



HAL
open science

Adsorption properties of functionalized α -glucans for the elaboration of innovative biobased materials

Aurore Delvart

► To cite this version:

Aurore Delvart. Adsorption properties of functionalized α -glucans for the elaboration of innovative biobased materials. Biotechnology. Nantes Université, 2022. English. NNT : 2022NANU4059 . tel-04041456

HAL Id: tel-04041456

<https://theses.hal.science/tel-04041456>

Submitted on 22 Mar 2023

HAL is a multi-disciplinary open access archive for the deposit and dissemination of scientific research documents, whether they are published or not. The documents may come from teaching and research institutions in France or abroad, or from public or private research centers.

L'archive ouverte pluridisciplinaire **HAL**, est destinée au dépôt et à la diffusion de documents scientifiques de niveau recherche, publiés ou non, émanant des établissements d'enseignement et de recherche français ou étrangers, des laboratoires publics ou privés.

THESE DE DOCTORAT DE

NANTES UNIVERSITE

ECOLE DOCTORALE N° 600

Ecole doctorale Ecologie, Géosciences, Agronomie et Alimentation

Spécialité : Sciences de l'aliment

Par

Aurore DELVART

Adsorption properties of functionalized α -glucans for the elaboration of innovative biobased materials

Thèse présentée et soutenue à Nantes, le 08/12/2022

Unité de recherche : INRAE, UR1268 BIA (Biopolymères, Interactions, Assemblages), Nantes

Rapporteurs avant soutenance :

Karine GLINEL Professeur in Biomaterials, Maître de Recherche FNRS –
Université catholique de Louvain, Belgique
Guy LADAM Professeur des Universités, HDR – Université Rouen Normandie

Composition du Jury :

Président : Guy LADAM Professeur des Universités, HDR – Université Rouen Normandie

Examineurs : Carmen FREIRE Principal researcher in Biopolymers – Université d'Aveiro, Portugal
 Stefan SPIRK Professeur Associé in Bioproduct and Cellulose technology –
 Patricia BERTONCINI Université technique de Graz, Autriche
 Maître de Conférences in Physics – Nantes Université

Dir. de thèse : Bernard CATHALA Directeur de Recherche in Cellulose materials – INRAE BIA, Nantes

Invités :

Co-dir. de thèse : Céline MOREAU Ingénieur de Recherche in Materials – INRAE BIA, Nantes

This PhD project has been funded by Agence National de la Recherche (ANR).

“Voies vertes pour la fonctionnalisation des α -Glucanes – GRaFTING”

Project ANR-18-CE43-0007

Remerciements

Ces travaux de thèse ont été réalisés au sein de l'unité de recherche Biopolymères, Interaction, Assemblages (BIA) à l'INRAE, institut national de recherche pour l'agriculture, l'alimentation et l'environnement, de Nantes. Je tiens à remercier son directeur d'unité, Bernard Cathala, et son ancien directeur d'unité, Marc Anton, de m'y avoir accueillie.

Cette thèse n'aurait jamais été possible sans mes encadrants de thèse, Bernard Cathala et Céline Moreau qui m'ont suivi durant ces trois ans. Merci infiniment à tous les deux, grâce à vous, j'ai beaucoup appris aussi bien scientifiquement que humainement. Je vous remercie pour le temps plus que conséquent que vous m'avez accordé durant ces trois années, pour votre patience et surtout vos très nombreux conseils durant la réalisation de cette thèse. Je continue mon petit chemin les bras remplis d'expériences, de méthodes et de motivation, et c'est grâce à vous !

Je remercie les membres du jury, Karine Glinel, Guy Ladam, Stefan Spirk, Carmen Freire et Patricia Bertocini pour avoir accepté de faire parti de mon jury et l'intérêt qu'ils porteront à mon manuscrit. J'adresse un grand merci à Chassenieux Christophe et Fouzia Bouldemais pour m'avoir suivi et évalué dans la plus grande gentillesse lors de mes comités de thèse. Merci également à Claire Moulis pour ces échanges passionnants lors des réunions de projets Grafting et lors de mes comités de thèse.

Un grand merci à Angéline D'Orlando pour son soutien et sa confiance sur les manipulations d'AFM ainsi que pour tous ses échanges scientifiques (ou non), riches en bonne humeur et en rire. Je tiens également à remercier Xavier Falourd et Luc Saulnier pour leur aide sur les analyses RMN and HPSEC respectivement. Et que seraient des remerciements sans mentionner Patrice Papineau *alias* Papi qui a toujours été présent pour résoudre mes problématiques mécaniques et techniques, pour le travail ou non. Toujours avec humour et bonne humeur. Merci beaucoup.

Merci aussi à Titouan Boureau, stagiaire, qui m'a aidé à finaliser mon projet de thèse lors de la dernière année.

Et si cette thèse s'est aussi bien déroulée, c'est très certainement grâce au soutien de toutes les personnes avec qui j'ai partagé cette aventure au quotidien. Merci à l'ensemble des

équipes NANO et MC2, merci à tous ceux qui ont animé mes pauses café, mes repas dans la bonne humeur, merci à tous ceux qui ont partagé mes hauts et mes bas durant ces trois dernières années. Et ce malgré une présence parfois en dents de scie au labo.

Avec tout cela, je me suis beaucoup baladé dans les bureaux du bâtiment Loire, et je tiens à faire un remerciement sincère à mes anciens et actuelles collègues de bureau : Nadège pour sa patience au quotidien et nos nombreuses discussions en tout genre, Karine pour son accueil et sa bienveillance, Pierre pour son aide et sa disponibilité à chaque instant. Je ne remercierai jamais assez Lisa pour cette année hors du commun dans notre petit cocoon entre sérieux et chansons, mais aussi Margaux qui a été mon pilier durant ces derniers mois de thèse grâce à sa bonne humeur et son aide pour finaliser le manuscrit.

Merci à tous les permanents de Loire pour leurs disponibilités, leurs conseils pleins de bienveillance et leurs aides qu'ils n'ont jamais hésité à me fournir : Isabelle Capron, Ana Villares, Hugo Voisin, Jean-Eudes Maigret, Denis Renard, Kamal Kansou, Denis Lourdin, Laurent Chaunier et Anne-Laure Réguerre. Merci aussi aux doctorants, post-doctorants et ingénieurs d'études avec qui j'ai partagé un bout de chemin, qui ont été là pour moi au quotidien : Maude, Yuzi, Rémy, Thomas, Maud, Aïcha, Dafné, Malika, Somia, Imen, Clara.

Ces trois ans ont connu des hauts et des bas, heureusement j'ai toujours pu compter sur mes amis, ici ou à l'autre bout de la France. Un merci particulier à Marie, Ipo et Camille pour votre soutien, merci infiniment. À mes (anciens) collègues et amis Gaëlle, Lisa, Margaux, Pierre, Anaïs, Mélanie, M&Ms, Hugo, Athénaïs, merci pour toutes ces soirées, voyages ou tout simplement tous ces souvenirs gravés dans ma mémoire. Un merci spécial à ma petite commu 'online' qui ont été toujours là pour m'écouter et m'aider à m'échapper et à relâcher la pression, vraiment merci à vous les filles !

Surtout, je remercie milles fois ma petite famille, à présent devenue grande ! Maman, Papa, Coraline, Ludo, Léo, Jeanne... Et particulièrement, je tiens à remercier de tout coeur ma petite soeur, Sélène, pour qui rien n'a été facile ces trois dernières années et qui malgré tout, a toujours été là pour les autres, pour moi. Ne baissons jamais les bras, petite soeur !

Et enfin, dédicace spéciale à mes deux boules de poils, Nyx et Lola. Ces trois ans auraient été bien plus difficiles sans leur réconfort quotidien !

Scientific contributions (2019-2022)

Publications in scientific journals

1. Delvart, A., Moreau, C., D'Orlando, A., Falourd, X., & Cathala, B. (2022). Dextran-based polyelectrolyte multilayers: Effect of charge density on film build-up and morphology. *Colloids and Surfaces B: Biointerfaces*, 210, 112258. <https://doi.org/10.1016/j.colsurfb.2021.112258>
2. Delvart, A., Moreau, C., & Cathala, B. (2022). Dextrans and dextran derivatives as polyelectrolytes in layer-by-layer processing materials – A review. *Carbohydrate Polymers*, 293, 119700. <https://doi.org/10.1016/j.carbpol.2022.119700>

Oral presentations

1. Delvart, A., Moreau, C., Leray, N., D'Orlando, A., Cathala, B. (2021). “Elaboration of innovative multi-layered materials based on functionalized α -glucans” in *7th EPNOE Meeting (European Polysaccharide Network of Excellence) – International Polysaccharide Conference* (Nantes, France).
2. Delvart, A., Moreau, C., Leray, N., D'Orlando, A., Cathala, B. (2021). “Functionalized dextrans multilayers: impact of the polymer structure on films growth” in *GDR SLAMM Meeting (Solliciter la Matière Molle) – National Soft Matter Conference* (Biarritz, France).
3. Delvart, A., Moreau, C., Leray, N., Cathala, B. (2022). “Functionalized α -glucans for multilayer films with tunable surface pattern and functionalities” in *Scientific Days of Doctorate School EGAAL (Ecologie, Géosciences, Agronomie et Alimentation) – Doctorate School Conference*.
4. Delvart, A., Boureau, T., Moreau, C., Leray, N., Cathala, B. (2022). “Dextrans for multilayer films with tunable surface pattern and functionalities” in *Young Researchers Days of INRAE BIA – Laboratory Conference*.
5. Delvart, A., Boureau, T., Moreau, C., Leray, N., Cathala, B. (2022). “Multilayers of α -glucans with engineered surface pattern and functionalities” in *5th EPNOE Junior*

Scientists Meeting (European Polysaccharide Network of Excellence) – International Polysaccharide Conference (Aveiro, Portugal).

Poster presentations

1. Delvart, A., Moreau, C., Leray, N., Cathala, B. (2021). “Adsorption properties of functionalized dextrans for the elaboration of innovative biobased materials” in *4th EPNOE Junior Scientists Meeting (European Polysaccharide Network of Excellence) – International Polysaccharide Visioconference.*
2. Delvart, A., Moreau, C., Leray, N., Cathala, B. (2021). “Multi-layered materials based on functionalized dextrans for the elaboration of innovative materials” in *Scientific Days of Doctorate School EGAAL (Ecologie, Géosciences, Agronomie et Alimentation) – Doctorate School Visioconference.*

Abbreviations

AFM : Atomic Force Microscopy

CHI : chitosan

DEAE : 2-(diethylamino) ethyl / diethylaminoethyl

Dex-DEAE : diethylaminoethyl-dextran

DexS H : dextran sulfate with high sulfate content / high charge density

DexS L : dextran sulfate with low sulfate content / low charge density

DexS : dextran sulfate

HPSEC : High-Performance Size-Exclusion Chromatography

LbL : layer-by-layer

Mw : molecular weight

NMR : nuclear magnetic resonance

Ox-Alt : TEMPO-oxidized alternan

Ox-Dex : TEMPO-oxidized Dex DSR-OK-a2

Ox-Reu : TEMPO-oxidized reuteran

PA : polyanion

PAA : poly(acrylic acid)

PAH : poly(allylamine) hydrochloride

PC : polycation

PE : polyelectrolyte

PEI : polyethyleneimine

PEM : polyelectrolyte multilayers

PLL : poly-L-lysine

QCM-D : Quartz Crystal Microbalance with Dissipation monitoring

RMS : Root Mean Square

SPR : Surface Plasmon Resonance

TEMPO : (2,2,6,6-tétraméthylpipéridin-1-yl)oxyl

Table of figures

Figure 1.1. Structures of cellobiose and maltose illustrating the different geometries of glycosidic bonds in polysaccharides: β -glycosidic bond (cellobiose on the left) and α -glycosidic bond (maltose on the right).	18
Figure 1.2. Classification of α -D-glucans by their typical main structures (α -D-(1 \rightarrow 4), α -D-(1 \rightarrow 6), α -D-(1 \rightarrow 3)) that are depending on their origins (mammals, bacteria, plants, algae, fungi and lichens). Families concerned by this work, bacterial α -D-glucans, are highlighted in red.	19
Figure 1.3. Illustration of the classical enzymatic production of α -glucans by the action of sucrases onto sucrose.	20
Figure 1.4. General structure of dextrans with a D-glucose main chain linked by α -(1 \rightarrow 6) glycosidic bonds and branches based on α -(1 \rightarrow 3), α -(1 \rightarrow 4) and α -(1 \rightarrow 2) bonds and main derivatives obtained by chemical functionalization of dextrans.	22
Figure 1.5. Overview of the most important applications of dextrans and their derivatives in industries. Adapted with permission from (Goodwin et al., 2009), © 2009 American Chemical Society. Adapted with permission from (Martwiset et al., 2006), © 2006 American Chemical Society. Adapted with permission from (Novak et al., 1955), © 1955 American Chemical Society. Adapted with permission from (Serizawa et al., 2000), © 2000 American Chemical Society. Adapted from (W.-S. Kim et al., 2019; Kokilavani et al., 2021; Lazić et al., 2020; Wolter et al., 2014), with permission from Elsevier. Adapted from (Parisi et al., 2017; Platt et al., 2010; Sethy et al., 2020; G. Sun et al., 2011).....	24
Figure 1.6. Schematic representation of the different steps in the preparation of polyelectrolyte multilayers (PEMs) by the layer-by-layer (LbL) method.	28
Figure 1.7. Schematic representation of the main LbL methods used for the fabrication of PEMs based on polycation (PC) and polyanion (PA). (A) Conventional immersion deposition of PEs, (B) Spray deposition of PEs, (C) Spin-assisted deposition of PEs, (D) Electromagnetic deposition of PEs, (E) Microfluidic assembly of PEs on microfluidic materials. (Petrila et al., 2021).....	29
Figure 1.8. Schematic representation of adsorption mechanism onto a surface, based on a simple system of polyelectrolyte (polycation) in aqueous solution with associated counterions (in red).....	31
Figure 1.9. Schematic representation of the linear and exponential growth regimes of LbL assembly observed on film thickness/film mass as a function of the number of adsorbed layers/bilayers. Adapted from (Silva et al., 2016).	33
Figure 1.10. Schematic representation of (a) Linear growth regime, (b) Exponential/non-linear/supra-linear growth regime of polyelectrolyte multilayers built with layer-by-layer method by (Silva et al., 2016) adapted from (Porcel et al., 2007).	34
Figure 1.11. Schematic representation of the main properties of polyelectrolyte multilayers, usually explored in literature, adapted from (Petrila et al., 2021).	36
Figure 1.12. Scheme of the changes in the conformation of weak polyelectrolytes (polycation in green, polyanion in blue) according to the pH of solutions.	38
Figure 1.13. Schematic representation of the impact of ionic strength, represented by salt/counterions addition (black dots) on polyelectrolyte conformation (here, a polyanion) according on the charge density of the polyelectrolytes.	40
Figure 1.14. QCM frequency shift as function of adsorbed layer number up to 10 bilayers of (CHI/DexS) films on silver quartz crystal at pH depending on added salt content, (a) 0 M NaCl and (b) 1M NaCl. Frequency shift and the corresponding thickness is indicated. Reprinted with permission from (Serizawa et al., 2000), © 2000 American Chemical Society. Thicknesses and roughnesses of 10 bilayers (CHI/DexS) films grown on silica wafer with (c) pH (at 0.5 M ionic strength) and (d) ionic strength (at pH 6) obtained with ellipsometer measurements, data from (Devi et al., 2014).	45

Figure 1.15. (a) AFM images ($10\ \mu\text{m} \times 10\ \mu\text{m}$, phase) of bare glass surface, (DEAE-Dex/DexS) multilayer, and (DEAE-Dex/DexS)-DEAE-Dex multilayer adsorbed on glass surfaces (Benni et al., 2014). (b) SEM images ($30\ \mu\text{m} \times 30\ \mu\text{m}$) of stent surfaces: bare metal stent, DexS coated stent and DEAE-Dex and DexS coated stent (Jang et al., 2019).	48
Figure 1.16. Schematic fabrication of micro- and nano- capsules based on LbL deposition principle onto sacrificial core template with (a) post-loading method and (b) pre-loading method.....	53
Figure 1.17. Schematic representation: principle of a filtration membrane based on polyelectrolyte multilayers.	57
Figure 1.18. Schematic representation of light reflected and optical interferences in (a) a multilayered structure based on two layers with different refractive index n_1 and n_2 and in (b) a single layer or a film appared to a single-layered structure based on layers with the same, or almost, refractive index n_{film}	59
Figure 1.19. Structural colors from LbL films of microfibrillated cellulose and poly(ethyleneimine) as a function of the number of layers (18 layers is 9 layers of microfibrillated cellulose and 9 layers of poly(ethyleneimine), from (Wågberg et al., 2008).	60
Figure 1.20. (a) Schematic representation of release system of encapsulated drug with enzymatic degradation, adapted with permission from (Itoh et al., 2006), © 2006 American Chemical Society. (b) Schematic representation of optical change induced by the action of enzymes on polyelectrolyte multilayers.	61
Figure 1.21. Enzyme-induced degradation photos of multilayer films composed of 5 bilayers and 8 bilayers of cellulose nanocrystals/xyloglucans after the deposition of enzyme droplet at different concentrations (spots 3 to 8) during 30 and 60 min.	63
Figure 2.1. Schematic representation of the spin-assisted methodology on the spin-coater system with the three-axis robot.....	94
Figure 2.2. Schematic representation of (a) the principle of Quartz crystal microbalance with dissipation monitoring (QCM-D), (b) the damping of oscillations depending on the type of layers and (c) the two main informations obtained using QCM-D (adapted from Biolin Scientific/Q-Sense).	95
Figure 2.3. Principle of SPR sensor. Surface plasmon resonance (SPR) sensors detect a refractive index (RI) change within a detection area ($<500\ \text{nm}$) as a change of resonance angle (RA) from (Yanase et al., 2014).	98
Figure 2.4. (a) Principle of Atomic Force Miscope (AFM): scanning probe microscope using interaction forces between the cantilever and the surface. (b) Different modes of AFM, including contact mode, tapping mode and non-contact mode. Adapted from AFM Handbook, JPK NanoWizard.	100
Figure 2.5. Schematic representation of light interferences, with constructive and destructive interferences for a thin film deposited of refractive index n_{film} on a substrate of refractive index $n_{\text{substrate}}$	101
Figure 2.6. Schematic representation of the contact angle formed by liquid drop on a surface with wetting and non-wetting situations, adapted from (Yuan & Lee, 2013).	103
Figure 3.1. Scheme of the LbL formation of films from polycation (orange chains), and polyanion (green chains) in solid substrate (grey bar).	116
Figure 3.2. Chemical structures of dextrans sulfate with high sulfate content DexS H (on the left) and low sulfate content DexS L (on the right); sulfation patterns of both DexS are indicated.	117
Figure 3.3. Chemical structure of poly(allylamine hydrochloride) (PAH).....	118
Figure 3.4. (a) Graph of $\Delta f_5/5$ vs time for (PAH/DexS) ₁₀ multilayer with DexS H40 (dark green) and DexS L40 (light green) building on gold coated surface. (b) Adsorbed mass evaluated with Voigt model for (PAH/DexS) ₁₀ multilayer with DexS H40 (dark green) and DexS L40 (light green). Bn corresponds to the n th (PAH/DexS) bilayer of the multilayer.	118
Figure 3.5. (a), (c) $\Delta f_n/n$ and ΔD_n as a function of time for (PAH/DexS 40) ₁₀ multilayers on gold coated quartz crystal using QCM-D. The frequency (blue) and dissipation (red) change for the third, fifth and seventh	

overtone is depicted. (b), (d) Zoom on the bilayer 10 build-up with adsorption of PAH (orange), rinsing with pure water (grey), adsorption of DexS 40 (green)..... 120

Figure 3.6. ΔD_5 as a function of $\Delta f_5/5$ of (a) the construction of (PAH/DexS H40)₁₀ films and (b) the construction of (PAH/DexS L40)₁₀. Relative softness calculated from ΔD_5 and $\Delta f_5/5$ for adsorption step of PAH layer (PAH 5) and DexS layer (DexS 5) of bilayer 5 and PAH layer (PAH 10) and DexS layer (DexS 10) of bilayer 10 for (c) (PAH/DexS H40)₁₀ and (d) (PAH/DexS L40)₁₀..... 122

Figure 3.7. Chemical structures of diethylaminoethyl-Dextran (Dex-DEAE). 123

Figure 3.8. (a) Graph of $\Delta f_5/5$ vs time for (Dex-DEAE 150/DexS)₁₀ multilayer with DexS H40 (dark green) and DexS L40 (light green) building on gold coated surface. (b) Adsorbed mass evaluated with Voigt model for (Dex-DEAE 150/DexS)₁₀ multilayer with DexS H40 (dark green) and DexS L40 (light green). B_n corresponds to the nth (Dex-DEAE 150/DexS) bilayer of the multilayer. (Adsorbed masses for bilayer 9 and bilayer 10 of (Dex-DEAE 150/DexS H40)₁₀ were not integrated in the data as the Voigt model does not fit for those two points). 124

Figure 3.9. (a), (b) $\Delta f_n/n$ and ΔD_n as a function of time for (Dex-DEAE 150/DexS 40)₁₀ multilayer on gold coated quartz crystal using QCM-D. The frequency (blue) and dissipation (red) changes for the third, fifth and seventh overtones are depicted with adsorption of Dex-DEAE 150 (orange) and adsorption of DexS 40 (green). 125

Figure 3.10. (a) Graph of $\Delta f_5/5$ vs time for (PAH/ α -glucan)₁₀ multilayer with PAH and neutral alternan (dark purple), Ox-Alt (light purple), neutral reuteran (dark orange), Ox1-Reu (orange) and Ox2-Reu (yellow) building on gold coated surface. (b) Adsorbed mass evaluated with Voigt model for 10 bilayers multilayer with PAH and oxidized α -glucan Ox-Alt (light purple), Ox1-Reu (orange) and Ox2-Reu (yellow). B_n corresponds to the nth (PAH/ α -glucan) bilayer of the multilayer. 128

Figure 3.11. (a), (b) $\Delta f_n/n$ and ΔD_n as a function of time for (PAH/Ox-Alt)₁₀ and (PAH/Ox1-Reu)₁₀ multilayer on gold coated quartz crystal using QCM-D. The frequency (blue) and dissipation (red) changes for the third, fifth and seventh overtones are depicted with adsorption of PAH (orange), adsorption of Ox-Alt (purple) and adsorption of Ox1-Reu (orange). 129

Figure 3.12. ΔD_5 as a function of $\Delta f_5/5$ of (a) the construction of (PAH/Ox-Alt)₁₀ films and (b) the construction of (PAH/Ox1-Reu)₁₀. 130

Figure 3.13. (a) Graph of $\Delta f_5/5$ vs time for (Dex-DEAE 150/ α -glucan)₁₀ multilayer with Dex-DEAE 150 and neutral Dex-DSR-OK-a2 (black), Ox1-Dex (brown), Ox2-Dex (dark orange) and Ox3-Dex (orange) built on gold coated surface. (b) Adsorbed mass evaluated with Voigt model for 10 bilayers multilayer with Dex-DEAE 150 and oxidized α -glucan Ox1-Dex (brown), Ox2-Dex (dark orange) and Ox3-Dex (orange). B_n corresponds to the nth (Dex-DEAE 150/ α -glucan) bilayer of the multilayer. 132

Figure 3.14. $\Delta f_n/n$ and ΔD_n as a function of time for (a) (Dex-DEAE 150/Ox1-Dex)₁₀ and (b) (Dex-DEAE 150/Ox3-Dex)₁₀ multilayer on gold coated quartz crystal using QCM-D. The frequency (blue) and dissipation (red) changes for the third, fifth and seventh overtones are depicted with adsorption of PAH (orange), adsorption of Ox1-Dex (brown) and adsorption of Ox3-Dex (orange)..... 133

Figure 3.15. ΔD_5 as a function of $\Delta f_5/5$ of (a) the construction of (Dex-DEAE 150/Ox1-Dex)₁₀ films and (b) the construction of (Dex-DEAE 150/Ox3-Dex)₁₀. 134

Figure 3.16. Schematic representation of the experimental approach to characterize multilayers: from growth of QCM-D to tentative mechanisms. 137

Figure 3.17. (a) Water content (%w/w) of the films calculated from the ratio of adsorbed mass obtained by SPR and adsorbed mass obtained by QCM-D on the 2nd bilayer and the value calculated from D₂O-H₂O exchange on the 2nd bilayer. (b) $\Delta f_5/5$ vs time for D₂O-H₂O exchange on the 2nd bilayer of (PAH/DexS H40) multilayer (dark green), of (PAH/DexS L40) multilayer (light green) and on bare gold (bare Au, grey). 139

Figure 3.18. AFM topography images from (a) (PAH/DexS H40) multilayer and (b) (PAH/DexS L40) multilayer of (at the top) the PAH 5 (bilayer 4.5 *i.e.* outermost layer of PAH before bilayer 5), the DexS 5 (bilayer 5), and of (at the bottom) PAH 10 (bilayer 9.5 *i.e.* outermost layer of PAH before bilayer 10) and DexS

10 (bilayer 10). Height profiles of (c) (PAH/DexS H40) ₁₀ and (d) (PAH/DexS L40) ₁₀ using AFM topography images on scratched surface (Annexes, Figure 3.A3).	140
Figure 3.19. Proposed mechanism for the build-up of (PAH/DexS H40) PEMs starting from bilayer 4 on PEMs previously ending with DexS.	142
Figure 3.A1. ¹ H NMR spectrum for DexS H and DexS L showing sulfation from peaks on C2 and C3 at 5.2-5.3 ppm, on C2 (5.1-5.2 ppm) and on C3 (4.9-5.0 ppm) and no sulfation from peaks at 4.8-4.9 ppm.	149
Figure 3.A2. Adsorbed mass obtained by SPR analysis on gold-coated sensors, where D _n represents the number of bilayers deposited. (PAH/DexS H40) is represented in dark green, (PAH/DexS L40) is represented in light green. In grey is indicated, the values where (PAH/DexS L40) seems to detach itself from the substrate and the total adsorbed mass detected drop during the measurement.	149
Figure 3.A3. AFM topography images (10 μm x 10 μm) and the corresponding height profiles of the 10th layer of DexS after scratching method applied on (a) (PAH/DexS H40) ₁₀ and (b) (PAH/DexS L40) ₁₀ PEMs. AFM scratching method applied on PEMs (PAH/DexS H40) and (PAH/DexS L40). Height profiles of (PAH/DexS H40) PEMs section on the top and of (PAH/DexS L40) PEMs section on the bottom. Height profiles of the 10th layer of DexS for (a) (PAH/DexS H40) and (b) (PAH/DexS L40).	150
Figure 3.A4. Δf _n /n and ΔD _n as function of time for (PAH/Ox2-Reu) ₁₀ multilayer on gold coated quartz crystal using QCM-D. The frequency (blue) and dissipation (red) changes for the third, fifth and seventh overtone are depicted with adsorption of PAH (orange) and adsorption of Ox2-Reu (yellow).	150
Figure 3.A5. Δf _n /n and ΔD _n as function of time for (Dex-DEAE 150/Ox2-Dex) ₁₀ multilayer on gold coated quartz crystal using QCM-D. The frequency (blue) and dissipation (red) changes for the third, fifth and seventh overtone are depicted with adsorption of Dex-DEAE 150 (orange) and adsorption of Ox2-Dex (dark orange).	151
Figure 4.1. (a) Graph of Δf ₅ /5 vs time for 5 bilayers of (PAH/DexS L5) films (light purple), (PAH/DexS H5) films (dark purple), (PAH/DexS L40) films (light green) and (PAH/DexS H40) films (dark green) built on gold coated surface. (b) ΔD ₅ as a function of Δf ₅ /5 of the construction of (PAH/DexS L5) ₅ films (light purple), (PAH/DexS H5) ₅ films (dark purple), (PAH/DexS L40) ₅ films (light green) and (PAH/DexS H40) ₅ films (dark green). Relative softness <i>i.e.</i> slopes in red.	160
Figure 4.2. (a) Graph of Δf ₅ /5 vs time for 5 bilayers of (Dex-DEAE 150/Ox1-Dex) films (brown), and (Dex-DEAE 150/Ox3-Dex) films (orange) built on gold coated surface. (b) ΔD ₅ as a function of Δf ₅ /5 of the construction of (Dex-DEAE 150/Ox1-Dex) ₅ films (brown) and (Dex-DEAE) ₅ films (orange).	162
Figure 4.3. AFM 2D and 3D images (10×10 μm) and photos of the surface for 40 bilayers of (a) (PAH/DexS H40) and (b) (PAH/DexS L40) built by spin-assisted dipping method onto silicon wafer at 25mM NaCl.	164
Figure 4.4. Contact angle images and corresponding values obtained for 40 bilayers of (a) (PAH/DexS H40) and (b) (PAH/DexS L40) built by spin-assisted dipping method onto silicon wafer at 25mM NaCl.	166
Figure 4.5. (a) Graph of Δf ₅ /5 vs time for 5 bilayers of (PAH/DexS H40) films for 0 mM NaCl (light grey), for 5 mM NaCl (grey) and for 25mM NaCl (dark grey) built on gold coated surface. (b) ΔD ₅ as a function of Δf ₅ of the construction of (PAH/DexS H40) ₅ films for 0 mM NaCl (light grey), for 5 mM NaCl (grey) and for 25mM NaCl (dark grey). Relative softness <i>i.e.</i> slopes in red.	169
Figure 4.6. (a) Graph of Δf ₅ /5 vs time for 5 bilayers of (PAH/DexS L40) films for 0 mM NaCl (light grey), for 5 mM NaCl (grey) and for 25mM NaCl (dark grey) built on gold coated surface. (b) ΔD ₅ as a function of Δf ₅ /5 of the construction of (PAH/DexS L40) ₅ films for 0 mM NaCl (light grey), for 5 mM NaCl (grey) and for 25mM NaCl (dark grey).	170
Figure 4.7. AFM 2D and 3D images (10×10 μm) and photos of the surface for 40 bilayers of (PAH/DexS H40) films at (a) 0mM NaCl, (b) 5mM NaCl and (c) 25mM NaCl, built by spin-assisted dipping method onto silicon wafer.	173
Figure 4.8. AFM 2D and 3D images (10×10 μm) and photos of the surface for 40 bilayers of (PAH/DexS L40) films at (a) 0mM NaCl, (b) 5mM NaCl and (c) 25mM NaCl, built by spin-assisted dipping method onto silicon wafer.	174

Figure 4.9. Contact angle images and contact angle values obtained for 40 bilayers of (a) (PAH/DexS H40) and (b) (PAH/DexS L40) at 0mM NaCl, 5mM NaCl and 25mM NaCl built by spin-assisted dipping method onto silicon wafer.....	175
Figure 4.10. (a) Graph of $\Delta f_5/5$ vs time for 5 bilayers of (PAH/DexS H5) films (dark purple), (PAH/DexS H40) films (dark green) and (PAH/DexS H500) films (red) built on gold coated surface. (b) ΔD_5 as a function of $\Delta f_5/5$ of the construction of (PAH/DexS H5) ₅ films (dark purple), (PAH/DexS H40) ₅ films (dark green) and (PAH/DexS H500) ₅ films (red). Relative rigidity <i>i.e.</i> slopes in red.....	178
Figure 4.11. AFM 2D and 3D images (10×10 μm) for 40 bilayers of (PAH/DexS H) films for DexS H with a molecular weight of (a) 5 000 g.mol ⁻¹ , (b) 40 000 g.mol ⁻¹ and (c) 500 000 g.mol ⁻¹ , built by spin-assisted dipping method onto silicon wafer at 25mM NaCl.....	180
Figure 4.12. Contact angle images and contact angle values obtained for 40 bilayers of (PAH/DexS H5), (PAH/DexS H40) and (PAH/DexS H500) built by spin-assisted dipping method onto silicon wafer at 25mM NaCl.....	181
Figure 5.1. Schematic presentation of (a) the concept proposed by Cerclier <i>et al.</i> for colorimetric biosensors for detection of enzymatic activity, (b) of the concept proposed in this thesis for more sensitive colorimetric biosensors for detection of enzymatic activity.....	194
Figure 5.2. Scheme of the concept proposed for the elaboration of colorimetric biosensors for the detection of enzymes, based on multilayers of functionalized α-glucans.....	196
Figure 5.3. Photos and colors of (a) (PAH/DexS) 40-bilayer films and (b) (PAH/oxidized α-glucans) and (DEAE-Dex 150/oxidized α-glucans) 40-bilayer films. Multilayers were built on silicon wafers at 25mM NaCl using spin-assisted coating method.....	198
Figure 5.4. Photos of (PAH/DexS L40) films for 30 bilayers, 40 bilayers, 60 bilayers and 80 bilayers. Multilayers were built on silica wafers at 25mM NaCl using spin-assisted coating method.....	199
Figure 5.5. (a) $\Delta f_n/n$ and ΔD_n as a function of time for deposition of (PAH/DexS H40) ₅ /(PAH/DexS L40) ₅ on gold coated surface using QCM-D. (b) ΔD_5 as a function of $\Delta f_5/5$ with the switch of regime between (PAH/DexS H40) ₅ and (PAH/DexS L40) ₅ in orange.....	201
Figure 5.6. Structure of ε-poly-L-lysine (PLL).....	202
Figure 5.7. $\Delta f_n/n$ and ΔD_n as a function of time for (a) (PLL/DexS H40) ₁₀ multilayer and (b) (PLL/DexS L40) ₁₀ multilayer on gold coated quartz crystal using QCM-D. The frequency (blue) and dissipation (red) changes for the third, fifth and seventh overtones are depicted.....	203
Figure 5.8. Photos and colors of (a) (PAH/DexS H40) ₄₀ film, of (b) (PAH/DexS H40) ₄₀ /(PLL/DexS H40) ₁ film and of (c) (PAH/DexS H40) ₄₀ /(PLL/DexS H40) ₁ /(PAH/DexS L40) ₄₀ film.....	204
Figure 5.9. Photos of (PAH/DexS H40) ₄₀ /(PLL/DexS H40) ₁₀ /(PAH/DexS L40) ₄₀ before and after dipping in presence of (a) 1 mg.mL ⁻¹ , (b) 0.1 mg.mL ⁻¹ and (c) 0.01 mg.mL ⁻¹ trypsin.....	205
Figure 5.A1. Δf_n and ΔD_n as a function of time for deposition of (PAH/DexS H40) ₅ /(PAH/DexS L40) ₅ /(PAH/DexS H40) ₅ on gold coated surface using QCM-D.....	211
Figure 5.A2. Photos of (PAH/DexS H40) ₄₀ /(PLL/DexS H40) ₁₀ /(PAH/DexS H40) ₄₀ before and after dipping in presence of (a) 0.01 mg.mL ⁻¹ , (b) 0.1 mg.mL ⁻¹ and (c) 1 mg.mL ⁻¹ trypsin.....	211
Figure R.1. Représentation schématique des différentes étapes de la fabrication de multicouches de polyélectrolytes (PEM) par la méthode couche par couche (layer-by-layer).....	221
Figure R.2. Masse adsorbée évaluée avec le modèle de Voigt pour un multicouche de (a) (PAH/DexS) ₁₀ and (b) (Dex-DEAE 150/DexS) ₁₀ avec DexS H40 (vert foncé) et DexS L40 (vert clair). Bn correspond à la nième bicouche du multicouche.....	222
Figure R.3. Mécanismes proposés pour la construction de (a) multicouche (PAH/DexS H40) et de (b) multicouche (PAH/DexS L40).....	224

Figure R.4. Images AFM 2D et 3D (10×10 μm) ainsi que les photos des surfaces pour 40 bicouches de (a) (PAH/DexS H40) et (b) (PAH/DexS L40) construites par la méthode de trempage assistée par rotation sur silicium à 25mM NaCl.	225
Figure R.5. Images AFM 2D et 3D (10×10 μm) ainsi que les photos des surfaces pour 40 bicouches de (PAH/DexS H) pour le DexS H avec un poids moléculaire de (a) (a) 5 000 g.mol ⁻¹ , (b) 40 000 g.mol ⁻¹ and (c) 500 000 g.mol ⁻¹ construites par la méthode de trempage assistée par rotation sur silicium à 25mM NaCl.	227
Figure R.6. Présentation schématique du concept proposé pour l'élaboration de biocapteurs colorimétriques pour la détection d'enzymes, basés sur des multicouches d'α-glucanes fonctionnalisés.....	228
Figure R.7. (a) Photo et couleurs d'un film de 40 bicouches (PAH/DexS L40). (b) $\Delta f_n/n$ et ΔD_n en fonction du temps pour le dépôt de (PAH/DexS H40) ₅ /(PAH/DexS L40) ₅ sur une surface d'or en utilisant QCM-D.....	229
Figure R.8. Photos de l'élaboration du film (PAH/DexS H40) ₄₀ /(PLL/DexS H40) ₁ /(PAH/DexS L40) ₄₀ et de sa dégradation par trempage en présence de (a) 0.01 mg.mL ⁻¹ , (b) 0.1 mg.mL ⁻¹ et (c) 1 mg.mL ⁻¹ de trypsine.....	230

List of tables

Table 1.1. Source and structure of different bacterial α -D-glucans, adapted from (Reddy Shetty et al., 2021). ..	21
Table 1.2. Summary of the most frequently used reactions and modifications for the obtention of dextran derivatives summarized from (Heinze et al., 2006).	23
Table 1.3. Chitosan and dextran sulfate (CHI/DexS) multilayered films reported in literature and their applications.	46
Table 1.4. Dextran derivatives as polyelectrolytes for drug delivery micro– and nano– capsules fabrication reported in literature.	54
Table 1.5. Polyelectrolytes and their specific enzymes used in enzyme-based degradation of multilayers that can be found in literature.	62
Table 2.1. Notation and summarized information of polyelectrolytes used for the formation of multilayered films in this thesis.	89
Table 3.1. Final frequency shift measured with QCM-D and mass obtained with Voigt model and Sauerbrey equation after 10 bilayers and rinsing step, for PAH/DexS 40 multilayers.	119
Table 3.2. Structure of different bacterial α -D-glucans synthesized and provided by TBI.	126
Table 3.3. Notation and oxidation degrees of the different oxidized α -glucans provided by TBI.	126
Table 3.4. Final frequency shift measured with QCM-D and mass obtained with Voigt model after 10 bilayers and rinsing step, for PAH/oxidized α -glucans multilayers.	128
Table 3.5. Final frequency shift measured with QCM-D and mass obtained with Voigt model after 10 bilayers and rinsing step, for Dex-DEAE 150/oxidized α -glucans multilayers.	132
Table 3.6. Summarized information on multilayers studied in section 1, after 10 bilayers formation.	135
Table 4.1. Systems based on different polyelectrolyte couples, charge type and charge density of polycation (PC) and polyanion (PA) used for each system.	159
Table 4.2. Systems based on different polyelectrolyte couples, charge density of polycation (PC) and polyanion (PA) and number of bilayers used for each system.	163
Table 4.3. Systems based on different polyelectrolyte couples, charge density and ionic strength (as NaCl concentration) of polycation (PC) and polyanion (PA) used for each system.	168
Table 4.4. Systems based on different polyelectrolyte couples. Molar masses of all polycations (PC) and polyanions (PA) used for each system.	177

General table of content

General introduction.....	1
Chapter 1 – Literature review	11
Chapter 2 – Material and methods.....	85
Chapter 3 – Layer-by-layer formation of α-glucans multilayers	109
Chapter 4 – Structure and surface properties modulation.....	153
Chapter 5 – α-glucans multilayers for detection of enzymatic activity	189
Conclusion and outlooks	213
Résumé en français.....	219

General introduction

General introduction

In response to declining oil resources and in a desire to reduce the environmental impact of human activities, it is necessary to find innovative and green solutions, particularly for the development of materials, both in terms of more energy-efficient and more environmentally friendly processes. Polymers represent a large part of the resources used in the materials industry and, today, they are mainly derived from petroleum. In the last decades, systems based on natural polymers, and in particular polysaccharides, have become a central topic in materials chemistry and nanotechnology due to their biocompatibility, biodegradability and low toxicity (Boddohi & Kipper, 2010; de Belder, 1996; Rinaudo, 2008).

Among the polysaccharides that are attracting the interest of the scientific community, α -glucans, synthesized by a variety of natural sources from bacteria, fungi, plants, algae, lichens, insects and mammals, are good candidates for the development of innovative materials (Liu et al., 2015; Rinaudo, 2008). Beyond their wide availability in nature, α -glucans display a large panel of structural variability: large range of molar mass, different branching patterns (Chludzinski et al., 1974; Hehre, 1956; Naessens et al., 2005). Moreover, there is a large variety of chemical functions that can be obtained by chemical functionalization (Antonini et al., 1964; Heinze et al., 2006; Mauzac & Jozefonvicz, 1984; Rogovin et al., 1972).

Bacterial α -glucans are of great interest for the scientific community due to their production by bacteria *i.e.* fermentation of sugar/sucrose and their possibility of functionalization by chemical way (Baptista & Freitas, 2021; Naessens et al., 2005). More recently, the notable progress made by a group of the Toulouse Biotechnology Institute on the production of α -glucans by enzymatic routes, has opened the field of possible enzymatic modifications of these polysaccharides by non-chemical route, *i.e.* with a lower environmental impact (Grimaud et al., 2018). These new “green” functionalization pathways would offer an opportunity for more massive use of α -glucans in industry. In particular, their use in the construction of materials would make it possible to replace some of the synthetic polymers filled to form materials.

The replacement of petroleum-derived polymers with bio-based polymers is therefore an important issue that need to meet the environmental and functional requirements of materials (Crouzier et al., 2010). The challenge is to understand and to control the interactions

of/with functionalized α -glucans to develop materials with new properties. A versatile and convenient technique to build such material is the layer-by-layer (LbL) assembly of polyelectrolytes, based on the alternated adsorption of polycations and polyanions onto a substrate (Decher, 1997; Decher & Hong, 1991).

In this context, the French National Research Agency project “Gràfting” aims to improve and diversify the production of charged α -glucans by developing green routes allowing the functionalization of α -glucans by enzymatic route. In parallel with this biological engineering of functionalization, the project also aspires to evaluate the possibility of elaborating new materials based on these new bio-sourced polyelectrolytes while exploring their interaction properties especially in LbL assembly.

The project gathers the competences of three laboratories:

- TBI, INRAE-INSA-CNRS (Toulouse, France) for the bacterial α -glucans production and the enzymatic functionalization of bacterial α -glucans
- INRAE Micalis (Jouy-en-Josas, France) for the enzymatic functionalization of bacterial α -glucans
- INRAE BIA, Nano Team (Nantes, France) for the adsorption by layer-by-layer technique and the formulation of novel materials with innovative properties

My thesis project was conducted in Nano Team at INRAE BIA (Biopolymers, Interactions and Assemblages) in Nantes (France) and was focused on three major objectives for the elaboration of innovative materials based on novel bacterial α -glucans multilayers:

1. Evaluation of the adsorption capacities of bacterial α -glucans
2. Control for the layer-by-layer (LbL) fabrication of bacterial α -glucans -based multilayers
3. Examination of the properties of multilayered films for the selection of specific applications

Anionic dextrans, *i.e.* dextrans sulfate (DexS), and a synthetic polycation, poly(allylamine) hydrochloride (PAH), that are commonly used for LbL assembly, were used to understand the interactions involved and the impact of experimental parameters on film construction (Feldötö et al., 2010; Serizawa et al., 2000). The extended analysis of the formation of PAH/DexS multilayers allowed us to propose growth mechanisms for α -glucans -based multilayers. Therefore, a general methodology was developed using PAH/DexS that

could be applied for the analysis of all functionalized α -glucans films. In particular, novel oxidized α -glucans prepared by the project partner TBI Team present a high molecular weight ($10^8 - 10^9 \text{ g.mol}^{-1}$). The use of polyelectrolytes with such high molar masses is to our knowledge a novelty in fabrication of multilayers.

We used Quartz Crystal Microbalance with Dissipation monitoring (QCM-D) that is a fast *in-situ* technique allowing online monitoring and requiring low amount of product. QCM-D gives access to the “hydrated” mass adsorbed of the film, but also to qualitative information on the material viscoelasticity (Dixon, 2008; Notley et al., 2005). In addition, we also studied/investigated the film construction by Surface Plasmon Resonance (SPR), an optical *in-situ* method, that gives access to the “dry” mass adsorbed of the film (Caruso et al., 1997). Particularly, the combination of QCM-D and SPR allows to obtain indication on the hydration state of the multilayers (Höök et al., 2001). Observation and analysis of multilayers by Atomic Force Microscopy (AFM) and contact angle measurements allowed acknowledging the notable properties of films: the surface morphology and wettability.

The work proposed in this thesis provides a comprehensive understanding of the formation of multilayered films based on sulfate dextrans and oxidized α -glucans, which could be generalized to any functionalized α -glucans independently of their charge and their molecular weight. Moreover, we have sought to give an overview on which type of properties can be obtained using those types of materials and how to modulate them. Especially, the tunable structural colors and wettability of the multilayers by modulation of their surface morphology, thickness, roughness had a potential for the development of bio-based innovative materials, such as fast-response colorful sensors for enzyme-detection.

Manuscript organization

The manuscript is divided into five chapters: a chapter for a literature review, a chapter for the presentation of materials and methods used and three chapters on results and discussion.

In **Chapter 1**, a *literature review describes the context of this Ph.D project* through a outline on bacterial α -glucans, a presentation of multilayers built by the layer-by-layer (LbL) method as well as the main applications of multilayers that we focus on during this thesis.

Extended details on the origin of bacterial α -glucans and on their uses are provided in Chapter 1, section 1. This draws the main challenge of the whole “Grafting” project and, thus, the challenges and the opportunities linked to the novel of my work. Chapter 1, section 2 focuses on a general introduction to polyelectrolyte multilayers (PEM) via an explanation of the layer-by-layer principle, the important key factors linked to the formation of multilayers and a highlight on the properties of such materials. In Chapter 1, section 3, an overview of the use of bacterial α -glucans in formation of polyelectrolyte multilayers that can be found in literature up to date. A last part, Chapter 1, section 4, we investigated the common applications of multilayers. In particular, this section focuses on studies on devices based on enzymatic degradation of multilayer films.

In **Chapter 2**, we present the materials and methods via a detailed description of the materials, the preparation procedures and the characterization techniques used during this thesis.

In **Chapter 3**, an evaluation of the *adsorption capacity of functionalized bacterial α -glucans for the formation of multilayers* with different charged α -glucans systems is proposed. The screening of the capacity of dextrans sulfate (DexS), diethylaminoethyl-dextran (Dex-DEAE) and various oxidized α -glucans (Ox-Dex, Ox-Reu, Ox-Alt) to form polyelectrolyte multilayers (PEMs) is presented in Chapter 3, section 1. We study the mass adsorbed and viscoelastic behavior during LbL assembly of functionalized bacterial α -glucans with both synthetic polyelectrolytes and other α -glucans derivatives (poly(allyamine) (PAH) and diethylaminoethyl-dextran (DEAE-Dex). Based on the observations realized on those film formations, we highlighted different film growth and viscoelastic characteristics for each system. Especially, we highlight how PAH and DexS can lead to different growth behavior depending on the charge density of DexS. Thus, in Chapter 3, section 2, we proposed a detailed analysis of physico-chemical characteristics of PAH and DexS films to understand their formation. With all the information on both films, we propose tentative multilayer growth mechanisms for (PAH/DexS) multilayers according to differences observed with two differently charged dextrans sulfate.

In **Chapter 4**, once we have established which polyelectrolyte systems allow the construction of multilayers and have distinguished formation mechanisms and properties of the two types, we investigate different experimental parameters to *tune the growth type of multilayers and their surface properties*. The impact of three key factors on the film growth

and on its structural and surface properties is presented. In Chapter 4, section 1, we propose to study the impact of the charge density of anionic functionalized dextrans (dextrans sulfate, oxidized dextrans) on films and their properties. In Chapter 4, section 2, we investigate the effect of ionic strength, on LbL built-up of multilayers and on their properties depending on the type of charges/polyelectrolytes. In Chapter 4, section 3, we explain how the molar mass of polyelectrolytes affects the film formation and its properties. The understanding of the contribution of each parameter on multilayers growth would result in a possible patterning of the surface and its properties.

In **Chapter 5**, we decided to take advantage of the properties obtained for the multilayers based on functionalized α -glucans to *develop novel systems for enzymatic assays*. In Chapter 5, we investigated the concept of a colorimetric device for detection of enzymatic activity based on a three-multilayer device with an enzyme-sensitive multilayer in the middle of two functionalized α -glucans multilayers. We have designed hydride multilayer thin films that exhibit structural colors. This kit includes a thin film composed of a polymer of interest, *i.e.* a polymer that is a substrate for the enzyme we want to detect, sandwiched between two larger multilayer thin films that do not degrade. When the sandwich film degrades, all of the top layers (sandwich + top layer) are removed, causing a color change that allows detection of enzyme activity. The purpose of this design was to try to increase the sensitivity of the assay, as the sandwich layers are thinner than the films normally used to detect enzymes. The amount of degradable polymer is lower than in commonly used films, so the expected sensitivity should be higher. A prototype device from an enzyme–polyelectrolyte model: trypsin/poly-L-lysine. The efficiency of a colorimetric sensor for the detection of trypsin based on the incorporation of a poly-L-lysine in the three-multilayer structures was studied by immersion in enzyme solution.

References

- Antonini, E., Bellelli, L., Bruzzesi, M. R., Caputo, A., Chiancone, E., & Rossi-Fanelli, A. (1964). Studies on dextran and dextran derivatives. I. Properties of native dextran in different solvents. *Biopolymers*, 2(1), 27–34. <https://doi.org/10.1002/bip.1964.360020105>
- Baptista, S., & Freitas, F. (2021). Bacterial Polysaccharides: Cosmetic Applications. In J. Oliveira, H. Radhouani, & R. L. Reis (Eds.), *Polysaccharides of Microbial Origin* (pp. 1–42). Springer International Publishing. https://doi.org/10.1007/978-3-030-35734-4_45-1
- Boddohi, S., & Kipper, M. J. (2010). Engineering Nanoassemblies of Polysaccharides. *Advanced Materials*, 22(28), 2998–3016. <https://doi.org/10.1002/adma.200903790>
- Caruso, F., Niikura, K., Furlong, D. N., & Okahata, Y. (1997). 1. Ultrathin Multilayer Polyelectrolyte Films on Gold: Construction and Thickness Determination. *Langmuir*, 13(13), 3422–3426. <https://doi.org/10.1021/la960821a>
- Chludzinski, A. M., Germaine, G. R., & Schachtele, C. F. (1974). Purification and properties of dextranase from *Streptococcus mutans*. *Journal of Bacteriology*, 118(1), 1–7.
- Crouzier, T., Boudou, T., & Picart, C. (2010). Polysaccharide-based polyelectrolyte multilayers. *Current Opinion in Colloid & Interface Science*, 15(6), 417–426. <https://doi.org/10.1016/j.cocis.2010.05.007>
- de Belder, D. (1996). *Polysaccharides in Medicinal Applications*. Marcel Dekker, New York, 505–524.
- Decher, G. (1997). Fuzzy Nanoassemblies: Toward Layered Polymeric Multicomposites. *Science*, 277(5330), 1232–1237. <https://doi.org/10.1126/science.277.5330.1232>
- Decher, G., & Hong, J.-D. (1991). Buildup of ultrathin multilayer films by a self-assembly process, I consecutive adsorption of anionic and cationic bipolar amphiphiles on charged surfaces. *Makromolekulare Chemie. Macromolecular Symposia*, 46(1), 321–327. <https://doi.org/10.1002/masy.19910460145>
- Dixon, M. C. (2008). Quartz crystal microbalance with dissipation monitoring: enabling real-time characterization of biological materials and their interactions. *Journal of Biomolecular Techniques: JBT*, 19(3), 151.
- Feldötö, Z., Varga, I., & Blomberg, E. (2010). Influence of Salt and Rinsing Protocol on the Structure of PAH/PSS Polyelectrolyte Multilayers. *Langmuir*, 26(22), 17048–17057. <https://doi.org/10.1021/la102351f>
- Grimaud, F., Faucard, P., Tarquis, L., Pizzut-Serin, S., Roblin, P., Morel, S., Gall, S. L., Falourd, X., Rolland-Sabaté, A., Lourdin, D., Moulis, C., Remaud-Siméon, M., & Potocki-Veronese, G. (2018). Enzymatic synthesis of polysaccharide-based copolymers. *Green Chemistry*, 20(17), 4012–4022. <https://doi.org/10.1039/C8GC01251B>
- Hehre, E. J. (1956). Natural synthesis of low molecular weight (clinical type) dextran by a *Streptococcus* strain. *Journal of Biological Chemistry*, 222(2), 739–750.
- Heinze, T., Liebert, T., Heublein, B., & Hornig, S. (2006). Functional Polymers Based on Dextran. In D. Klemm (Ed.), *Polysaccharides II* (Vol. 205, pp. 199–291). Springer Berlin Heidelberg. https://doi.org/10.1007/12_100
- Höök, F., Kasemo, B., Nylander, T., Fant, C., Sott, K., & Elwing, H. (2001). Variations in Coupled Water, Viscoelastic Properties, and Film Thickness of a Mefp-1 Protein Film during Adsorption and Cross-Linking: A Quartz Crystal Microbalance with Dissipation Monitoring, Ellipsometry, and Surface Plasmon Resonance Study. *Analytical Chemistry*, 73(24), 5796–5804. <https://doi.org/10.1021/ac0106501>
- Liu, J., Willför, S., & Xu, C. (2015). A review of bioactive plant polysaccharides: Biological activities, functionalization, and biomedical applications. *Bioactive Carbohydrates and Dietary Fibre*, 5(1), 31–61. <https://doi.org/10.1016/j.bcdf.2014.12.001>
- Mauzac, M., & Jozefonvicz, J. (1984). Anticoagulant activity of dextran derivatives. Part I: Synthesis and characterization. *Biomaterials*, 5(5), 301–304. [https://doi.org/10.1016/0142-9612\(84\)90078-4](https://doi.org/10.1016/0142-9612(84)90078-4)
- Naessens, M., Cerdobbel, A., Soetaert, W., & Vandamme, E. J. (2005). *Leuconostoc* dextranase and dextran: production, properties and applications. *Journal of Chemical Technology & Biotechnology*, 80(8), 845–860. <https://doi.org/10.1002/jctb.1322>
- Notley, S. M., Eriksson, M., & Wågberg, L. (2005). Visco-elastic and adhesive properties of adsorbed polyelectrolyte multilayers determined in situ with QCM-D and AFM measurements. *Journal of Colloid and Interface Science*, 292(1), 29–37. <https://doi.org/10.1016/j.jcis.2005.05.057>
- Rinaudo, M. (2008). Main properties and current applications of some polysaccharides as biomaterials. *Polymer International*, 57(3), 397–430. <https://doi.org/10.1002/pi.2378>
- Rogovin, Z. A., Vernik, A. D., Khomiakov, K. P., Laletina, O. P., & Penenzhik, M. A. (1972). Study of the Synthesis of Dextran Derivatives. *Journal of Macromolecular Science: Part A - Chemistry*, 6(3), 569–593. <https://doi.org/10.1080/10601327208056860>
- Serizawa, T., Yamaguchi, M., Matsuyama, T., & Akashi, M. (2000). Alternating bioactivity of polymeric layer-by-layer assemblies: Anti- vs procoagulation of human blood on chitosan and dextran sulfate layers. *Biomacromolecules*, 1(3), 306–309. <https://doi.org/10.1021/bm000006g>

Chapter 1

Literature review

Table of content

Introduction	15
1. α-glucans and derivatives	17
<u>1.1. Bacterial α-glucans: sugar sources to bacterial polymers.....</u>	<u>17</u>
<i>1.1.1. Polysaccharides and α-glucans.....</i>	<i>17</i>
<i>1.1.2. α-glucans from bacterial origin: sugar fermentation to polymers.....</i>	<i>19</i>
<u>1.2. Dextrans and dextran derivatives</u>	<u>21</u>
<i>1.2.1. Structure and properties in solution.....</i>	<i>21</i>
<i>1.2.2. Functionalization routes of dextrans.....</i>	<i>22</i>
<i>1.2.3. Applications of dextrans and their derivatives.....</i>	<i>24</i>
2. Introduction to Polyelectrolytes Multilayers (PEMs)	27
<u>2.1. Layer-by-layer assembly</u>	<u>27</u>
<i>2.1.1. Introduction to the principle of layer-by-layer (LbL) assembly.....</i>	<i>27</i>
<i>2.1.2. Deposition methods</i>	<i>28</i>
<u>2.2. Formation of polyelectrolyte multilayers</u>	<u>31</u>
<i>2.2.1. Driving forces.....</i>	<i>31</i>
<i>2.2.2. Linear growth regime vs Exponential growth.....</i>	<i>32</i>
<u>2.3. Tailoring properties of polyelectrolyte films.....</u>	<u>35</u>
<i>2.3.1. Main properties of polyelectrolyte multilayers</i>	<i>35</i>
<i>2.3.2. Factors controlling multilayers build-up</i>	<i>38</i>
3. Functionalized bacterial α-glucans for elaboration of multilayer materials	44
<u>3.1. Dextran sulfates-based polyelectrolyte multilayers.....</u>	<u>44</u>
<i>3.1.1. Dextran sulfates and chitosan multilayered films</i>	<i>44</i>
<i>3.1.2. Dextran sulfates and polyelectrolyte-based multilayered films.....</i>	<i>47</i>
<u>3.2. Dextran sulfates and proteins multilayered films</u>	<u>49</u>

3.3. Other α -glucans derivatives in multilayered films	50
4. Applications of multilayers: overview, specific applications for the thesis.....	52
<u>4.1. Main applications of polyelectrolyte multilayers: biomedical, environment.....</u>	<u>52</u>
4.1.1. <i>Biomedical applications</i>	52
4.1.2. <i>Environmental applications</i>	56
<u>4.2. Colorimetric devices for enzyme detection.....</u>	<u>58</u>
4.2.1. <i>Structural colors of multilayer films</i>	58
4.2.2. <i>Enzyme-sensitive multilayers</i>	60
Conclusion.....	64
References	66

This chapter on literature is adapted from the review:

Delvart, A., Moreau, C., & Cathala, B. (2022). Dextrans and dextran derivatives as polyelectrolytes in layer-by-layer processing materials – A review. Carbohydrate Polymers, 293, 119700. <https://doi.org/10.1016/j.carbpol.2022.119700>

Introduction

The development of alternative materials and systems based on natural polymers is currently a challenge, yet it is one of the key issues in materials chemistry and nanotechnology mainly due to current environmental concerns. The scientific community has focused on polysaccharides due to their biocompatibility, biodegradability and low toxicity (de Belder, 1996; Hernández-Rivas et al., 2020; J. Liu et al., 2015; Rinaudo, 2008). Polysaccharides are a large family of polymers, obtained from biomass (animals, plants, bacteria, algae, and fungi), with diverse structures and functionalities. They exhibit a wide variety of structures resulting from the absolute configuration of the asymmetric carbons, the stereochemistry of the bonds as well as the branching pattern of the polymers which differ according to their type and source (J. Liu et al., 2015). Thus, they have been widely studied and used for their functional properties in the pharmaceutical industry, cosmetic formulation, paper industry, food industry, petroleum extraction and many other application fields (J. Liu et al., 2015).

Among all polysaccharides, α -glucans are polymers naturally produced by microorganisms, including dextrans which are the most widely used bacterial α -glucans in many fields, both in industry and research (Mehvar, 2000; Naessens et al., 2005; Yalpani & Hedman, 1985). The dextran family are D-glucose polysaccharides with a large majority of α -(1 \rightarrow 6) glycosidic linkages whose structures are production dependent due to the origin of the glucose and the bacteria involved (Taylor et al., 1985). These bacterial polysaccharides are of great interest to the scientific community and have many applications in various fields, especially in the development of bio-based materials: their wide availability, diverse structures, different branching patterns, "clean" production, as well as the possibility of functionalization with a great variety of active groups or sites. Charged dextrans, in particular, have been studied as potential alternatives to many synthetic polyelectrolytes in the

elaboration of nanomaterials such as thin films and coatings, capsules, nanoparticles, etc. The presence of chemical groups on their polymer chain promotes the formation of electrostatic interactions and facilitates their inclusion with other charged compounds. Pioneering research on the integration of polysaccharides into multilayer films, using well-known methods such as the layer-by-layer (LbL) method, began in the mid-1990s (Lvov et al., 1998). The specific integration of dextrans into these thin films, started in the early 2000s and their applications have been gradually developing since then (Hartley et al., 2002; Serizawa et al., 2000).

Polyelectrolyte films have become an indispensable way to functionalize surfaces and create ordered nanostructures, which have found diverse applications from biomedical devices to the environmental field (Boudou et al., 2010; Gribova et al., 2012; Jaber & Schlenoff, 2006; Joseph et al., 2014). The commonly used principle for polyelectrolyte multilayers is the formation of an LbL film based on the alternating adsorption of polyanions (PA) and polycations (PC) from aqueous solutions, which was first studied by Decher and Hong in the late 1980s. Revised by Decher *et al.* in the early 1990s, the first generation of research extended the method to polyelectrolyte films with various materials as well as characterization of the films (Ariga et al., 1997; Decher, 1997; Decher & Hong, 1991b; Lvov et al., 1995). The construction of a polyelectrolyte film relies primarily on electrostatic interactions between charged polymers and is highly dependent on the charge balance of the polyelectrolytes and the experimental conditions (Schoeler et al., 2002; Voigt et al., 2002). Indeed, the properties of the films can be controlled by modulating the deposition conditions (deposition time, temperature, etc.), the characteristics of the polyelectrolytes (charge density, molecular weight, etc.) and the polyelectrolyte solution parameters (concentration, pH, ionic strength, etc.) (Dubas & Schlenoff, 1999; Guzmán et al., 2020). Over the last two decades, the interest of the research community in bio-sourced alternatives for the assembly of LbLs from charged polypeptides and polysaccharides, including dextran derivatives, has significantly increased (Crouzier et al., 2010; Elbert et al., 1999; Picart et al., 2001, 2002).

1. α -glucans and derivatives

1.1. Bacterial α -glucans: sugar sources to bacterial polymers

1.1.1. Polysaccharides and α -glucans

Polysaccharides are a large family of polymers, derived from biomass (including microalgae), animal, bacterial, and fungal, with diverse structures and functionalities. They have been widely studied and used for their functional properties in the pharmaceutical, cosmetic, paper industry, food industry, and in oil extraction (Q. Li et al., 2020; J. Liu et al., 2015; Srivastava et al., 2021). More recently, the scientific community has begun to focus on polysaccharides for new applications due to their biocompatibility, biodegradability, and nontoxicity, especially in the biomedical field. From a chemical point of view, polysaccharides are polymers of high molar mass of the carbohydrate family and consist of monosaccharides, which are linked together by O-glycosidic bonds. The structure of these polymers can be very varied and complex. In particular, there are homopolysaccharides, composed of a single monosaccharide, and heteropolysaccharides, composed of several oses. Polysaccharides can also be linear or branched and have one or more functional groups. Among this group of polysaccharides, we distinguish the glucans or polyglucans, polysaccharides containing glucose units, which are the most abundant in terrestrial biomass (Heinze et al., 2006). They present a wide variety of structures resulting from the absolute configuration of the asymmetric carbons, the stereochemistry of the glycosidic bond as well as the branching pattern of the polymers. In particular, we differentiate between L-(-)-glucose or D-(+)-glucose based glucans, the two enantiomers of glucose but also β -glucans and α -glucans, the glycosidic bonds of the former being in the equatorial position while those of the α -glucans are in the axial position as represented in Figure 1. Thus, glucans are classified according to their structure into three major groups, *i.e.* α -D-glucans, β -D-glucans and mixed α , β -D-glucans.

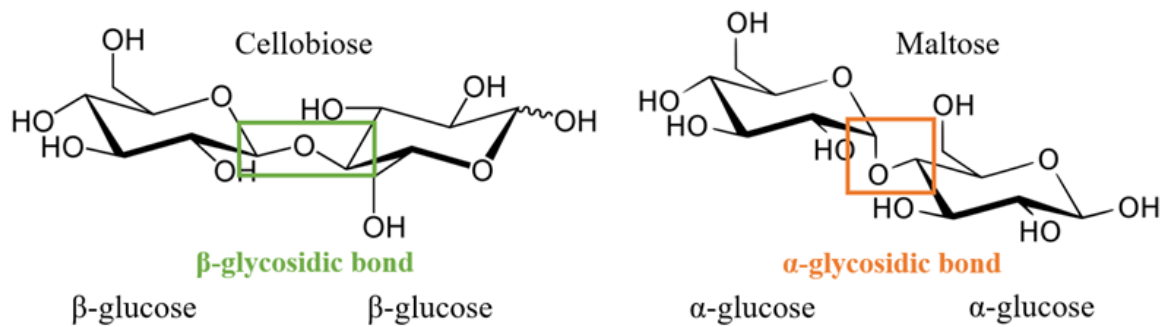


Figure 1.1. Structures of cellobiose and maltose illustrating the different geometries of glycosidic bonds in polysaccharides: β -glycosidic bond (cellobiose on the left) and α -glycosidic bond (maltose on the right).

α -D-glucans can be synthesized by a variety of natural sources from bacteria, fungi, plants, algae, lichens, insects to mammals. Their function also differs depending on the source and their structures but also their structural characteristics such as linkage pattern and branching as presented on Figure 1.2. When α -D-(1 \rightarrow 4) glucans function mainly as an energy source (starch in plant, amylose and glycogen in fungi, glycogen in animals and bacteria), α -D-(1 \rightarrow 3) glucans mainly exist as a cell wall element in fungi and as an exopolysaccharide in bacteria.

Among this set of polyglucans, one type stands out: the α -D-glucans produced naturally by bacterial activity. This is a family of polysaccharides whose main chain is made up of D-glucose units linked by α -(1 \rightarrow 6) glycosidic bonds of varying size and with different branching depending on the bacteria involved in production (Taylor et al., 1985). Thus, several other families of α -glucans of bacterial origin exist: dextrans, alternans, mutans and reuterans. Among them, the most used bacterial polysaccharides are dextrans that are commonly used in food or cosmetic formulations, in chemistry, in the health field or as probiotics (Heinze et al., 2006; Mehvar, 2000; Naessens et al., 2005; Reddy Shetty et al., 2021; Yalpani & Hedman, 1985).

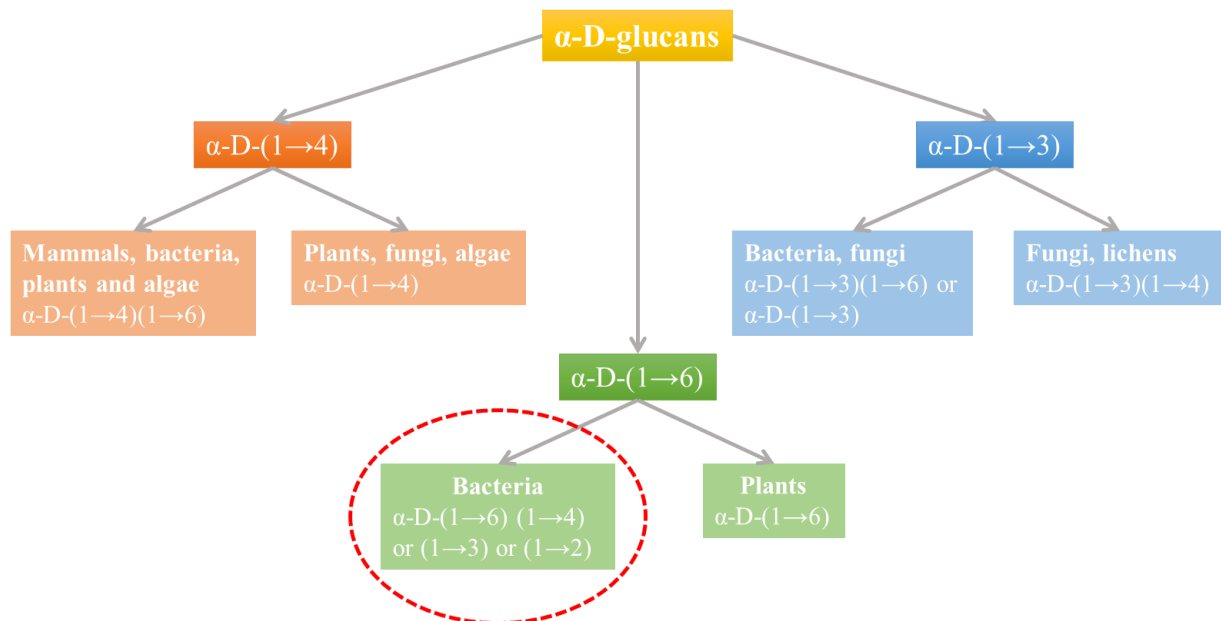


Figure 1.2. Classification of α -D-glucans by their typical main structures (α -D-(1 \rightarrow 4), α -D-(1 \rightarrow 6), α -D-(1 \rightarrow 3)) that are depending on their origins (mammals, bacteria, plants, algae, fungi and lichens). Families concerned by this work, bacterial α -D-glucans, are highlighted in red.

1.1.2. α -glucans from bacterial origin: sugar fermentation to polymers

First studies on α -glucans are in fact linked to the discovery of the natural production of dextrans by sugar fermentation. The primary reports of dextran focused on the studies of "viscous fermentation" by early chemists when the understanding of fermentative mechanisms was not related to microorganisms yet (Braconnot, 1813). Later on, observations on "viscous fermentation" (dextrans) were done in the 1800s by Desfosses who explained that sugar was able to form a viscous material with carbonic acid and hydrogen emissions. Further analysis suggested that "sugar water" contained a material able to transform sugar into a viscous substance without any gas emission (Desfosses, 1829). A few years later, Gay-Lussac and Pelouze discovered that mannite and lactic acid compounds were the result of viscous fermentation of sugar beet juice (Gay-Lussac & Pelouze, 1833). In 1861, Pasteur had found that slimes on fermented food with plant origins were caused by microbial action that he reported as "viscous fermentation" or "alcoholic fermentation" (Pasteur, 1861). The term "dextran" was first used to name the segregated carbohydrate found in aging sugar juices in 1874 by Scheibler, who demonstrated that dextran was a carbohydrate with the formula $(C_6H_{10}O_6)_n$ and with a positive optical rotation (Scheibler, 1874). Back in 1878, Van Tieghem named the bacterium responsible, for that mysterious thickening gum that he called "gomme

de sucrerie”, *Leuconostoc mesenteroides* (Van Tieghem, 1878). Later studies have shown that this family of α -D-glucans can be produced from sucrose by several bacterial strains, mostly gram-positive cocci, including *Leuconostoc*, *Gluconobacter*, *Streptococcus* and *Lactobacillus* strains (Chludzinski et al., 1974; Hehre, 1956; Jeanes et al., 1954).

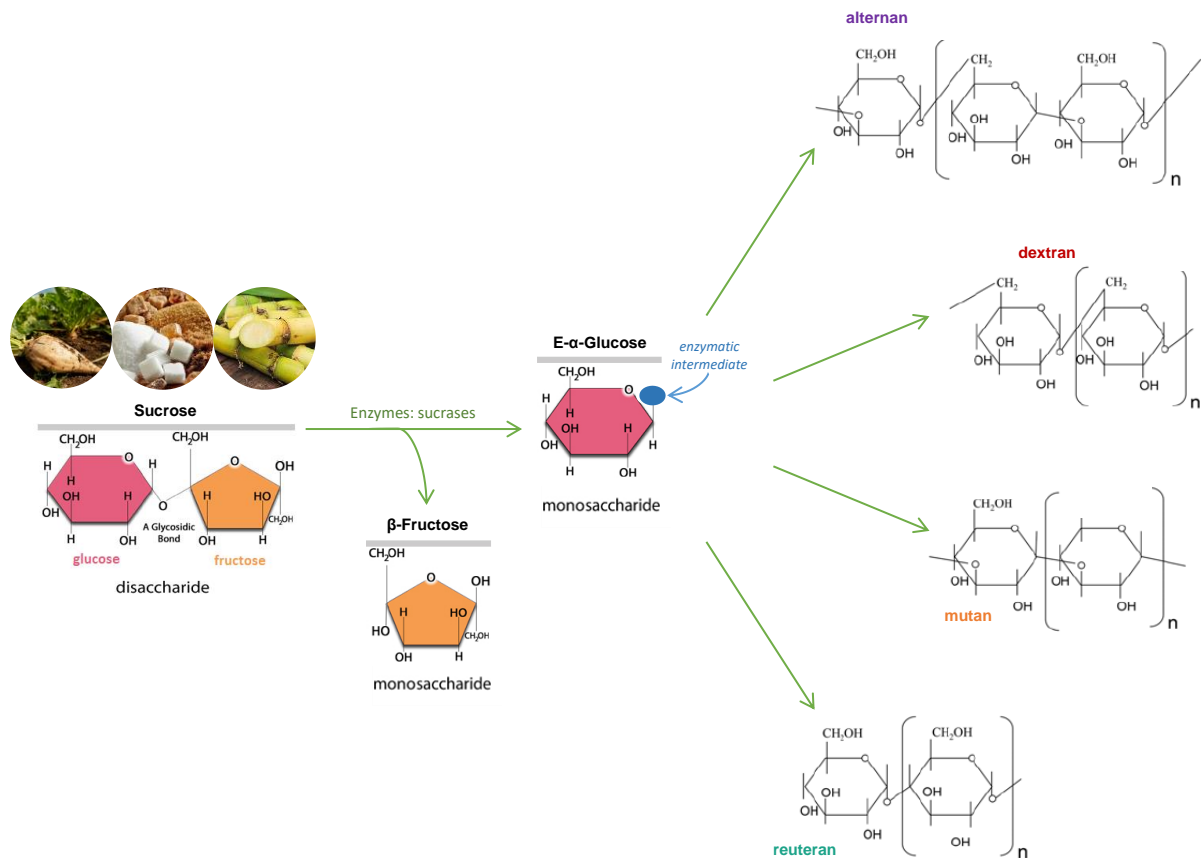


Figure 1.3. Illustration of the classical enzymatic production of α -glucans by the action of sucrases onto sucrose.

In general, bacterial extracellular enzymes, sucrases, can commonly form bacterial α -D-glucans including alternan, dextran mutan and reuteran with their action on sucrose as illustrated of Figure 1.3. Literature reports showed that α -D-glucans such as dextran, mutan, alternan and reuteran can be produced by action of different mesophilic and thermophilic bacteria on sucrose as presented on Table 1.1. The structures of α -D-glucans differ mainly by their α -glycosidic linkages and the arrangement of glucose units in the chain by presenting linear and/or more or less branched parts. Depending of their bacterial sources, the position, the quantity as well as the linkage involved in the side chains of the α -D-glucans structures can vary.

Table 1.1. Source and structure of different bacterial α -D-glucans, adapted from (Reddy Shetty et al., 2021).

Bacterial species	Name	Type of α -linkages	References
<i>Lactobacillus species</i> <i>Leuconostoc mesenteroides</i> <i>Leuconostoc dextranicum</i> <i>Streptococcus mutans</i> <i>Weissella species</i>	Dextran	Linear chain of (1 \rightarrow 6) with side chains of (1 \rightarrow 3), (1 \rightarrow 4) and/or (1 \rightarrow 2)	(Monsan et al., 2001; Naessens et al., 2005)
<i>Lactobacillus reuteri</i> <i>Streptococcus mutans</i> <i>Streptococcus salivarius</i> <i>Streptococcus sownei</i>	Mutan	Linear chain of (1 \rightarrow 3) with side chains of (1 \rightarrow 6)	(Monsan et al., 2001; Torino et al., 2015)
<i>Leuconostoc mesenteroides</i> <i>Streptococcus salivarius</i>	Alternan	Alternating (1 \rightarrow 3) and (1 \rightarrow 6) with side chains of (1 \rightarrow 3)	(Monsan et al., 2001; Torino et al., 2015)
<i>Lactobacillus reuteri</i>	Reuteran	Linear chain of (1 \rightarrow 4) (major) and (1 \rightarrow 6) (minor)	(Kralj et al., 2005)
<i>Mycobacterium tuberculosis</i>		Linear chain of (1 \rightarrow 4)	(Lemassu et al., 1996; Ortalo-Magne et al., 1995)
<i>Streptomyces venezuelae</i>		Linear chain of (1 \rightarrow 4)	(Miah et al., 2016)

1.2. Dextrans and dextran derivatives

1.2.1. Structure and properties in solution

Dextrans are a family of neutral polysaccharides, synthesized from sucrose and dextranase, whose main chain consists of D-glucose units, as illustrated in Figure 4. The structure of these α -glucans is highly dependent on the bacterial strains from which they are produced, leading to dextrans of various sizes and substitution patterns (Díaz-Montes, 2021). Dextran is a glucose homopolymer with a number of consecutive α -(1 \rightarrow 6) linkages in the main chain that can vary from 50 to 97% of the total glycosidic linkages (Leathers, 2002). The side chains of the D-glucose units occur as α -(1 \rightarrow 3), α -(1 \rightarrow 4), and α -(1 \rightarrow 2) linkages as shown in Figure 1.4. The production of dextran determines the density of the branches and their nature on the polymer backbone as well as its molecular weight (Hehre, 1956; Ruckel & Schuerch, 1967). Dextrans exhibit a wide range of average molecular weights (Mw) (10^5 to 10^8 g.mol⁻¹) with different polydispersity (Mw/Mn = 1 – 25) that tends to increase with the degree of branching (Antonini et al., 1964; Bovey, 1959; Confer & Logan, 1997; Ioan et al., 2000).

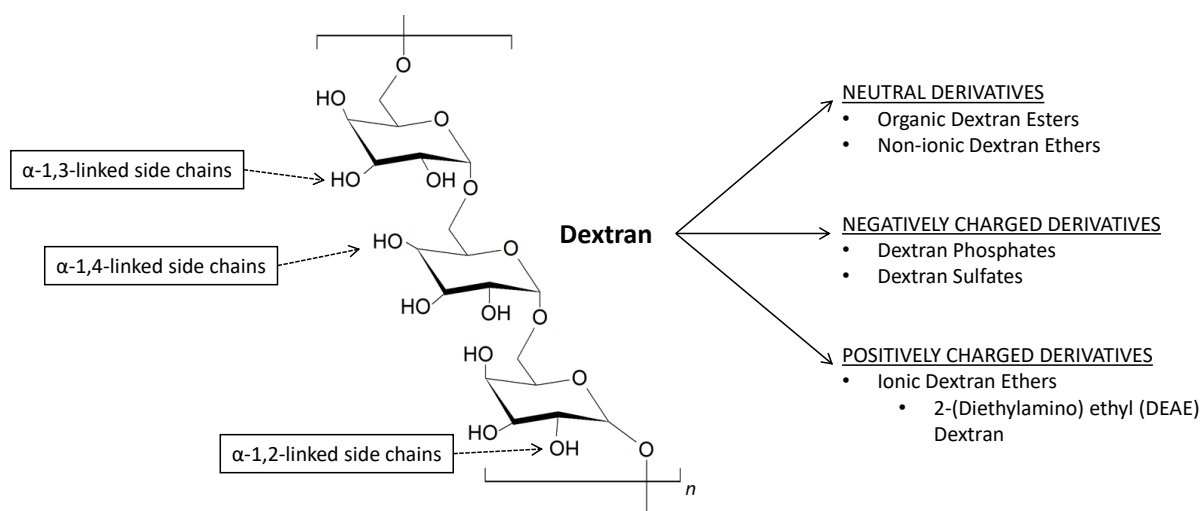


Figure 1.4. General structure of dextrans with a D-glucose main chain linked by α -(1 \rightarrow 6) glycosidic bonds and branches based on α -(1 \rightarrow 3), α -(1 \rightarrow 4) and α -(1 \rightarrow 2) bonds and main derivatives obtained by chemical functionalization of dextrans.

The high content of α -(1 \rightarrow 6) linkages leads to significant chain mobility because the presence of α -(1 \rightarrow 6) linkages between sugar rings provides a considerably wider range of accessible relative orientations of successive sugar rings in the dextrans chain (Burton & Brant, 1983; Kadkhodaei et al., 1991). Because of this chain flexibility and the presence of hydroxyl groups, dextrans exhibit good solubility in water and most polar solvents, including organic and alcoholic solvents (Heinze et al., 2006; Leathers, 2002; Masuelli, 2013). Most dextrans demonstrate that increasing the concentration of the polymer impacts the viscosity of the solution that allows hydrogel formation (McCurdy et al., 1994).

1.2.2. Functionalization routes of dextrans

Due to the occurrence of hydroxyl groups on the surface of dextrans main chain and branches, the polymer promotes a large possibility of functionalization to a large variety of neutral and charged dextran derivatives as indicated on Figure 1.4 and summarized in Table 1.2 (Ahmad et al., 2015; Heinze et al., 2006; Lindenbaum et al., 1977). The two major chemical modifications are esters of dextrans and ethers of dextrans that allow to obtain both neutral and charged dextran derivatives as reported on Table 2 (Heinze et al., 2006; R. Li et al., 2017).

Table 1.2. Summary of the most frequently used reactions and modifications for the obtention of dextran derivatives summarized from (Heinze et al., 2006).

Reaction	Group of modifications	Name / type of dextran	References
Esterification	Inorganic Esters of Dextran	Dextran Phosphate	(Sato et al., 2004; Suzuki et al., 1977)
		Dextran sulfuric Acid Half esters (Dextran Sulfate)	(Mauzac & Jozefonvicz, 1984; Papy-Garcia et al., 2005)
	Organic Esters of Dextran	Unsaturated Dextran Ether	(S. H. Kim et al., 1999; Sánchez-Chaves et al., 1989)
		Dextran Esters with Bioactive Moieties	(Larsen, 1989; Mehvar, 2000)
Etherification	Non-ionic dextran Ethers	Alkyl Dextran	(Larm et al., 1971; R. Zhang et al., 2005)
		Hydroxyalkyl and Hydroxyalkyl Aryl Ethers of Dextran	(Imbert et al., 2002; Rotureau et al., 2004)
		Poly(Ethylene Glycol)-Alkyl Dextran Ether	(Francis et al., 2004, 2006)
	Ionic Dextran Ethers	Anionic Amphiphilic Dextran Ether	(Covis et al., 2013; Rotureau et al., 2007)
		Carboxymethyl Dextran	(Huynh et al., 1998; Khalil et al., 1990)
		2-(Diethylamino)ethyl (DEAE) Dextran	(Gubenšek & Lapanje, 1968; Nichifor et al., 2004)

Neutral dextrans include both organic esters of dextrans and non-ionic ethers. Organic esters of dextrans demonstrate a larger interest as they are used for the coupling with bioactive compounds and for the binding of unsaturated moieties. Among the etherification reactions, about twenty of them are considered as the most frequently used for dextrans modifications and lead to both neutral and charged dextrans (Heinze et al., 2006; Rogovin et al., 1972). Out of the inorganic esters of dextran, mainly negatively charged dextrans, only dextran sulfates (dextran sulfuric acid half esters) and dextran phosphates present a notable interest as they lead to polyelectrolytes presenting interesting biological activity and properties (Bamford et al., 1986; Kagimura et al., 2015; R. Li et al., 2017; Mei et al., 2015). In fact, dextran sulfates have shown anti-inflammatory properties in several studies, anticoagulant capacity as well as anti-viral activity for a few viruses (de Raucourt et al., 1998; Hall & Ricketts, 1952; Jing et al., 2016; Mauzac & Jozefonvicz, 1984; Mitsuya et al., 1988). The introduction of ether-type groups in dextrans structure often results in stable positively charged dextran derivatives such as 2-(diethylamino) ethyl (DEAE) dextrans, with new biological properties such as immunological properties and new physico-chemical properties such as complexing or adhesives properties (Naessens et al., 2005). Even though chemical modifications remained

major, other types of functionalization including cross-linking and grafting are also included in the current interest to form dextran derivatives (Heinze et al., 2006; R. Li et al., 2017).

1.2.3. Applications of dextrans and their derivatives

There is a significant literature on the various uses of dextrans from bacterial origins and their derivatives for medical and industrial applications as summarized on Figure 1.5.

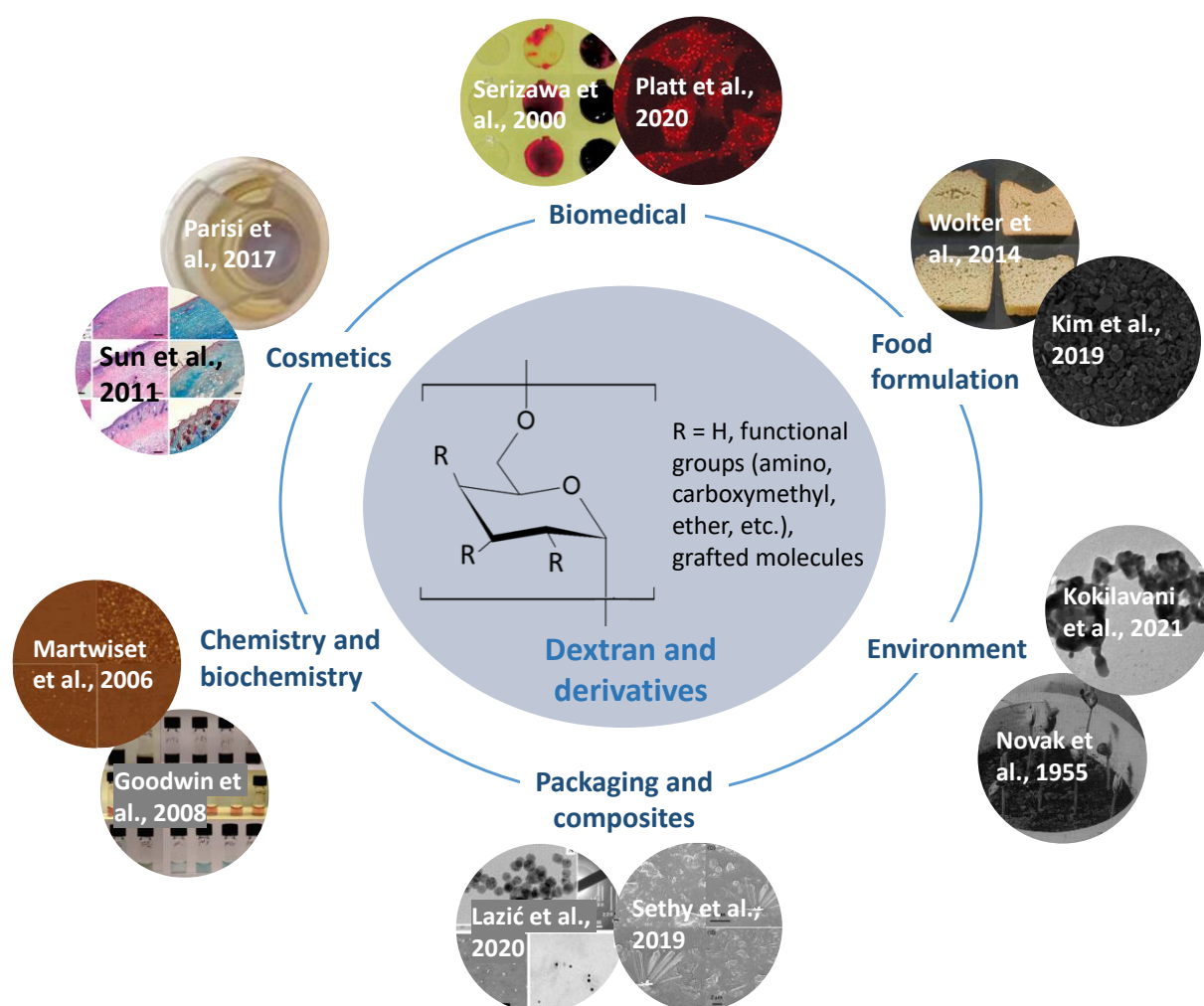


Figure 1.5. Overview of the most important applications of dextrans and their derivatives in industries. Adapted with permission from (Goodwin et al., 2009), © 2009 American Chemical Society. Adapted with permission from (Martwiset et al., 2006), © 2006 American Chemical Society. Adapted with permission from (Novak et al., 1955), © 1955 American Chemical Society. Adapted with permission from (Serizawa et al., 2000), © 2000 American Chemical Society. Adapted from (W.-S. Kim et al., 2019; Kokilavani et al., 2021; Lazić et al., 2020; Wolter et al., 2014), with permission from Elsevier. Adapted from (Parisi et al., 2017; Platt et al., 2010; Sethy et al., 2020; G. Sun et al., 2011).

Dextrans and dextran derivatives have been widely used for years in the biomedical field, as dextrans are physiologically harmless biopolymers. Unlike high molecular weight native dextrans, dextrans with low molecular weight (40 000 – 100 000 g.mol⁻¹) are suitable as therapeutic agents in restoring moderate blood volume (Robyt, 1985). The retention of low molecular weight dextrans in plasma is high enough to lead to a volume expansion without causing clogging. In addition, they help to improve blood flow by reducing blood viscosity and inhibiting erythrocyte aggregation (de Belder, 1996). However, sulfate esters of dextrans are mostly used for their anticoagulant properties, similar to the ones of heparin ; by forming complexes with several proteins, dextran sulfates avoid clotting mechanism of blood (de Raucourt et al., 1998; Hall & Ricketts, 1952; Mauzac & Jozefonvicz, 1984; Serizawa et al., 2000). Studies also highlight the use of dextran sulfates as antiviral drugs, laboratory tests showing the possibility of dextrans as anti-HIV (human immunodeficiency virus) agents as well as anti-viral against several other viruses (Mitsuya et al., 1988; Platt et al., 2010).

Beside the medical field, the variety of structures and functionalities found in dextrans and dextran derivatives presents a great interest in numerous industrial domains, mainly in cosmetics formulation and in food formulation. The occurrence of hydroxyl groups and high molecular weights of native dextrans is a source of hydrogen bonds for the formulation of viscous solutions and hydrogels, that are suitable as emulsifiers and as thickening agents (Leemhuis et al., 2013; McCurdy et al., 1994). Dextrans and dextran derivatives present a great biocompatibility, moistening properties and excellent solubility, which make them great candidates for the formulation of skin-care products in several cases such as skin regeneration (G. Sun et al., 2011). In 2017, Parisi *et al.* also highlighted the potential of dextran derivatives as polymeric antioxidants for skin whitening (Parisi et al., 2017).

Moreover, they are often used in the preparation of baked products to improve baking properties and sensory profiles (Lacaze et al., 2007). For instance, dextrans can be used to improve softness, crumb texture and loaf volume in the formulation of gluten-free and wheat breads (Wolter et al., 2014). Dextrans can also find applications as additives to give improved rheological (gelling, thickening) or physico-chemical (emulsion stabilization, particle suspension, etc.) properties in several industrial products (Kothari et al., 2014). Recently, more and more studies used dextrans for the elaboration of functional foods such as probiotics, that can provide health benefits and protection against risk of several diseases (W.-S. Kim et al., 2019). Since α -(1→6) linkages and α -(1→2) linkages are known to be resistant

to human intestinal enzymes, the digestion of dextrans is relatively slow yielding prebiotic activity (Olano-Martin et al., 2000).

Dextran derivatives have potential for the conception of functional materials with great biocompatibility and degradability in the fields of chemistry and biochemistry as they provide a large range of charged or neutral biomacromolecules with different types of substituents, degrees of substitution and molecular weights (Naessens et al., 2005). For example, it was shown that amphiphilic dextrans form stable layers onto surfaces that improve *in vivo* imaging and encapsulation yield (Goodwin et al., 2009). Another study highlighted how grafted dextrans and oxidized dextrans on silicon wafer lead to non-fouling surfaces that can be valorized in the elaboration of biomaterials (Martwiset et al., 2006).

In the environmental applications, charged dextran derivatives are used for separation and detection of particles, soil conditioners, explosives, oil drilling muds, recovery of petroleum or high-viscosity gums. Ionic dextran derivatives have shown potential of flocculants for cleaning of wastewater, as they presented high efficacy for removal of both inorganic and organic particles (Ghimici et al., 2009; Ghimici & Nichifor, 2018). More recently, Kokilavani *et al.* proposed multifunctional materials based on Cu–Ag nanocomposites stabilized with dextrans for selective and sensitive detection of mercury (Kokilavani et al., 2021). Authors also highlighted that this dextran-based nanocomposite presents efficient photocatalytic and anti-microbial behavior. Dextrans and dextran derivatives also found uses in agriculture as, in the late 1900s, studies proved that inclusion of certain dextrans affects several aspects of soils. Depending on dextran structure, increasing wet-sieve stability of soils studied, percent seedling emergence, rate of plant growth and crop yield for plant used were observed (Novak et al., 1955).

Among packaging applications, dextrans and derivatives can be employed in different ways, such as coating for improving compatibility of particles or performance in food packaging as suggested by Lazić *et al.* (Lazić et al., 2020). In this study, dextran used as coating on silver nanoparticles helped to improve barrier properties, *i.e.* oxygen permeability and anti-microbial activity of nanocellulose films. Dextran-composites are also widely studied for the elaboration of biocompatible and eco-friendly packaging materials. Sethy *et al.* proposed matrix of dextran-grafted poly(acrylic acid) hybrid nanocomposites and nano-CaCO₃ filler to design materials with oxygen barrier, thermal, and antimicrobial properties (Sethy et al., 2020).

2. Introduction to Polyelectrolytes Multilayers (PEMs)

2.1. Layer-by-layer assembly

2.1.1. Introduction to the principle of layer-by-layer (LbL) assembly

In current technologies, nanostructures and nanomaterials found an important place in the development of ultra-small devices and are mainly prepared by top-down fabrication techniques (Baig et al., 2021; L. Cheng et al., 2020; Khin et al., 2012; Moon et al., 2011; Pomerantseva et al., 2019; Roduner, 2006; X. Wang et al., 2021). However, due to physical limitations of those techniques, bottom-up techniques are presently gaining in interest and micro- or nano- materials based on self-assembly approaches are becoming more and more present in nanotechnologies (Abid et al., 2022; Lombardo et al., 2020). These methods have great potential in all fields of research: biomedical (Deng et al., 2010), paper industry (T. Wu & Farnood, 2014), functional materials (Damasceno Borges et al., 2018), composites (Sher et al., 2010), cosmetics (Yoo et al., 2016), food (Treviño-Garza et al., 2017), electronics (de Oliveira Farias et al., 2015) or even the environment (Ma et al., 2011). Among bottom-up approaches, the LbL method is a way to build complex self-assemblies from charged molecules/nanoparticles with controlled architectures.

Introduced by Iler in 1966, the LbL method was firstly applied to the alternate deposition of oppositely charged colloidal particles for the electrostatic self-assembly of multilayers (Iler, 1966). In 1991-1992, Decher's group revised for the first time the principle of manufacturing polyelectrolyte multilayers on a solid substrate as illustrated by Figure 1.6 (Decher et al., 1992; Decher & Hong, 1991a, 1991b). The formation of LbL films onto a substrate is based on the alternate immersion of the substrate in oppositely charged polymer solutions. In those studies, the authors presented a simple method to achieve "soft" multilayered films with controlled architectures by adsorption of polyelectrolytes (Decher, 1997). The advantages of the LbL assembly techniques include its simplicity, its versatility but also the control of the film architecture (thickness, mass, porosity, etc.). The properties of the system are governed to the greatest extent by the choice of the polyelectrolytes pair. Since the Decher group's works, LbL assemblies are traditionally produced by dipping deposition, *i.e.* immersive LbL assembly (Decher et al., 1992; Decher & Hong, 1991a, 1991b; Lvov et al., 1994, 1998).

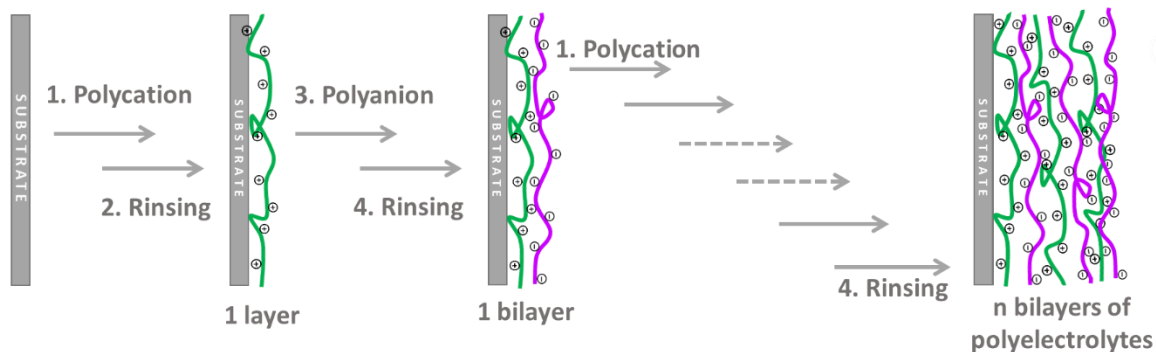


Figure 1.6. Schematic representation of the different steps in the preparation of polyelectrolyte multilayers (PEMs) by the layer-by-layer (LbL) method.

The dipping or immersion deposition method is presented in Figure 1.6 and in Figure 1.7(A). To form the multilayer, the substrate is immersed in the first polyelectrolyte (polycation or polyanion) solution (Decher & Hong, 1991b). During the immersion, the polymer is adsorbed onto the surface due to favorable interactions between the polyelectrolyte and the substrate. After adsorption, an intermediate rinsing step allows to wash off the excess of polyelectrolyte and remove the loosely bound material leading to the formation of a layer. The immersion step is repeated with the opposite charged polymer to form a bilayer; the substrate is immersed in the solution for adsorption and then rinsed. Afterward, the process is repeated x times until a multilayer with n bilayers, composed of two layers of polyelectrolytes with opposite charges, is obtained. As illustrated in Figure 1.6, a polycation (PC) is absorbed on the substrate then rinsed, leading to a positively charged surface. Then, a polyanion (PA) is absorbed onto it and rinsed, leading to a negatively charged surface. Each adsorption step allows a charge inversion at the surface and the adsorption of the oppositely charged polyelectrolyte that allow the growth of the next layer.

2.1.2. Deposition methods

In order to produce multilayers, several methods can be used depending on the materials to be assembled, the conditions required for the deposition as well as the nature of the substrate. The main methods to build multilayers based on polycation (PC) and polyanion (PA) are summarized in Figure 1.7: dipping, *i.e.* immersion deposition, spray deposition, centrifugal deposition, *i.e.* spin-assisted deposition, electrodeposition, *i.e.* electromagnetic deposition and microfluidic deposition (Guzmán et al., 2020; Petrila et al., 2021; Richardson

et al., 2015). The dipping, *i.e.* immersion deposition method, is presented in the previous section.

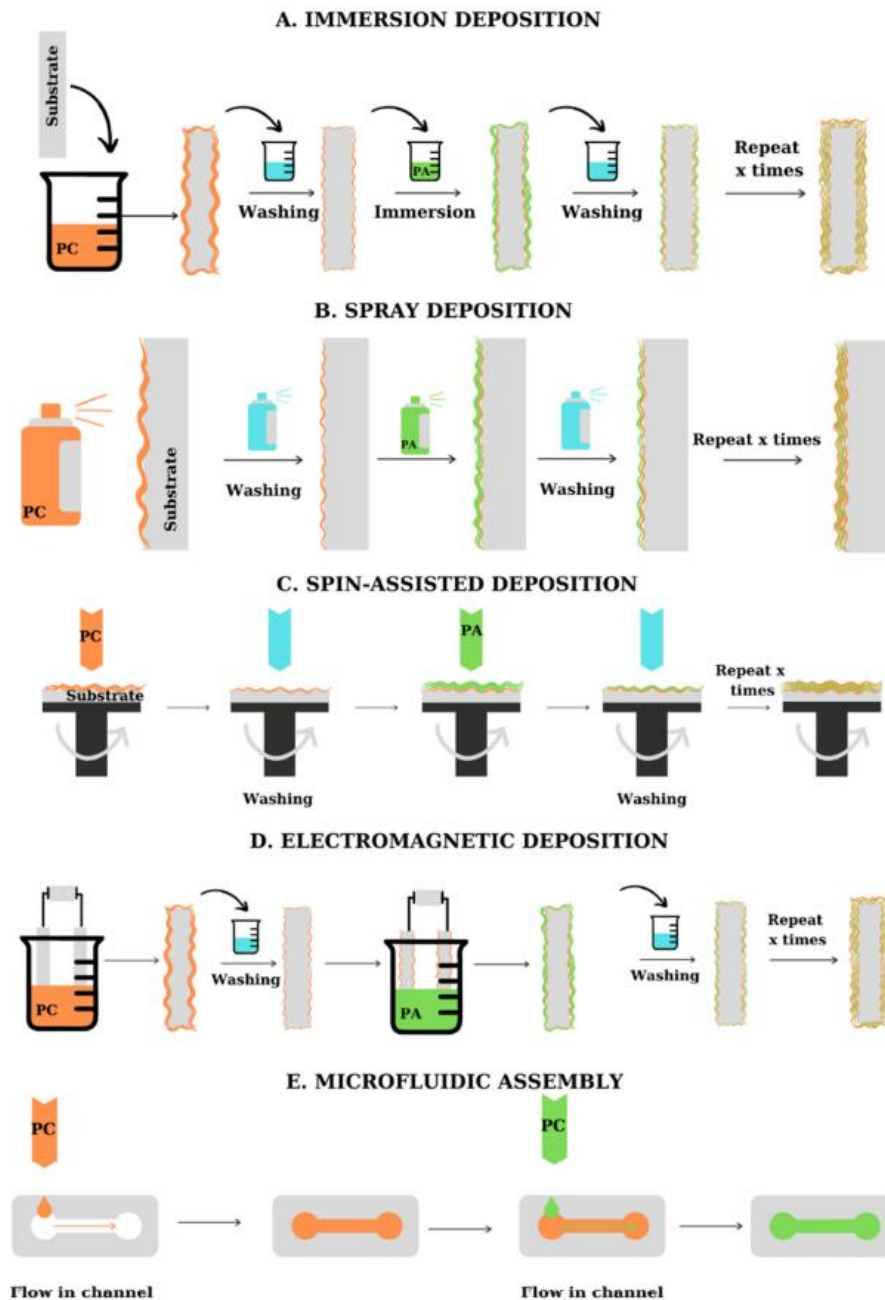


Figure 1.7. Schematic representation of the main LbL methods used for the fabrication of PEMs based on polycation (PC) and polyanion (PA). (A) Conventional immersion deposition of PEs, (B) Spray deposition of PEs, (C) Spin-assisted deposition of PEs, (D) Electromagnetic deposition of PEs, (E) Microfluidic assembly of PEs on microfluidic materials. (Petřila et al., 2021).

Spray deposition is another LbL method (Figure 1.7(B)) where polyelectrolyte multilayers are assembled by aerosolizing polymer solutions, sequentially spraying

polyelectrolyte solutions and alternatively spraying washing solution onto substrates (Schlenoff et al., 2000). Using this method, the deposition is often achieved by spraying the polyelectrolyte solution perpendicular to position of the substrate, allowing an easy removal of unbound material from the surface due to gravitational drainage. Spray-assisted deposition of polyelectrolytes is a quick production of films and allows to form multilayers onto large substrates. However, the position of the substrate can lead to the deposition of inhomogeneous films that can be reduced by coupling with spinning (Krogman et al., 2007; Richardson et al., 2015).

Film fabrication by spin-coating, illustrated in Figure 1.7(C), is based on alternative deposition of charged polymer solutions onto a solid substrate immediately followed by a rinsing and drying step, while the substrate undergoes spinning at constant velocity. In the majority of spin assembly, polymers are enforced to adsorb during the “classical” spin-coating procedure by casting the solution onto a spinning substrate. Spin-assisted LbL assembly of thin films from polyelectrolytes and/or biopolymers have been used in cases where polymers are allowed to adsorb onto stationary substrate before spinning steps (C. Cerclier et al., 2010). During the substrate rotation, the polymer solutions spread onto the surface to obtain layers with complete evaporation of the solvent, generally water.

Electromagnetic deposition of polyelectrolyte multilayers is based on the use of an applied electric or magnetic field to drive the layer formation as illustrated on Figure 1.7(D). In the standard electrodeposition, an electrode coated with the deposition substrate and the reference electrode are immersed in a polyelectrolyte solution with opposite charge to the substrate and the application of a potential difference induces the formation of the film (Richardson et al., 2015; J. Sun et al., 2001). After deposition, the electrodes are washed and placed in polymer solutions of opposite charge. By repeating the process, polyelectrolyte multilayers with a small number of layers can be built (Guzmán et al., 2020). Another method to perform electrodeposition is to place the substrate between the two electrodes.

Microfluidic or fluidic assembly/deposition of polyelectrolyte multilayers is used for the deposition of layers of polyelectrolytes using fluidic channels, to coat the walls and a substrate immobilized in the capillaries/channels of a fluidic system (Figure 1.7(E)). In the general set-up, the LbL assembly is usually performed under vacuum or pressure to alternatively inject polyelectrolyte solutions and rinsing solution into the microfluidic system *via* tubing and/or capillaries (Katayama et al., 1998; Richardson et al., 2015). In addition to

being faster than immersive deposition, microfluidic deposition provides a way to form polyelectrolyte multilayers on substrate with special forms that are not accessible by other LbL methods or the use of masks to obtain region-specific patterning (Shchukin et al., 2004).

2.2. Formation of polyelectrolyte multilayers

2.2.1. Driving forces

The formation or the growth of LbL polyelectrolyte films is based on spontaneous adsorption, of at least two species, usually driven and limited by the increase of entropy in the system (illustrated in Figure 1.8) and Coulombic interactions. However, it is important to note that the driving forces involved in multilayers construction are not only restricted to electrostatic interactions. More and more polymers/macromolecules are being exploited for their ability to form multilayer films *via* other interactions than electrostatic ones. Hydrogen bonds, hydrophobic interactions and van der Waals forces also operate in the formation of the layers and influence the stability of the LbL assemblies (Borges & Mano, 2014; Clark & Hammond, 2000; Kotov, 1999). Here is an exhaustive list of the main interactions that can occur in LbL assembly: electrostatic interactions, hydrogen bonds, hydrophobic interactions, charge transfer interactions, coordination bonds, supramolecular-type interactions, covalent bonds, stereo complexation-type interactions.

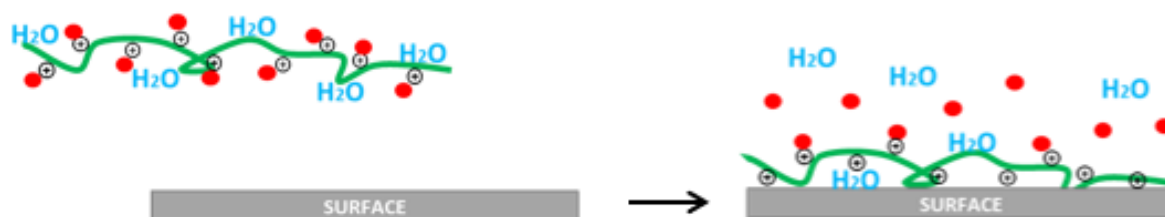


Figure 1.8. Schematic representation of adsorption mechanism onto a surface, based on a simple system of polyelectrolyte (polycation) in aqueous solution with associated counterions (in red).

To understand these interactions contribution, it is necessary to consider the impact of two different aspects on the assembly: 1) the different components of the system (polyelectrolytes, substrate, solvent, counterions) and 2) the contribution of electrostatic interactions (enthalpic factor) and entropic factor (Borges & Mano, 2014; Dubas & Schlenoff, 1999; Petrilu et al., 2021). For polyelectrolytes, the charge inversion has been considered the driving force leading to multilayer formation in the early studies on the subject. In fact, the

deposition of layer is not stopped when the neutralization of the surface charge is reached, but when a certain degree of opposite charge appears onto the surface. However, later on, studies on potential measurements at the surface showed that a change in potential sign of the surface charge is not necessary for the formation of layers (Neff, Naji, et al., 2006; Neff, Wunderlich, et al., 2006). Thus, that electrostatic attraction between the polyelectrolytes and/or the substrate is not the main reason for LbL assembly. This is rather the result of the entropy gain of the system, and other interactions can lead to PEMs growth.

During the formation of a multilayered films based on polyelectrolytes, the complexes formed from adsorption between a polycation and a polyanion lead to the release of counterions associated to the polymer backbone (v. Klitzing, 2006). The release of those counterions leads to two phenomena: 1) “intrinsic” charge compensation, 2) “extrinsic” charge compensation (Schönhoff, 2003). Films from intrinsically compensated multilayers presents a very low concentration of counterions while films from extrinsically compensated multilayers present a higher concentration of counterions within their structures. In the first case, a large quantity of counterions is released from the polymer chains during the layer formation. The release of the counterions leads to a decrease of the free energy of the system. The decrease of free energy is associated to an entropy gain that is the driving force of the assembly of intrinsically compensated LbL films. In the contrary, the systems with extrinsic compensation need the presence of counterions to ensure the electroneutrality of the multilayer. Their presence within the structure reduces the impact of the entropy on the assembly of extrinsic compensated multilayers.

2.2.2. Linear growth regime vs Exponential growth

The adsorption process includes charge inversion of the surface; indeed adsorption does not yield to surface neutralization but end with charge overcompensation of the surface that induces repulsive interactions with polymers in solution (Hoogeveen et al., 1996; Schlenoff & Dubas, 2001). The surface charge reversal allows the adsorption of the following layer with the oppositely charged polyelectrolyte, initiating the growth of the film. From literature, two types of film’s growths can be distinguished: linear and non-linear or exponential growths as presented on Figure 1.9. The growth type depends on the polymer couple and experimental conditions and can be identified by the relationship between the

deposited/absorbed mass or the layer thickness and the number of bilayers (Elzbieciak et al., 2009; Y. Li et al., 2012; Schlenoff & Dubas, 2001). The transition between linear and exponential growth regime (Figure 1.9) occurs mostly when the growth becomes independent of the physico-chemical characteristics of the substrate.

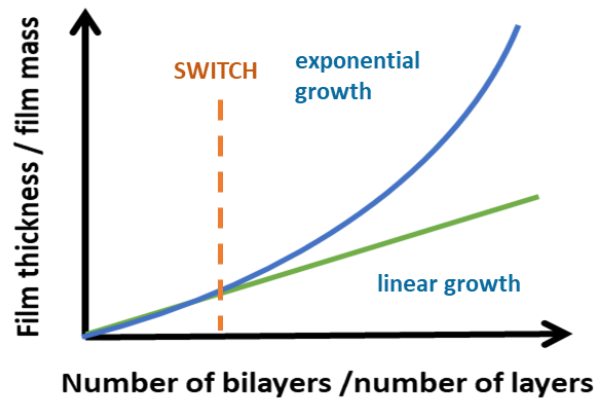


Figure 1.9. Schematic representation of the linear and exponential growth regimes of LbL assembly observed on film thickness/film mass as a function of the number of adsorbed layers/bilayers. Adapted from (Silva et al., 2016).

In the first case, the growth of polyelectrolyte multilayers shows a linear increase of the mass and/or the thickness adsorbed onto the surface after each layer/bilayer deposition (Decher, 1997). In these films, the charged polyelectrolytes interact with oppositely charged ones constituting the external surface of the film by forming a new layer with constant thickness. In Figure 1.10a, the scheme (i) represents a single layer of charged polyelectrolyte. The scheme (ii) represents the adsorption of a polyelectrolyte of opposite charges on (i) constituting a second layer with a thickness Δd equivalent to the layer (i). The layers (ii) correspond to a so-called bilayer, consisting of a polycation layer and a polyanion layer. A homogenization between adjacent layers occurs during the film formation, giving to the film a homogeneity of structure and of charge distribution (Schmitt et al., 1993; v. Klitzing, 2006). A relevant example of this growth type is the poly(allylamine hydrochloride)/poly(styrene sulfonate) (PAH/PSS) system that has been widely studied (Decher et al., 1992).

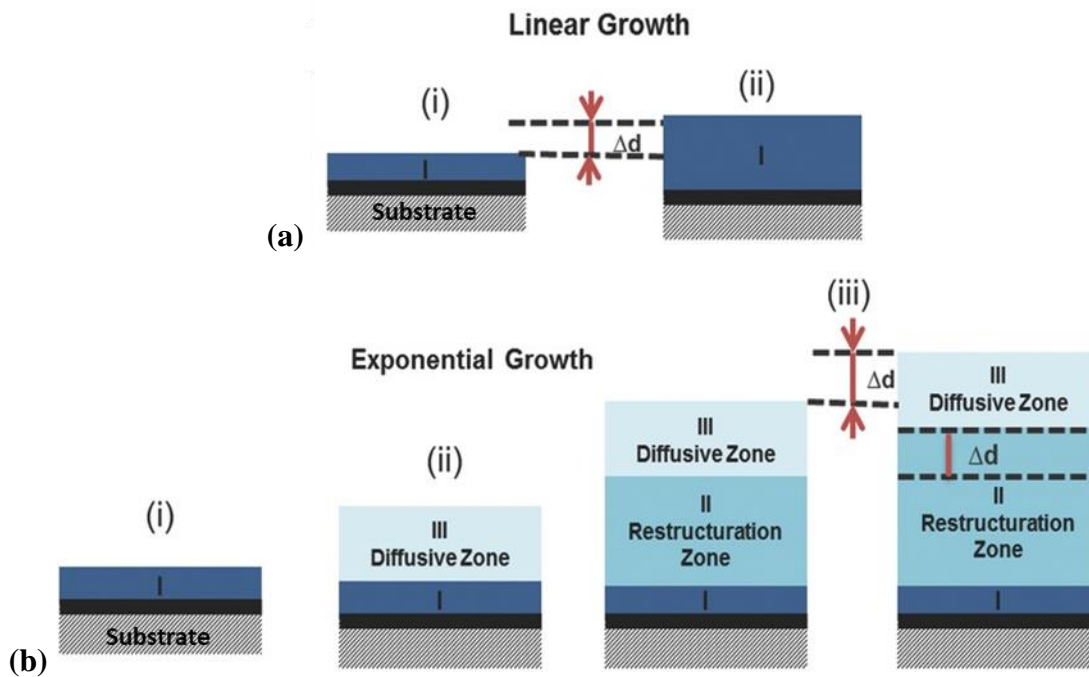


Figure 1.10. Schematic representation of (a) Linear growth regime, (b) Exponential/non-linear/supra-linear growth regime of polyelectrolyte multilayers built with layer-by-layer method by (Silva et al., 2016) adapted from (Porcel et al., 2007).

In the second case, films present a non-linear increase of mass (or thickness) with each adsorbed bilayer, also called supra-linear or exponential growth (Haynie et al., 2011). The films are characterized by a quantity of adsorbed polyelectrolytes per bilayer that increases with the number of bilayers deposited. First, work from Elbert *et al.* suggested that complexation between polycations and polyanions (on the last adsorbed layers) could be the reason of the non-linear growth of some multilayers (Elbert et al., 1999). Later on, non-linear growth has been mainly related to the presence of a weak polyelectrolyte, that can favor diffusion processes inside the adsorbed layers and hydrogen bonding interactions within the film (Haynie et al., 2011; Picart et al., 2002; Porcel et al., 2007; Silva et al., 2016). This growth regime is largely due to the diffusion in and out of at least one of the two polyelectrolytes used through the film during the formation of bilayers as illustrated on Figure 1.10b.

- (i) The scheme represents the deposition of the first layer onto the surface.
- (ii) The scheme represents the adsorption of oppositely charged polyelectrolyte on previous layer. The interactions with the two layers lead to a diffusive zone III where the new layer diffuse into the layer represented on (i).

- (iii) The scheme represents the deposition of third layer (same polyelectrolyte as for the first layer) onto the layers formed in (ii). The adsorption leads to a new diffusion zone III on the top while the previous diffusion zone III results in a restructuration zone II. For each new layer adsorbed, the thickness Δd of the restructuration zone II increases while the diffusion zone III remains constant.

Studies has shown that films based on most biologically relevant polyelectrolytes, such as polypeptides and polysaccharides, showed exponential growth in most cases (Elbert & Hubbell, 1998; Lavalle et al., 2002; Picart et al., 2001). The growth mechanisms depend on the characteristics of the polymers and the processing parameters (Elzbieciak et al., 2009; Picart et al., 2002; Schlenoff & Dubas, 2001). More generally, polyelectrolyte multilayers films and their characteristics are related to the nature of polyelectrolytes and assembly conditions and result in films with different internal structures and physico-chemical properties (Borges & Mano, 2014; Dubas & Schlenoff, 1999; Guzmán et al., 2020).

2.3. Tailoring properties of polyelectrolyte films

2.3.1. Main properties of polyelectrolyte multilayers

The internal structure and physico-chemical properties of multilayers are linked to the characteristics of the polyelectrolytes used, to the deposition conditions and to the characteristics of substrate as well. Polyelectrolytes multilayers offer a large variety of material fabrication possibilities with different properties, and control over those properties. The main properties of multilayers studied in literature are summarized in Figure 1.11.

The stability of multilayers is dependent on the charge equilibrium in the system (ionic strength, pH) and on the acido-basic characteristics of the functional groups of the polyelectrolytes (type of charges, charge density) (Hoogeveen et al., 1996). It is possible to improve the film stability by adding a cross-linking step to the fabrication of films (Ghiorghita et al., 2019; Reurink et al., 2020; Richert et al., 2004). Cross-linking between the adsorption steps or at the end of the film build-up allows to create chemical bonds between opposite charges within the structure. The introduction of chemical bonds between polyelectrolytes enhances then the stability.

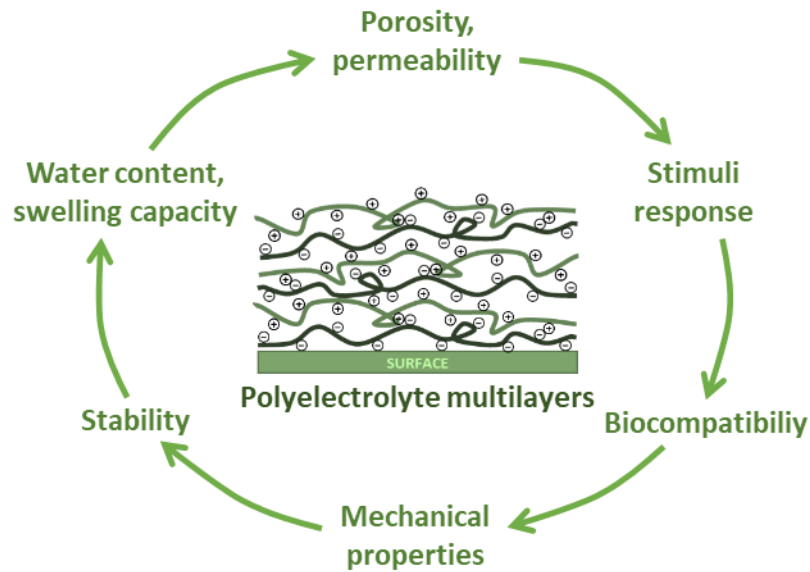


Figure 1.11. Schematic representation of the main properties of polyelectrolyte multilayers, usually explored in literature, adapted from (Petřila et al., 2021).

One of the key properties of multilayers for environmental and biomedical applications is the water content. The water embedded within the films has an important impact on the dynamic behavior of the films and their structure, as it affects the local molecular interactions and so the complexation between polyelectrolytes. The water content can be separated into two types: 1) hydration, 2) swelling (Dodoo, 2011; Schönhoff, 2003). In general, the hydration water of polyelectrolyte multilayers is high, up to 80% of the adsorbed mass, and are strongly dependent of the number of layers deposited / the thickness of the film (Crouzier & Picart, 2009; Guzmán, Cavallo, et al., 2011). The swelling capacity of multilayers can be affected by the environmental conditions (*i.e.* relative humidity), but also by the ionic strength and the type of ions used during their formation (Dodoo et al., 2011, 2013; Dubas & Schlenoff, 2001). The swelling degree is dependent of the interactions within the structure, thus of the ionic pairing and physico-chemical properties of polyelectrolytes.

In addition to a swelling capacity, polyelectrolytes multilayers may present a selective permeability, which is an important feature for exchange with external environment (W. Dong et al., 2005; Kempe et al., 2014; Qiu et al., 2001). Many parameters have an influence on the porosity of multilayers: characteristics of polyelectrolytes, experimental conditions (ionic strength, pH, temperature, mechanical deformation, ultrasounds) (Antipov et al., 2001; Petřila et al., 2021). Especially, studies focus on controlling the permeability of multilayers *via* the

ionic strength and pH, as stimuli-response materials, or deposition conditions (Ali Said et al., 2020; Antipov et al., 2003; Tong et al., 2005, 2006).

As mentioned, multilayer films can present stimuli-responsive properties, including permeability and swelling that are of interest since the beginning of 2000s. Different stimuli-responsive multilayers have been studied based on the modulation of different parameters by varying several conditions, which are particularly used for drug release applications. The most classic parameter used for the development of such systems is the pH, to trigger a specific response (Cai et al., 2019; Diez-Pascual & Shuttleworth, 2014; Guzmán, Cavallo, et al., 2011; Tong et al., 2006). A change in pH can lead to different porosity and can also induce a total deconstruction of the film. More recently, the response of multilayers to microorganisms has also been studied as a stimulus to generate a change in properties (C. V. Cerclier et al., 2013; Itoh et al., 2006; Schaubeder et al., 2022; Serizawa et al., 2002). Action of specific microorganisms, such as development of bacteria or enzyme action, can also affect the permeability and release properties by partial or total degradation of the multilayer.

The biocompatibility is one the most researched feature for the development of materials based on multilayers, mainly in biomedical, food or cosmetic applications (Jaber & Schlenoff, 2006; Petrilă et al., 2021). In fact, many multilayer films are built using biocompatible polyelectrolytes, from both natural (polysaccharides, proteins, polypeptides, etc.) and synthetic origins (Boudou et al., 2010; Crouzier et al., 2010; Sharma & Sundaramurthy, 2020). The fabrication of polyelectrolyte multilayers with good biological compatibility is essential for good acceptance by the human organism as well as high degradability in the short or long terms.

The internal structure and physico-chemical properties of the film has an essential impact on the mechanical properties of polyelectrolyte multilayers. In particular, the hydration water and film composition are correlated to the viscoelastic behavior of the film and thus, to the material flexibility (Guzmán et al., 2020; Patro & Wagner, 2011). Addition of inorganic species, such as clays, metal oxides or ceramics, within multilayers can improve the rigidity and decrease the flexibility (Bonderer et al., 2008; J. Wang et al., 2014). Lastly, ionic pairing (ionic strength, charge density, pH) can also induce a shift of viscoelastic behavior of the multilayers *i.e.* a change of their mechanical properties (Guzmán et al., 2009; Heuvingh et al., 2005).

2.3.2. Factors controlling multilayers build-up

Some experimental parameters are crucial for the assembly of polyelectrolyte multilayers and resulting properties: physico-chemical characteristics of substrates, physico-chemical characteristics of the polyelectrolytes, solution parameters (ionic strength, pH, concentration) and experimental parameters of the deposition procedure (adsorption time, drying step, temperature).

Physico-chemical characteristics of substrates. Due to the versatility of layer-by-layer principle and the different methods of deposition, a wide variety of substrate can be used to assemble polyelectrolyte multilayers: organic, inorganic, metallic, flat, spherical, etc. Chemical nature, surface morphology as well as size of substrates can affect the film growth and, as the result, the properties of the films. Surface charge density and hydrophilicity/hydrophobicity characteristics of the substrate are critical parameters for film formation as the interactions between polyelectrolytes and substrates are driving the first-layers adsorption (Decher & Schlenoff, 2003). Moreover, roughness, porosity and presence of impurities also present a non-negligible impact onto the internal structure of the films and their stability (Azzaroni & Lau, 2011; Ladam, Schaad, et al., 2000; Sukhishvili & Granick, 1998).

Physico-chemical characteristics of the polyelectrolytes. The intrinsic properties of polyelectrolytes involved in the formation of multilayers also present a great impact on the films and their properties. In particular, the charge density, the molar mass, and the conformation of polymers in solution were highlighted as critical factors to the LbL assembly.

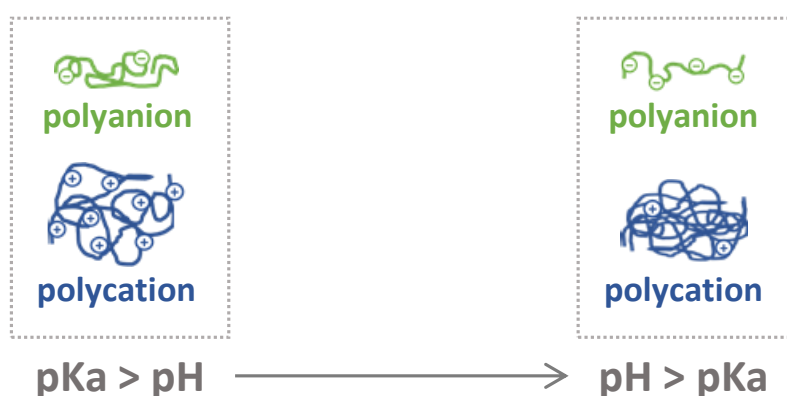


Figure 1.12. Scheme of the changes in the conformation of weak polyelectrolytes (polycation in green, polyanion in blue) according to the pH of solutions.

Polyelectrolytes can be classified into two parts: strong vs weak polyelectrolytes. Strong polyelectrolytes are polyions for which the degree of ionization in solution is independent of the pH value of the solution ($pK_a < 0$ or $pK_a > 14$) (Schönhoff, 2003) (Figure 1.12). Strong polyelectrolytes are always charged in solution (Cramer et al., 2017; Glinel et al., 2002; Voigt et al., 2003). The degree of ionization in solution of weak polyelectrolytes can be adjusted by the pH of the solution ($0 < pK_a < 14$). The formation of multilayers based on one and two weak polyelectrolytes can be affected by the pH values of either polyelectrolyte solution (Bieker & Schönhoff, 2010; Choi & Rubner, 2005; Elzbieciak et al., 2009). Especially in the case of two weak polyions, the pH influences the thickness increments with layer deposition and external stimuli can lead to change in dissociation of weak polyions (Elzbieciak et al., 2009; Shiratori & Rubner, 2000). Thus, weak polyelectrolytes are often used for the build-up of multilayers with stimuli-responsive properties as they are sensitive to pH variations (Devi et al., 2014; Glinel et al., 2007; Mauser et al., 2006; Sharma & Sundaramurthy, 2020).

The impact of the molecular weight of the polyelectrolyte on the film growth is also to be considered. There is a lack of consensus in the literature on the correlation between adsorbed mass and molar masses of polyelectrolytes. Sui *et al.* reported that thicker multilayers were obtained by increasing molar masses of polyelectrolytes, while Yu *et al.* reported the opposite observation (Sui et al., 2003; J. Yu et al., 2017). However, in general, higher molecular mass tends to increase the amount of absorbed polymer and film stability (Cramer et al., 2017; Porcel et al., 2007; Towle et al., 2020). Moreover, the risk of “stripping”, a phenomenon occurring when a polyelectrolyte pulls off the last layer instead of adsorbing on it, increases at certain molecular weight ranges due to charge distribution into the multilayers or when there is an important difference between the molecular weights of the polyelectrolytes used (Alkekhia & Shukla, 2019; Sui et al., 2003; Towle et al., 2020).

As electrostatic interactions often have an important contribution in the LbL assembly, charge density of the polyelectrolyte is one of the most studied impact (Lundström-Hämälä et al., 2010; Schoeler et al., 2002; Voigt et al., 2002). It is well known that low charge density generally leads to the formation of thin or unstable multilayers and that a too high charge density can induce the delamination of the film (Choi & Rubner, 2005). On Figure 1.13, at the bottom, we have a schematic representation of polyelectrolytes at high charge density (right) and at low charge density (left). In the case of high charge density, a lot of charges of the same sign are presented on the polymer chain and they repulse each other. The important

occurrence of charges results in an extended configuration of the polyelectrolyte called “stretched” configuration. In the case of low charge density, the lower presence of charges from the same sign leads to a lower electrostatic repulsion and thus, a more “coiled” configuration of the polymer. In addition, a minimum value for charge density was considered for strong polyelectrolytes below which the interactions are too weak to obtain stable films. Depending on the charge equilibrium between polyelectrolytes, it can lead to desorption of the last layer adsorbed instead of adsorbing and/or formation of polyelectrolyte complexes (Glinel et al., 2002; Voigt et al., 2003).

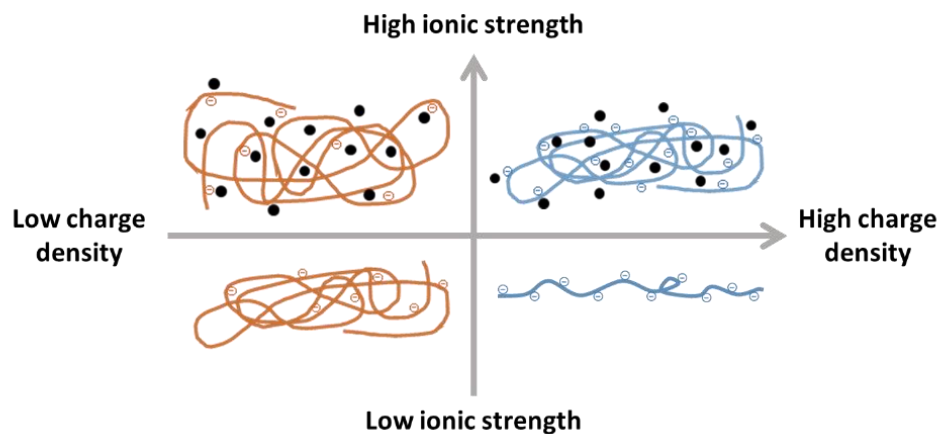


Figure 1.13. Schematic representation of the impact of ionic strength, represented by salt/counterions addition (black dots) on polyelectrolyte conformation (here, a polyanion) according on the charge density of the polyelectrolytes.

Properties of polyelectrolyte solutions. The change of the ionic strength of the solutions can strongly affect the adsorption behavior of polyelectrolytes, which makes it one of the most important parameters to control for the multilayer formation. The modification in ionic strength is mostly controlled by the addition of salt in the polyelectrolyte solution (Farhat et al., 1999; Feldötö et al., 2010; Glinel et al., 2002). The addition of counterions to the system modifies the balance between the enthalpic and entropic contributions in the system resulting in a change in the adsorption capacity. On the top of Figure 1.13., we can see the effect of the introduction of ions *i.e.* the increase of the ionic strength for the two types of charge density. In both cases, the presence of counterions in polymer solution leads to a screening effect by decreasing their effective charge. Thus, the intra- and inter-chains repulsions between the polyelectrolytes decrease resulting in conformation changes of the polyelectrolytes, from “stretched” to “coiled” (Figure1.13).

Depending on the “stretched” or “coiled” conformation type, the interaction ability between polyelectrolytes and/or the substrate can be modified (Guzmán et al., 2009). In addition, not only the salt concentration has an impact on the assembly of multilayers, but also the nature of the counterions involved. “Small ions” have a high electric field and a large hydration shell meaning a low interaction with the polyelectrolytes, while “large ions” present a small shell due to a weak electric shell (Salomäki et al., 2004). This refers to the Hofmeister series, which is a series to classify anions and cations by their ability to precipitate a given protein. An anionic series is $F^- > Cl^- > Br^-$ (Feldötö et al., 2010; Leontidis, 2002). To the left of chloride, the ions are referred as “large ions” while on the right, they are referred as “small ions”. A cationic series is $NH_4^+ > K^+ > Na^+ > Li^+$ (Heuvingh et al., 2005). As with the low ionic strength, the large hydration shell causes a strong chain repulsion between polyelectrolytes affecting their conformation (Wong et al., 2009). However, Heuvingh *et al.* found out that the effect of different cations was weak compared to the effect of anions (Heuvingh et al., 2005). Therefore, salt concentration and its nature influences both stability and physical characteristics of multilayers such as their morphology.

Other conditions of polyelectrolyte solutions affect the formation and properties of multilayers built, especially the solution’s pH, concentration and the nature of the solvent.

In the case of weak polyelectrolytes, even minor variations in pH around the pKa value of the polyelectrolyte lead to change of the ionization of functional groups and charge density (Guzmán, Cavallo, et al., 2011; Itano et al., 2005).

As illustrated in Figure 1.12, at $pH < pKa$, weak polycation appear in “stretched” conformation while weak polyanion appears in “coiled” conformation and the opposite is observed at $pH > pKa$. The opposite is observed for weak polyanions. The contribution of each weak polyelectrolytes and their conformation during the LbL assembly can lead to different growth types, as it was studied for hyaluronic acid/poly-L-lysine system (Bütergerds et al., 2017). Besides a modification of structural conformation, it impacts the interactions between polyelectrolytes and/or with the substrate as well (Bieker & Schönhoff, 2010). Moreover, the formation of layers requires an exposure of the substrate/previous layer to polyelectrolytes long enough to deposit stable layers and ensure charge inversion onto the surface.

In some cases of LbL assembly, multilayers can be obtained with polyelectrolyte in aqueous solution, as water is a good solvent for a lot of polyelectrolytes and allows to avoid toxicity of organic solvents (Dubas & Schlenoff, 1999). However, it is possible to change the role and the contribution of interactions by using solvents with different polarities, such as ethanol, dimethylformamide, dimethylsulfoxide or chloroform (Park et al., 2014; Poptoshev et al., 2004; Tuo et al., 2005).

Processing condition. In addition to the deposition method used, contact time, rinsing, drying as well as temperature were highlighted as critical parameters to control the LbL assembly.

Contact time was found to have a significant effect in most cases where interdiffusion of polymer (layers) is involved in the multilayer formation, leading to structure differences. Still, contact times allowing the adsorption of polyelectrolytes remain short. A range of 10 seconds to 180 seconds is observed in which there is an impact on the morphology of poly(allylamine hydrochloride)/poly(sodium styrene sulfonate) multilayers built by spray-assisted deposition or spin-coating (Kharlampieva et al., 2009). Shorter contact time can result in kinetics arrest of the interdiffusion while long contact time can result in weakening the structure due to restructuration (Bellanger et al., 2017; Guzmán, Ritacco, et al., 2011). However, the decrease of the contact time can improve the homogeneity of the multilayers as a result of the limited polymer diffusion (Krogman et al., 2007).

The removal of the loosely bound material by rinsing is also an important step in the formation as the presence of weakly absorbed polyelectrolytes onto the surface can lead to inter-polyelectrolyte complexation (Decher & Schlenoff, 2003; Feldötö et al., 2010). The formation and the precipitation of polyelectrolyte complexes can alter both the internal structure of multilayers and their properties.

As the LbL principle is a wet method (in water or other solvents), final and/or intermediate drying steps can affect the properties of multilayers built (Decher & Schlenoff, 2003). Drying is a fundamental step in the film formation, as it creates bonds between polyions (mostly H-bonds) and allows the stability of the films (Moreau et al., 2012). Drying between each absorbed layer is known to affect the film growth and internal structures, while drying at the final step of film build-up can have an impact on the final structure and the general swelling of the multilayer. Moreover, drying temperature affects the solubility and the

degree of ionization of polyelectrolytes, but also adsorption kinetics (Lvov et al., 1993; Salomäki et al., 2005; Vikulina et al., 2016). Several studies have shown its influence on the structure of polyelectrolyte multilayers, their swelling capacity, and their stability. Also, temperature changes are a way to switch from linear growth to exponential growth during the LbL build-up.

3. Functionalized bacterial α -glucans for elaboration of multilayer materials

3.1. Dextran sulfates-based polyelectrolyte multilayers

Among the dextrans used in multilayered materials, dextran sulfates (DexS) are commonly encountered since different molecular weights and sulfate contents are commercially available, expanding the range of materials implementation. Dextran sulfates are bio-based anionic polymers with SO_3^- groups with a pKa around 1.5. Regarding their pKa, dextrans sulfates are almost always ionized in water ($\text{pH} > 1.5$), which makes them close to a strong polyelectrolyte.

3.1.1. Dextran sulfates and chitosan multilayered films

One of the most employed polycation used in combination with DexS is chitosan (CHI), poly[(1 \rightarrow 4)- β -linked 2-amino-2-deoxy-D-glucose], a biocompatible and biodegradable anionic biopolymer with $\text{NH}_2/\text{NH}_3^+$ groups (pKa between 6 and 7). CHI is prepared by N-deacetylation of chitin extracted from the outer shells of crustaceans or insect wings (Jayakumar et al., 2010; Shukla et al., 2013). The first studies about CHI/DexS based materials were reported by Kikuchi and Fukuda in the 1970s (Fukuda & Kikuchi, 1977, 1978; Kikuchi & Fukuda, 1974). The authors highlight the ability of DexS and CHI to form polyelectrolyte complexes and the water-insoluble complex created was sensitive to the reaction conditions such as pH and concentration of the polyelectrolyte solutions (Fukuda & Kikuchi, 1978). This polyelectrolyte pair was later applied to multilayers for the first time in the 2000s by Serizawa's research group who used LbL principle to build DexS/CHI films (Sakaguchi et al., 2003; Serizawa et al., 2000, 2002; Serizawa, Yamaguchi, Kishida, et al., 2003).

In 2000, Serizawa *et al.* investigated the assembly process of CHI/DexS films and a key parameter of the construction of multilayers: the impact of salt addition on the film growth (Figure 1.14a,b). Using Quartz crystal microbalance (QCM) to investigate the films' growth and thickness increments, the authors found out that 10 bilayers of CHI/DexS with no salt addition leads to thin films displaying a quartz frequency shift of $\Delta f = -163$ Hz (corresponding to a thickness of 3.7 nm) while adding 1M NaCl to both polymer solutions leads to $\Delta f = -9946$ Hz (an increase of the thickness of the films of 227 nm) as reported on

Figure 1.14a. In the case of no salted film with low thickness, a possible incomplete coverage of the surface and uneven repartition of the polymer on the surface were assumed by the authors. It can also be due to the inaccurate measurements from the QCM-D technique. Nevertheless, results showed a shift from linear film growth at 0M NaCl (figure 1.14a) to an exponential film growth at 1M NaCl (figure 1.14b) as well as an increase of mass/thickness with the salt addition.

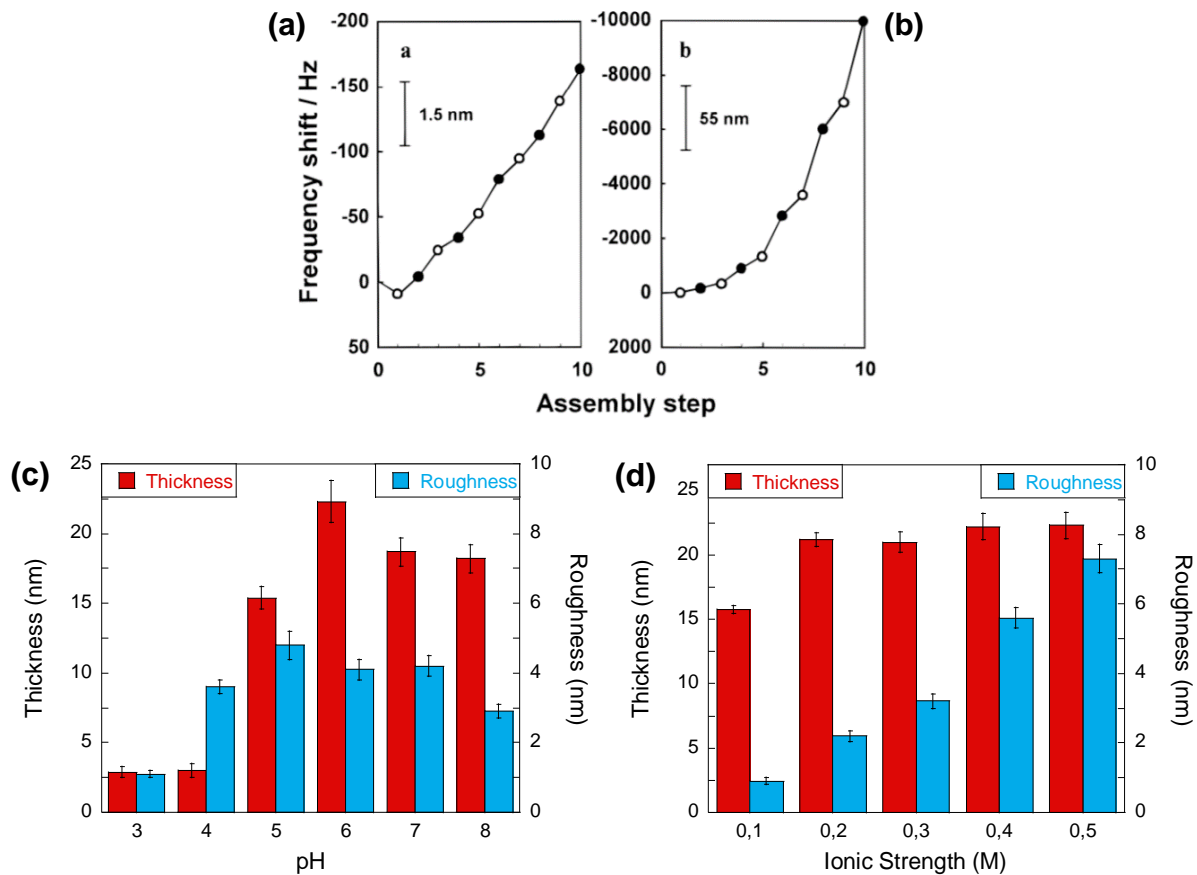


Figure 1.14. QCM frequency shift as function of adsorbed layer number up to 10 bilayers of (CHI/DexS) films on silver quartz crystal at pH depending on added salt content, (a) 0 M NaCl and (b) 1M NaCl. Frequency shift and the corresponding thickness is indicated. Reprinted with permission from (Serizawa et al., 2000), © 2000 American Chemical Society. Thicknesses and roughnesses of 10 bilayers (CHI/DexS) films grown on silica wafer with (c) pH (at 0.5 M ionic strength) and (d) ionic strength (at pH 6) obtained with ellipsometer measurements, data from (Devi et al., 2014).

In 2014, Devi *et al.* studied the formation of 10 bilayers DexS/CHI film on silica using the dipping method (Devi et al., 2014). Authors observed an exponential growth in thickness of the CHI/DexS film with increasing number of layers at 0.5M NaCl and explained that after the 4th layer, the film growth changes from linear to exponential showing the influence of the substrate on the first adsorbed layers. This observed exponential growth mechanism is related

to the ability of the CHI to diffuse in and out of CHI/DexS film and is often observed for CHI-based multilayered films (Salomäki & Kankare, 2009; Z. Song et al., 2009).

Devi *et al.* also investigate the impact of ionic strength and pH on the surface morphology of CHI/DexS films (Devi et al., 2014). By increasing ionic strength, *i.e.* increasing NaCl concentration from 0.1M to 0.5M (Figure 1.14d), the film thickness increased from 15 nm to 25 nm. The presence of ions induces a screening of the polyelectrolyte charges leading to a decrease of the electrostatic repulsion from identical charges on the polymer chain. Thus, polyelectrolytes display random coil conformation allowing a bigger polymer amount to be adsorbed onto a surface due to the highest compaction and decreased repulsion between polymer coils. At low ionic strength, polyelectrolytes are in an extended conformation and higher repulsion between chains occurs. Variation of pH from 3 to 8 at fixed ionic strength (Figure 1.14c) highlighted a clear dependence of the film growth with pH which was observed for other multilayers based on chitosan (Guzmán, Cavallo, et al., 2011). As displayed on Figure 1.14c, average thickness of adsorbed layers increases when increasing pH from 1 to 6, then the thickness decreases by increasing pH to 8 with an optimum at 23 nm for 10 bilayers at pH 6. In fact, at high pH (> 6), CHI becomes deprotonated and electrostatic-driven LbL assembly cannot occur between CHI and DexS. At low pH (pH<5), amino groups of chitosan are protonated allowing a successful LbL adsorption. However, at very low pH, authors explained that protonation of chitosan leads to an excess of positive charges from DexS and immediate dissolution of multilayers. The variation of charge equilibrium, here by changing the ionic strength and pH, also affects morphology of layers as illustrated on Figure 1.14c, d, by analyzing the roughness and the surface morphologies by AFM. Roughness increases from 3.75 nm to 8 nm by increasing ionic strength from 0.1 M NaCl to 0.5 M NaCl and pH variation induces also a significant change of both parameters.

Table 1.3. Chitosan and dextran sulfate (CHI/DexS) multilayered films reported in literature and their applications.

Application(s)	Films	Targeted properties	Ref
Biomedical	(CHI-DexS)-CHI (CHI-DexS) _{1 to 40}	Alternating anti- vs procoagulant activity, biodegradability	(Serizawa et al., 2000, 2002)
		Control of blood coagulation, antithrombogenic surface	(Sakaguchi et al., 2003; D.-G. Yu, Jou, et al., 2007; D.-G. Yu, Lin, et al., 2007)
		Drug delivery	(Xie et al., 2016; F. Zhang et

Tissue engineering	(CHI-DexS)-CHI (CHI-DexS) _{1 to 4}	Bioactivity, fibroblast cell compatibility	al., 2019) (Kulikouskaya et al., 2018; Serizawa, Yamaguchi, Kishida, et al., 2003)
--------------------	--	--	---

By considering the physico-chemical properties of chitosan and dextran sulfate and the capacity to form films with controlled architecture, (DexS/CHI) multilayers found potential uses in different fields and mainly in biomedical applications. Table 1.3 outlines the applications and main targeted properties of (CHI/DexS) films found in literature. Thanks to the ability of dextran sulfate to prevent blood coagulation, Serizawa's research group highlighted the potential of CHI/DexS multilayers in blood related devices to control blood coagulation (Sakaguchi et al., 2003; Serizawa et al., 2000; D.-G. Yu, Jou, et al., 2007; D.-G. Yu, Lin, et al., 2007). Moreover, integration of chitosan into multilayers films allows to block anticoagulation of DexS and open the possibility to form biodegradable films with both anti-coagulation and pro-coagulation properties (Serizawa et al., 2000, 2002). More recently, the interest of the scientific community in CHI/DexS as potential alternatives as multilayered coating for drug nanocarriers increased. In addition of both polyelectrolytes being biocompatible, their use as surface functionalization can improve their dispersibility in physiological conditions, as it was observed with graphene oxide nanosheets (Xie et al., 2016; F. Zhang et al., 2019). Moreover, DexS/CHI multilayers were proven to be useful for cell attachment and their growth on surfaces (Kulikouskaya et al., 2018; Serizawa, Yamaguchi, Kishida, et al., 2003). Cell adhesion seems to depend mainly on the stiffness of the multilayers, which can be related to the growth pattern and thus of the choice of polycations and polyanions and the number of bilayers deposited (Kulikouskaya et al., 2018). Kulikouskaya *et al.* demonstrated that multilayered films are formed by alternating adsorption of negatively charged polysaccharides switched from linear to exponential growth by changing the polycation from polyethyleneimine (PEI) to CHI (Kulikouskaya et al., 2018). Authors also showed that those films built with exponential growth had different properties as the surface roughness increased and the mechanical properties changed from elastic to viscous by increasing the number of bilayers.

3.1.2. Dextran sulfates and polyelectrolyte-based multilayered films

Apart from chitosan, other polycations were associated with DexS. These include synthetic and natural polyelectrolytes as well as other dextran derivatives allowing building

different film structures. In 1995, Elferink et de Koster introduced diethylaminoethyl dextran (DEAE-Dex), polycation derivate from dextran with physiological effects (antibacterial, antifungal, and antitumor) as a good candidate to substitute synthetic polymers in biomedical applications (Elferink & de Koster, 1995). The use of DEAE-Dex into LbL assembly associated with DexS was proposed later by Benni *et al.* to control surface morphology of films to tune protein adsorption and cell adhesion (Benni et al., 2014). The authors studied the surface morphology of (DEAE-Dex/DexS)₄ and (DEAE-Dex/DexS)₄-DEAE-Dex films and their properties on glass surface depending on the last layer adsorbed (polycation or polyanion). Comparison between multilayers ending with a polycation DEAE-Dex layer and multilayers ending with a polyanion DexS layer highlighted significant differences in terms of roughness.

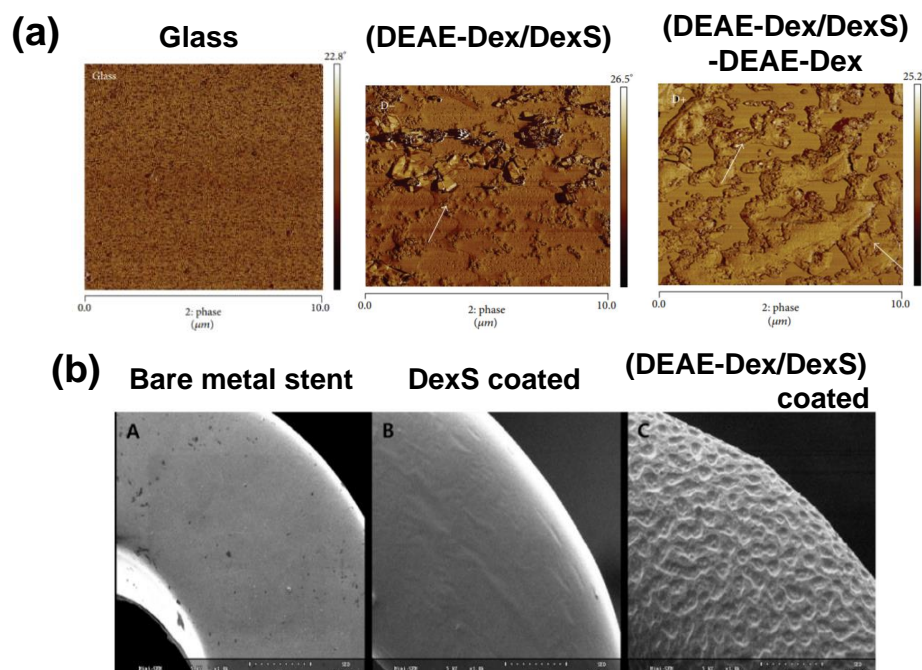


Figure 1.15. (a) AFM images ($10\ \mu\text{m} \times 10\ \mu\text{m}$, phase) of bare glass surface, (DEAE-Dex/DexS) multilayer, and (DEAE-Dex/DexS)-DEAE-Dex multilayer adsorbed on glass surfaces (Benni et al., 2014). (b) SEM images ($30\ \mu\text{m} \times 30\ \mu\text{m}$) of stent surfaces: bare metal stent, DexS coated stent and DEAE-Dex and DexS coated stent (Jang et al., 2019).

AFM images (Figure 5a) showed that (DEAE-Dex/DexS) and (DEAE-Dex/DexS)-DEAE-Dex multilayers display high coverage of the surface and their topographical morphologies present clusters or granules. Analysis of the multilayers showed an increase of surface roughness with values of 47 nm for (DEAE-Dex/DexS) and 72 nm for (DEAE-Dex/DexS)-DEAE-Dex multilayers while the bare glass's roughness ranges about 3 nm. The monitoring of advancing contact angles displays the decrease of hydrophilicity, which can be

related to an increase in surface roughness with the number of adsorption steps in general. Also, a higher hydrophobicity of the surface was observed with (DEAE-Dex/DexS)-DEAE-Dex multilayers than for (DEAE-Dex/DexS) multilayers. In 2019, Jang *et al.* demonstrated similar effect of DEAE-Dex/DexS multilayered coatings on metal stent, both increasing the hydrophilicity and inhibiting cell adhesion of metal stent (Jang *et al.*, 2019). In this study, AFM images (Figure 5b) showed an increase of roughness with DEAE-Dex/DexS coating compared to DexS coating. Moreover, water contact angle of (DEAE-Dex/DexS) coated metal stent was significantly higher than water contact angle of the bare metal stent as well, confirming the potential of (DEAE-Dex/DexS) multilayers in tuning surfaces for various applications including protein and cell adhesion.

3.2. Dextran sulfates and proteins multilayered films

Proteins were associated with DexS to build multilayers for mainly targeting biomedical applications due to the biocompatibility of dextran sulfates and biological activity of protein. Investigation of interactions between polysaccharides and proteins in multilayers films constitutes a topic of interest in biomedical field in order to build films with controlled organization of proteins (Brynda & Houska, 1998; J. Zhang *et al.*, 2005). The use of LbL technique and the choice of both assembly parameters and nature of polyelectrolyte-protein couple allow to build multilayers with a structured morphology but also the regulation of the protein conformation within the film (Hong *et al.*, 1993; Lvov *et al.*, 1994, 1995). As well as the polyelectrolytes usually encountered, the nature of the protein and the processing parameters (pH, salt concentration, compound concentrations, temperature, etc.) are of importance for the construction of polyelectrolyte-protein multilayer films (Müller *et al.*, 2001; vander Straeten *et al.*, 2018, 2020). Overall, pH was found to be a key parameter in the LbL assembly of proteins with polyelectrolyte to promote interactions between them, and pH of the protein solution has to be set far from the isoelectric point (Kayitmazer *et al.*, 2013; Lvov *et al.*, 1995; vander Straeten *et al.*, 2018). In general, proteins are susceptible to conformation changes depending on solution conditions and surface properties, which have an important impact on protein adsorption and multilayer formation.

In 1999, Brynda *et al.* used DexS as a building block to fabricate LbL assembly with human b2-microglobulin antibody cross-linked with glutaraldehyde. The resulting flexible film can be used as immunosensor for b2-microglobulin (Brynda *et al.*, 1999). More recently,

Damanik *et al.* investigated the growth of collagen/DexS 4 bilayers on PEI/ PSS 2 bilayers in order to develop high loading efficiency systems for biomedical applications. This study highlights the effect of collagen/DexS multilayers: collagen at pH 7 leads to linear growth while an exponential growth is obtained with collagen at pH 3. At pH 3, collagen used by authors with basal isoelectric point 7.8 interacts strongly with DexS through electrostatic interactions and displays more likely a compact conformation leading to exponential film growth. Moreover, they were able to optimize the immobilization of heparin in such multilayer systems, *i.e.* the bioactivity of heparin is retained on (PEI/PSS)₂+(collagen/DexS)₄ for 14 days by using collagen in acidic pH and exponential growth of collagen/DexS 4 bilayers (Damanik *et al.*, 2020). He and Hu first reported in 2004 a study on the interactions of hemoglobin or myoglobin with DexS. Authors suggested that localized electrostatic interactions are the driving force in protein/polymer LbL assemblies due to net positive charges or net negative charges of heme proteins (hemoglobin or myoglobin) depending on the pH solution (He & Hu, 2004). Houska *et al.* published a report on the influence of polyelectrolyte chain length on the LbL formation with proteins, especially albumin. The authors compared multilayers of albumin/DexS with different molecular weights of DexS and they showed that the assembly of globular proteins and linear strong polyanions at pH below the IEP of the protein is affected by the chain length of the polyanion (Houska *et al.*, 2004). The study suggested that at lower molecular weights of DexS, competition with adsorbing protein and absorbed protein might lead to resolubilization of the polyelectrolyte. Interactions between polysaccharides and proteins in LbL process were further investigated by Jourdain *et al.* using caseinate to understand mechanisms at interfaces for emulsion stabilization (L. Jourdain *et al.*, 2008; L. S. Jourdain *et al.*, 2009). LbL construction of (Caseinate/DexS) layers displays linear increase of shear viscosity with time explained by strong interactions between caseinate and DexS that produce flat conformation of the layer followed by a slow reorganization of protein and DexS.

3.3. Other α -glucans derivatives in multilayered films

In the late 2000s, Lee, Choi and Tsutsumi built polyaniline and carboxydextran multilayer films that present an interesting activity for the oxidation of ascorbic acid but also an excellent electron-transfer mediating capability for oxidation of glucose (Lee *et al.*, 2009). Oxidized dextrans were used to form a bilayer with PEI to immobilize biocatalyst of β -1,4-

endoxylanase by surface coating for the production of xylooligosaccharides (Romero-Fernandez et al., 2018). PEI was associated with an amine-substituted dextran, aminodextran (AMD), as well as with oxidized dextrans using the dipping technique to build multilayers (Heurich et al., 2011; Romero-Fernandez et al., 2018). Heurich *et al.* proposed the use of biointerfaces for increasing cell compatibility. In order to develop bioink for 3-dimensional printing, another dextran derivative, hydroxyethyl-methacrylate-derivatized dextran, was paired with hyaluronic acid (HA) to produce bio-based hydrogels *i.e.* bioink (Pescosolido et al., 2011). In 2019, a boronic derivative (the phenylboronic acid-modified alginate) and a diol biopolymer (a dextran derivative) were applied to the fabrication of H₂O₂-responsive microparticles by Mansour, Joukhar and Belbekhouche (Mansour et al., 2019). As far as we know, no studies on the use of other α -glucans derivatives from alternans, reuterans or mutans in multilayers can be found in literature.

4. Applications of multilayers: overview, specific applications for the thesis

In the last two decades, polyelectrolyte multilayers have been developed as nanomaterials for a wide range of fields, from medical field to nanotechnology, with different applications: optical devices, membranes for filtration or with active features, photodiodes, drug delivery or specific coatings. In this part, we focus on the use of multilayers in biomedical and environmental fields, as they were the two main applications targeted for my thesis. In particular, after a global presentation of the biomedical and environmental applications of polyelectrolyte multilayers, we describe their use as sensors for enzymes detection and as gas-barrier coatings.

4.1. Main applications of polyelectrolyte multilayers: biomedical, environment

4.1.1. Biomedical applications

Encapsulation of active compounds. The interest of the scientific community is particularly focused on the potential for drug delivery applications that imply loading of active molecules into multi-layered objects and their release. The versatility of LbL technique allows the fabrication of micro-objects with various colloid sizes, shapes, compositions and functionalities that address the issues of drug delivery devices (Ariga et al., 2011; De Cock et al., 2010; Tong et al., 2012). Especially, the choice of polyelectrolytes can also provide interesting properties to capsules such as sensitive permeability, with a stimuli-responsive (pH, ionic strength) character, that is a key property for encapsulation and drug delivery (Delcea et al., 2011; Sukhorukov et al., 2001). Multilayer objects, used as loaded objects, are also called shell objects. They consist of polyelectrolyte layers that are formed in the presence of a template produced by LbL assembly, resulting of a multilayer of specific shape (of an engineered shape). ‘Hollow’ multilayer objects and capsules are mainly fabricated by coating core particles, which serve as sacrificial templates. Those templates can be both organic and inorganic molecules/polymers, such as silica, polystyrene, metallic nanoparticles, melamine formamide or mineral cores. In addition to different sacrificial templates for LbL sequential adsorption, two different approaches for loading active content can be found in literature: pre-loading and post-loading that are illustrated on Figure 1.16a and 1.16b.

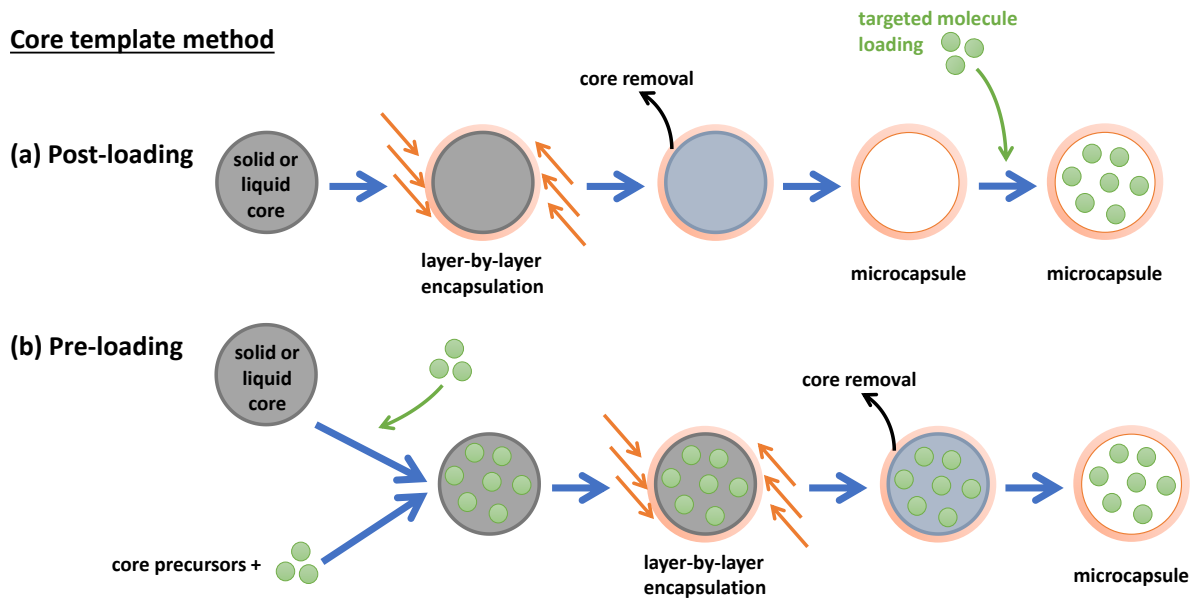


Figure 1.16. Schematic fabrication of micro- and nano- capsules based on LbL deposition principle onto sacrificial core template with (a) post-loading method and (b) pre-loading method.

With pre-loading procedures, core templates already contain the molecules to encapsulate. It is the case for all the micro-aggregate's precursors, as the first step is the fabrication of the core by complexation of substance of interest with one of the two coating substances (Averin et al., 2016; N. G. Balabushevich et al., 2006, 2016; Crecente-Campo & Jose Alonso, 2019). For example, Averin and co-workers developed doxorubicin containing micro- and nano- particles by preparing insoluble (Doxorubicin-DexS) particles before coating them with $(\text{CHI}/\text{DexS}/\text{CHI})_1$ (Averin et al., 2016). Pre-loading is also observed with dextran derivatives, using solid templates by adding loaded content directly within the cores during their preparation and keeping/retaining active compounds inside the hollow shell after core dissolution. Selina *et al.* proposed $(\text{DexS}/\text{PLL})_3$ biodegradable microcapsules using CaCO_3 core with entrapped protein (DNA) as template (Selina et al., 2009).

This is the application where dextrans and dextran derivatives are the more present as polyelectrolytes. Table 1.4 reports the preparation of dextrans-based capsules dedicated to drug delivery. The principal dextran derivatives used, dextran sulfates (DexS) were shown to be suitable for the encapsulation with various macromolecules with control on the quantity and the delivery time of the encapsulated substance.

Table 1.4. Dextran derivatives as polyelectrolytes for drug delivery micro- and nano-capsules fabrication reported in literature.

Coating Components	Encapsulated species	Ref
DexS/Chitosan	FITC-albumin; basic fibroblast growth factor; vascular endothelial growth factor; rifampicin; ciprofloxacin; ceftriaxone sodium salt; gentamicin sulphate; FITC	(Devi et al., 2015; Geetha Devi et al., 2021; Gnanadhas et al., 2013; Itoh et al., 2004, 2006, 2008a, 2008b)
	bovine serum albumin; polyphenol; protein (DNA); antibiotic	(Ali Said et al., 2020; Ferrari et al., 2017; Paini et al., 2015; Selina et al., 2009)
	doxorubicin; vitamin E and lecithin	(Averin et al., 2016; Crecente-Campo & Jose Alonso, 2019)
	N-benzoyl-L-arginine ethyl ester; N-benzoyl-L-tyrosine ethyl ester; insulin	(N. G. Balabushevich et al., 2006, 2013)
	Phosphate ions; 1-hydroxy pyrene-3,6,8-trisulfonic acid; amphiphilic alendronate; non-ionic glucose	(Fukui & Fujimoto, 2009, 2011)
	silver	(Livanovich & Shutava, 2019)
DexS/PAH	silver	(Anandhakumar et al., 2011, 2012)
DexS/poly-L-arginine	rhodamine B	(Gao et al., 2016)
	proteins; rhodamine B; messenger RNA; albumin and acid tannic; doxycycline; multikinase inhibitor sorafenib; alpha-2-macroglobulin	(Canova et al., 2015; De Temmerman et al., 2011a, 2011b; Ermakov et al., 2019; Kakran et al., 2015; Karamitros et al., 2013; Kochetkova et al., 2013; W. Liu et al., 2014; Lomova et al., 2015; D. Luo et al., 2016; Novoselova et al., 2020; Poojari et al., 2016)
	Tannic acid	(Kashcooli et al., 2016; Lomova et al., 2010)
DexS/protamine	proteins, enzymes, peroxidases	(N. Balabushevich et al., 2005; N. G. Balabushevich & Larionova, 2009)
	kidney cells, various cells	(Reibetanz et al., 2006, 2010, 2011)
	proteins, anti-inflammatory, doxorubicin substances	(N. G. Balabushevich et al., 2016; Rathmann et al., 2011; Trushina et al., 2018, 2019)
	insulin	(N. Balabushevich & Larionova, 2004)
DexS/poly-L-lysine	erythrocyte	(R. Luo, Mutukumaraswamy, et al., 2012)
	poly(DL-lactide-co-glycolide)	(R. Luo, Neu, et al., 2012)
	curcumin	(Mancarella et al., 2015)
	bioactive compounds	(Pan & Nitin, 2015)
Animated dextran/ carboxylated nanocellulose	curcumin	(Anirudhan et al., 2019)
Carboxymethyldextran/poly-L-lysine	quantum dots	(Chen et al., 2003)
Diol-dextran/ modified alginate	rhodamine b	(Mansour et al., 2019)

Although there is a wide range of counter-polyelectrolytes, literature overview (Table 1.4) emphasizes that most studies focus on the capsules based on dextrans and bio-based

polyelectrolytes (chitosan (CHI), polyarginine including protamine and PLL) for the fabrication of biodegradable and biocompatible objects. Similarly, for the construction of LbL films, (DexS/CHI) is a common polyelectrolytes couple for the fabrication of micro- and nano- capsules, as reported in Table 1.4. Since they are biocompatible, biodegradable and pH responsive, (CHI/DexS) capsules present different advantages for drug delivery systems, especially for release control since they offer different possibilities for drug release that can be triggered either by chemical or enzymatic action (Itoh et al., 2004, 2006, 2008a, 2008b).

Tissue engineering. Besides their sensibility to external stimuli, polyelectrolytes multilayers can provide a great ability to interact with biological molecules (proteins, nucleic acids, enzymes, etc.). For those specific applications, multilayers are mainly build-up with bio-based polymers such as chitosan, hyaluronic acid, sodium alginate, collagen, chondroitin sulfate, heparin or dextrans sulfate (Gribova et al., 2012; Khan & Ahmad, 2013; Tang et al., 2006). One advantage of these natural components is their bioactivity, their bioavailability, and their possible biodegradability in tissue and/or biological fluids. Moreover, multilayers based on natural polyelectrolytes present unique features such as adhesion of a specific biological molecules or stimulation of a specific cellular response. In the early 2000s, Serizawa *et al.* proposed an anti- vs procoagulant device based on chitosan (CHI) and dextran sulfate (DexS), where DexS layer showing procoagulant behavior and CHI layer an anti-coagulant behavior (Sakaguchi et al., 2003; Serizawa et al., 2000). Later on, the research group highlights the difference of gene expression in fibroblasts, depending on their adhesion on DexS layer or their adhesion on CHI layer (Serizawa, Yamaguchi, Kishida, et al., 2003). In general, dextran derivatives have been shown to form film with a surface favorable for cell adhesion and development, due to their surface roughness (Benni et al., 2014; Jang et al., 2019; Kulikouskaya et al., 2018).

Film with antimicrobial properties. Adhesion of microorganisms at the surface of materials is the first step in microbial development and post-surgical infections (Costerton et al., 1999; Stickler & McLean, 1995). Adhesion of bacteria on a surface can be the result of non-specific interactions (electrostatic, hydrophobic, Van der Waals forces) and specific interactions (receptor–adhesion interactions) (Nagel et al., 1996). One way to reduce the interactions and the adhesion of microorganisms is to add a coating that repels the adsorption of macromolecules (Korica et al., 2018; Ladam, Gergely, et al., 2000; Ratner et al., 2004). Since many polyelectrolytes have inhibitory activity on bacteria, multilayers based on polyelectrolytes have been used for the development of coating with antimicrobial or non-

adhesion properties. In 2021, Petrila *et al.* reported that CHI (chitosan) and HA (hyaluronic acid) were the most commonly used for this type of materials. In particular, CHI/HA multilayer coating has been found to reduce the development of *Escherichia coli*, *Staphylococcus aureus* and *Candida albicans* onto the surfaces (Taketa *et al.*, 2021). Moreover, the integration in multilayer films of inorganic compounds with antibacterial activity, such as silver nanoparticles, can further inhibit the microorganisms (Francesko *et al.*, 2018; Taketa *et al.*, 2021).

Electrochemical biosensors. The development of biosensors for the easy identification and quantification of biological signals is one of the great challenges in biomedical research. The electrical properties of polyelectrolytes and their ability to interact with charged macromolecules makes them great candidates for the elaboration of electrochemical biosensors (Brynda *et al.*, 1998; Iost & Crespilho, 2012). In fact, the immobilization of active compounds such as proteins, enzymes or DNA in polyelectrolyte multilayers allows a better stability of biosensors, as well as a selective barrier for the substrate analyzed (Taketa *et al.*, 2020; Zhao *et al.*, 2006). The principle of such biosensors is the specific chemical reaction between immobilized compounds and substrate. The chemical response results in an electrical response that can be detected by an electrode. Moreover, the variety of species that can be immobilized in multilayers for biosensors is another advantage of the method. From 1995, Lvov *et al.* proposed the assembly of LbL films with water-soluble proteins such as cytochrome, myoglobin, lysozyme, hemoglobin, glucoamylase and glucose oxidase (Lvov *et al.*, 1995). An example of biosensors is reported by Calvo *et al.* who proposed the use of glucose oxidase in organized multilayers, constituted by alternative enzyme layers and layers of an osmium derivatized poly(allylamine), acting as redox relays (Calvo *et al.*, 2002). Authors successfully controlled the chemical reaction and electrical signal by varying the position of active enzyme within the film.

4.1.2. Environmental applications

Pollutants in water and water waste are the normal result of human activity, which leads to the degradation of ecosystems and numerous health risks for species, including humans. Apart from the high plastic pollution in water (especially in ocean), a high diversity of contaminants can be found in water waste, called emerging contaminants (Abdulrazaq *et*

al., 2020; Rasheed et al., 2019). Those emerging contaminants are identified by the NORMAN network in an updated list, which highlights pharmaceuticals, pesticides, endocrine disruptors, parabens, repellents, UV filters, dyes as the main contaminants. Due to their low degradability in aqueous media, their dangers are especially concerning in the long term. Moreover, their low concentration and specificity (size, chemical properties) makes them difficult to be removed by conventional depollution methods (Neerugatti et al., 2022).

Filtration membranes. The modification of porous materials by LbL coating allows to control the pores sizes/permeability for filtration but also the charges on the surface of the material for a high selectivity (Boyd & Zydney, 1997; Escobar-Ferrand et al., 2014; Fong et al., 2021; Joseph et al., 2014). The functionalization of porous materials *via* the introduction of charges leads to attraction/repulsion of oppositely charged compounds, which can be used for separation of pollutants from water. The development of membranes based on polyelectrolytes multilayers and in particular, for nanofiltration, ultrafiltration, reverse osmosis and solvent resistant nanofiltration, are promising techniques for environmental depollution using polyelectrolyte multilayers (Joseph et al., 2014). The efficiency of such polyelectrolyte membranes can vary with the structure and morphology of the multilayer, and thus, by adjusting the experimental conditions of the LbL assembly. Nanofiltration, ultrafiltration and reverse osmosis are pressure-driven membrane techniques, for which the difference results in the pressure range: 1 to 5 bar for ultrafiltration, 5 to 20 bar for nanofiltration and from 10 bar upwards for reverse osmosis (S. Cheng et al., 2011; Joseph et al., 2014). The solute is transported through the material depending on both the pore size and the charge of the membrane. The retention of the solutes, illustrated on Figure 1.17, occurs through electrostatic and sieving effects/steric hindrance.

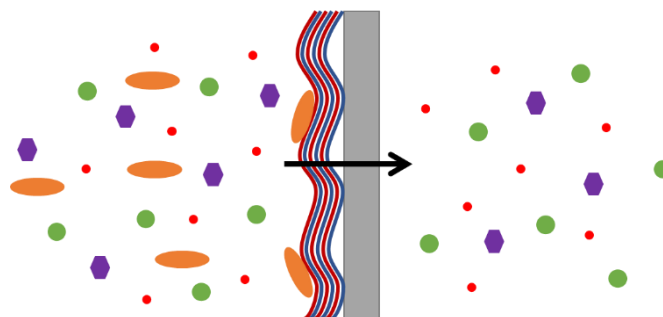


Figure 1.17. Schematic representation: principle of a filtration membrane based on polyelectrolyte multilayers.

In particular, poly(acrylic acid)/poly(allylamine hydrochloride) PAA/PAH multilayers deposition has shown great potential for filtration. Ilyas *et al.* demonstrated that its retention capacity and selectivity were highly dependent on the pH of membrane formation: at pH = 6, the retention was better for organic pollutants, while a pH = 3.5 for PAA and/or PAH results in a better retention for charged micropollutants (Ilyas *et al.*, 2015). PAH/PAA multilayers membranes also present a great efficiency for sulfamethoxazole, SO_4^{2-} ions and other pharmaceutical molecules' removal from water (L. Liu *et al.*, 2018; Werber *et al.*, 2016). The same membranes also present potential for desalination of seawater with respectively 58% and 65% sodium ions rejection for 60 bilayers and 120 bilayers on polysulfone membrane (Fadhillah *et al.*, 2013). On the same principle, polyelectrolytes multilayers have been studied for the elaboration of solvent resistant nanofiltration for contaminants in organic feeds (Ahmadiannamini *et al.*, 2012; Ilyas *et al.*, 2016; X. Li *et al.*, 2008).

Multilayers sorbents. Polyelectrolyte multilayers has been used to develop sorbents *i.e.* composites with good sorption properties. Among the polyelectrolyte multilayers studied for the development of sorbents, it should be noted that weak polyelectrolytes are the most used because of their ionic groups which can interact with pollutants (Bucatariu *et al.*, 2021; Ding *et al.*, 2009). One of the applications of those materials is the removal of heavy metals as proposed by Bucatariu *et al.* The research group reported the formation of PEI/PAA multilayer cross-linked with glutaraldehyde coating on silica for the retention of Cu^{2+} , Ni^{2+} , Co^{2+} and Cd^{2+} ions (Bucatariu, Schwarz, *et al.*, 2020). They also formed composites with PEI, PLL, poly(vinyl alcohol) PVA, PAH and PAA on silica as well, with high affinity with metal ions (Bucatariu, Ghiorghita, *et al.*, 2020). The multilayer sorbents showed a better sorption capacity with the increase of functional groups available to interact with ions.

4.2. Colorimetric devices for enzyme detection

4.2.1. Structural colors of multilayer films

One of the features of multilayers films can be the structural colors obtained due to interferences phenomena between the light reflected from the air/film and film/substrate interfaces. This phenomenon *i.e.* quarter-wave Bragg stack is well known as the cause of intense coloration of butterfly wings, skin of snakes, hummingbirds and the shell of arthropods (Fu *et al.*, 2016). It results from reflective interferences by stacked thin film layers

of alternating high and low index of refraction materials as illustrated on Figure 1.18a (Macleod & Macleod, 2010). Alternating regions of high and low refractive index cause constructive and destructive interferences of the incident light, yielding a reflectance band centered at the desired wavelength. In some variety of animal species, it has been proved that alternating layers of chitin with different refractive index are responsible of their apparent color (Leertouwer et al., 2011). The architectures of multilayers can mimic the layered structure of natural systems that leads to optical interferences effect and structural colors. When the thin film is composed of alternating layers with refraction indexes close to each other, the film can be assimilated to a single layer films with a reflectance determined by film thickness as described in Figure 1.18b (Schauer et al., 2003). Thus, the phenomenon has been observed for several type of thin films based on alternative layers of two or more compounds, including spin-coated natural polymer multilayers (C. Cerclier et al., 2010; Cranston & Gray, 2006; Schauer et al., 2003).

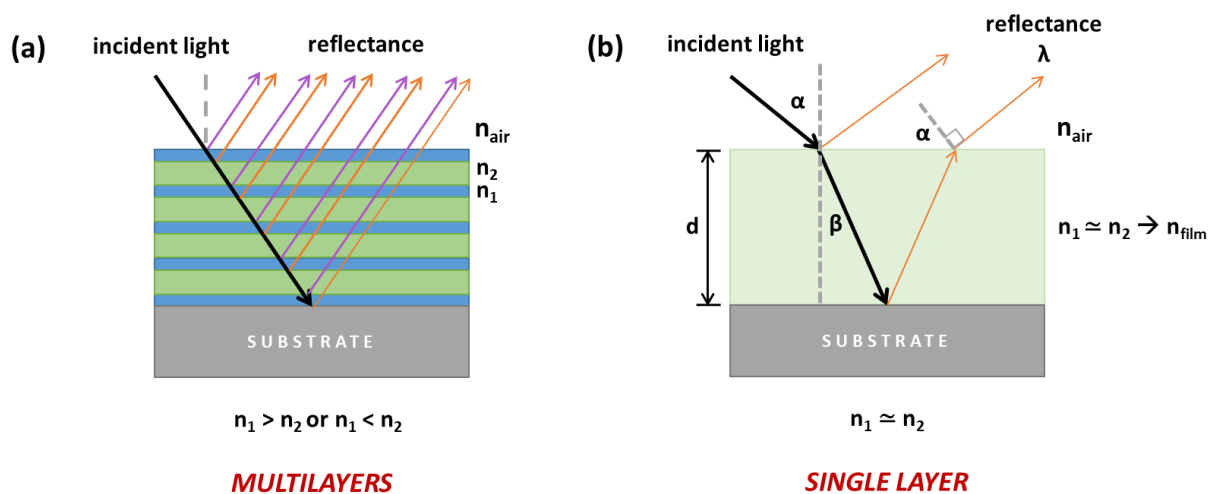


Figure 1.18. Schematic representation of light reflected and optical interferences in (a) a multilayered structure based on two layers with different refractive index n_1 and n_2 and in (b) a single layer or a film appared to a single-layered structure based on layers with the same, or almost, refractive index n_{film} .

For single layer films (Figure 1.18b) and $n_{film} > n_{air}$, the wavelength of the reflectance light can be predicted by Bragg's law (Alfrey et al., 1969). It can be related to the thickness of the film and the refractive index of the film by the simple relationship given by Equation 0, which results from the constructive interferences of the incident light.

$$\lambda = 2d \cdot n_{film} m \quad (0)$$

where d is the thickness of the film, λ is the wavelength of the incident light, n_{film} is the refractive index of the film, and m ($m=0, 1, 2, 3, \dots$) is an integer related to the number of reflection maxima.

Thus, the structural colors of those films can change due to the modification of different optical properties and their thickness. First, a change or an alteration in the physico-chemical properties of layers can lead to a different index of refraction n_{film} for the multilayer film (Z. Dong et al., 2019; Kurt et al., 2009). Multiple factors can result in such a change such as modification of the experimental conditions, degradation of the film or change in porosity due to stimuli-responsivity (C. V. Cerclier et al., 2013). Secondly, the optical distance d can be modified by increasing the number of layers/bilayers, changing the experimental conditions and/or by a swelling or shrinking of the LbL assembly. For instance, Wågberg *et al.* studied the change of interference colors of films based on microfibrillated cellulose and different polycations, at different ionic strength and different pH (Wågberg et al., 2008). They reported a really visible change in structural colors with increasing the number of layers of microfibrillated cellulose and poly(ethyleneimine) films (Figure 1.19).

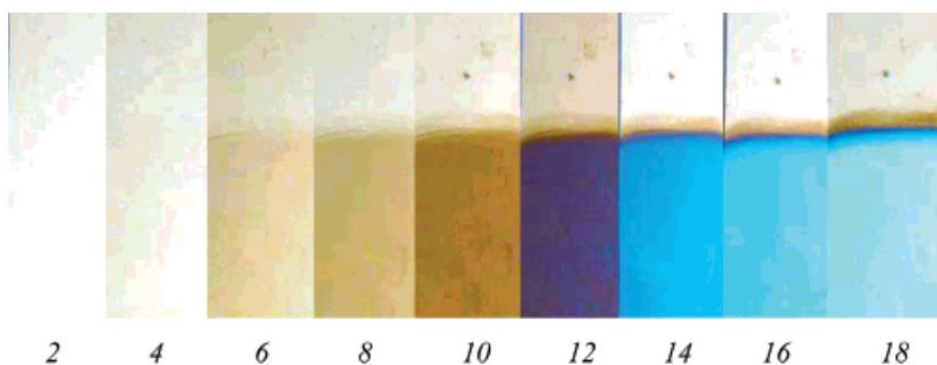


Figure 1.19. Structural colors from LbL films of microfibrillated cellulose and poly(ethyleneimine) as a function of the number of layers (18 layers is 9 layers of microfibrillated cellulose and 9 layers of poly(ethyleneimine)), from (Wågberg et al., 2008).

4.2.2. Enzyme-sensitive multilayers

The advantage of choosing natural polymers for polyelectrolytes-based structures is their sensitivity to enzymes allowing the elaboration of enzyme-degradable devices (Itoh et al., 2006, 2008a). In these systems, the release of active molecules is controlled by the selection of the type and quantity of enzymes. The first use of the sensitivity of natural

polymers to enzymes is the enzyme-triggered release of active molecules for drug delivery, which is illustrated in Figure 1.20a. Itoh's research group demonstrated the biodegradability of (CHI/DexS) capsules by using chitosanase that hydrolyzes CHI resulting in capsules deformation and degradation (Itoh et al., 2006). Later on, authors also proposed to tune the degradation of multilayered composites containing other enzyme-sensitive polyelectrolytes such as poly-L-lysine (PLL) that can be degraded by α -chymotrypsin. The formation of (CHI/DexS/PLL) allowed the stepwise release of multiple proteins at different times from i) degradation of PLL in a first step and then ii) degradation of CHI. More combinations for a controlled release can be designed based on the choice of polyelectrolyte/enzyme couple and on the characteristics (porosity, pH-responsivity, *etc.*) of the multilayer obtained.

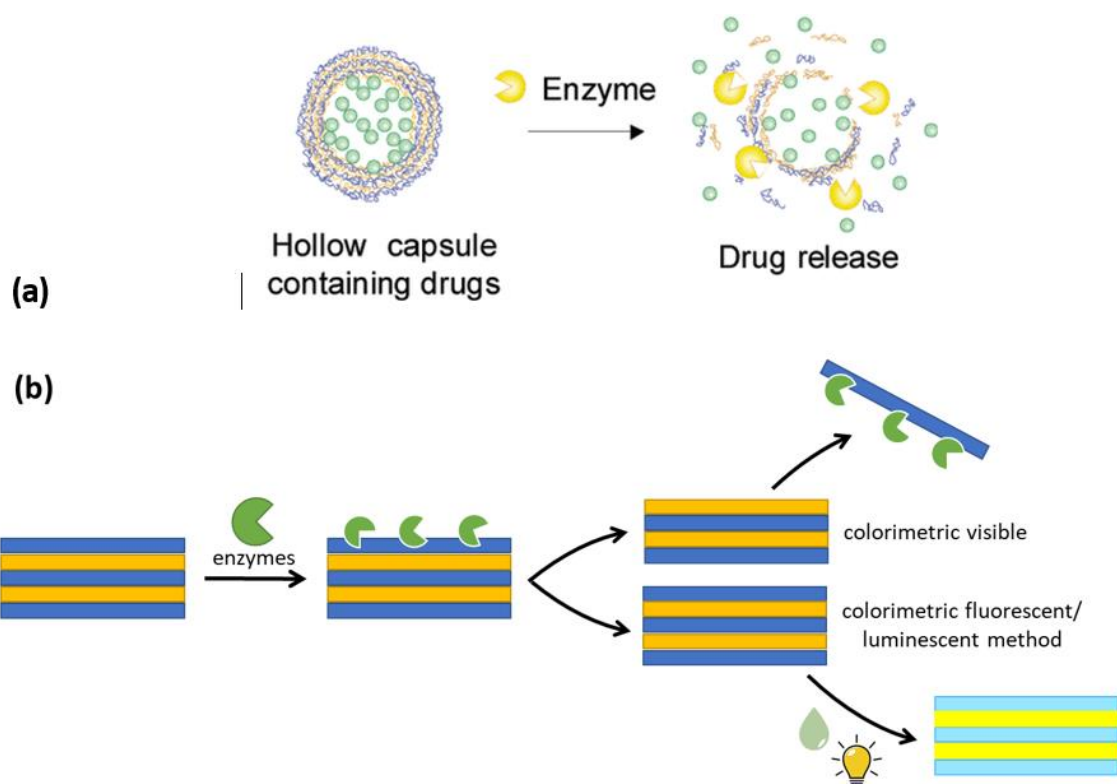


Figure 1.20. (a) Schematic representation of release system of encapsulated drug with enzymatic degradation, adapted with permission from (Itoh et al., 2006), © 2006 American Chemical Society. (b) Schematic representation of optical change induced by the action of enzymes on polyelectrolyte multilayers.

The sensitivity of polyelectrolytes to specific enzymes is also an approach to develop biosensors for enzyme detection based on a biorecognition of enzymes in the environment. For electrochemical biosensors, detailed in section 4.1.1., the chemical reaction between the substrate and the enzymes results in an electric signal that can be detected with an electrode.

However, the action of enzymes on multilayers can also be used for the development of optical biosensors. The reaction of a specific polyelectrolyte to the enzyme then causes an optical interaction, directly or by applying a colorimetric fluorescent as described in Figure 1.20b. Especially, the use of bio-sourced polyelectrolytes, such as polysaccharides and/or polypeptides, offer a wide range of possibilities due to their enzymatic sensitivity. Main bio-based polyelectrolytes/enzyme pairs found in literature are summarized in Table 1.5.

Table 1.5. Polyelectrolytes and their specific enzymes used in enzyme-based degradation of multilayers that can be found in literature.

Polyelectrolyte (polycation/polyanion)	Enzyme(s)	Ref
Poly-L-lysine (polycation)	trypsin, α -chymotrypsin, pronase	(Itoh et al., 2006; Marchenko et al., 2012; Ren et al., 2006)
Chitosan (polycation)	chitosanase, lysozyme	(Picart et al., 2005; Serizawa et al., 2002)
Hyaluronan	hyaluronidase	(Picart et al., 2005)
Protamine (polycation)	trypsin	(Radhakrishnan & Raichur, 2012)
DNA (polyanion)	endonuclease deoxyribonuclease I	(Serizawa, Yamaguchi, & Akashi, 2003)
Poly-L-arginine (polycation)	pronase, trypsin, α -chymotrypsin, glutamyl endopeptidase	(Craig et al., 2012; Lomova et al., 2015; Marchenko et al., 2012; Webber et al., 2017)
Poly-L-aspartic acid (polyanion)	pronase	(Marchenko et al., 2012)
Poly-L-glumatic acid (polyanion)	pronase, glutamyl endopeptidase	(Craig et al., 2012; Marchenko et al., 2012)
Herapin (polyanion)	herapinase	(L. Sun et al., 2017)
Cellulose (polyanion)	cellulase	(C. Cerclier et al., 2010; C. V. Cerclier et al., 2013)
Cationic xylan (polycation)	xylanase	(Dammak et al., 2013; Schaubeder et al., 2022)

In addition to polyelectrolytes sensitive to enzymes, LbL technique allows to integrate uncharged macromolecules into multilayers by adsorption, which can be sensitive to certain microorganisms. In the early 2010s, Cerclier *et al.* from our research team proposed to form multilayer films with xyloglucan, irreversibly adsorbed by hydrogen bonding and van der Waals forces onto nanocellulose. As function of film thickness, the brown or blue films were obtained (Figure 1.21) and were subjected to the action of cellulase mixture, as cellulolytic enzymes can hydrolyze both cellulose and xyloglucans (C. Cerclier et al., 2010). The demonstration of the enzymatic degradation (Figure 1.21) is evidenced through the change to the naked eye of the structural colors of the thin films, resulting from the interferences phenomena described in section 4.2.1. Later on, they demonstrated the impact of different factors and different architectural features on the enzymatic degradation (polysaccharides accessibility, porosity, cross-linking) (C. V. Cerclier et al., 2013; Guyomard-Lack et al.,

2012). Our research team also studied the degradation of cellulose multilayers coated with cationic xylan by action of xylanase (Dammak et al., 2013). This work then inspired the development of a xylan-cellulose thin film platform to study the digestion of xylans by xylanase (Schaubeder et al., 2022).

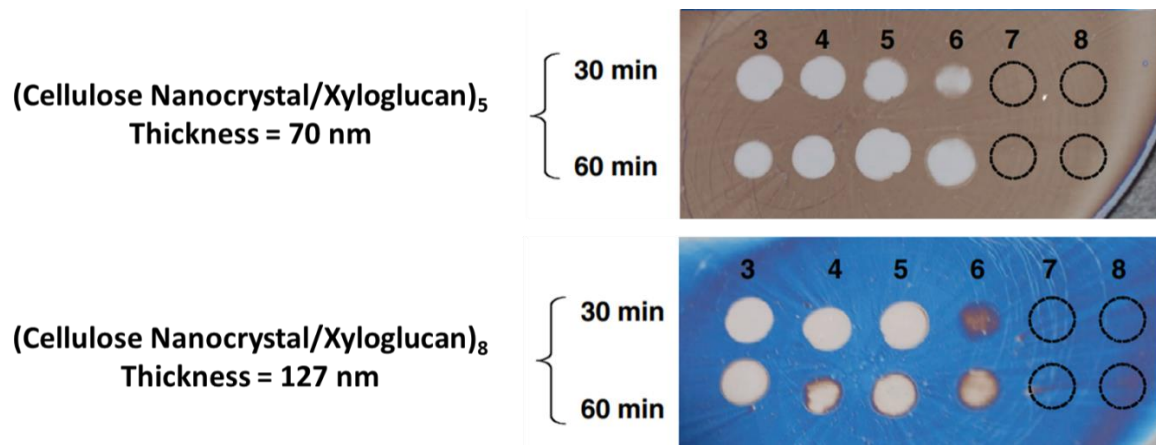


Figure 1.21. Enzyme-induced degradation photos of multilayer films composed of 5 bilayers and 8 bilayers of cellulose nanocrystals/xyloglucans after the deposition of enzyme droplet at different concentrations (spots 3 to 8) during 30 and 60 min.

Conclusion

Nanomaterials based on dextran and dextran derivatives built by LbL method present promising applications in biomedical fields due to their biocompatibility and their biodegradability. Dextrans and dextran derivatives have been successfully introduced into multilayer films and structures with control over film growth and characteristics by adjusting processing parameters. Among derivatives, dextran sulfate seems to present the greatest interest for the research community for its many biological properties such as anticoagulant, anti-inflammatory and anti-viral properties. Moreover, its great compatibility with other polysaccharides (chitosan, cellulose, etc.), polyarginines, poly-L-lysine (PLL) and protein (insulin, etc.), allow to form biodegradable multilayers useful for drug delivery systems in particular.

Although studies on the applicability of dextrans and dextran derivatives into multilayers and multilayered objects can be found with various polyelectrolytes, there is a need for deeper understanding of most dextran-based LbL assemblies beside the well-studied DexS. Works considering other dextran derivatives, such as carboxymethyl dextran, diethylaminoethyl dextran (DEAE-Dex) or other aminated dextrans, are seldom and dedicated to specific applications so that it is difficult to determine the key parameters controlling the film growth. Commercially available dextran derivatives are still restricted and the chemical functionalization of dextrans limits the employment of dextran derivatives in the development of innovative structures. Development of new functionalization routes for dextrans is promising to extend the range of dextran derivatives, with a better environmental impact and diversified functional properties. One of them is to explore an enzymatic approach to the custom synthesis of polyelectrolytes based on microbial polysaccharides such as dextrans. In addition to finely controlled structures and molar masses of dextrans, designed enzymes may improve the properties of α -glucans with charged groups (Moulis et al., 2021).

Moreover, apart from extensive research on (CHI/DexS) multilayer films and structures, only a few studies reported LbL assemblies with other polyelectrolyte counterparts than chitosan. Functional groups in dextran derivatives as well as their wide variety of chemical structures offer possibilities for adsorption. A wider range of other biocompatible and biodegradable functional species from mineral nanoparticles to polypeptides needs to be explored in the coming years and will give opportunities for controlled elaboration of dextran-based multilayer nanoobjects.

Finally, studies and applications mostly focused on biomedical fields with drug delivery applications. The possibility to control the film morphology and the surface pattern of dextran-based multilayers give new opportunities to create specific surfaces or specific objects that can be used in broader application areas. This includes nano-printing and nano-lithography processes used to fabricate patterns at nanometric scales (Vigneswaran et al., 2014) but also, the possibility of obtaining super-hydrophobic coating by tuning hydrophobicity found and developed for cell adhesion and proliferation (Jafari et al., 2019; Sethi & Manik, 2018; W. Song et al., 2010). In this thesis, we have chosen to study the capacity of dextran-based multilayers for the development of colorimetric assay (especially for enzyme detection) due to the presence of visible structural colors.

References

- Abdulrazaq, Y., Abdulsalam, A., Rotimi, A. L., Abdulbasit, A. A., Clifford, O., Abdulsalam, O. A., Racheal, O. N., Joy, A. A., Victor, F. O., Johannes, Z. M., & others. (2020). Classification, potential routes and risk of emerging pollutants/contaminant. In *Emerging Contaminants*. IntechOpen.
- Abid, N., Khan, A. M., Shujait, S., Chaudhary, K., Ikram, M., Imran, M., Haider, J., Khan, M., Khan, Q., & Maqbool, M. (2022). Synthesis of nanomaterials using various top-down and bottom-up approaches, influencing factors, advantages, and disadvantages: A review. *Advances in Colloid and Interface Science*, 300, 102597. <https://doi.org/10.1016/j.cis.2021.102597>
- Ahmad, N. H., Mustafa, S., & Man, Y. B. C. (2015). Microbial Polysaccharides and Their Modification Approaches: A Review. *International Journal of Food Properties*, 18(2), 332–347. <https://doi.org/10.1080/10942912.2012.693561>
- Ahmadiannamini, P., Li, X., Goyens, W., Joseph, N., Meesschaert, B., & Vankelecom, I. F. J. (2012). Multilayered polyelectrolyte complex based solvent resistant nanofiltration membranes prepared from weak polyacids. *Journal of Membrane Science*, 394–395, 98–106. <https://doi.org/10.1016/j.memsci.2011.12.032>
- Alfrey, T., Gurnee, E. F., & Schrenk, W. J. (1969). Physical optics of iridescent multilayered plastic films. *Polymer Engineering and Science*, 9(6), 400–404. <https://doi.org/10.1002/pen.760090605>
- Ali Said, F., Bousserhine, N., Alphonse, V., Michely, L., & Belbekhouche, S. (2020). Antibiotic loading and development of antibacterial capsules by using porous CaCO₃ microparticles as starting material. *International Journal of Pharmaceutics*, 579, 119175. <https://doi.org/10.1016/j.ijpharm.2020.119175>
- Alkekha, D., & Shukla, A. (2019). Influence of poly- L -lysine molecular weight on antibacterial efficacy in polymer multilayer films. *Journal of Biomedical Materials Research Part A*, 107(6), 1324–1339. <https://doi.org/10.1002/jbm.a.36645>
- Anandhakumar, S., Mahalakshmi, V., & Raichur, A. M. (2012). Silver nanoparticles modified nanocapsules for ultrasonically activated drug delivery. *Materials Science & Engineering C-Materials for Biological Applications*, 32(8), 2349–2355. <https://doi.org/10.1016/j.msec.2012.07.006>
- Anandhakumar, S., Vijayalakshmi, S. P., Jagadeesh, G., & Raichur, A. M. (2011). Silver Nanoparticle Synthesis: Novel Route for Laser Triggering of Polyelectrolyte Capsules. *ACS Applied Materials & Interfaces*, 3(9), 3419–3424. <https://doi.org/10.1021/am200651t>
- Anirudhan, T. S., Sekhar, C., V., Shainy, F., & Thomas, J. P. (2019). Effect of dual stimuli responsive dextran/nanocellulose polyelectrolyte complexes for chemophotothermal synergistic cancer therapy. *International Journal of Biological Macromolecules*, 135, 776–789. <https://doi.org/10.1016/j.ijbiomac.2019.05.218>
- Antipov, A. A., Shchukin, D., Fedutik, Y., Petrov, A. I., Sukhorukov, G. B., & Möhwald, H. (2003). Carbonate microparticles for hollow polyelectrolyte capsules fabrication. *Colloids and Surfaces A: Physicochemical and Engineering Aspects*, 224(1–3), 175–183. [https://doi.org/10.1016/S0927-7757\(03\)00195-X](https://doi.org/10.1016/S0927-7757(03)00195-X)
- Antipov, A. A., Sukhorukov, G. B., Donath, E., & Möhwald, H. (2001). Sustained Release Properties of Polyelectrolyte Multilayer Capsules. *The Journal of Physical Chemistry B*, 105(12), 2281–2284. <https://doi.org/10.1021/jp002184+>
- Antonini, E., Bellelli, L., Bruzzesi, M. R., Caputo, A., Chiancone, E., & Rossi-Fanelli, A. (1964). Studies on dextran and dextran derivatives. I. Properties of native dextran in different solvents. *Biopolymers*, 2(1), 27–34. <https://doi.org/10.1002/bip.1964.360020105>
- Ariga, K., Lvov, Y., & Kunitake, T. (1997). Assembling Alternate Dye–Polyion Molecular Films by Electrostatic Layer-by-Layer Adsorption. *Journal of the American Chemical Society*, 119(9), 2224–2231. <https://doi.org/10.1021/ja963442c>
- Ariga, K., Lvov, Y. M., Kawakami, K., Ji, Q., & Hill, J. P. (2011). Layer-by-layer self-assembled shells for drug delivery. *Advanced Drug Delivery Reviews*, 63(9), 762–771. <https://doi.org/10.1016/j.addr.2011.03.016>
- Arnon-Rips, H., & Poverenov, E. (2018). Improving food products’ quality and storability by using Layer by Layer edible coatings. *Trends in Food Science & Technology*, 75, 81–92. <https://doi.org/10.1016/j.tifs.2018.03.003>
- Averin, P. S., de Gerenyu, A. V. L., & Balabushevich, N. G. (2016). Polyelectrolyte Micro- and Nanoparticles with Doxorubicin. *Moscow University Chemistry Bulletin*, 71(2), 140–145. <https://doi.org/10.3103/S0027131416020012>
- Azzaroni, O., & Lau, K. H. A. (2011). Layer-by-layer assemblies in nanoporous templates: nano-organized design and applications of soft nanotechnology. *Soft Matter*, 7(19), 8709. <https://doi.org/10.1039/c1sm05561e>
- Baig, N., Kammakam, I., & Falath, W. (2021). Nanomaterials: a review of synthesis methods, properties, recent progress, and challenges. *Materials Advances*, 2(6), 1821–1871. <https://doi.org/10.1039/D0MA00807A>
- Balabushevich, N. G., de Guereny, A. V. L., Feoktistova, N. A., Skirtach, A. G., & Volodkin, D. (2016). Protein-Containing Multilayer Capsules by Templating on Mesoporous CaCO₃ Particles: POST- and PRE-Loading Approaches. *Macromolecular Bioscience*, 16(1), 95–105. <https://doi.org/10.1002/mabi.201500243>
- Balabushevich, N. G., & Larionova, N. I. (2009). Protein-loaded microspheres prepared by sequential adsorption of dextran sulphate and protamine on melamine formaldehyde core. *Journal of Microencapsulation*, 26(7), 571–579. <https://doi.org/10.3109/02652040802518145>
- Balabushevich, N. G., Lebedeva, O. V., Vinogradova, O. I., & Larionova, N. I. (2006). Polyelectrolyte assembling for protein microencapsulation. *Journal of Drug Delivery Science and Technology*, 16(4), 315–319. [https://doi.org/10.1016/S1773-2247\(06\)50056-5](https://doi.org/10.1016/S1773-2247(06)50056-5)

- Balabushevich, N. G., Pechenkin, M. A., Shibanova, E. D., Volodkin, D. V., & Mikhalechik, E. V. (2013). Multifunctional Polyelectrolyte Microparticles for Oral Insulin Delivery. *Macromolecular Bioscience*, 13(10), 1379–1388. <https://doi.org/10.1002/mabi.201300207>
- Balabushevich, N., & Larionova, N. (2004). Fabrication and characterization of polyelectrolyte microparticles with protein. *Biochemistry-Moscow*, 69(7), 757–762. <https://doi.org/10.1023/B:BIRY.0000040200.61663.01>
- Balabushevich, N., Sukhorukov, G., & Larionova, N. (2005). Polyelectrolyte multilayer microspheres as carriers for bienzyme system: Preparation and characterization. *Macromolecular Rapid Communications*, 26(14), 1168–1172. <https://doi.org/10.1002/marc.200500141>
- Bamford, C. H., Middleton, I. P., & Al-Lamee, K. G. (1986). Studies of the esterification of dextran: routes to bioactive polymers and graft copolymers. *Polymer*, 27(12), 1981–1985. [https://doi.org/10.1016/0032-3861\(86\)90194-1](https://doi.org/10.1016/0032-3861(86)90194-1)
- Bastarrachea, L., Wong, D., Roman, M., Lin, Z., & Goddard, J. (2015). Active Packaging Coatings. *Coatings*, 5(4), 771–791. <https://doi.org/10.3390/coatings5040771>
- Bellanger, H., Casdorff, K., Muff, L. F., Ammann, R., Burgert, I., & Michen, B. (2017). Layer-by-layer deposition on a heterogeneous surface: Effect of sorption kinetics on the growth of polyelectrolyte multilayers. *Journal of Colloid and Interface Science*, 500, 133–141. <https://doi.org/10.1016/j.jcis.2017.02.048>
- Benni, S., Avramoglou, T., Hlawaty, H., & Mora, L. (2014). Dynamic Contact Angle Analysis of Protein Adsorption on Polysaccharide Multilayer's Films for Biomaterial Reendothelialization. *Biomed Research International*. <https://doi.org/10.1155/2014/679031>
- Bieker, P., & Schönhoff, M. (2010). Linear and Exponential Growth Regimes of Multilayers of Weak Polyelectrolytes in Dependence on pH. *Macromolecules*, 43(11), 5052–5059. <https://doi.org/10.1021/ma1007489>
- Biji, K. B., Ravishankar, C. N., Mohan, C. O., & Srinivasa Gopal, T. K. (2015). Smart packaging systems for food applications: a review. *Journal of Food Science and Technology*, 52(10), 6125–6135. <https://doi.org/10.1007/s13197-015-1766-7>
- Bonderer, L. J., Studart, A. R., & Gauckler, L. J. (2008). Bioinspired Design and Assembly of Platelet Reinforced Polymer Films. *Science*, 319(5866), 1069–1073. <https://doi.org/10.1126/science.1148726>
- Borges, J., & Mano, J. F. (2014). Molecular Interactions Driving the Layer-by-Layer Assembly of Multilayers. *Chemical Reviews*, 114(18), 8883–8942. <https://doi.org/10.1021/cr400531v>
- Boudou, T., Crouzier, T., Ren, K., Blin, G., & Picart, C. (2010). Multiple Functionalities of Polyelectrolyte Multilayer Films: New Biomedical Applications. *Advanced Materials*, 22(4), 441–467. <https://doi.org/10.1002/adma.200901327>
- Bovey, F. A. (1959). Enzymatic polymerization. I. Molecular weight and branching during the formation of dextran. *Journal of Polymer Science*, 35(128), 167–182. <https://doi.org/10.1002/pol.1959.1203512813>
- Boyd, R., & Zydney, A. (1997). Sieving characteristics of multilayer ultrafiltration membranes. *Journal of Membrane Science*, 131(1–2), 155–165. [https://doi.org/10.1016/S0376-7388\(97\)00045-8](https://doi.org/10.1016/S0376-7388(97)00045-8)
- Braconnot, H. (1813). Expériences Sur un Acide Particulier qui se Développe Dans les Matières Acescentes. *Ann. Chim*, 86, 84–100.
- Brynda, E., & Houska, M. (1998). Preparation of organized protein multilayers. *Macromolecular Rapid Communications*, 19(4), 173–176. [https://doi.org/10.1002/\(SICI\)1521-3927\(19980401\)19:4<173::AID-MARC173>3.0.CO;2-S](https://doi.org/10.1002/(SICI)1521-3927(19980401)19:4<173::AID-MARC173>3.0.CO;2-S)
- Brynda, E., Houska, M., Brandenburg, A., Wikerstal, A., & Skvor, J. (1999). The detection of human beta(2)-microglobulin by grating coupler immunosensor with three dimensional antibody networks. *Biosensors & Bioelectronics*, 14(4), 363–368. [https://doi.org/10.1016/S0956-5663\(99\)00013-5](https://doi.org/10.1016/S0956-5663(99)00013-5)
- Brynda, E., Houska, M., Skvor, J., & Ramsden, J. (1998). Immobilisation of multilayer bioreceptor assemblies on solid substrates. *Biosensors & Bioelectronics*, 13(2), 165–172. [https://doi.org/10.1016/S0956-5663\(97\)00107-3](https://doi.org/10.1016/S0956-5663(97)00107-3)
- Bucatariu, F., Ghiorghita, C.-A., Zaharia, M.-M., Schwarz, S., Simon, F., & Mihai, M. (2020). Removal and Separation of Heavy Metal Ions from Multicomponent Simulated Waters Using Silica/Polyethyleneimine Composite Microparticles. *ACS Applied Materials & Interfaces*, 12(33), 37585–37596. <https://doi.org/10.1021/acsami.0c10283>
- Bucatariu, F., Schwarz, D., Zaharia, M., Steinbach, C., Ghiorghita, C.-A., Schwarz, S., & Mihai, M. (2020). Nanostructured polymer composites for selective heavy metal ion sorption. *Colloids and Surfaces A: Physicochemical and Engineering Aspects*, 603, 125211. <https://doi.org/10.1016/j.colsurfa.2020.125211>
- Bucatariu, F., Teodosiu, C., Morosanu, I., Fighir, D., Ciobanu, R., Petrila, L.-M., & Mihai, M. (2021). An Overview on Composite Sorbents Based on Polyelectrolytes Used in Advanced Wastewater Treatment. *Polymers*, 13(22), 3963. <https://doi.org/10.3390/polym13223963>
- Burton, B. A., & Brant, D. A. (1983). Comparative flexibility, extension, and conformation of some simple polysaccharide chains. *Biopolymers*, 22(7), 1769–1792. <https://doi.org/10.1002/bip.360220712>
- Bütergerds, D., Cramer, C., & Schönhoff, M. (2017). pH-Dependent Growth Laws and Viscoelastic Parameters of Poly- L - Lysine/Hyaluronic Acid Multilayers. *Advanced Materials Interfaces*, 4(1), 1600592. <https://doi.org/10.1002/admi.201600592>
- Cai, H., Wang, P., & Zhang, D. (2019). pH-responsive linkages-enabled layer-by-layer assembled antibacterial and antiadhesive multilayer films with polyelectrolyte nanocapsules as biocide delivery vehicles. *Journal of Drug Delivery Science and Technology*, 54. <https://doi.org/10.1016/j.jddst.2019.101251>

- Calvo, E. J., Danilowicz, C., & Wolosiuk, A. (2002). Molecular “Wiring” Enzymes in Organized Nanostructures. *Journal of the American Chemical Society*, 124(11), 2452–2453. <https://doi.org/10.1021/ja017802u>
- Canova, D. F., Pavlov, A. M., Norling, L. V., Gobetti, T., Brunelleschi, S., Le Fauder, P., Cenac, N., Sukhorukov, G. B., & Perretti, M. (2015). Alpha-2-macroglobulin loaded microcapsules enhance human leukocyte functions and innate immune response. *Journal of Controlled Release*, 217, 284–292. <https://doi.org/10.1016/j.jconrel.2015.09.021>
- Carosio, F., Colonna, S., Fina, A., Rydzek, G., Hemmerlé, J., Jierry, L., Schaaf, P., & Boulmedais, F. (2014). Efficient Gas and Water Vapor Barrier Properties of Thin Poly(lactic acid) Packaging Films: Functionalization with Moisture Resistant Nafion and Clay Multilayers. *Chemistry of Materials*, 26(19), 5459–5466. <https://doi.org/10.1021/cm501359e>
- Cerclier, C., Cousin, F., Bizot, H., Moreau, C., & Cathala, B. (2010). Elaboration of Spin-Coated Cellulose-Xyloglucan Multilayered Thin Films. *Langmuir*, 26(22), 17248–17255. <https://doi.org/10.1021/la102614b>
- Cerclier, C. V., Guyomard-Lack, A., Cousin, F., Jean, B., Bonnin, E., Cathala, B., & Moreau, C. (2013). Xyloglucan–Cellulose Nanocrystal Multilayered Films: Effect of Film Architecture on Enzymatic Hydrolysis. *Biomacromolecules*, 14(10), 3599–3609. <https://doi.org/10.1021/bm400967e>
- Chen, Y., Ji, T., & Rosenzweig, Z. (2003). Synthesis of glyconanospheres containing luminescent CdSe–ZnS quantum dots. *Nano Letters*, 3(5), 581–584. <https://doi.org/10.1021/nl034086g>
- Cheng, L., Wang, X., Gong, F., Liu, T., & Liu, Z. (2020). 2D Nanomaterials for Cancer Theranostic Applications. *Advanced Materials*, 32(13), 1902333. <https://doi.org/10.1002/adma.201902333>
- Cheng, S., Oatley, D. L., Williams, P. M., & Wright, C. J. (2011). Positively charged nanofiltration membranes: Review of current fabrication methods and introduction of a novel approach. *Advances in Colloid and Interface Science*, 164(1–2), 12–20. <https://doi.org/10.1016/j.cis.2010.12.010>
- Chludzinski, A. M., Germaine, G. R., & Schachtele, C. F. (1974). Purification and properties of dextransucrase from *Streptococcus mutans*. *Journal of Bacteriology*, 118(1), 1–7.
- Cho, C., Xiang, F., Wallace, K. L., & Grunlan, J. C. (2015). Combined Ionic and Hydrogen Bonding in Polymer Multilayer Thin Film for High Gas Barrier and Stretchiness. *Macromolecules*, 48(16), 5723–5729. <https://doi.org/10.1021/acs.macromol.5b01279>
- Choi, J., & Rubner, M. F. (2005). Influence of the Degree of Ionization on Weak Polyelectrolyte Multilayer Assembly. *Macromolecules*, 38(1), 116–124. <https://doi.org/10.1021/ma048596o>
- Clark, S. L., & Hammond, P. T. (2000). The Role of Secondary Interactions in Selective Electrostatic Multilayer Deposition. *Langmuir*, 16(26), 10206–10214. <https://doi.org/10.1021/la000418a>
- Confer, D. R., & Logan, B. E. (1997). Molecular weight distribution of hydrolysis products during the biodegradation of model macromolecules in suspended and biofilm cultures. II. Dextran and dextrin. *Water Research*, 31(9), 2137–2145. [https://doi.org/10.1016/S0043-1354\(97\)00050-X](https://doi.org/10.1016/S0043-1354(97)00050-X)
- Costerton, J. W., Stewart, P. S., & Greenberg, E. P. (1999). Bacterial Biofilms: A Common Cause of Persistent Infections. *Science*, 284(5418), 1318–1322. <https://doi.org/10.1126/science.284.5418.1318>
- Covis, R., Ladaviere, C., Desbrieres, J., Marie, E., & Durand, A. (2013). Hydrophobic modification of dextran with 1,2-epoxyalkanes in aqueous micellar medium: Competition between interfacial and bulk reactions and consequences on polymer properties. *Colloids and Surfaces A: Physicochemical and Engineering Aspects*, 436, 744–750. <https://doi.org/10.1016/j.colsurfa.2013.07.045>
- Craig, M., Bordes, R., & Holmberg, K. (2012). Polypeptide multilayer self-assembly and enzymatic degradation on tailored gold surfaces studied by QCM-D. *Soft Matter*, 8(17), 4788. <https://doi.org/10.1039/c2sm25124h>
- Cramer, A. D., Dong, W.-F., Benbow, N. L., Webber, J. L., Krasowska, M., Beattie, D. A., & Ferri, J. K. (2017). The influence of polyanion molecular weight on polyelectrolyte multilayers at surfaces: elasticity and susceptibility to saloplasticity of strongly dissociated synthetic polymers at fluid–fluid interfaces. *Physical Chemistry Chemical Physics*, 19(35), 23781–23789. <https://doi.org/10.1039/C7CP02614E>
- Cranston, E. D., & Gray, D. G. (2006). Morphological and Optical Characterization of Polyelectrolyte Multilayers Incorporating Nanocrystalline Cellulose. *Biomacromolecules*, 7(9), 2522–2530. <https://doi.org/10.1021/bm0602886>
- Crecente-Campo, J., & Jose Alonso, M. (2019). Engineering, on-demand manufacturing, and scaling-up of polymeric nanocapsules. *Bioengineering & Translational Medicine*, 4(1), 38–50. <https://doi.org/10.1002/btm2.10118>
- Crouzier, T., Boudou, T., & Picart, C. (2010). Polysaccharide-based polyelectrolyte multilayers. *Current Opinion in Colloid & Interface Science*, 15(6), 417–426. <https://doi.org/10.1016/j.cocis.2010.05.007>
- Crouzier, T., & Picart, C. (2009). Ion Pairing and Hydration in Polyelectrolyte Multilayer Films Containing Polysaccharides. *Biomacromolecules*, 10(2), 433–442. <https://doi.org/10.1021/bm8012378>
- Damanik, F. F. R., Brunelli, M., Pastorino, L., Ruggiero, C., van Blitterswijk, C., Rotmans, J., & Moroni, L. (2020). Sustained delivery of growth factors with high loading efficiency in a layer by layer assembly. *Biomaterials Science*, 8(1), 174–188. <https://doi.org/10.1039/c9bm00979e>
- Damasceno Borges, D., Woellner, C. F., Autreto, P. A. S., & Galvao, D. S. (2018). Insights on the mechanism of water-alcohol separation in multilayer graphene oxide membranes: Entropic versus enthalpic factors. *Carbon*, 127, 280–286. <https://doi.org/10.1016/j.carbon.2017.11.020>

- Dammak, A., Moreau, C., Beury, N., Schwikal, K., Winter, H. T., Bonnin, E., Saake, B., & Cathala, B. (2013). Elaboration of multilayered thin films based on cellulose nanocrystals and cationic xylans: application to xylanase activity detection. *Holzforschung*, 67(5), 579–586. <https://doi.org/10.1515/hf-2012-0176>
- de Belder, D. (1996). *Polysaccharides in Medicinal Applications*. Marcel Dekker, New York, 505–524.
- de Oliveira Farias, E. A., dos Santos, M. C., de Araujo Dionísio, N., Quelemes, P. V., de Souza Almeida Leite, J. R., Eaton, P., da Silva, D. A., & Eiras, C. (2015). Layer-by-Layer films based on biopolymers extracted from red seaweeds and polyaniline for applications in electrochemical sensors of chromium VI. *Materials Science and Engineering: B*, 200, 9–21. <https://doi.org/10.1016/j.mseb.2015.05.004>
- de Raucourt, E., Mauray, S., Chaubet, F., Maiga-Revel, O., Jozefowicz, M., & Fischer, A. M. (1998). Anticoagulant activity of dextran derivatives. *Journal of Biomedical Materials Research*, 41(1), 49–57. [https://doi.org/10.1002/\(SICI\)1097-4636\(199807\)41:1<49::AID-JBM6>3.0.CO;2-Q](https://doi.org/10.1002/(SICI)1097-4636(199807)41:1<49::AID-JBM6>3.0.CO;2-Q)
- De Temmerman, M.-L., Rejman, J., Grooten, J., De Beer, T., Vervaet, C., Demeester, J., & De Smedt, S. C. (2011a). Lyophilization of Protein-Loaded Polyelectrolyte Microcapsules. *Pharmaceutical Research*, 28(7), 1765–1773. <https://doi.org/10.1007/s11095-011-0411-z>
- De Temmerman, M.-L., Rejman, J., Grooten, J., De Beer, T., Vervaet, C., Demeester, J., & De Smedt, S. C. (2011b). Lyophilization of Protein-Loaded Polyelectrolyte Microcapsules. *Pharmaceutical Research*, 28(7), 1765–1773. <https://doi.org/10.1007/s11095-011-0411-z>
- Decher, G. (1997). Fuzzy Nanoassemblies: Toward Layered Polymeric Multicomposites. *Science*, 277(5330), 1232–1237. <https://doi.org/10.1126/science.277.5330.1232>
- Decher, G., & Hong, J. D. (1991a). Buildup of Ultrathin Multilayer Films by a Self-Assembly Process: II. Consecutive Adsorption of Anionic and Cationic Bipolar Amphiphiles and Polyelectrolytes on Charged Surfaces. *Berichte Der Bunsengesellschaft Für Physikalische Chemie*, 95(11), 1430–1434. <https://doi.org/10.1002/bbpc.19910951122>
- Decher, G., Hong, J. D., & Schmitt, J. (1992). Buildup of ultrathin multilayer films by a self-assembly process: III. Consecutively alternating adsorption of anionic and cationic polyelectrolytes on charged surfaces. *Thin Solid Films*, 210–211, 831–835. [https://doi.org/10.1016/0040-6090\(92\)90417-A](https://doi.org/10.1016/0040-6090(92)90417-A)
- Decher, G., & Hong, J.-D. (1991b). Buildup of ultrathin multilayer films by a self-assembly process, 1 consecutive adsorption of anionic and cationic bipolar amphiphiles on charged surfaces. *Makromolekulare Chemie. Macromolecular Symposia*, 46(1), 321–327. <https://doi.org/10.1002/masy.19910460145>
- Decher, G., & Schlenoff, J. B. (Eds.). (2003). *Multilayer thin films: sequential assembly of nanocomposite materials*. Wiley-VCH.
- De Cock, L. J., De Koker, S., De Geest, B. G., Grooten, J., Vervaet, C., Remon, J. P., Sukhorukov, G. B., & Antipina, M. N. (2010). Polymeric Multilayer Capsules in Drug Delivery. *Angewandte Chemie International Edition*, 49(39), 6954–6973. <https://doi.org/10.1002/anie.200906266>
- Delcea, M., Möhwald, H., & Skirtach, A. G. (2011). Stimuli-responsive LbL capsules and nanoshells for drug delivery. *Advanced Drug Delivery Reviews*, 63(9), 730–747. <https://doi.org/10.1016/j.addr.2011.03.010>
- Deng, Y., Wu, Y., Qian, Y., Ouyang, X., Yang, D., & Qiu, X. (2010). ADSORPTION AND DESORPTION BEHAVIORS OF LIGNOSULFONATE DURING THE SELF-ASSEMBLY OF MULTILAYERS. *BioResources*, 5(2), 2.
- Desfosses. (1829). Observations sur la fermentation visqueuse et sur le mutisme. *Journal de pharmacie et des sciences accessoires*, 15(series 2), 602.
- Devi, M. G., Dutta, S., Al Hinai, A. T., & Feroz, S. (2014). Surface Morphology Study of Chitosan-Dextran Sulphate Multilayer Thin Films. *Journal of Chitin and Chitosan Science*, 2(4), 245–258. <https://doi.org/10.1166/jcc.2014.1069>
- Devi, M. G., Dutta, S., Al Hinai, A. T., & Feroz, S. (2015). Studies on encapsulation of Rifampicin and its release from chitosan-dextran sulfate capsules. *Korean Journal of Chemical Engineering*, 32(1), 118–124. <https://doi.org/10.1007/s11814-014-0161-9>
- Diez-Pascual, A. M., & Shuttleworth, P. S. (2014). Layer-by-Layer Assembly of Biopolyelectrolytes onto Thermo/pH-Responsive Micro/Nano-Gels. *Materials*, 7(11), 7472–7512. <https://doi.org/10.3390/ma7117472>
- Ding, Y., Zhao, Y., Tao, X., Zheng, Y.-Z., & Chen, J.-F. (2009). Assembled alginate/chitosan micro-shells for removal of organic pollutants. *Polymer*, 50(13), 2841–2846. <https://doi.org/10.1016/j.polymer.2009.04.046>
- Dodoo, S. (2011). Structure and swelling behaviour of polyelectrolyte multilayers.
- Dodoo, S., Balzer, B. N., Hugel, T., Laschewsky, A., & Klitzing, R. von. (2013). Effect of Ionic Strength and Layer Number on Swelling of Polyelectrolyte Multilayers in Water Vapour. *Soft Materials*, 11(2), 157–164. <https://doi.org/10.1080/1539445X.2011.607203>
- Dodoo, S., Steitz, R., Laschewsky, A., & von Klitzing, R. (2011). Effect of ionic strength and type of ions on the structure of water swollen polyelectrolyte multilayers. *Physical Chemistry Chemical Physics*, 13(21), 10318. <https://doi.org/10.1039/c0cp01357a>
- Dong, W., Liu, S., Wan, L., Mao, G., Kurth, D., & Mohwald, H. (2005). Controlled permeability in polyelectrolyte films via solvent treatment. *Chemistry of Materials*, 17(20), 4992–4999. <https://doi.org/10.1021/cm051090f>

- Dong, Z., Zhang, N., Wang, Y., Wu, J., Gan, Q., & Li, W. (2019). Photopatternable Nanolayered Polymeric Films with Fast Tunable Color Responses Triggered by Humidity. *Advanced Functional Materials*, 29(43), 1904453. <https://doi.org/10.1002/adfm.201904453>
- Dubas, S. T., & Schlenoff, J. B. (1999). Factors Controlling the Growth of Polyelectrolyte Multilayers. *Macromolecules*, 32(24), 8153–8160. <https://doi.org/10.1021/ma981927a>
- Dubas, S. T., & Schlenoff, J. B. (2001). Swelling and Smoothing of Polyelectrolyte Multilayers by Salt. *Langmuir*, 17(25), 7725–7727. <https://doi.org/10.1021/la0112099>
- Elbert, D. L., Herbert, C. B., & Hubbell, J. A. (1999). Thin Polymer Layers Formed by Polyelectrolyte Multilayer Techniques on Biological Surfaces. *Langmuir*, 15(16), 5355–5362. <https://doi.org/10.1021/la9815749>
- Elbert, D. L., & Hubbell, J. A. (1998). Self-assembly and steric stabilization at heterogeneous, biological surfaces using adsorbing block copolymers. *Chemistry & Biology*, 5(3), 177–183. [https://doi.org/10.1016/S1074-5521\(98\)90062-X](https://doi.org/10.1016/S1074-5521(98)90062-X)
- Elferink, J. G. R., & de Koster, B. M. (1995). The role of calcium ions in DEAE-dextran-induced stimulation of neutrophil migration. *Chemico-Biological Interactions*, 95(1), 203–214. [https://doi.org/10.1016/0009-2797\(94\)03360-9](https://doi.org/10.1016/0009-2797(94)03360-9)
- Elzbieciak, M., Kolaszińska, M., Zapotoczny, S., Krastev, R., Nowakowska, M., & Warszyński, P. (2009). Nonlinear growth of multilayer films formed from weak polyelectrolytes. *Colloids and Surfaces A: Physicochemical and Engineering Aspects*, 343(1–3), 89–95. <https://doi.org/10.1016/j.colsurfa.2009.01.034>
- Elzbieciak, M., Zapotoczny, S., Nowak, P., Krastev, R., Nowakowska, M., & Warszyński, P. (2009). Influence of pH on the Structure of Multilayer Films Composed of Strong and Weak Polyelectrolytes. *Langmuir*, 25(5), 3255–3259. <https://doi.org/10.1021/la803988k>
- Ermakov, A., V., Inozemtseva, O. A., Gorin, D. A., Sukhorukov, G. B., Belyakov, S., & Antipina, M. N. (2019). Influence of Heat Treatment on Loading of Polymeric Multilayer Microcapsules with Rhodamine B. *Macromolecular Rapid Communications*, 40(5, SI). <https://doi.org/10.1002/marc.201800200>
- Escobar-Ferrand, L., Li, D., Lee, D., & Durning, C. J. (2014). All-Nanoparticle Layer-by-Layer Surface Modification of Micro- and Ultrafiltration Membranes. *Langmuir*, 30(19), 5545–5556. <https://doi.org/10.1021/la5002489>
- Fadhillah, F., Zaidi, S. M. J., Khan, Z., Khaled, M. M., Rahman, F., & Hammond, P. T. (2013). Development of polyelectrolyte multilayer thin film composite membrane for water desalination application. *Desalination*, 318, 19–24. <https://doi.org/10.1016/j.desal.2013.03.011>
- Farhat, T., Yassin, G., Dubas, S. T., & Schlenoff, J. B. (1999). Water and Ion Pairing in Polyelectrolyte Multilayers. *Langmuir*, 15(20), 6621–6623. <https://doi.org/10.1021/la990631a>
- Feldtötö, Z., Varga, I., & Blomberg, E. (2010). Influence of Salt and Rinsing Protocol on the Structure of PAH/PSS Polyelectrolyte Multilayers. *Langmuir*, 26(22), 17048–17057. <https://doi.org/10.1021/la102351f>
- Ferrari, P. F., Aliakbarian, B., Zattera, E., Pastorino, L., Palombo, D., & Perego, P. (2017). ENGINEERED CACO(3) NANOPARTICLES WITH TARGETING ACTIVITY: A SIMPLE APPROACH FOR A VASCULAR INTENDED DRUG DELIVERY SYSTEM. *Canadian Journal of Chemical Engineering*, 95(9), 1683–1689. <https://doi.org/10.1002/cjce.22871>
- Fong, D., Cummings, L. J., Chapman, S. J., & Sanaei, P. (2021). On the performance of multilayered membrane filters. *Journal of Engineering Mathematics*, 127(1), 23. <https://doi.org/10.1007/s10665-021-10118-2>
- Francesko, A., Ivanova, K., Hoyo, J., Pérez-Rafael, S., Petkova, P., Fernandes, M. M., Heinze, T., Mendoza, E., & Tzanov, T. (2018). Bottom-up Layer-by-Layer Assembling of Antibacterial Freestanding Nanobiocomposite Films. *Biomacromolecules*, 19(9), 3628–3636. <https://doi.org/10.1021/acs.biomac.8b00626>
- Francis, M. F., Cristea, M., & Winnik, F. M. (2004). Polymeric micelles for oral drug delivery: Why and how. *Pure and Applied Chemistry*, 76(7–8), 1321–1335. <https://doi.org/10.1351/pac200476071321>
- Francis, M. F., Piredda, M., Cristea, M., & Winnik, F. M. (2006). Synthesis and Evaluation of Hydrophobically-Modified Polysaccharides as Oral Delivery Vehicles for Poorly Water-Soluble Drugs. In *Polymeric Drug Delivery I* (pp. 55–67).
- Fu, Y., Tippets, C. A., Donev, E. U., & Lopez, R. (2016). Structural colors: from natural to artificial systems. *WIREs Nanomedicine and Nanobiotechnology*, 8(5), 758–775. <https://doi.org/10.1002/wnan.1396>
- Fukuda, H., & Kikuchi, Y. (1977). Polyelectrolyte Complexes of Sodium Dextran Sulfate with Chitosan. *Makromolekulare Chemie-Macromolecular Chemistry and Physics*, 178(10), 2895–2899.
- Fukuda, H., & Kikuchi, Y. (1978). In vitro Clot Formation on Polyelectrolyte Complexes of Sodium Dextran Sulfate with Chitosan. *Journal of Biomedical Materials Research*, 12(4), 531–539. <https://doi.org/10.1002/jbm.820120408>
- Fukui, Y., & Fujimoto, K. (2009). The Preparation of Sugar Polymer-Coated Nanocapsules by the Layer-by-Layer Deposition on the Liposome. *Langmuir*, 25(17), 10020–10025. <https://doi.org/10.1021/la9008834>
- Fukui, Y., & Fujimoto, K. (2011). Control in Mineralization by the Polysaccharide-Coated Liposome via the Counter-Diffusion of Ions. *Chemistry of Materials*, 23(21), 4701–4708. <https://doi.org/10.1021/cm201211n>
- Gao, H., Goryacheva, O. A., Tarakina, N. V., & Sukhorukov, G. B. (2016). Intracellularly Biodegradable Polyelectrolyte/Silica Composite Microcapsules as Carriers for Small Molecules. *ACS Applied Materials & Interfaces*, 8(15), 9651–9661. <https://doi.org/10.1021/acsami.6b01921>
- Gay-Lussac, J., & Pelouze, J. (1833). Sur l'acide lactique. *Annales de Chimie et de Physique*, 52, 410–424.

- Geetha Devi, M., Dutta, S., Al Hinai, A. T., & Feroz, S. (2021). Nano engineered biodegradable capsules for the encapsulation and kinetic release studies of ciprofloxacin hydrochloride. *Journal of the Indian Chemical Society*, 98(8), 100109. <https://doi.org/10.1016/j.jics.2021.100109>
- Ghimici, L., Morariu, S., & Nichifor, M. (2009). Separation of clay suspension by ionic dextran derivatives. *Separation and Purification Technology*, 68(2), 165–171.
- Ghimici, L., & Nichifor, M. (2018). Dextran derivatives application as flocculants. *Carbohydrate Polymers*, 190, 162–174. <https://doi.org/10.1016/j.carbpol.2018.02.075>
- Ghiorghita, C.-A., Bucatariu, F., & Dragan, E. S. (2019). Influence of cross-linking in loading/release applications of polyelectrolyte multilayer assemblies. A review. *Materials Science and Engineering: C*, 105, 110050. <https://doi.org/10.1016/j.msec.2019.110050>
- Glinel, K., Déjgnat, C., Prevot, M., Schöler, B., Schönhoff, M., & Klitzing, R. v. (2007). Responsive polyelectrolyte multilayers. *Colloids and Surfaces A: Physicochemical and Engineering Aspects*, 303(1–2), 3–13. <https://doi.org/10.1016/j.colsurfa.2007.02.052>
- Glinel, K., Moussa, A., Jonas, A. M., & Laschewsky, A. (2002). Influence of Polyelectrolyte Charge Density on the Formation of Multilayers of Strong Polyelectrolytes at Low Ionic Strength. *Langmuir*, 18(4), 1408–1412. <https://doi.org/10.1021/la0113670>
- Gnanadhas, D. P., Ben Thomas, M., Elango, M., Raichur, A. M., & Chakravorty, D. (2013). Chitosan-dextran sulphate nanocapsule drug delivery system as an effective therapeutic against intraphagosomal pathogen Salmonella. *Journal of Antimicrobial Chemotherapy*, 68(11), 2576–2586. <https://doi.org/10.1093/jac/dkt252>
- Goodwin, A. P., Tabakman, S. M., Welscher, K., Sherlock, S. P., Prencipe, G., & Dai, H. (2009). Phospholipid–Dextran with a Single Coupling Point: A Useful Amphiphile for Functionalization of Nanomaterials. *Journal of the American Chemical Society*, 131(1), 289–296. <https://doi.org/10.1021/ja807307e>
- Gribova, V., Auzely-Velty, R., & Picart, C. (2012). Polyelectrolyte Multilayer Assemblies on Materials Surfaces: From Cell Adhesion to Tissue Engineering. *Chemistry of Materials*, 24(5), 854–869. <https://doi.org/10.1021/cm2032459>
- Gubenšek, F., & Lapanje, S. (1968). Potentiometric Titration Studies of Diethyl aminoethyl Dextran Base. *Journal of Macromolecular Science: Part A - Chemistry*, 2(5), 1045–1054. <https://doi.org/10.1080/10601326808051455>
- Guyomard-Lack, A., Cerclier, C., Beury, N., Jean, B., Cousin, F., Moreau, C., & Cathala, B. (2012). Nano-structured cellulose nanocrystals-xyloglucan multilayered films for the detection of cellulase activity. *The European Physical Journal Special Topics*, 213(1), 291–294. <https://doi.org/10.1140/epjst/e2012-01676-1>
- Guzmán, E., Cavallo, J. A., Chuliá-Jordán, R., Gómez, C., Strumia, M. C., Ortega, F., & Rubio, R. G. (2011). pH-Induced Changes in the Fabrication of Multilayers of Poly(acrylic acid) and Chitosan: Fabrication, Properties, and Tests as a Drug Storage and Delivery System. *Langmuir*, 27(11), 6836–6845. <https://doi.org/10.1021/la200522r>
- Guzmán, E., Ritacco, H., Ortega, F., & Rubio, R. G. (2011). Evidence of the influence of adsorption kinetics on the internal reorganization of polyelectrolyte multilayers. *Colloids and Surfaces A: Physicochemical and Engineering Aspects*, 384(1–3), 274–281. <https://doi.org/10.1016/j.colsurfa.2011.04.005>
- Guzmán, E., Ritacco, H., Rubio, J. E. F., Rubio, R. G., & Ortega, F. (2009). Salt-induced changes in the growth of polyelectrolyte layers of poly(diallyl-dimethylammonium chloride) and poly(4-styrene sulfonate of sodium). *Soft Matter*, 5(10), 2130. <https://doi.org/10.1039/b901193e>
- Guzmán, E., Rubio, R. G., & Ortega, F. (2020). A closer physico-chemical look to the Layer-by-Layer electrostatic self-assembly of polyelectrolyte multilayers. *Advances in Colloid and Interface Science*, 282, 102197. <https://doi.org/10.1016/j.cis.2020.102197>
- Hall, M., & Ricketts, C. R. (1952). The Use of Dextran Sulphate as a Blood Anticoagulant in Biological Research. *Journal of Clinical Pathology*, 5(4), 366–366. <https://doi.org/10.1136/jcp.5.4.366>
- Han, J.-W., Ruiz-Garcia, L., Qian, J.-P., & Yang, X.-T. (2018). Food Packaging: A Comprehensive Review and Future Trends: Food packaging: Review and future trends.... *Comprehensive Reviews in Food Science and Food Safety*, 17(4), 860–877. <https://doi.org/10.1111/1541-4337.12343>
- Hartley, P., McArthur, S., McLean, K., & Griesser, H. (2002). Physicochemical properties of polysaccharide coatings based on grafted multilayer assemblies. *Langmuir*, 18(7), 2483–2494. <https://doi.org/10.1021/la001801i>
- Haynie, D. T., Cho, E., & Waduge, P. (2011). “In and Out Diffusion” Hypothesis of Exponential Multilayer Film Buildup Revisited. *Langmuir*, 27(9), 5700–5704. <https://doi.org/10.1021/la104516a>
- He, P., & Hu, N. (2004). Interactions between Heme Proteins and Dextran Sulfate in Layer-by-Layer Assembly Films. *The Journal of Physical Chemistry B*, 108(35), 13144–13152. <https://doi.org/10.1021/jp049974u>
- Hehre, E. J. (1956). Natural synthesis of low molecular weight (clinical type) dextran by a Streptococcus strain. *Journal of Biological Chemistry*, 222(2), 739–750.
- Heinze, T., Liebert, T., Heublein, B., & Hornig, S. (2006). Functional Polymers Based on Dextran. In D. Klemm (Ed.), *Polysaccharides II* (Vol. 205, pp. 199–291). Springer Berlin Heidelberg. https://doi.org/10.1007/12_100
- Hernández-Rivas, M., Guzmán, E., Fernández-Peña, L., Akanno, A., Greaves, A., Léonforte, F., Ortega, F., Rubio, R., & Luengo, G. S. (2020). Deposition of Synthetic and Bio-Based Polycations onto Negatively Charged Solid Surfaces: Effect of

- the Polymer Cationicity, Ionic Strength, and the Addition of an Anionic Surfactant. *Colloids and Interfaces*, 4(3), 33. <https://doi.org/10.3390/colloids4030033>
- Heurich, E., Zankovych, S., Beyer, M., Schnabelrauch, M., Berg, A., & Jandt, K. D. (2011). A Comparison of the Cell Compatibility of Poly(ethyleneimine) with that of other Cationic Biopolymers Used in Applications at Biointerfaces. *Advanced Engineering Materials*, 13(9), B285–B295. <https://doi.org/10.1002/adem.201080105>
- Heuvingh, J., Zappa, M., & Fery, A. (2005). Salt Softening of Polyelectrolyte Multilayer Capsules. *Langmuir*, 21(7), 3165–3171. <https://doi.org/10.1021/la047388m>
- Hong, J. D., Lowack, K., Schmitt, J., & Decher, G. (1993). Layer-by-layer deposited multilayer assemblies of polyelectrolytes and proteins: from ultrathin films to protein arrays. In P. Laggner & O. Glatter (Eds.), *Trends in Colloid and Interface Science VII* (Vol. 93, pp. 98–102). Steinkopff. <https://doi.org/10.1007/BFb0118482>
- Hoogeveen, N. G., Cohen Stuart, M. A., Fleer, G. J., & Böhmer, M. R. (1996). Formation and Stability of Multilayers of Polyelectrolytes. *Langmuir*, 12(15), 3675–3681. <https://doi.org/10.1021/la951574y>
- Houska, M., Brynda, E., & Bohata, K. (2004). The effect of polyelectrolyte chain length on layer-by-layer protein/polyelectrolyte assembly-an experimental study. *Journal of Colloid and Interface Science*, 273(1), 140–147. <https://doi.org/10.1016/j.jcis.2003.12.056>
- Huynh, R., Chaubet, F., & Jozefonvicz, J. (1998). Carboxymethylation of dextran in aqueous alcohol as the first step of the preparation of derivatized dextrans. *Die Angewandte Makromolekulare Chemie*, 254, 61–65.
- Iler, R. K. (1966). Multilayers of colloidal particles. *Journal of Colloid and Interface Science*, 21(6), 569–594. [https://doi.org/10.1016/0095-8522\(66\)90018-3](https://doi.org/10.1016/0095-8522(66)90018-3)
- Ilyas, S., de Grooth, J., Nijmeijer, K., & de Vos, W. M. (2015). Multifunctional polyelectrolyte multilayers as nanofiltration membranes and as sacrificial layers for easy membrane cleaning. *Journal of Colloid and Interface Science*, 446, 386–393. <https://doi.org/10.1016/j.jcis.2014.12.019>
- Ilyas, S., Joseph, N., Szymczyk, A., Volodin, A., Nijmeijer, K., de Vos, W. M., & Vankelecom, I. F. J. (2016). Weak polyelectrolyte multilayers as tunable membranes for solvent resistant nanofiltration. *Journal of Membrane Science*, 514, 322–331. <https://doi.org/10.1016/j.memsci.2016.04.073>
- Imbert, P., Sadtler, V. M., & Dellacherie, E. (2002). Phenoxy-substituted dextrans as emulsifying agent: *Colloids and Surfaces A: Physicochemical and Engineering Aspects*, 211(2–3), 157–164. [https://doi.org/10.1016/S0927-7757\(02\)00257-1](https://doi.org/10.1016/S0927-7757(02)00257-1)
- Ioan, C. E., Aberle, T., & Burchard, W. (2000). Structure Properties of Dextran. 2. Dilute Solution. *Macromolecules*, 33(15), 5730–5739. <https://doi.org/10.1021/ma000282n>
- Iost, R. M., & Crespihlo, F. N. (2012). Layer-by-layer self-assembly and electrochemistry: Applications in biosensing and bioelectronics. *Biosensors and Bioelectronics*, 31(1), 1–10. <https://doi.org/10.1016/j.bios.2011.10.040>
- Itano, K., Choi, J., & Rubner, M. F. (2005). Mechanism of the pH-Induced Discontinuous Swelling/Deswelling Transitions of Poly(allylamine hydrochloride)-Containing Polyelectrolyte Multilayer Films. *Macromolecules*, 38(8), 3450–3460. <https://doi.org/10.1021/ma047667g>
- Itoh, Y., Matsusaki, M., Kida, T., & Akashi, M. (2004). Preparation of biodegradable hollow nanocapsules by silica template method. *Chemistry Letters*, 33(12), 1552–1553. <https://doi.org/10.1246/cl.2004.1552>
- Itoh, Y., Matsusaki, M., Kida, T., & Akashi, M. (2006). Enzyme-responsive release of encapsulated proteins from biodegradable hollow capsules. *Biomacromolecules*, 7(10), 2715–2718. <https://doi.org/10.1021/bm060289y>
- Itoh, Y., Matsusaki, M., Kida, T., & Akashi, M. (2008a). Time-modulated release of multiple proteins from enzyme-responsive multilayered capsules. *Chemistry Letters*, 37(3), 238–239. <https://doi.org/10.1246/cl.2008.238>
- Itoh, Y., Matsusaki, M., Kida, T., & Akashi, M. (2008b). Locally controlled release of basic fibroblast growth factor from multilayered capsules. *Biomacromolecules*, 9(8), 2202–2206. <https://doi.org/10.1021/bm800321w>
- Jaber, J. A., & Schlenoff, J. B. (2006). Recent developments in the properties and applications of polyelectrolyte multilayers. *Current Opinion in Colloid & Interface Science*, 11(6), 324–329. <https://doi.org/10.1016/j.cocis.2006.09.008>
- Jafari, R., Cloutier, C., Allahdini, A., & Momen, G. (2019). Recent progress and challenges with 3D printing of patterned hydrophobic and superhydrophobic surfaces. *The International Journal of Advanced Manufacturing Technology*, 103(1–4), 1225–1238. <https://doi.org/10.1007/s00170-019-03630-4>
- Jang, E.-J., Lee, S.-Y., Bae, I.-H., Park, D. S., Jeong, M. H., & Park, J.-K. (2019). Fabrication and Evaluation of Polyelectrolyte Complexes of Dextran Derivatives for Drug Coating of Coronary Stents. *Applied Chemistry for Engineering*, 30(5), 586–590. <https://doi.org/10.14478/ace.2019.1057>
- Jayakumar, R., Menon, D., Manzoor, K., Nair, S. V., & Tamura, H. (2010). Biomedical applications of chitin and chitosan based nanomaterials—A short review. *Carbohydrate Polymers*, 82(2), 227–232. <https://doi.org/10.1016/j.carbpol.2010.04.074>
- Jeanes, A., Haynes, W. C., Wilham, C. A., Rankin, J. C., Melvin, E. H., Austin, M. J., Cluskey, J. E., Fisher, B. E., Tsuchiya, H. M., & Rist, C. E. (1954). Characterization and classification of dextrans from ninety-six strains of bacterial. *Journal of the American Chemical Society*, 76(20), 5041–5052.

- Jing, Y., Zhang, C., Fu, T., Jiang, C., Ma, K., Zhang, D., Hou, S., Dai, J., Wang, H., Zhang, X., Kou, G., & Guo, Y. (2016). Combination of dextran sulfate and recombinant trypsin on aggregation of Chinese hamster ovary cells. *Cytotechnology*, 68(2), 241–248. <https://doi.org/10.1007/s10616-014-9774-4>
- Joseph, N., Ahmadiannamini, P., Hoogenboom, R., & Vankelecom, Ivo. F. J. (2014). Layer-by-layer preparation of polyelectrolyte multilayer membranes for separation. *Polymer Chemistry*, 5(6), 1817–1831. <https://doi.org/10.1039/C3PY01262J>
- Jourdain, L., Leser, M. E., Schmitt, C., Michel, M., & Dickinson, E. (2008). Stability of emulsions containing sodium caseinate and dextran sulfate: Relationship to complexation in solution. *Food Hydrocolloids*, 22(4), 647–659. <https://doi.org/10.1016/j.foodhyd.2007.01.007>
- Jourdain, L. S., Schmitt, C., Leser, M. E., Murray, B. S., & Dickinson, E. (2009). Mixed Layers of Sodium Caseinate plus Dextran Sulfate: Influence of Order of Addition to Oil-Water Interface. *Langmuir*, 25(17), 10026–10037. <https://doi.org/10.1021/la900919w>
- Kadkhodaei, M., Wu, H., & Brant, D. A. (1991). Comparison of the conformational dynamics of the (1 → 4)- and (1 → 6)-linked α -D-glucans using ¹³C-NMR relaxation. *Biopolymers*, 31(13), 1581–1592. <https://doi.org/10.1002/bip.360311313>
- Kagimura, F. Y., da Cunha, M. A. A., Barbosa, A. M., Dekker, R. F. H., & Malfatti, C. R. M. (2015). Biological activities of derivatized d-glucans: A review. *International Journal of Biological Macromolecules*, 72, 588–598. <https://doi.org/10.1016/j.ijbiomac.2014.09.008>
- Kakran, M., Muratani, M., Tng, W. J., Liang, H., Trushina, D. B., Sukhorukov, G. B., Ng, H. H., & Antipina, M. N. (2015). Layered polymeric capsules inhibiting the activity of RNases for intracellular delivery of messenger RNA. *Journal of Materials Chemistry B*, 3(28), 5842–5848. <https://doi.org/10.1039/c5tb00615e>
- Karamitros, C. S., Yashchenok, A. M., Moehwald, H., Skirtach, A. G., & Konrad, M. (2013). Preserving Catalytic Activity and Enhancing Biochemical Stability of the Therapeutic Enzyme Asparaginase by Biocompatible Multilayered Polyelectrolyte Microcapsules. *Biomacromolecules*, 14(12), 4398–4406. <https://doi.org/10.1021/bm401341k>
- Kashcooli, Y., Park, K., Bose, A., Greenfield, M., & Bothun, G. D. (2016). Patchy Layersomes Formed by Layer-by-Layer Coating of Liposomes with Strong Biopolyelectrolytes. *Biomacromolecules*, 17(11), 3838–3844. <https://doi.org/10.1021/acs.biomac.6b01467>
- Katayama, H., Ishihama, Y., & Asakawa, N. (1998). Stable Cationic Capillary Coating with Successive Multiple Ionic Polymer Layers for Capillary Electrophoresis. *Analytical Chemistry*, 70(24), 5272–5277. <https://doi.org/10.1021/ac9805221>
- Kayitmazer, A. B., Seeman, D., Minsky, B. B., Dubin, P. L., & Xu, Y. (2013). Protein–polyelectrolyte interactions. *Soft Matter*, 9(9), 2553. <https://doi.org/10.1039/c2sm27002a>
- Kempe, K., Noi, K. F., Ng, S. L., Muellner, M., & Caruso, F. (2014). Multilayered polymer capsules with switchable permeability. *Polymer*, 55(25), 6451–6459. <https://doi.org/10.1016/j.polymer.2014.09.074>
- Kerry, J. P., O’Grady, M. N., & Hogan, S. A. (2006). Past, current and potential utilisation of active and intelligent packaging systems for meat and muscle-based products: A review. *Meat Science*, 74(1), 113–130. <https://doi.org/10.1016/j.meatsci.2006.04.024>
- Khalil, M. I., Hashem, A., & Hebeish, A. (1990). Carboxymethylation of Maize Starch. *Starch - Stärke*, 42(2), 60–63. <https://doi.org/10.1002/star.19900420209>
- Khan, F., & Ahmad, S. R. (2013). Polysaccharides and Their Derivatives for Versatile Tissue Engineering Application. *Macromolecular Bioscience*, 13(4), 395–421. <https://doi.org/10.1002/mabi.201200409>
- Kharlampieva, E., Kozlovskaya, V., Chan, J., Ankner, J. F., & Tsukruk, V. V. (2009). Spin-Assisted Layer-by-Layer Assembly: Variation of Stratification as Studied with Neutron Reflectivity. *Langmuir*, 25(24), 14017–14024. <https://doi.org/10.1021/la9014042>
- Khin, M. M., Nair, A. S., Babu, V. J., Murugan, R., & Ramakrishna, S. (2012). A review on nanomaterials for environmental remediation. *Energy & Environmental Science*, 5(8), 8075. <https://doi.org/10.1039/c2ee21818f>
- Kikuchi, Y., & Fukuda, H. (1974). Polyelectrolyte Complex of Sodium Dextran Sulfate with Chitosan. *Makromolekulare Chemie-Macromolekulare Chemistry and Physics*, 175(12), 3593–3596.
- Kim, S. H., Won, C. Y., & Chu, C. C. (1999). Synthesis and characterization of dextran-maleic acid based hydrogel. *Journal of Biomedical Materials Research*, 46(2), 160–170. [https://doi.org/10.1002/\(sici\)1097-4636\(199908\)46:2%3C160::aid-jbm4%3E3.0.co;2-p](https://doi.org/10.1002/(sici)1097-4636(199908)46:2%3C160::aid-jbm4%3E3.0.co;2-p)
- Kim, W.-S., Han, G. G., Hong, L., Kang, S.-K., Shokouhimehr, M., Choi, Y.-J., & Cho, C.-S. (2019). Novel production of natural bacteriocin via internalization of dextran nanoparticles into probiotics. *Biomaterials*, 218, 119360. <https://doi.org/10.1016/j.biomaterials.2019.119360>
- Kochetkova, O. Y., Kazakova, L. I., Moshkov, D. A., Vinokurov, M. G., & Shabarchina, L. I. (2013). Incorporation of proteins into polyelectrolyte microcapsules by coprecipitation and adsorption. *Russian Journal of Bioorganic Chemistry*, 39(5), 504–509. <https://doi.org/10.1134/S1068162013050087>
- Kokilavani, S., Syed, A., Thomas, A. M., Elgorban, A. M., Bahkali, A. H., Marraiki, N., Raju, L. L., Das, A., & Khan, S. S. (2021). Development of multifunctional Cu sensitized Ag-dextran nanocomposite for selective and sensitive detection of mercury from environmental sample and evaluation of its photocatalytic and anti-microbial applications. *Journal of Molecular Liquids*, 321, 114742. <https://doi.org/10.1016/j.molliq.2020.114742>

- Korica, M., Fras Zemljič, L., Bračić, M., Kargl, R., Spirk, S., Reishofer, D., Mihajlovski, K., & Kostić, M. (2018). Novel protein-repellent and antimicrobial polysaccharide multilayer thin films. *Holzforchung*, 73(1), 93–103. <https://doi.org/10.1515/hf-2018-0094>
- Kothari, D., Das, D., Patel, S., & Goyal, A. (2014). Dextran and Food Application. In K. G. Ramawat & J.-M. Mérillon (Eds.), *Polysaccharides* (pp. 1–16). Springer International Publishing. https://doi.org/10.1007/978-3-319-03751-6_66-1
- Kotov, N. A. (1999). Layer-by-layer self-assembly: The contribution of hydrophobic interactions. *Nanostructured Materials*, 12(5), 789–796. [https://doi.org/10.1016/S0965-9773\(99\)00237-8](https://doi.org/10.1016/S0965-9773(99)00237-8)
- Kralj, S., Stripling, E., Sanders, P., van Geel-Schutten, G. H., & Dijkhuizen, L. (2005). Highly Hydrolytic Reuteransucrase from Probiotic *Lactobacillus reuteri* Strain ATCC 55730. *Applied and Environmental Microbiology*, 71(7), 3942–3950. <https://doi.org/10.1128/AEM.71.7.3942-3950.2005>
- Krogman, K. C., Zacharia, N. S., Schroeder, S., & Hammond, P. T. (2007). Automated Process for Improved Uniformity and Versatility of Layer-by-Layer Deposition. *Langmuir*, 23(6), 3137–3141. <https://doi.org/10.1021/la063085b>
- Kulikouskaya, V. I., Pinchuk, S. V., Hileuskaya, K. S., Kraskouski, A. N., Vasilevich, I. B., Matievski, K. A., Agabekov, V. E., & Volotovskii, I. D. (2018). Layer-by-layer buildup of polysaccharide-containing films: Physico-chemical properties and mesenchymal stem cells adhesion. *Journal of Biomedical Materials Research Part A*, 106(8), 2093–2104. <https://doi.org/10.1002/jbm.a.36408>
- Kurt, P., Banerjee, D., Cohen, R. E., & Rubner, M. F. (2009). Structural color via layer-by-layer deposition: layered nanoparticle arrays with near-UV and visible reflectivity bands. *Journal of Materials Chemistry*, 19(47), 8920. <https://doi.org/10.1039/b912211g>
- Lacaze, G., Wick, M., & Cappelletti, S. (2007). Emerging fermentation technologies: Development of novel sourdoughs. *Food Microbiology*, 24(2), 155–160. <https://doi.org/10.1016/j.fm.2006.07.015>
- Ladam, G., Gergely, C., Senger, B., Decher, G., Voegel, J.-C., Schaaf, P., & Cuisinier, F. J. G. (2000). Protein Interactions with Polyelectrolyte Multilayers: Interactions between Human Serum Albumin and Polystyrene Sulfonate/Polyallylamine Multilayers. *Biomacromolecules*, 1(4), 674–687. <https://doi.org/10.1021/bm005572q>
- Ladam, G., Schaad, P., Voegel, J. C., Schaaf, P., Decher, G., & Cuisinier, F. (2000). In Situ Determination of the Structural Properties of Initially Deposited Polyelectrolyte Multilayers. *Langmuir*, 16(3), 1249–1255. <https://doi.org/10.1021/la990650k>
- Larm, O., Lindberg, B., & Svensson, S. (1971). Studies on the length of the side chains of the dextran elaborated by *Leuconostoc mesenteroides* NRRL B-512. *Carbohydrate Research*, 20(1), 39–48. [https://doi.org/10.1016/S0008-6215\(00\)84947-2](https://doi.org/10.1016/S0008-6215(00)84947-2)
- Larsen, C. (1989). Dextran prodrugs — structure and stability in relation to therapeutic activity. *Advanced Drug Delivery Reviews*, 3(1), 103–154. [https://doi.org/10.1016/0169-409X\(89\)90006-9](https://doi.org/10.1016/0169-409X(89)90006-9)
- Lavalle, Ph., Gergely, C., Cuisinier, F. J. G., Decher, G., Schaaf, P., Voegel, J. C., & Picart, C. (2002). Comparison of the Structure of Polyelectrolyte Multilayer Films Exhibiting a Linear and an Exponential Growth Regime: An in Situ Atomic Force Microscopy Study. *Macromolecules*, 35(11), 4458–4465. <https://doi.org/10.1021/ma0119833>
- Lazić, V., Vivod, V., Peršin, Z., Stojiljković, M., Ratnayake, I. S., Ahrenkiel, P. S., Nedeljković, J. M., & Kokol, V. (2020). Dextran-coated silver nanoparticles for improved barrier and controlled antimicrobial properties of nanocellulose films used in food packaging. *Food Packaging and Shelf Life*, 26, 100575. <https://doi.org/10.1016/j.fpsl.2020.100575>
- Leathers, T. D. (2002). Dextran. *Biopolymers*, 5, 299–321.
- Lee, S., Choi, B., & Tsutsumi, A. (2009). Electrochemical properties of polyaniline/carboxydextran (PANI/carDEX) composite films for biofuel cells in neutral aqueous solutions. *Biotechnology Letters*, 31(6), 851–855. <https://doi.org/10.1007/s10529-009-9944-1>
- Leemhuis, H., Pijning, T., Dobruchowska, J. M., van Leeuwen, S. S., Kralj, S., Dijkstra, B. W., & Dijkhuizen, L. (2013). Glucansucrases: Three-dimensional structures, reactions, mechanism, α -glucan analysis and their implications in biotechnology and food applications. *Journal of Biotechnology*, 163(2), 250–272. <https://doi.org/10.1016/j.jbiotec.2012.06.037>
- Leertouwer, H. L., Wilts, B. D., & Stavenga, D. G. (2011). Refractive index and dispersion of butterfly chitin and bird keratin measured by polarizing interference microscopy. *Optics Express*, 19(24), 24061. <https://doi.org/10.1364/OE.19.024061>
- Lemassu, A., Ortalo-Magné, A., Bardou, F., Silve, G., Lanéelle, M.-A., & Daffé, M. (1996). Extracellular and surface-exposed polysaccharides of non-tuberculous mycobacteria. *Microbiology*, 142(6), 1513–1520. <https://doi.org/10.1099/13500872-142-6-1513>
- Leontidis, E. (2002). Hofmeister anion effects on surfactant self-assembly and the formation of mesoporous solids. *Current Opinion in Colloid & Interface Science*, 7(1–2), 81–91. [https://doi.org/10.1016/S1359-0294\(02\)00010-9](https://doi.org/10.1016/S1359-0294(02)00010-9)
- Li, F., Biagioni, P., Finazzi, M., Tavazzi, S., & Piergiovanni, L. (2013). Tunable green oxygen barrier through layer-by-layer self-assembly of chitosan and cellulose nanocrystals. *Carbohydrate Polymers*, 92(2), 2128–2134. <https://doi.org/10.1016/j.carbpol.2012.11.091>
- Li, Q., Wang, S., Jin, X., Huang, C., & Xiang, Z. (2020). The Application of Polysaccharides and Their Derivatives in Pigment, Barrier, and Functional Paper Coatings. *Polymers*, 12(8), 8. <https://doi.org/10.3390/polym12081837>
- Li, R., Zeng, T., Wu, M., Zhang, H., & Hu, X. (2017). Effects of esterification on the structural, physicochemical, and flocculation properties of dextran. *Carbohydrate Polymers*, 174, 1129–1137. <https://doi.org/10.1016/j.carbpol.2017.07.034>

- Li, X., De Feyter, S., Chen, D., Aldea, S., Vandezande, P., Du Prez, F., & Vankelecom, I. F. J. (2008). Solvent-Resistant Nanofiltration Membranes Based on Multilayered Polyelectrolyte Complexes. *Chemistry of Materials*, 20(12), 3876–3883. <https://doi.org/10.1021/cm703072k>
- Li, Y., Wang, X., & Sun, J. (2012). Layer-by-layer assembly for rapid fabrication of thick polymeric films. *Chemical Society Reviews*, 41(18), 5998. <https://doi.org/10.1039/c2cs35107b>
- Lindenbaum, G. M., Mirgorodskaya, O. A., & Moskvichev, B. V. (1977). Chemical modification of water-soluble dextrans. *Pharmaceutical Chemistry Journal*, 11(6), 806–809. <https://doi.org/10.1007/BF00779300>
- Liu, J., Willför, S., & Xu, C. (2015). A review of bioactive plant polysaccharides: Biological activities, functionalization, and biomedical applications. *Bioactive Carbohydrates and Dietary Fibre*, 5(1), 31–61. <https://doi.org/10.1016/j.bcdf.2014.12.001>
- Liu, L., Kang, H., Wang, W., Xu, Z., Mai, W., Li, J., Lv, H., Zhao, L., & Qian, X. (2018). Layer-by-layer self-assembly of polycation/GO/OCNTs nanofiltration membrane with enhanced stability and flux. *Journal of Materials Science*, 53(15), 10879–10890. <https://doi.org/10.1007/s10853-018-2317-1>
- Liu, W., Wang, X., Bai, K., Lin, M., Sukhorukov, G., & Wang, W. (2014). Microcapsules functionalized with neuraminidase can enter vascular endothelial cells in vitro. *Journal of the Royal Society Interface*, 11(101). <https://doi.org/10.1098/rsif.2014.1027>
- Livanovich, K., & Shutava, T. (2019). Influence of Chitosan/Dextran Sulfate Layer-by-Layer Shell on Colloidal Properties of Silver Nanoparticles. *International Journal of Nanoscience*, 18(3–4, SI). <https://doi.org/10.1142/S0219581X19400775>
- Lombardo, D., Calandra, P., Pasqua, L., & Magazù, S. (2020). Self-Assembly of Organic Nanomaterials and Biomaterials: The Bottom-Up Approach for Functional Nanostructures Formation and Advanced Applications. *Materials*, 13(5), 1048. <https://doi.org/10.3390/ma13051048>
- Lomova, M. V., Brichkina, A. I., Kiryukhin, M. V., Vasina, E. N., Pavlov, A. M., Gorin, D. A., Sukhorukov, G. B., & Antipina, M. N. (2015). Multilayer Capsules of Bovine Serum Albumin and Tannic Acid for Controlled Release by Enzymatic Degradation. *ACS Applied Materials & Interfaces*, 7(22), 11732–11740. <https://doi.org/10.1021/acsami.5b03263>
- Lomova, M. V., Sukhorukov, G. B., & Antipina, M. N. (2010). Antioxidant Coating of Micronsize Droplets for Prevention of Lipid Peroxidation in Oil-in-Water Emulsion. *ACS Applied Materials & Interfaces*, 2(12), 3669–3676. <https://doi.org/10.1021/am100818j>
- Lundström-Hämälä, L., Johansson, E., & Wågberg, L. (2010). Polyelectrolyte Multilayers from Cationic and Anionic Starch: Influence of Charge Density and Salt Concentration on the Properties of the Adsorbed Layers. *Starch - Stärke*, 62(2), 102–114. <https://doi.org/10.1002/star.200900176>
- Luo, D., Gould, D. J., & Sukhorukov, G. B. (2016). Local and Sustained Activity of Doxycycline Delivered with Layer-by-Layer Microcapsules. *Biomacromolecules*, 17(4), 1466–1476. <https://doi.org/10.1021/acs.biomac.6b00070>
- Luo, R., Mutukumaraswamy, S., Venkatraman, S. S., & Neu, B. (2012). Engineering of erythrocyte-based drug carriers: control of protein release and bioactivity. *Journal of Materials Science-Materials in Medicine*, 23(1), 63–71. <https://doi.org/10.1007/s10856-011-4485-2>
- Luo, R., Neu, B., & Venkatraman, S. S. (2012). Surface Functionalization of Nanoparticles to Control Cell Interactions and Drug Release. *Small*, 8(16), 2585–2594. <https://doi.org/10.1002/sml.201200398>
- Lvov, Y., Ariga, K., Ichinose, I., & Kunitake, T. (1995). Assembly of Multicomponent Protein Films by Means of Electrostatic Layer-by-Layer Adsorption. *Journal of the American Chemical Society*, 117(22), 6117–6123. <https://doi.org/10.1021/ja00127a026>
- Lvov, Y., Ariga, K., & Kunitake, T. (1994). Layer-by-Layer Assembly of Alternate Protein/Polyion Ultrathin Films. *Chemistry Letters*, 23(12), 2323–2326. <https://doi.org/10.1246/cl.1994.2323>
- Lvov, Y., Decher, G., & Moehwald, H. (1993). Assembly, structural characterization, and thermal behavior of layer-by-layer deposited ultrathin films of poly(vinyl sulfate) and poly(allylamine). *Langmuir*, 9(2), 481–486. <https://doi.org/10.1021/la00026a020>
- Lvov, Y., Onda, M., Ariga, K., & Kunitake, T. (1998). Ultrathin films of charged polysaccharides assembled alternately with linear polyions. *Journal of Biomaterials Science, Polymer Edition*, 9(4), 345–355. <https://doi.org/10.1080/09205063.1998.9753060>
- Ma, Y., Zhang, Y., Wu, B., Sun, W., Li, Z., & Sun, J. (2011). Polyelectrolyte Multilayer Films for Building Energetic Walking Devices. *Angewandte Chemie*, 123(28), 6378–6381. <https://doi.org/10.1002/ange.201101054>
- Macleod, H. A., & Macleod, H. A. (2010). *Thin-film optical filters*. CRC press.
- Mancarella, S., Greco, V., Baldassarre, F., Vergara, D., Maffia, M., & Leporatti, S. (2015). Polymer-Coated Magnetic Nanoparticles for Curcumin Delivery to Cancer Cells. *Macromolecular Bioscience*, 15(10), 1365–1374. <https://doi.org/10.1002/mabi.201500142>
- Mansour, O., El Joukhar, I., & Belbekhouche, S. (2019). H2O2-sensitive delivery microparticles based on the boronic acid chemistry: (Phenylboronic-alginate derivative/dextran) system. *Reactive & Functional Polymers*, 145. <https://doi.org/10.1016/j.reactfunctpolym.2019.104377>
- Marchenko, I., Yashchenok, A., Borodina, T., Bukreeva, T., Konrad, M., Möhwald, H., & Skirtach, A. (2012). Controlled enzyme-catalyzed degradation of polymeric capsules templated on CaCO₃: Influence of the number of LbL layers,

- conditions of degradation, and disassembly of multicompartments. *Journal of Controlled Release*, 162(3), 599–605. <https://doi.org/10.1016/j.jconrel.2012.08.006>
- Martwiset, S., Koh, A. E., & Chen, W. (2006). Nonfouling Characteristics of Dextran-Containing Surfaces. *Langmuir*, 22(19), 8192–8196. <https://doi.org/10.1021/la061064b>
- Masuelli, M. A. (2013). Dextrans in Aqueous Solution. Experimental Review on Intrinsic Viscosity Measurements and Temperature Effect. *Journal of Polymer and Biopolymer Physics Chemistry*, 1(1), 1. <https://doi.org/10.12691/jpbpc-1-1-3>
- Mateos, A. J., Cain, A. A., & Grunlan, J. C. (2014). Large-Scale Continuous Immersion System for Layer-by-Layer Deposition of Flame Retardant and Conductive Nanocoatings on Fabric. *Industrial & Engineering Chemistry Research*, 53(15), 6409–6416. <https://doi.org/10.1021/ie500122u>
- Mauser, T., Déjugnat, C., Möhwald, H., & Sukhorukov, G. B. (2006). Microcapsules Made of Weak Polyelectrolytes: Templating and Stimuli-Responsive Properties. *Langmuir*, 22(13), 5888–5893. <https://doi.org/10.1021/la060088f>
- Mauzac, M., & Jozefonvicz, J. (1984). Anticoagulant activity of dextran derivatives. Part I: Synthesis and characterization. *Biomaterials*, 5(5), 301–304. [https://doi.org/10.1016/0142-9612\(84\)90078-4](https://doi.org/10.1016/0142-9612(84)90078-4)
- McCurdy, R. D., Goff, H. D., & Stanley, D. W. (1994). Properties of dextran as a cryoprotectant in ice cream. *Food Hydrocolloids*, 8(6), 625–633. [https://doi.org/10.1016/S0268-005X\(09\)80069-6](https://doi.org/10.1016/S0268-005X(09)80069-6)
- Mehvar, R. (2000). Dextrans for targeted and sustained delivery of therapeutic and imaging agents. *Journal of Controlled Release*, 69(1), 1–25. [https://doi.org/10.1016/S0168-3659\(00\)00302-3](https://doi.org/10.1016/S0168-3659(00)00302-3)
- Mei, J.-Q., Zhou, D.-N., Jin, Z.-Y., Xu, X.-M., & Chen, H.-Q. (2015). Effects of citric acid esterification on digestibility, structural and physicochemical properties of cassava starch. *Food Chemistry*, 187, 378–384. <https://doi.org/10.1016/j.foodchem.2015.04.076>
- Miah, F., Bibb, M. J., Barclay, J. E., Findlay, K. C., & Bornemann, S. (2016). Developmental delay in a *Streptomyces venezuelae* glgE null mutant is associated with the accumulation of α -maltose 1-phosphate. *Microbiology*, 162(7), 1208–1219. <https://doi.org/10.1099/mic.0.000296>
- Mitsuya, H., Looney, D., Kuno, S., Ueno, R., Wong-Staal, F., & Broder, S. (1988). Dextran sulfate suppression of viruses in the HIV family: inhibition of virion binding to CD4+ cells. *Science*, 240(4852), 646–649. <https://doi.org/10.1126/science.2452480>
- Monsan, P., Bozonnet, S., Albenne, C., Joucla, G., Willemot, R.-M., & Remaud-Siméon, M. (2001). Homopolysaccharides from lactic acid bacteria. *International Dairy Journal*, 11(9), 675–685. [https://doi.org/10.1016/S0958-6946\(01\)00113-3](https://doi.org/10.1016/S0958-6946(01)00113-3)
- Moon, R. J., Martini, A., Nairn, J., Simonsen, J., & Youngblood, J. (2011). Cellulose nanomaterials review: structure, properties and nanocomposites. *Chemical Society Reviews*, 40(7), 3941. <https://doi.org/10.1039/c0cs00108b>
- Moreau, C., Beury, N., Delorme, N., & Cathala, B. (2012). Tuning the Architecture of Cellulose Nanocrystal–Poly(allylamine hydrochloride) Multilayered Thin Films: Influence of Dipping Parameters. *Langmuir*, 28(28), 10425–10436. <https://doi.org/10.1021/la301293r>
- Moulis, C., Guieysse, D., Morel, S., Séverac, E., & Remaud-Siméon, M. (2021). Natural and engineered transglycosylases: Green tools for the enzyme-based synthesis of glycoproducts. *Current Opinion in Chemical Biology*, 61, 96–106. <https://doi.org/10.1016/j.cbpa.2020.11.004>
- Müller, M., Rieser, T., Dubin, P. L., & Lunkwitz, K. (2001). Selective Interaction Between Proteins and the Outermost Surface of Polyelectrolyte Multilayers: Influence of the Polyanion Type, pH and Salt. *Macromolecular Rapid Communications*, 22(6), 390–395. [https://doi.org/10.1002/1521-3927\(20010301\)22:6<390::AID-MARC390>3.0.CO;2-B](https://doi.org/10.1002/1521-3927(20010301)22:6<390::AID-MARC390>3.0.CO;2-B)
- Naessens, M., Cerdobbel, A., Soetaert, W., & Vandamme, E. J. (2005). *Leuconostoc* dextranase and dextran: production, properties and applications. *Journal of Chemical Technology & Biotechnology*, 80(8), 845–860. <https://doi.org/10.1002/jctb.1322>
- Nagel, J. A., Dickinson, R. B., & Cooper, S. L. (1996). Bacterial adhesion to polyurethane surfaces in the presence of pre-adsorbed high molecular weight kininogen. *Journal of Biomaterials Science, Polymer Edition*, 7(9), 769–780. <https://doi.org/10.1163/156856296X00110>
- Neerugatti, K. R. E., Veldurthi, N. K., & Heo, J. (2022). Emerging pollutants in water bodies. In *Nano-Enabled Technologies for Water Remediation* (pp. 23–38). Elsevier. <https://doi.org/10.1016/B978-0-323-85445-0.00005-9>
- Neff, P. A., Naji, A., Ecker, C., Nickel, B., von Klitzing, R., & Bausch, A. R. (2006). Electrical Detection of Self-Assembled Polyelectrolyte Multilayers by a Thin Film Resistor. <https://doi.org/10.48550/ARXIV.COND-MAT/0601090>
- Neff, P. A., Wunderlich, B. K., Lud, S. Q., & Bausch, A. R. (2006). Silicon-on-insulator based thin film resistors for quantitative biosensing applications. *Physica Status Solidi (a)*, 203(14), 3417–3423. <https://doi.org/10.1002/pssa.200622387>
- Nichifor, M., Stanciu, M. C., & Zhu, X. X. (2004). Bile acids covalently bound to polysaccharides: 2. Dextran with pendant cholic acid groups. *Reactive and Functional Polymers*, 59(2), 141–148. <https://doi.org/10.1016/j.reactfunctpolym.2004.01.003>
- Novak, L. J., Witt, E. E., & Hiler, M. J. (1955). Soil Conditioners, Dextran and Dextran Products as Soil-Conditioning Materials. *Journal of Agricultural and Food Chemistry*, 3(12), 1028–1033.

- Novoselova, M. V., Loh, H. M., Trushina, D. B., Ketkar, A., Abakumova, T. O., Zatsepin, T. S., Kakran, M., Brzozowska, A. M., Lau, H. H., Gorin, D. A., Antipina, M. N., & Brichkina, A. I. (2020). Biodegradable Polymeric Multilayer Capsules for Therapy of Lung Cancer. *ACS Applied Materials & Interfaces*, 12(5), 5610–5623. <https://doi.org/10.1021/acsami.9b21381>
- Olano-Martin, E., Mountzouris, K. C., Gibson, G. R., & Rastall, R. A. (2000). In vitro fermentability of dextran, oligodextran and maltodextrin by human gut bacteria. *British Journal of Nutrition*, 83(3), 247–255. <https://doi.org/10.1017/S0007114500000325>
- Ortalo-Magne, A., Dupont, M.-A., Lemassu, A., Andersen, A. B., Gounon, P., & Mamadou, D. (1995). Molecular composition of the outermost capsular material of the tubercle bacillus. *Microbiology*, 141(7), 1609–1620. <https://doi.org/10.1099/13500872-141-7-1609>
- Paini, M., Aliakbarian, B., Casazza, A. A., Perego, P., Ruggiero, C., & Pastorino, L. (2015). Chitosan/dextran multilayer microcapsules for polyphenol co-delivery. *Materials Science & Engineering C-Materials for Biological Applications*, 46, 374–380. <https://doi.org/10.1016/j.msec.2014.10.047>
- Pan, Y., & Nitin, N. (2015). Effect of layer-by-layer coatings and localization of antioxidant on oxidative stability of a model encapsulated bioactive compound in oil-in-water emulsions. *Colloids and Surfaces B-Biointerfaces*, 135, 472–480. <https://doi.org/10.1016/j.colsurfb.2015.08.003>
- Papy-Garcia, D., Barbier-Chassefière, V., Rouet, V., Kerros, M.-E., Klochendler, C., Tournaire, M.-C., Barritault, D., Caruelle, J.-P., & Petit, E. (2005). Nondegradative Sulfation of Polysaccharides. Synthesis and Structure Characterization of Biologically Active Heparan Sulfate Mimetics. *Macromolecules*, 38(11), 4647–4654. <https://doi.org/10.1021/ma048485p>
- Parisi, O., Malivindi, R., Amone, F., Ruffo, M., Malanchin, R., Carlomagno, F., Piangiolo, C., Nobile, V., Pezzi, V., Scrivano, L., & Puoci, F. (2017). Safety and Efficacy of Dextran-Rosmarinic Acid Conjugates as Innovative Polymeric Antioxidants in Skin Whitening: What Is the Evidence? *Cosmetics*, 4(3), 28. <https://doi.org/10.3390/cosmetics4030028>
- Park, M., Kim, Y., Ko, Y., Cheong, S., Ryu, S. W., & Cho, J. (2014). Amphiphilic Layer-by-Layer Assembly Overcoming Solvent Polarity between Aqueous and Nonpolar Media. *Journal of the American Chemical Society*, 136(49), 17213–17223. <https://doi.org/10.1021/ja509168g>
- Pasteur, L. (1861). Expériences et vues nouvelles sur la nature des fermentations.
- Patro, T. U., & Wagner, H. D. (2011). Layer-by-layer assembled PVA/Laponite multilayer free-standing films and their mechanical and thermal properties. *Nanotechnology*, 22(45), 455706. <https://doi.org/10.1088/0957-4484/22/45/455706>
- Pescosolido, L., Schuurman, W., Malda, J., Matricardi, P., Alhaique, F., Coviello, T., van Weeren, P. R., Dhert, W. J. A., Hennink, W. E., & Vermonden, T. (2011). Hyaluronic Acid and Dextran-Based Semi-IPN Hydrogels as Biomaterials for Bioprinting. *Biomacromolecules*, 12(5), 1831–1838. <https://doi.org/10.1021/bm200178w>
- Petrila, L.-M., Bucatariu, F., Mihai, M., & Teodosiu, C. (2021). Polyelectrolyte Multilayers: An Overview on Fabrication, Properties, and Biomedical and Environmental Applications. *Materials*, 14(15), 4152. <https://doi.org/10.3390/ma14154152>
- Picart, C., Lavallo, Ph., Hubert, P., Cuisinier, F. J. G., Decher, G., Schaaf, P., & Voegel, J.-C. (2001). Buildup Mechanism for Poly(L-lysine)/Hyaluronic Acid Films onto a Solid Surface. *Langmuir*, 17(23), 7414–7424. <https://doi.org/10.1021/la010848g>
- Picart, C., Mutterer, J., Richert, L., Luo, Y., Prestwich, G. D., Schaaf, P., Voegel, J.-C., & Lavallo, P. (2002). Molecular basis for the explanation of the exponential growth of polyelectrolyte multilayers. *Proceedings of the National Academy of Sciences*, 99(20), 12531–12535. <https://doi.org/10.1073/pnas.202486099>
- Picart, C., Schneider, A., Etienne, O., Mutterer, J., Schaaf, P., Egles, C., Jessel, N., & Voegel, J.-C. (2005). Controlled Degradability of Polysaccharide Multilayer Films In Vitro and In Vivo. *Advanced Functional Materials*, 15(11), 1771–1780. <https://doi.org/10.1002/adfm.200400588>
- Platt, E. J., Kozak, S. L., Durnin, J. P., Hope, T. J., & Kabat, D. (2010). Rapid Dissociation of HIV-1 from Cultured Cells Severely Limits Infectivity Assays, Causes the Inactivation Ascribed to Entry Inhibitors, and Masks the Inherently High Level of Infectivity of Virions. *Journal of Virology*, 84(6), 3106–3110. <https://doi.org/10.1128/JVI.01958-09>
- Pomerantseva, E., Bonaccorso, F., Feng, X., Cui, Y., & Gogotsi, Y. (2019). Energy storage: The future enabled by nanomaterials. *Science*, 366(6468), eaan8285. <https://doi.org/10.1126/science.aan8285>
- Poojari, R., Kini, S., Srivastava, R., & Panda, D. (2016). Intracellular interactions of electrostatically mediated layer-by-layer assembled polyelectrolytes based sorafenib nanoparticles in oral cancer cells. *Colloids and Surfaces B-Biointerfaces*, 143, 131–138. <https://doi.org/10.1016/j.colsurfb.2016.03.024>
- Poptoshev, E., Schoeler, B., & Caruso, F. (2004). Influence of Solvent Quality on the Growth of Polyelectrolyte Multilayers. *Langmuir*, 20(3), 829–834. <https://doi.org/10.1021/la035485u>
- Porcel, C., Lavallo, Ph., Decher, G., Senger, B., Voegel, J.-C., & Schaaf, P. (2007). Influence of the Polyelectrolyte Molecular Weight on Exponentially Growing Multilayer Films in the Linear Regime. *Langmuir*, 23(4), 1898–1904. <https://doi.org/10.1021/la062728k>
- Poyatos-Racionero, E., Ros-Lis, J. V., Vivancos, J.-L., & Martínez-Mañez, R. (2018). Recent advances on intelligent packaging as tools to reduce food waste. *Journal of Cleaner Production*, 172, 3398–3409. <https://doi.org/10.1016/j.jclepro.2017.11.075>
- Priolo, M. A., Gamboa, D., Holder, K. M., & Grunlan, J. C. (2010). Super Gas Barrier of Transparent Polymer-Clay Multilayer Ultrathin Films. *Nano Letters*, 10(12), 4970–4974. <https://doi.org/10.1021/nl103047k>

- Qiu, X., Donath, E., & Mohwald, H. (2001). Permeability of ibuprofen in various polyelectrolyte multilayers. *Macromolecular Materials and Engineering*, 286(10), 591–597. [https://doi.org/10.1002/1439-2054\(20011001\)286:10<591::AID-MAME591>3.0.CO;2-I](https://doi.org/10.1002/1439-2054(20011001)286:10<591::AID-MAME591>3.0.CO;2-I)
- Radhakrishnan, K., & Raichur, A. M. (2012). Biologically triggered exploding protein based microcapsules for drug delivery. *Chemical Communications*, 48(17), 2307. <https://doi.org/10.1039/c2cc17344a>
- Rasheed, T., Bilal, M., Nabeel, F., Adeel, M., & Iqbal, H. M. N. (2019). Environmentally-related contaminants of high concern: Potential sources and analytical modalities for detection, quantification, and treatment. *Environment International*, 122, 52–66. <https://doi.org/10.1016/j.envint.2018.11.038>
- Rathmann, S., Schoenberg, M., Lessig, J., & Reibetanz, U. (2011). Interaction, Uptake, and Processing of LbL-Coated Microcarriers by PMNs. *Cytometry Part A*, 79A(12), 979+. <https://doi.org/10.1002/cyto.a.21145>
- Ratner, B. D., Hoffman, A. S., Schoen, F. J., & Lemons, J. E. (2004). *Biomaterials science: an introduction to materials in medicine*. San Diego, California, 162–4.
- Realini, C. E., & Marcos, B. (2014). Active and intelligent packaging systems for a modern society. *Meat Science*, 98(3), 404–419. <https://doi.org/10.1016/j.meatsci.2014.06.031>
- Reddy Shetty, P., Batchu, U. R., Buddana, S. K., Sambasiva Rao, K., & Penna, S. (2021). A comprehensive review on α -D-Glucans: Structural and functional diversity, derivatization and bioapplications. *Carbohydrate Research*, 503, 108297. <https://doi.org/10.1016/j.carres.2021.108297>
- Reibetanz, U., Chen, M. H. A., Mutukumaraswamy, S., Liaw, Z. Y., Oh, B. H. L., Donath, E., & Neu, B. (2011). Functionalization of Calcium Carbonate Microparticles as a Combined Sensor and Transport System for Active Agents in Cells. *Journal of Biomaterials Science-Polymer Edition*, 22(14), 1845–1859. <https://doi.org/10.1163/092050610X528552>
- Reibetanz, U., Claus, C., Typlt, E., Hofmann, J., & Donath, E. (2006). Defoliation and plasmid delivery with layer-by-layer coated colloids. *Macromolecular Bioscience*, 6(2), 153–160. <https://doi.org/10.1002/mabi.200500163>
- Reibetanz, U., Lessig, J., Hoyer, J., & Neundorf, I. (2010). Surface Functionalized Colloidal Microparticles for Fast Endocytotic Cell Uptake. *Advanced Engineering Materials*, 12(9, SI), B488–B495. <https://doi.org/10.1002/adem.200980074>
- Ren, K., Ji, J., & Shen, J. (2006). Construction and enzymatic degradation of multilayered poly-L-lysine/DNA films. *Biomaterials*, 27(7), 1152–1159. <https://doi.org/10.1016/j.biomaterials.2005.07.021>
- Reurink, D. M., Willott, J. D., Roesink, H. D. W., & de Vos, W. M. (2020). Role of Polycation and Cross-Linking in Polyelectrolyte Multilayer Membranes. *ACS Applied Polymer Materials*, 2(11), 5278–5289. <https://doi.org/10.1021/acsapm.0c00992>
- Richardson, J. J., Björnalm, M., & Caruso, F. (2015). Technology-driven layer-by-layer assembly of nanofilms. *Science*, 348(6233), aaa2491. <https://doi.org/10.1126/science.aaa2491>
- Richert, L., Boulmedais, F., Lavalle, P., Mutterer, J., Ferreux, E., Decher, G., Schaaf, P., Voegel, J.-C., & Picart, C. (2004). Improvement of Stability and Cell Adhesion Properties of Polyelectrolyte Multilayer Films by Chemical Cross-Linking. *Biomacromolecules*, 5(2), 284–294. <https://doi.org/10.1021/bm0342281>
- Rinaudo, M. (2008). Main properties and current applications of some polysaccharides as biomaterials. *Polymer International*, 57(3), 397–430. <https://doi.org/10.1002/pi.2378>
- Robyt, J. F. (1985). Dextran. *Encyclopaedia of Polymer Science*. Wiley-Vch, 4, 753–767.
- Roduner, E. (2006). Size matters: why nanomaterials are different. *Chemical Society Reviews*, 35(7), 583. <https://doi.org/10.1039/b502142c>
- Rogovin, Z. A., Vernik, A. D., Khomiakov, K. P., Laletina, O. P., & Penenzhik, M. A. (1972). Study of the Synthesis of Dextran Derivatives. *Journal of Macromolecular Science: Part A - Chemistry*, 6(3), 569–593. <https://doi.org/10.1080/10601327208056860>
- Romero-Fernandez, M., Moreno-Perez, S., Martins de Oliveira, S., Santamaria, R. I., Guisan, J. M., & Rocha-Martin, J. (2018). Preparation of a robust immobilized biocatalyst of beta-1,4-endoxylanase by surface coating with polymers for production of xylooligosaccharides from different xylan sources. *New Biotechnology*, 44, 50–58. <https://doi.org/10.1016/j.nbt.2018.04.007>
- Rotureau, E., Leonard, M., Dellacherie, E., & Durand, A. (2004). Emulsifying properties of neutral and ionic polymer surfactants based on dextran. *Phys. Chem. Chem. Phys.*, 6(7), 1430–1438. <https://doi.org/10.1039/B314454M>
- Rotureau, E., Marie, E., Dellacherie, E., & Durand, A. (2007). From polymeric surfactants to colloidal systems (3): Neutral and anionic polymeric surfactants derived from dextran. *Colloids and Surfaces A: Physicochemical and Engineering Aspects*, 301(1–3), 229–238. <https://doi.org/10.1016/j.colsurfa.2006.12.062>
- Ruckel, E. R., & Schuerch, C. (1967). Chemical synthesis of a dextran model, poly- α -(1 \rightarrow 6)-anhydro-D-glucopyranose. *Biopolymers: Original Research on Biomolecules*, 5(6), 515–523.
- Sakaguchi, H., Serizawa, T., & Akashi, M. (2003). Layer-by-layer assembly on hydrogel surfaces and control of human whole blood coagulation. *Chemistry Letters*, 32(2), 174–175. <https://doi.org/10.1246/cl.2003.174>
- Salomäki, M., & Kankare, J. (2009). Influence of Synthetic Polyelectrolytes on the Growth and Properties of Hyaluronan–Chitosan Multilayers. *Biomacromolecules*, 10(2), 294–301. <https://doi.org/10.1021/bm8010177>

- Salomäki, M., Tervasmäki, P., Areva, S., & Kankare, J. (2004). The Hofmeister Anion Effect and the Growth of Polyelectrolyte Multilayers. *Langmuir*, 20(9), 3679–3683. <https://doi.org/10.1021/la036328y>
- Salomäki, M., Vinokurov, I. A., & Kankare, J. (2005). Effect of Temperature on the Buildup of Polyelectrolyte Multilayers. *Langmuir*, 21(24), 11232–11240. <https://doi.org/10.1021/la051600k>
- Sánchez-Chaves, M., Arranz, F., & Díaz, C. (1989). Synthesis and characterization of 2-acetoxybenzoic acid-dextran ester conjugates. *Die Makromolekulare Chemie*, 190(10), 2391–2396. <https://doi.org/10.1002/macp.1989.021901005>
- Sato, T., Nishimura-Uemura, J., Shimosato, T., Kawai, Y., Kitazawa, H., & Saito, T. (2004). Dextran from *Leuconostoc mesenteroides* Augments Immunostimulatory Effects by the Introduction of Phosphate Groups. *Journal of Food Protection*, 67(8), 1719–1724. <https://doi.org/10.4315/0362-028X-67.8.1719>
- Schaubeder, J. B., Ravn, J. L., Orzan, E. J. Q., Manfrão-Netto, J. H. C., Geijer, C., Nypelö, T., & Spirk, S. (2022). Xylan-cellulose thin film platform for assessing xylanase activity. *Carbohydrate Polymers*, 294, 119737. <https://doi.org/10.1016/j.carbpol.2022.119737>
- Schauer, C. L., Chen, M.-S., Chatterley, M., Eisemann, K., Welsh, E. R., Price, R. R., Schoen, P. E., & Ligler, F. S. (2003). Color changes in chitosan and poly(allyl amine) films upon metal binding. *Thin Solid Films*, 434(1–2), 250–257. [https://doi.org/10.1016/S0040-6090\(03\)00055-5](https://doi.org/10.1016/S0040-6090(03)00055-5)
- Scheibler, C. (1874). Investigation on the nature of the gelatinous excretion (so-called frog's spawn) which is observed in production of beet-sugar juices. *Z Dtsch Zucker-Ind*, 24, 309–335.
- Schlenoff, J. B., & Dubas, S. T. (2001). Mechanism of Polyelectrolyte Multilayer Growth: Charge Overcompensation and Distribution. *Macromolecules*, 34(3), 592–598. <https://doi.org/10.1021/ma0003093>
- Schlenoff, J. B., Dubas, S. T., & Farhat, T. (2000). Sprayed Polyelectrolyte Multilayers. *Langmuir*, 16(26), 9968–9969. <https://doi.org/10.1021/la001312i>
- Schmitt, J., Gruenewald, T., Decher, G., Pershan, P. S., Kjaer, K., & Loesche, M. (1993). Internal structure of layer-by-layer adsorbed polyelectrolyte films: a neutron and x-ray reflectivity study. *Macromolecules*, 26(25), 7058–7063. <https://doi.org/10.1021/ma00077a052>
- Schoeler, B., Kumaraswamy, G., & Caruso, F. (2002). Investigation of the Influence of Polyelectrolyte Charge Density on the Growth of Multilayer Thin Films Prepared by the Layer-by-Layer Technique. *Macromolecules*, 35(3), 889–897. <https://doi.org/10.1021/ma011349p>
- Schönhoff, M. (2003). Self-assembled polyelectrolyte multilayers. *Current Opinion in Colloid & Interface Science*, 8(1), 86–95. [https://doi.org/10.1016/S1359-0294\(03\)00003-7](https://doi.org/10.1016/S1359-0294(03)00003-7)
- Selina, O. E., Belov, S. Yu., Vlasova, N. N., Balyшева, V. I., Churin, A. I., Bartkoviak, A., Sukhorukov, G. B., & Markvicheva, E. A. (2009). Biodegradable microcapsules with entrapped DNA for development of new DNA vaccines. *Russian Journal of Bioorganic Chemistry*, 35(1), 103–110. <https://doi.org/10.1134/S1068162009010130>
- Serizawa, T., Yamaguchi, M., & Akashi, M. (2002). Enzymatic hydrolysis of a layer-by-layer assembly prepared from chitosan and dextran sulfate. *Macromolecules*, 35(23), 8656–8658. <https://doi.org/10.1021/ma012153s>
- Serizawa, T., Yamaguchi, M., & Akashi, M. (2003). Time-Controlled Desorption of Ultrathin Polymer Films Triggered by Enzymatic Degradation. *Angewandte Chemie International Edition*, 42(10), 1115–1118. <https://doi.org/10.1002/anie.200390293>
- Serizawa, T., Yamaguchi, M., Kishida, A., & Akashi, M. (2003). Alternating gene expression in fibroblasts adhering to multilayers of chitosan and dextran sulfate. *Journal of Biomedical Materials Research Part A*, 67A(3), 1060–1063. <https://doi.org/10.1002/jbm.a.10150>
- Serizawa, T., Yamaguchi, M., Matsuyama, T., & Akashi, M. (2000). Alternating bioactivity of polymeric layer-by-layer assemblies: Anti- vs procoagulation of human blood on chitosan and dextran sulfate layers. *Biomacromolecules*, 1(3), 306–309. <https://doi.org/10.1021/bm000006g>
- Sethi, S. K., & Manik, G. (2018). Recent Progress in Super Hydrophobic/Hydrophilic Self-Cleaning Surfaces for Various Industrial Applications: A Review. *Polymer-Plastics Technology and Engineering*, 57(18), 1932–1952. <https://doi.org/10.1080/03602559.2018.1447128>
- Sethy, P. K., Prusty, K., Mohapatra, P., & Swain, S. K. (2020). Nano-CaCO₃-embodied polyacrylicacid/dextran nanocomposites for packaging applications. *Journal of Applied Polymer Science*, 137(3), 48298. <https://doi.org/10.1002/app.48298>
- Sharma, V., & Sundaramurthy, A. (2020). Multilayer capsules made of weak polyelectrolytes: a review on the preparation, functionalization and applications in drug delivery. *Beilstein Journal of Nanotechnology*, 11, 508–532. <https://doi.org/10.3762/bjnano.11.41>
- Shchukin, D. G., Kommireddy, D. S., Zhao, Y., Cui, T., Sukhorukov, G. B., & Lvov, Y. M. (2004). Polyelectrolyte Micropatterning Using a Laminar-Flow Microfluidic Device. *Advanced Materials*, 16(5), 389–393. <https://doi.org/10.1002/adma.200305776>
- Sher, P., Custódio, C. A., & Mano, J. F. (2010). Layer-By-Layer Technique for Producing Porous Nanostructured 3D Constructs Using Moldable Freeform Assembly of Spherical Templates. *Small*, 6(23), 2644–2648. <https://doi.org/10.1002/sml.201001066>

- Shiratori, S. S., & Rubner, M. F. (2000). pH-Dependent Thickness Behavior of Sequentially Adsorbed Layers of Weak Polyelectrolytes. *Macromolecules*, 33(11), 4213–4219. <https://doi.org/10.1021/ma991645q>
- Shukla, S. K., Mishra, A. K., Arotiba, O. A., & Mamba, B. B. (2013). Chitosan-based nanomaterials: A state-of-the-art review. *International Journal of Biological Macromolecules*, 59, 46–58. <https://doi.org/10.1016/j.ijbiomac.2013.04.043>
- Silva, J. M., Reis, R. L., & Mano, J. F. (2016). Biomimetic Extracellular Environment Based on Natural Origin Polyelectrolyte Multilayers. *Small*, 12(32), 4308–4342. <https://doi.org/10.1002/sml.201601355>
- Song, W., Gaware, V. S., Rúnarsson, Ö. V., Másson, M., & Mano, J. F. (2010). Functionalized superhydrophobic biomimetic chitosan-based films. *Carbohydrate Polymers*, 81(1), 140–144. <https://doi.org/10.1016/j.carbpol.2010.01.041>
- Song, Y., Tzeng, P., & Grunlan, J. C. (2016). Super Oxygen and Improved Water Vapor Barrier of Polypropylene Film with Polyelectrolyte Multilayer Nanocoatings. *Macromolecular Rapid Communications*, 37(12), 963–968. <https://doi.org/10.1002/marc.201600140>
- Song, Z., Yin, J., Luo, K., Zheng, Y., Yang, Y., Li, Q., Yan, S., & Chen, X. (2009). Layer-by-Layer Buildup of Poly(L-glutamic acid)/Chitosan Film for Biologically Active Coating. *Macromolecular Bioscience*, 9(3), 268–278. <https://doi.org/10.1002/mabi.200800164>
- Srivastava, R. K., Sushant, P., Sathvik, A. S., Kolluru, V. C., Ahamad, M. I., Alharthi, M. A., & Luqman, M. (2021). Sources and industrial applications of polysaccharides. In *Food, Medical, and Environmental Applications of Polysaccharides* (pp. 511–530). Elsevier. <https://doi.org/10.1016/B978-0-12-819239-9.00022-1>
- Stickler, D. J., & McLean, R. J. (1995). Biomaterials associated infections: the scale of the problem. *Cells and Materials*, 5(2), 6.
- Sui, Z., Salloum, D., & Schlenoff, J. B. (2003). Effect of Molecular Weight on the Construction of Polyelectrolyte Multilayers: Stripping versus Sticking. *Langmuir*, 19(6), 2491–2495. <https://doi.org/10.1021/la026531d>
- Sukhishvili, S. A., & Granick, S. (1998). Polyelectrolyte adsorption onto an initially-bare solid surface of opposite electrical charge. *The Journal of Chemical Physics*, 109(16), 6861–6868. <https://doi.org/10.1063/1.477253>
- Sukhorukov, G., Antipov, A., Voigt, A., Donath, E., & Mohwald, H. (2001). pH-controlled macromolecule encapsulation in and release from polyelectrolyte multilayer nanocapsules. *Macromolecular Rapid Communications*, 22(1), 44–46. [https://doi.org/10.1002/1521-3927\(20010101\)22:1<44::AID-MARC44>3.0.CO;2-U](https://doi.org/10.1002/1521-3927(20010101)22:1<44::AID-MARC44>3.0.CO;2-U)
- Sullivan, D. M., & Bruening, M. L. (2003). Ultrathin, Gas-Selective Polyimide Membranes Prepared from Multilayer Polyelectrolyte Films. *Chemistry of Materials*, 15(1), 281–287. <https://doi.org/10.1021/cm020639x>
- Sun, G., Zhang, X., Shen, Y.-I., Sebastian, R., Dickinson, L. E., Fox-Talbot, K., Reinblatt, M., Steenbergen, C., Harmon, J. W., & Gerecht, S. (2011). Dextran hydrogel scaffolds enhance angiogenic responses and promote complete skin regeneration during burn wound healing. *Proceedings of the National Academy of Sciences*, 108(52), 20976–20981. <https://doi.org/10.1073/pnas.1115973108>
- Sun, J., Gao, M., & Feldmann, J. (2001). Electric Field Directed Layer-by-Layer Assembly of Highly Fluorescent CdTe Nanoparticles. *Journal of Nanoscience and Nanotechnology*, 1(2), 133–136. <https://doi.org/10.1166/jnn.2001.029>
- Sun, L., Xiong, X., Zou, Q., Ouyang, P., & Krastev, R. (2017). Controlled heparinase-catalyzed degradation of polyelectrolyte multilayer capsules with heparin as responsive layer. *Journal of Applied Polymer Science*, 134(23). <https://doi.org/10.1002/app.44916>
- Suzuki, M., Mikami, T., Matsumoto, T., & Suzuki, S. (1977). Preparation and antitumor activity of O-palmitoyldextran phosphates, O-palmitoyldextrans, and dextran phosphate. *Carbohydrate Research*, 53(2), 223–229. [https://doi.org/10.1016/S0008-6215\(00\)88090-8](https://doi.org/10.1016/S0008-6215(00)88090-8)
- Taketa, T. B., Bataglioli, R. A., Rocha Neto, J. B. M., & Beppu, M. M. (2021). Probing axial metal distribution on biopolymer-based layer-by-layer films for antimicrobial use. *Colloids and Surfaces B: Biointerfaces*, 199, 111505. <https://doi.org/10.1016/j.colsurfb.2020.111505>
- Taketa, T. B., Bataglioli, R. A., Rocha Neto, J. B. M., de Carvalho, B. G., de la Torre, L. G., & Beppu, M. M. (2020). Fundamentals and biomedical applications of biopolymer-based layer-by-layer films. In *Biopolymer Membranes and Films* (pp. 219–242). Elsevier. <https://doi.org/10.1016/B978-0-12-818134-8.00009-2>
- Tang, Z., Wang, Y., Podsiadlo, P., & Kotov, N. A. (2006). Biomedical Applications of Layer-by-Layer Assembly: From Biomimetics to Tissue Engineering. *Advanced Materials*, 18(24), 3203–3224. <https://doi.org/10.1002/adma.200600113>
- Taylor, C., Cheetham, N. W. H., & Walker, G. J. (1985). Application of high-performance liquid chromatography to a study of branching in dextrans. *Carbohydrate Research*, 137, 1–12. [https://doi.org/10.1016/0008-6215\(85\)85144-2](https://doi.org/10.1016/0008-6215(85)85144-2)
- Tong, W., Dong, W., Gao, C., & Mohwald, H. (2005). Charge-controlled permeability of polyelectrolyte microcapsules. *Journal of Physical Chemistry B*, 109(27), 13159–13165. <https://doi.org/10.1021/jp0511092>
- Tong, W., Gao, C., & Mohwald, H. (2006). Stable weak polyelectrolyte microcapsules with pH-responsive permeability. *Macromolecules*, 39(1), 335–340. <https://doi.org/10.1021/ma0517648>
- Tong, W., Song, X., & Gao, C. (2012). Layer-by-layer assembly of microcapsules and their biomedical applications. *Chemical Society Reviews*, 41(18), 6103. <https://doi.org/10.1039/c2cs35088b>
- Torino, M. I., Font de Valdez, G., & Mozzi, F. (2015). Biopolymers from lactic acid bacteria. Novel applications in foods and beverages. *Frontiers in Microbiology*, 6. <https://doi.org/10.3389/fmicb.2015.00834>

- Towle, E. G., Ding, I., & Peterson, A. M. (2020). Impact of molecular weight on polyelectrolyte multilayer assembly and surface properties. *Journal of Colloid and Interface Science*, 570, 135–142. <https://doi.org/10.1016/j.jcis.2020.02.114>
- Treviño-Garza, M. Z., García, S., Heredia, N., Alanís-Guzmán, Ma. G., & Arévalo-Niño, K. (2017). Layer-by-layer edible coatings based on mucilages, pullulan and chitosan and its effect on quality and preservation of fresh-cut pineapple (*Ananas comosus*). *Postharvest Biology and Technology*, 128, 63–75. <https://doi.org/10.1016/j.postharvbio.2017.01.007>
- Trushina, D. B., Akasov, R. A., Khovankina, A. V., Borodina, T. N., Bukreeva, T. V., & Markvicheva, E. A. (2019). Doxorubicin-loaded biodegradable capsules: Temperature induced shrinking and study of cytotoxicity in vitro. *Journal of Molecular Liquids*, 284, 215–224. <https://doi.org/10.1016/j.molliq.2019.03.152>
- Trushina, D. B., Bukreeva, T. V., Borodina, T. N., Belova, D. D., Belyakov, S., & Antipina, M. N. (2018). Heat-driven size reduction of biodegradable polyelectrolyte multilayer hollow capsules assembled on CaCO₃ template. *Colloids and Surfaces B-Biointerfaces*, 170, 312–321. <https://doi.org/10.1016/j.colsurfb.2018.06.033>
- Tuo, X., Chen, D., Cheng, H., & Wang, X. (2005). Fabricating Water-Insoluble Polyelectrolyte into Multilayers with Layer-by-layer Self-assembly. *Polymer Bulletin*, 54(6), 427–433. <https://doi.org/10.1007/s00289-005-0387-0>
- v. Klitzing, R. (2006). Internal structure of polyelectrolyte multilayer assemblies. *Physical Chemistry Chemical Physics*, 8(43), 5012. <https://doi.org/10.1039/b607760a>
- Van Tieghem, P. (1878). On sugar-mill gum. *Ann Sci Nature Bot Biol Veg*, 7, 180–203.
- vander Straeten, A., Bratek-Skicki, A., Jonas, A. M., Fustin, C.-A., & Dupont-Gillain, C. (2018). Integrating Proteins in Layer-by-Layer Assemblies Independently of their Electrical Charge. *ACS Nano*, 12(8), 8372–8381. <https://doi.org/10.1021/acsnano.8b03710>
- vander Straeten, A., Lefèvre, D., Demoustier-Champagne, S., & Dupont-Gillain, C. (2020). Protein-based polyelectrolyte multilayers. *Advances in Colloid and Interface Science*, 280, 102161. <https://doi.org/10.1016/j.cis.2020.102161>
- Vigneswaran, N., Samsuri, F., Ranganathan, B., & Padmapriya. (2014). Recent Advances in Nano Patterning and Nano Imprint Lithography for Biological Applications. *Procedia Engineering*, 97, 1387–1398. <https://doi.org/10.1016/j.proeng.2014.12.420>
- Vikulina, A. S., Anissimov, Y. G., Singh, P., Prokopović, V. Z., Uhlig, K., Jaeger, M. S., von Klitzing, R., Duschl, C., & Volodkin, D. (2016). Temperature effect on the build-up of exponentially growing polyelectrolyte multilayers. An exponential-to-linear transition point. *Physical Chemistry Chemical Physics*, 18(11), 7866–7874. <https://doi.org/10.1039/C6CP00345A>
- Voigt, U., Jaeger, W., Findenegg, G. H., & Klitzing, R. v. (2003). Charge Effects on the Formation of Multilayers Containing Strong Polyelectrolytes. *The Journal of Physical Chemistry B*, 107(22), 5273–5280. <https://doi.org/10.1021/jp0256488>
- Voigt, U., Khrenov, V., Tauer, K., Hahn, M., Jaeger, W., & Klitzing, R. von. (2002). The effect of polymer charge density and charge distribution on the formation of multilayers. *Journal of Physics: Condensed Matter*, 15(1), S213–S218. <https://doi.org/10.1088/0953-8984/15/1/327>
- Wågberg, L., Decher, G., Norgren, M., Lindström, T., Ankerfors, M., & Axnäs, K. (2008). The Build-Up of Polyelectrolyte Multilayers of Microfibrillated Cellulose and Cationic Polyelectrolytes. *Langmuir*, 24(3), 784–795. <https://doi.org/10.1021/la702481v>
- Wang, J., Cheng, Q., Lin, L., & Jiang, L. (2014). Synergistic Toughening of Bioinspired Poly(vinyl alcohol)–Clay–Nanofibrillar Cellulose Artificial Nacre. *ACS Nano*, 8(3), 2739–2745. <https://doi.org/10.1021/nn406428n>
- Wang, X., Zhong, X., Li, J., Liu, Z., & Cheng, L. (2021). Inorganic nanomaterials with rapid clearance for biomedical applications. *Chemical Society Reviews*, 50(15), 8669–8742. <https://doi.org/10.1039/D0CS000461H>
- Wang, Y., Zucker, I., Boo, C., & Elimelech, M. (2021). Removal of Emerging Wastewater Organic Contaminants by Polyelectrolyte Multilayer Nanofiltration Membranes with Tailored Selectivity. *ACS ES&T Engineering*, 1(3), 404–414. <https://doi.org/10.1021/acsestengg.0c00160>
- Webber, J. L., Benbow, N. L., Krasowska, M., & Beattie, D. A. (2017). Formation and enzymatic degradation of poly-L-arginine/fucoidan multilayer films. *Colloids and Surfaces B: Biointerfaces*, 159, 468–476. <https://doi.org/10.1016/j.colsurfb.2017.08.005>
- Werber, J. R., Osuji, C. O., & Elimelech, M. (2016). Materials for next-generation desalination and water purification membranes. *Nature Reviews Materials*, 1(5), 16018. <https://doi.org/10.1038/natrevmats.2016.18>
- Wolter, A., Hager, A.-S., Zannini, E., Czerny, M., & Arendt, E. K. (2014). Influence of dextran-producing *Weissella cibaria* on baking properties and sensory profile of gluten-free and wheat breads. *International Journal of Food Microbiology*, 172, 83–91. <https://doi.org/10.1016/j.ijfoodmicro.2013.11.015>
- Wong, J. E., Zastrow, H., Jaeger, W., & von Klitzing, R. (2009). Specific Ion versus Electrostatic Effects on the Construction of Polyelectrolyte Multilayers. *Langmuir*, 25(24), 14061–14070. <https://doi.org/10.1021/la901673u>
- Wu, F., Misra, M., & Mohanty, A. K. (2021). Challenges and new opportunities on barrier performance of biodegradable polymers for sustainable packaging. *Progress in Polymer Science*, 117, 101395. <https://doi.org/10.1016/j.progpolymsci.2021.101395>
- Wu, T., & Farnood, R. (2014). Cellulose fibre networks reinforced with carboxymethyl cellulose/chitosan complex layer-by-layer. *Carbohydrate Polymers*, 114, 500–505. <https://doi.org/10.1016/j.carbpol.2014.08.053>

- Xiang, F., Givens, T. M., & Grunlan, J. C. (2015). Fast Spray Deposition of Super Gas Barrier Polyelectrolyte Multilayer Thin Films. *Industrial & Engineering Chemistry Research*, 54(19), 5254–5260. <https://doi.org/10.1021/acs.iecr.5b01367>
- Xie, M., Lei, H., Zhang, Y., Xu, Y., Shen, S., Ge, Y., Li, H., & Xie, J. (2016). Non-covalent modification of graphene oxide nanocomposites with chitosan/dextran and its application in drug delivery. *RSC Advances*, 6(11), 9328–9337. <https://doi.org/10.1039/c5ra23823d>
- Yalpani, M., & Hedman, P. O. (1985). Preparation and Applications of Dextran-Derived Products in Biotechnology and Related Areas. *Critical Reviews in Biotechnology*, 3(4), 375–421. <https://doi.org/10.3109/07388558509150789>
- Yildirim, S. (2011). Active packaging for food biopreservation. In *Protective Cultures, Antimicrobial Metabolites and Bacteriophages for Food and Beverage Biopreservation* (pp. 460–489). Elsevier. <https://doi.org/10.1533/9780857090522.3.460>
- Yoo, G., Choi, S. L., Lee, S., Yoo, B., Kim, S., & Oh, M. S. (2016). Enhancement-mode operation of multilayer MoS₂ transistors with a fluoropolymer gate dielectric layer. *Applied Physics Letters*, 108(26), 263106. <https://doi.org/10.1063/1.4955024>
- Yu, D.-G., Jou, C.-H., Lin, W.-C., & Yang, M.-C. (2007). Surface modification of poly(tetramethylene adipate-co-terephthalate) membrane via layer-by-layer assembly of chitosan and dextran sulfate polyelectrolyte multilayer. *Colloids and Surfaces B-Biointerfaces*, 54(2), 222–229. <https://doi.org/10.1016/j.colsurfb.2006.10.026>
- Yu, D.-G., Lin, W.-C., Lin, C.-H., Yeh, Y.-H., & Yang, M.-C. (2007). Construction of antithrombogenic polyelectrolyte multilayer on thermoplastic polyurethane via layer-by-layer self-assembly technique. *Journal of Biomedical Materials Research Part B-Applied Biomaterials*, 83B(1), 105–113. <https://doi.org/10.1002/jbm.b.30772>
- Yu, J., Meharg, B. M., & Lee, I. (2017). Adsorption and interlayer diffusion controlled growth and unique surface patterned growth of polyelectrolyte multilayers. *Polymer*, 109, 297–306. <https://doi.org/10.1016/j.polymer.2016.12.055>
- Zhang, C., Li, C., Aliakbarlu, J., Cui, H., & Lin, L. (2022). Typical application of electrostatic layer-by-layer self-assembly technology in food safety assurance. *Trends in Food Science & Technology*, 129, 88–97. <https://doi.org/10.1016/j.tifs.2022.09.006>
- Zhang, F., Xie, M., Zhao, Y., Zhang, Y., Yang, M., Yang, N., Deng, T., Zhang, M., & Xie, J. (2019). Chitosan and dextran stabilized GO-iron oxide nanosheets with high dispersibility for chemotherapy and photothermal ablation. *Ceramics International*, 45(5), 5996–6003. <https://doi.org/10.1016/j.ceramint.2018.12.070>
- Zhang, J., Senger, B., Vautier, D., Picart, C., Schaaf, P., Voegel, J.-C., & Lavallo, P. (2005). Natural polyelectrolyte films based on layer-by layer deposition of collagen and hyaluronic acid. *Biomaterials*, 26(16), 3353–3361. <https://doi.org/10.1016/j.biomaterials.2004.08.019>
- Zhang, R., Tang, M., Bowyer, A., Eisenthal, R., & Hubble, J. (2005). A novel pH- and ionic-strength-sensitive carboxy methyl dextran hydrogel. *Biomaterials*, 26(22), 4677–4683. <https://doi.org/10.1016/j.biomaterials.2004.11.048>
- Zhao, W., Xu, J.-J., & Chen, H.-Y. (2006). Electrochemical Biosensors Based on Layer-by-Layer Assemblies. *Electroanalysis*, 18(18), 1737–1748. <https://doi.org/10.1002/elan.200603630>
- Zhou, B., Hu, Y., Li, J., & Li, B. (2014). Chitosan/phosvitin antibacterial films fabricated via layer-by-layer deposition. *International Journal of Biological Macromolecules*, 64, 402–408. <https://doi.org/10.1016/j.ijbiomac.2013.12.016>

Chapter 2

Material and methods

Table of content

1. Materials	89
1.1. Chemical products.....	89
1.2. Polyelectrolytes	89
1.2.1. Polycations.....	90
1.2.2. Polyanions.....	91
2. Methods	92
2.1. Characterization of polyelectrolytes.....	92
2.1.1. Molar masses.....	92
2.2.2. Chemical structure	93
2.2. Fabrication of polyelectrolyte multilayers by layer-by-layer method	93
2.2.1. Multilayered films by dipping deposition.....	93
2.2.2. Multilayered films by spin-assisted deposition.....	94
2.3. Layer(s) formation analysis by QCM-D and SPR.....	94
2.3.1. Quartz Crystal Microbalance with Dissipation Monitoring (QCM-D).....	94
2.3.2. Surface Plasmon Resonance Measurement (SPR)	97
2.4. Multilayer film characterization.....	99
2.4.1. Evaluation of water content in the films.....	99
2.4.2. Layer morphology by Atomic Force Microscopy Measurement (AFM).....	100
2.4.3. Evaluation of thickness using structural colors	101
2.4.4. Contact angles by drop tensiometer.....	103
2.4.4. Visual detection of enzymatic activity	104
References	105

1. Materials

1.1. Chemical products

All commercial chemical compounds were used without further purification. Deuterium oxide D₂O (98%) used for D₂O/H₂O exchange and 99.96% D₂O for NMR experiments were purchased from Euriso-Top (France). All the water used was Milli-Q water: 18.2 mΩ, Millipore Milli-Q purification system. Sodium chloride (NaCl) ≥99.5% for solution preparation was purchased from Sigma Aldrich (Germany).

The enzyme used for the detection of enzymatic activity is trypsin from bovine pancreas purchased from Sigma Aldrich (Germany). This trypsin, a type I with an activity of ~10 000 units/mg protein, was prepared in 0.1 M phosphate buffer (pH 6). The trypsin and trypsin solutions were stocked at -20°C.

1.2. Polyelectrolytes

All the commercial and synthesized polyelectrolytes, polycations and polyanions, used for the buildup of the multilayered films are listed in Table 2.1.

Table 2.1. Notation and summarized information of polyelectrolytes used for the formation of multilayered films in this thesis.

Name	Notation	Polycation (PC) / polyanion (PA)	Charge density	Molar mass (g.mol ⁻¹)
<i>Poly(allylamine hydrochloride)</i>	<i>PAH</i>	PC	1 charge / 1 monomer	120 – 200 000
<i>Dextran sulfates</i>	<i>DexS H500</i>	PA	1.75 charge / 1 monomer	500 000
	<i>DexS H40</i>	PA	1.75 charge / 1 monomer	40 000
	<i>DexS L40</i>	PA	0.6 charge / 1 monomer	40 000
	<i>DexS H5</i>	PA	1.75 charge / 1 monomer	5 000
	<i>DexS L5</i>	PA	0.6 charge / 1 monomer	5 000
<i>Diethylaminoethyl-Dextran</i>	<i>Dex-DEAE 500</i>	PC	0.33 charge / 1 monomer	500 000
	<i>Dex-DEAE 150</i>	PC	0.33 charge / 1 monomer	150 000
	<i>Dex-DEAE 40</i>	PC	0.33 charge / 1 monomer	40 000
	<i>Dex-DEAE 10</i>	PC	0.33 charge / 1 monomer	10 000
<i>Oxidized dextran</i>	<i>Ox1-Dex</i>	PA	1 charge / 1 monomer	~ 10 ⁸
	<i>Ox2-Dex</i>	PA	0.92 charge / 1 monomer	~ 10 ⁸
	<i>Ox3-Dex</i>	PA	0.77 charge / 1 monomer	~ 10 ⁸

<i>Oxidized alternan</i>	<i>Ox-Alt</i>	PA	1.1 charge / 1 monomer	~ 10 ⁸
<i>Oxidized reuteran</i>	<i>Ox1-Reu</i>	PA	1.34 charge / 1 monomer	~ 10 ⁸
	<i>Ox2-Reu</i>	PA	0.88 charge / 1 monomer	~ 10 ⁸
<i>Poly-L-lysine</i>	<i>PLL</i>	PC	1 charge / 1 monomer	40 – 60 000

Aqueous solutions of polyelectrolytes were prepared in Milli-Q water and the solutions were stocked at 4°C. The characteristics and preparation of each of the polyelectrolytes are detailed below.

The concentrations of polyelectrolyte solution were chosen according to a preliminary study of multilayer build-up on Quartz Crystal Microbalance with Dissipation Monitoring (QCM-D).

1.2.1. Polycations

Poly(allylamine hydrochloride) (PAH) is a synthetic polycation with a molecular mass in the range of 120 – 200 000 g.mol⁻¹ purchased from Polysciences (Germany). PAH was dissolved in 0mM, 5mM or 25mM NaCl solution using Milli-Q water at a concentration of 0.1 g.L⁻¹ during 12 hours at room temperature under agitation. The pH of the solution was measured between pH 6 – 6.5.

Diethylaminoethyl-Dextran (DEAE-Dex) is a polycation derivated from dextran. The functionalization of dextran to DEAE-Dex is a chemical functionalization. DEAE-Dex with different molecular masses ($M_w \sim 500\,000$ g.mol⁻¹, $M_w \sim 40\,000$ g.mol⁻¹ and $M_w \sim 10\,000$ g.mol⁻¹) was purchased from Sigma Aldrich (Germany). According to their molar masses, DEAE-Dex were noted as: DEAE-Dex 500, DEAE-Dex 40 and DEAE-Dex 10. DEAE-Dex was dissolved in 0mM, 5mM or 25mM NaCl solution using Milli-Q water at a concentration of 0.1 g.L⁻¹ during 12 hours at room temperature under agitation. The pH of the solution was measured between pH 6 – 6.5.

Poly-L-lysine (PLL) is a positively charged amino acid polymer with a molecular mass in the range of 40 – 60 000 g.mol⁻¹ purchased from Sigma Aldrich (Germany). PLL was dissolved in 25mM NaCl solution using Milli-Q water at a concentration of 0.1 g.L⁻¹ during 12 hours at 4°C. The pH of the solution was measured between pH 6 – 6.5.

1.2.2. Polyanions

Dextrans sulfate (DexS) is a polyanion, a dextran derivative functionalized by chemical modifications. Different molar masses ($M_w \sim 500\,000 \text{ g}\cdot\text{mol}^{-1}$, $M_w \sim 40\,000 \text{ g}\cdot\text{mol}^{-1}$ and $M_w \sim 5\,000 \text{ g}\cdot\text{mol}^{-1}$) and different charge densities obtained from Sigma Aldrich (Germany) were employed as polyanions in the multilayer buildup. Two dextrans sulfate with different sulfate contents were purchased: one noted as high sulfate content (H) and the another one as low sulfate content (L). According to their molar masses and their sulfate content, DexS were noted as: DexS H500, DexS H40, DexS L40, DexS H5 and DexS L5.

Oxidized bacterial α -glucans are derivated from neutral Dex DSR-OK, Dex DSR-OK-a3, Dex DSR-OK-a2, Dex DSR-S, Dex DSR-S-a3, Dex DSR-S-a2, alternan and reuteran from TEMPO-oxidation. Neutral α -glucans were obtained by TBI team (Toulouse, France) by synthesis of saccharose with enzymes. The reactions were done in 50mM sodium acetate buffer at pH 5.75 for 24h at 30°C under agitation, followed by 15min at 95°C before stopping the reaction. Oxidized α -glucans were obtained by action of (2,2,6,6-tétraméthylpipéridin-1-yl)oxyl (TEMPO) on neutral polymers in the presence of laccase, for different polymers concentration leading to different oxidation degree.

All polyanions were dissolved at a concentration of $0.5 \text{ g}\cdot\text{L}^{-1}$ with Milli-Q water in 0mM, 5mM and 25mM NaCl during 12 hours at room temperature under agitation. The pH of polyanions solutions was measured between pH 6 – 6.5.

2. Methods

2.1. Characterization of polyelectrolytes

2.1.1. Molar masses

Molar masses of dextrans sulfate were determined using High-Performance Size-Exclusion Chromatography (HPSEC) with OMNISEC Reveal and OMNISEC Resolve (Malvern Panalytical Ltd., Malvern, UK). DexS were dissolved at 5 g.L⁻¹ in deionized water (18.2 mΩ, Millipore Milli-Q purification system) and filtrated at 0.45 μm before measurement. The DexS samples were eluted at a range of 0.7 mL/min with 50mM NaNO₃ containing 0.02% NaN₃. The column used was a polymethyl-methacrylate (A-series) A5000 column (300 mm x 7.8 mm) and intrinsic viscosity determinations were performed using a viscometer included in multi angle light scattering detector Viscotek SEC-MALS 9 (Malvern Panalytical Ltd., Malvern, UK). Intrinsic viscosity data were recorded using OMNISEC 11.01 software (Malvern Panalytical Ltd., Malvern, UK). Molar masses were obtained using Mark-Houwink equation:

$$(1) \quad [\eta] = K \times \frac{M_v^\alpha}{M_0}$$

where $[\eta]$ (dL.g⁻¹) is intrinsic viscosity obtained with HPSEC, M_v (g.mol⁻¹) is the polymer viscosity-average molar mass, M_0 is 1 g.mol⁻¹ and K (dL.g⁻¹), α are viscosity-molecular weight constants for particular polymer-solvent combination. Values of K and α were assumed to be respectively 7.337×10^{-4} dL.g⁻¹ and 0.533 according to value for dextrans at 20°C reported by Güner (Güner, 1999). Molar masses obtained were consistent with supplier data.

Molar masses used for other commercial polyelectrolytes, PAH and Dex-DEAE, were given by the supplier. Molar masses of other functionalized α -glucans including oxidized-dextran, oxidized-alternan and oxidized-reuteran were determined by the TBI team (INRAE, Toulouse).

2.2.2. Chemical structure

Information of the structure of DexS were obtained by nuclear magnetic resonance (NMR). ^1H NMR experiments were carried out on a Bruker AvanceIII 400 NB spectrometer operating for ^1H , equipped with a double-resonance H/X BBo 5-mm probe. Between 90 and 95 mg of dextrans sulfate were solubilized in 1 g of 99.96% D_2O . All spectra were recorded at 30°C using a ^1H 90° pulse of $10.2\ \mu\text{s}$ and 128 accumulation with a recycle delay of 10 s. Acquisition parameters included a water signal pre-saturation applied to decrease the HDO signal in the same order of magnitude than the others peaks. NMR spectra deconvolution was performed using the PeakFit® software (Systat Software, Inc., US). Peak chemical shifts and relative contribution were assigned according to the study report by Neville *et al.* (Neville *et al.*, 1991).

2.2. Fabrication of polyelectrolyte multilayers by layer-by-layer method

Multilayered films were deposited on silicon wafers as solid substrates for AFM analysis, ellipsometry measurements and contact angle measurements. Surfaces were cleaned in piranha bath (mixture of $\text{H}_2\text{O}_2/\text{H}_2\text{SO}_4$ at 70%/30% v/v) for 30 minutes for silicon wafers, then they were extensively rinsed in pure deionized water and dried under a N_2 stream.

In this thesis, we used two deposition methods: 1) dipping method for Quartz Crystal Microbalance with Dissipation monitoring and films below 10 bilayers, 2) automatized spin-assisted deposition method for the construction of films with a high number of bilayers (above 10 bilayers).

2.2.1. Multilayered films by dipping deposition

Multilayered films were formed by the LbL method using dipping procedure (Decher, 1997; Moreau *et al.*, 2012). Silicon substrates were alternately immersed in polycation solution and polyanion solution for 5 minutes. Between each adsorption step, the surfaces were rinsed in 3 water baths containing no NaCl. The dipping sequence was repeated n times to form n bilayers, where a bilayer ($n = 1$) consists in a double layer composed from a single polycation layer and a single polyanion layer. All surfaces were dried under N_2 stream.

2.2.2. Multilayered films by spin-assisted deposition

Multilayered films were formed by the LbL method using a spin-assisted deposition procedure (Cerclier et al., 2013), method illustrated on Figure 2.1. The automated spin-coater is composed of a spin-coater created at BIA, 4 peristaltic pumps and an interface box that connects these 5 elements to a three-axis robot that is controlled by a handmade software (I&J7100, Fisnar).

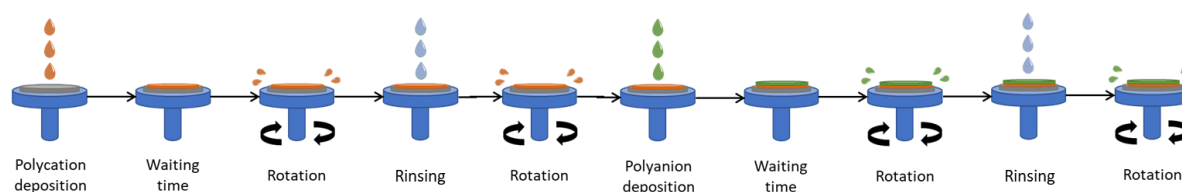


Figure 2.1. Schematic representation of the spin-assisted methodology on the spin-coater system with the three-axis robot.

Polycation and polyanion solutions were alternately deposited on a static silicon substrate cleaned by piranha bath. First, the polycation was deposited on the surface followed by a waiting adsorption step for 275 seconds. Then, the substrate was rotated with a speed of 60 tr.s^{-2} (3600 rpm) for 60 seconds (acceleration of 3.0 tr.s^{-2} , deceleration of 3.0 tr.s^{-2}) to remove the excess of solution. The sequence was repeated n times to form n bilayers, with n between 10 and 80 bilayers.

2.3. Layer(s) formation analysis by QCM-D and SPR

2.3.1. Quartz Crystal Microbalance with Dissipation Monitoring (QCM-D)

Principle of QCM-D. Quartz crystal microbalance with dissipation monitoring (QCM-D) is an acoustic technique developed by Sauerbrey in the 1950s, similar to a piezoelectric balance (Figure 2.2a). This technique is used to study the adsorption of molecules/particles or macromolecules on a substrate. The principle relies on a frequency generator that stimulates the quartz crystal with a sinusoidal voltage of frequency f_0 . This frequency successively takes the value of the fundamental resonance frequency of the crystal (5 MHz) and its harmonics ($n = 3, 5, 7, 9, 11$ and 13 corresponding to frequencies 15, 25, 35,

45, 55 and 65 MHz) on the deformation of a quartz crystal when an electrical potential difference is applied on it (Figure 2.2a). After the end of the excitation, for each resonance ($n = 1$ to 13), the crystal oscillates at a resonance frequency close to the excitation frequency of the quartz crystal. Its mechanical oscillations generate electrical oscillations, which are recorded and processed by the device. The oscillations are damped because of the energy dissipated in the crystal, but especially in the film and in the media in contact with the crystal *i.e.* the “hydrated mass” deposited on the surface. The evaluation of the damping gives access to the dissipation factor D of the system (Figure 2.2b).

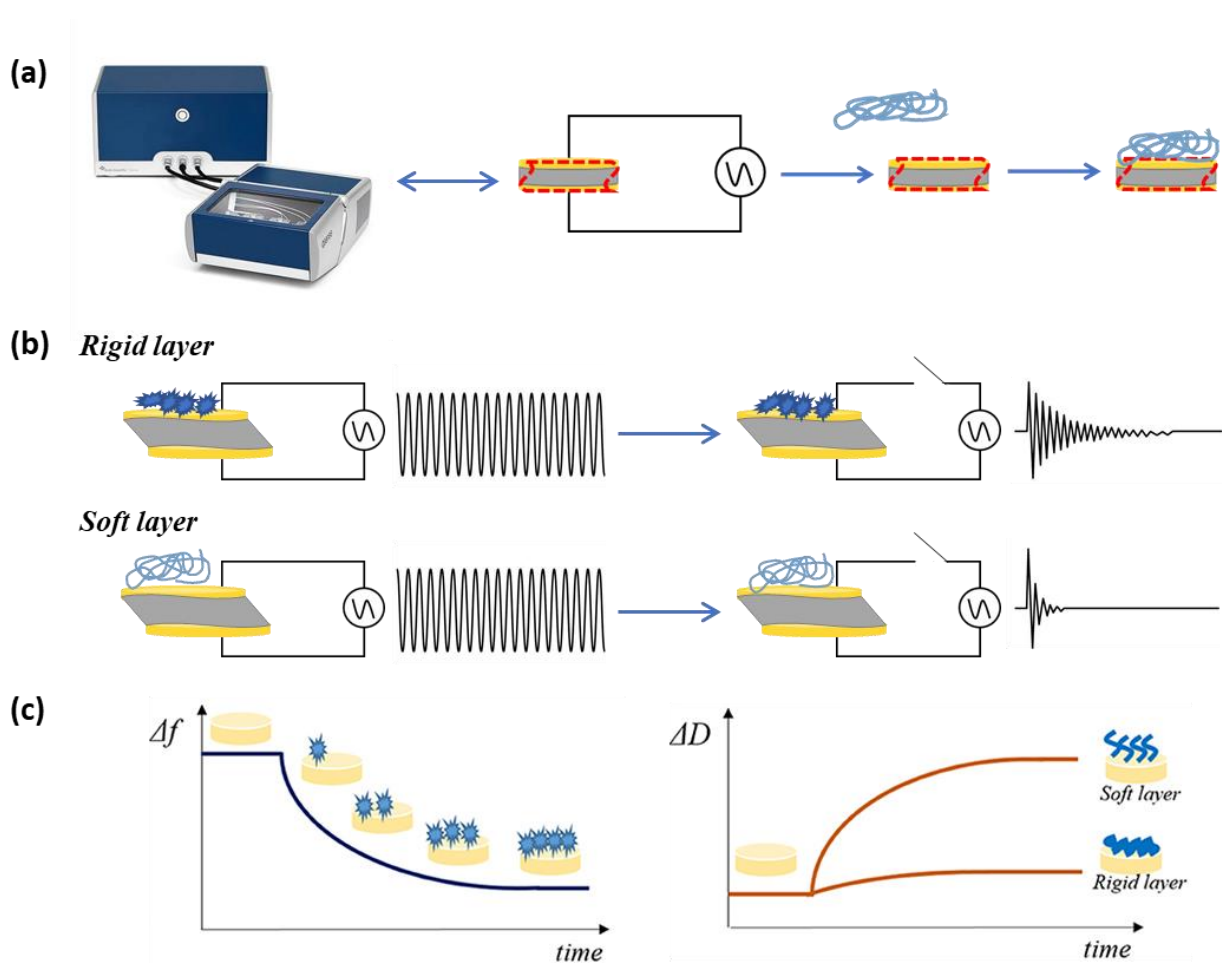


Figure 2.2. Schematic representation of (a) the principle of Quartz crystal microbalance with dissipation monitoring (QCM-D), (b) the damping of oscillations depending on the type of layers and (c) the two main informations obtained using QCM-D (adapted from Biolin Scientific/Q-Sense).

When a mass m is deposited on the surface of the quartz crystal, the resonance frequency f is associated to the quartz changes (Figure 2.2c). The monitoring of the resonance frequency shift, $\Delta f = f_0 - f_x$, (time=0 and time= x) allows to follow the adsorption process in real time and allow the determination of the “hydrated” mass deposited (Δm) on the surface.

QCM-D is a common technique to follow the formation of polyelectrolyte multilayers with a sensitivity out of the order of 18 ng.cm^{-2} . Normalized shifts in frequency ($\Delta f_n/n$) due to additional mass on the sensor surface can be linked to the adsorbed mass (Δm) using Sauerbrey equation (equation 2) for rigid films (dissipation $\Delta D_n/n < 2 \times 10^{-6}$) or using viscoelastic modeling for non-rigid films (dissipation $\Delta D_n/n > 2 \times 10^{-6}$) (Höök et al., 1998; Sauerbrey, 1959).

$$(2) \quad \Gamma_{\text{QCM-D}} = -C \frac{\Delta f_n}{n}$$

where n is the overtone number and C , called the Sauerbrey constant, is a mass sensitivity constant that depends on the thickness and on the inherent properties of the quartz crystal used. For the most common sensors with a fundamental resonance frequency of about 5MHz, $C \approx 18 \text{ ng/cm}^2/\text{Hz}$.

QCM-D also measures an additional parameter, the dissipation factor D (Figure 2.2c) which is defined as the proportion of energy lost E_{lost} at each crystal oscillation versus the energy stocked E_{stored} in the oscillator (equation 3).

$$(3) \quad D = \frac{E_{\text{lost}}}{2\pi E_{\text{stored}}}$$

The dissipation gives information about the energy losses in the system and are particularly useful in the study of viscoelasticity properties of layers (Rodahl et al., 1995). The dissipation factor D can be obtained by stopping regularly the excitation of the quartz crystal and measuring the relaxation time of the system when the resonator energy is dissipating. As the relaxation time is inversely proportional to the damping constant of the system, QCM-D gives the dissipation shift ΔD at each frequency, $\Delta D_n = D_0 - D_x$ (time=0 and time=x) and provides qualitative information on viscoelasticity properties (soft/rigid material) of the film (Dunér et al., 2013; Höök et al., 2001).

Experimental setup. A QCM-D equipment (E4 Q-Sense instrument, AB, Sweden) was used to investigate the adsorption process of polyelectrolytes in the formation of multilayered films. Films were deposited on gold-coated quartz crystals (QSX301, Q-Sense) which were cleaned in piranha bath for 5 minutes. The quartz crystals used are AT-cut quartz crystal coated with a gold layer (100 nm) with a nominal resonance frequency of 5 MHz (f_0) and a C constant of $17.7 \text{ ng.cm}^{-2}.\text{Hz}^{-1}$. Quartz crystals were introduced into the cell and water was introduced at a flow rate of $50 \mu\text{L.min}^{-1}$ at 20°C for at least 1 hour until a stable baseline was obtained. First, the polycation solution was injected at the same flow rate for 5 minutes,

followed by 5 minutes of water rinsing. Then, the polyanion solution was injected at 50 $\mu\text{L}\cdot\text{min}^{-1}$ for 5 minutes, once again followed a 5-minutes rinsing step. The variations in frequency (Δf) and dissipation (ΔD) signals were recorded at the fundamental resonance frequency and its overtones (from 3rd overtone to 7th overtone) (QSoft® software). All experiments were repeated at least 3 times.

In this thesis, the data interpretation was done with Dfind Smartfit model and Sauerbrey equation on QSense Dfind® Software (version 1.2.6, Biolin Scientific, Q-Sense, Sweden), which integrates both frequency and dissipation assuming a film density ρ of 1.200 $\text{g}\cdot\text{cm}^{-3}$ for all films (Serizawa et al., 2000, 2002). The film built under LbL process was assumed to have a uniform thickness and a uniform density. The model, based on Kelvin-Voigt model, was fitted with at least four overtones with a good signal-to-noise S/N ratio and gave access to film thickness, shear elastic modulus and shear viscosity (Höök et al., 2001). Only values from fit with quality indicator higher than 0.70 were used. The adsorbed mass $\Gamma_{\text{QCM-D}}$ ($\text{ng}\cdot\text{cm}^{-2}$) of the polymer layer in hydrated state was calculated as follows:

$$(3) \quad \Gamma_{\text{QCM-D}} = d_{\text{QCM-D}} \cdot \rho$$

where $d_{\text{QCM-D}}$ is the film thickness (cm) obtained with QCM-D technique and ρ is the assumed density of the film ($\text{ng}\cdot\text{cm}^{-3}$).

2.3.2. Surface Plasmon Resonance Measurement (SPR)

Principle of SPR. Surface plasmon resonance (SPR) is an *in-situ* method, based on an optical phenomenon that allows one to follow processes and interactions between particles/macromolecules and a solid surface. The method is based on the light reflection that happens when a beam of light passes from a material into another material with a different refractive index (Figure 2.3). SPR measurements reports changes in the refractive index (n) of a surface, caused by the adsorption of molecules on it. A change in the refractive index induces a variation in the angle of incidence of the light on the interface $\Delta\theta$, which is detected by SPR equipment (Höök et al., 2001; J. D. Kittle et al., 2012; Stenberg et al., 1991).

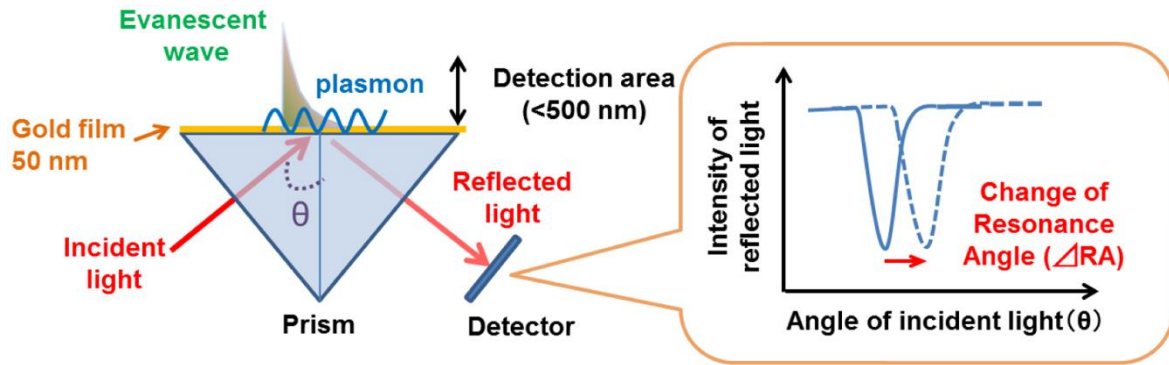


Figure 2.3. Principle of SPR sensor. Surface plasmon resonance (SPR) sensors detect a refractive index (RI) change within a detection area (<500 nm) as a change of resonance angle (RA) from (Yanase et al., 2014).

The refractive index n , and so $\Delta\theta$, is related to the thickness and mass concentration of the adsorbed layers without associated water and the thickness d_{SPR} (nm) was determined using the following equation derived from Feijter et al. equation (Feijter et al., 1978):

$$(4) \quad d_{SPR} = \frac{l_d}{2} \frac{\Delta\theta}{m(n_a - n_s)}$$

where l_d is a characteristic decay length of the evanescent electromagnetic field estimated at 0.37 of the light wavelengths ($\lambda_d = 281.2$ nm), m is a sensitivity factor for the sensor obtained after calibration of the SPR ($101.93^\circ/\text{RI}$), n_s is the refractive index of the bulk solution ($n_s = 1.33371$), n_a is the refractive index of the adsorbed species in rigid and compact film.

Experimental setup. Building of polyelectrolyte multilayers was followed by SPR on a Biacore $\times 100$ instrument (Sweden) using gold-coated chips (SIA kit Au, GE Healthcare, France) cleaned in piranha bath for 5 minutes. The sensor was slid into the equipment flow cell, where Milli-Q water was injected at a flow rate of $30 \mu\text{L}\cdot\text{min}^{-1}$ at 20°C until baseline stabilization. Then the polycation and polyanion solutions were alternately introduced for 5 minutes, followed by a 5-minutes injection of deionized water at $30 \mu\text{L}\cdot\text{min}^{-1}$ flow rate.

In this thesis, the refractive index n_a was assumed to be 1.49 and 1.48 respectively for PAH and dextrans and other α -glucans derivatives, which are values for rigid dry films entirely made of the polymer (Kim et al., 2006; Silva et al., 2016). The adsorbed mass Γ_{SPR} ($\text{ng}\cdot\text{cm}^{-2}$) was calculated as follows:

$$(5) \quad \Gamma_{SPR} = d_{SPR} \cdot \rho$$

where d_{SPR} is the film thickness (cm) and ρ is the density of the film ($\text{ng}\cdot\text{cm}^{-3}$).

2.4. Multilayer film characterization

2.4.1. Evaluation of water content in the films

The determination of the water content / hydration of the films was done using two different methods:

- 1) Comparing the “hydrated” mass obtained with QCM-D and the “dry” mass obtained with SPR.
- 2) Performing a solvent exchange between H₂O and D₂O using QCM-D.

Calculated QCM-D mass, Γ_{QCM-D} , represents the “hydrated” mass, *i.e.* the adsorbed polymer and the coupled water while calculated SPR mass, Γ_{SPR} , is related to the “dry” mass, *i.e.* the polymer without associated water (Davantès et al., 2019; Stokes et al., 2011). Using both techniques, the water content of films, $H_2O_{SPR/QCM}$ (%) is calculated as follow:

$$(6) \quad H_2O_{SPR/QCM}(\%) = \frac{\Gamma_{QCM-D} - \Gamma_{SPR}}{\Gamma_{QCM-D}} \times 100\%$$

The water content was calculated using QCM-D by switching the solvent from water to deuterium oxide D₂O (J. Kittle et al., 2021; J. D. Kittle et al., 2012; Villares et al., 2017). The H₂O/D₂O solvent exchange was performed with one bilayer constructed in the same conditions as described in the section 2.3.1 “QCM-D”. After layer stabilization in H₂O at a flow rate of 50 $\mu\text{l}\cdot\text{min}^{-1}$, D₂O is injected for 5 minutes followed by rinsing with H₂O during 30 minutes. The same experiment was done using the bare quartz substrate as reference system.

The changes in frequency between bare quartz crystal $(\Delta f/n)_{bare}$ and quartz crystals covered by layers $(\Delta f/n)_{film}$ allow to determine the frequency shift $(\Delta f/n)_{water}$ caused by solvent exchange with the following equation (J. Kittle et al., 2021):

$$(7) \quad \left(\frac{\Delta f}{n}\right)_{water} = \frac{\left(\frac{\Delta f}{n}\right)_{film} - \left(\frac{\Delta f}{n}\right)_{bare}}{\left(\frac{\rho_{D_2O}}{\rho_{H_2O}}\right) - 1}$$

where n is the overtone number and ρ the densities of solvent, 0.998 $\text{g}\cdot\text{cm}^{-3}$ for H₂O and 1.106 $\text{g}\cdot\text{cm}^{-3}$ for D₂O at 20°C. The water content from H₂O/D₂O exchange, $H_2O_{exchange}$ (%), can then be calculated as:

$$(8) \quad H_2O_{exchange}(\%) = 100\% \times \frac{\left(\frac{\Delta f}{n}\right)_{water}}{\left(\frac{\Delta f}{n}\right)_{film}}$$

2.4.2. Layer morphology by Atomic Force Microscopy Measurement (AFM)

Principle of AFM. Atomic force microscopy (AFM) is based on the measurement of the short-range interaction forces of the atoms of the fine probe with those of the surface (McClelland et al., 1987; Mermut et al., 2003). This high-resolution scanning probe microscope allows to image the surface of samples with a lateral resolution of 30 Ångstroms (Å) and a vertical resolution of 1 Å. The operating principle of this microscope is described in Figure 2.4.

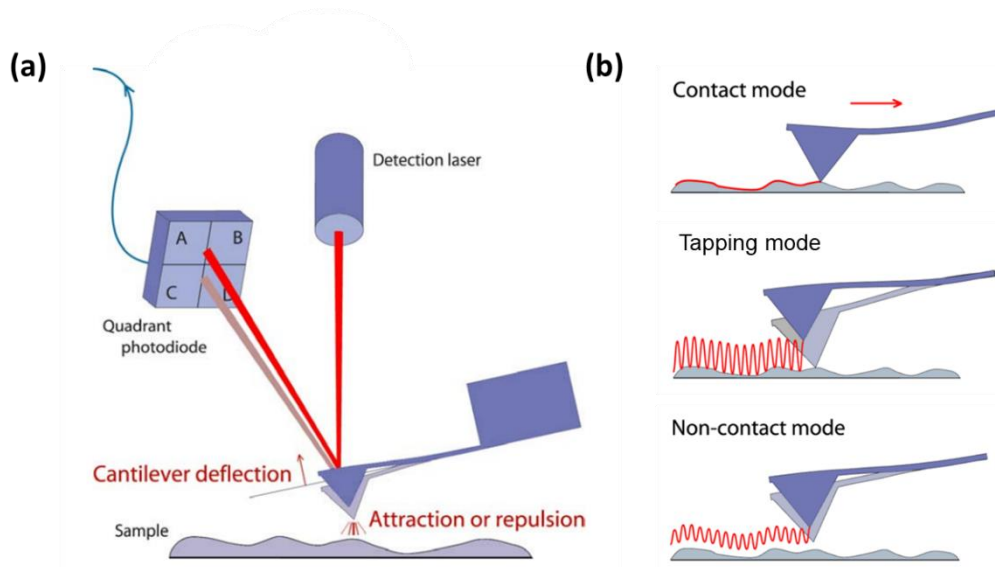


Figure 2.4. (a) Principle of Atomic Force Microscope (AFM): scanning probe microscope using interaction forces between the cantilever and the surface. (b) Different modes of AFM, including contact mode, tapping mode and non-contact mode. Adapted from AFM Handbook, JPK NanoWizard.

The force sensor is a cantilever (probe) with an extremely fine sharp tip (a few nm). The interaction forces between the tip and the surface modify the deflection or the torsion (static or oscillating) of the cantilever. The measurement of the deformations is done by the deflection of a laser beam reflected by the tip of the cantilever. As required, the forces applied between the tip and the surface can be measured to detect mechanical contact force, magnetic forces, van der Waals interaction, electrostatic, capillary, chemical and steric forces.

Three modes of operation are often used in an AFM unit: contact mode, non-contact mode and tap mode as presented in Figure 2.4.

Experimental setup. AFM images (height, error-signal and phase images) of multilayered films adsorbed on silicon wafers were recorded in air employing INNOVA AFM from Bruker (France). Images were registered with low scan rates (0.3 Hz) using nitride

coated silicon probes with spring constants of 37 N.m^{-1} (TESPA-VS, Bruker, France) or 2.8 N.m^{-1} (FESPA-V2, Bruker, France). All images were taken at both $10 \mu\text{m} \times 10 \mu\text{m}$ and $5 \mu\text{m} \times 5 \mu\text{m}$ at a resolution of 512×512 points or 1024×1024 points. Treatment to improve AFM images and their analysis were done using Gwyddion Software (version 2.58, developed by Czech Metrology Institute). Based on three AFM images per surface, the surface root mean squared (RMS) roughness was quantified. In addition of RMS, scratching method was realized to obtain average height and height profiles by analysis eight zones of a surface scratched with a razor blade. When the morphology of surface showed aggregates (peaks, beads, *etc.*), a statistic analysis of their size was performed by measuring the width of 20 patterns with Gwyddion Software.

2.4.3. Evaluation of thickness using structural colors

A structural color is a color component due to interference of light, diffraction, refractive dispersion, differential scattering or differential polarization. As presented in literature chapter (chapter 1), structural colors in thin films such as multilayers is mostly caused by the first type: light interferences. Thin-film interference is a type of structural coloration in which two or more semi-transparent surfaces are layered, causing constructive and destructive interference as illustrated in Figure 2.5.

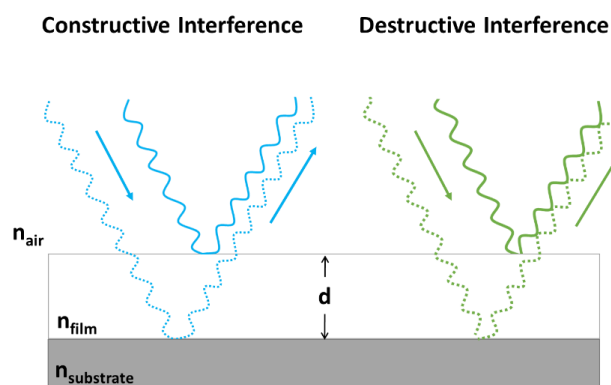


Figure 2.5. Schematic representation of light interferences, with constructive and destructive interferences for a thin film deposited of refractive index n_{film} on a substrate of refractive index $n_{\text{substrate}}$.

As explained before (details in chapter 1, section 4.2.1), the multilayer films can be related to thin films with only one refractive index change if the thin films are composed of alternating layers with refraction indexes close to each other. With the Bragg's law, the

wavelength resulting from constructive interferences and destructive interferences can be related to both the refractive index of the film and its thickness.

In the case of $n_{film} > n_{air}$ and $n_{film} < n_{substrate}$, the wavelength resulting from the constructive interferences is given by Equation 9 and the wavelength resulting from destructive interferences is given by Equation 10.

$$(9) \quad \lambda = 2d \cdot n_{film} m$$

$$(10) \quad \lambda = 2d \cdot n_{film} \left(m + \frac{1}{2} \right)$$

where d is the thickness of the film, λ is the wavelength of the incident light, n_{film} is the refractive index of the film, and m ($m=0, 1, 2, 3, \dots$) is an integer related to the number of reflection maxima.

In the case of $n_{film} > n_{air}$ and $n_{film} > n_{substrate}$, the wavelength resulting in the constructive interferences is given by Equation 11 and the wavelength resulting from destructive interference is given by Equation 12.

$$(11) \quad \lambda = 2d \cdot n_{film} \left(m + \frac{1}{2} \right)$$

$$(12) \quad \lambda = 2d \cdot n_{film} m$$

The multilayers prepared in this thesis were composed of polycation and polyanion with refraction index of around 1.48 for α -glucans and 1.49 for PAH. Thus, we decide to assimilate them as thin films with a theoretical refractive index of 1.48. Moreover, the films are built on silicon wafers with a refractive index around 2.10. So, we have for all film in this thesis $n_{film} < n_{substrate}$ and we used equation 9 and equation 10 to determine the thickness d for our film using their structural colors.

For colors composed of a unique wavelength (e.g. blue, green or red), the theoretical thickness was calculated using the wavelength of the color and equation 9 for constructive interferences. For colors composed of a mixture of wavelengths (e.g. magenta or brown), the theoretical thickness was calculated using the wavelength of the opposite color and equation

10 for destructive interferences. In fact, we supposed that the color observed was a result of destructive interferences with the wavelength of the opposite optical color.

The structural colors were observed under white light with naked eyes and recorded at a vertical angle using a 64MP camera of a smartphone.

2.4.4. Contact angles by drop tensiometer

Principle of wettability and contact angle. Wettability characterizes the ease with which a drop of liquid spreads on a solid surface. Wettability is characterized by the contact angle θ (or wetting angle) of a drop of liquid placed on the solid (Giridhar et al., 2017; Good, 1992; Yuan & Lee, 2013). This angle is dependent on solid-liquid γ_{SL} interfacial tension, surface energy of the solid γ_{SV} and surface tension of the liquid γ_{LV} . At equilibrium, the sum of the three forces applied to the surface is zero, and the contact angle can be described by the equation of Young, equation 13.

$$(13) \quad \gamma_{LV} \cos \theta = \gamma_{SV} - \gamma_{SL}$$

The equation indicates that when a liquid is strongly attracted to the solid surface, *i.e.* solid-liquid γ_{SL} interfacial tension is low and the surface energy of the solid high, the liquid drop will completely spread out on the solid surface, corresponding to a contact angle of 0° . This is the case for hydrophilic surfaces and water that result in a good wetting as illustrated on Figure 2.6. In the opposite, it is often considered that the contact angle will be larger than 90° corresponding to a nonwetting situation with hydrophobic surface. Surfaces with a contact angle greater than 150° are called superhydrophobic surfaces.

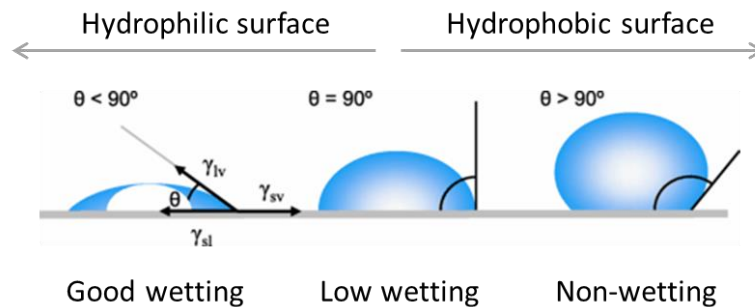


Figure 2.6. Schematic representation of the contact angle formed by liquid drop on a surface with wetting and non-wetting situations, adapted from (Yuan & Lee, 2013).

Experiment set-up. The contact angles of multilayer films absorbed on silicon wafers were measured using an automatic drop tensiometer TRACKER from Teclis Scientific (France). The device is composed of a syringe mounted on a motor to control the volume of the drops and a tray on which we deposit our samples. A CCD camera (640x480) with an extension tube to increase the magnification and a telecentric lens is used to photograph the deposit of the drop on the surface and calculate the contact angles. The volume of the drop, the data acquisition and the analysis of the angles were performed automatically by the Windrop software. For the contact angles of the films prepared in our work, the drop volume chosen was 2 μ L. The acquisition time was 80 seconds, with a measurement every 2 seconds to observe and choose the angle stability time. Final contact angles were calculated at 80 seconds. The average contact angle was calculated by repeating the measurements 6 times at different locations on the surfaces.

2.4.4. Visual detection of enzymatic activity

To evaluate the possibility of detecting enzymatic activity, multilayer films were made by spin-assisted deposition on a quarter silicon wafer. Trypsin enzyme solutions were prepared at different concentrations (1 mg.mL⁻¹, 0.1 mg.mL⁻¹ and 0.01 mg.mL⁻¹) in 0.1 M phosphate buffer (pH 6). The tests were performed by dipping the films in a beaker containing the enzyme solution at 38°C for 30 minutes. After this time, the films were rinsed with MilliQ water and dried by N₂ flow. The degradation of the films is evidenced by the change in film color due to the light interference phenomenon described in chapter 1 (section 4.2.1) and in chapter 2 (section 2.4.3).

References

- Cerclier, C. V., Guyomard-Lack, A., Cousin, F., Jean, B., Bonnin, E., Cathala, B., & Moreau, C. (2013). Xyloglucan–Cellulose Nanocrystal Multilayered Films: Effect of Film Architecture on Enzymatic Hydrolysis. *Biomacromolecules*, 14(10), 3599–3609. <https://doi.org/10.1021/bm400967e>
- Davantès, A., Nigen, M., Sanchez, C., d’Orlando, A., & Renard, D. (2019). Adsorption of Hyperbranched Arabinogalactan-Proteins from Plant Exudate at the Solid–Liquid Interface. *Colloids and Interfaces*, 3(2), 2. <https://doi.org/10.3390/colloids3020049>
- Decher, G. (1997). Fuzzy Nanoassemblies: Toward Layered Polymeric Multicomposites. *Science*, 277(5330), 1232–1237. <https://doi.org/10.1126/science.277.5330.1232>
- Dunér, G., Thormann, E., & Dédinaité, A. (2013). Quartz Crystal Microbalance with Dissipation (QCM-D) studies of the viscoelastic response from a continuously growing grafted polyelectrolyte layer. *Journal of Colloid and Interface Science*, 408, 229–234. <https://doi.org/10.1016/j.jcis.2013.07.008>
- Feijter, J. A. D., Benjamins, J., & Veer, F. A. (1978). Ellipsometry as a tool to study the adsorption behavior of synthetic and biopolymers at the air–water interface. *Biopolymers*, 17(7), 1759–1772. <https://doi.org/10.1002/bip.1978.360170711>
- Giridhar, G., Manepalli, R. K. N. R., & Apparao, G. (2017). Contact Angle Measurement Techniques for Nanomaterials. In *Thermal and Rheological Measurement Techniques for Nanomaterials Characterization* (pp. 173–195). Elsevier. <https://doi.org/10.1016/B978-0-323-46139-9.00008-6>
- Good, R. J. (1992). Contact angle, wetting, and adhesion: a critical review. *Journal of Adhesion Science and Technology*, 6(12), 1269–1302. <https://doi.org/10.1163/156856192X00629>
- Güner, A. (1999). Unperturbed dimensions and the theta temperature of dextran in aqueous solutions. *Journal of Applied Polymer Science*, 72(7), 871–876. [https://doi.org/10.1002/\(SICI\)1097-4628\(19990516\)72:7<871::AID-APP2>3.0.CO;2-R](https://doi.org/10.1002/(SICI)1097-4628(19990516)72:7<871::AID-APP2>3.0.CO;2-R)
- Höök, F., Kasemo, B., Nylander, T., Fant, C., Sott, K., & Elwing, H. (2001). Variations in Coupled Water, Viscoelastic Properties, and Film Thickness of a Mefp-1 Protein Film during Adsorption and Cross-Linking: A Quartz Crystal Microbalance with Dissipation Monitoring, Ellipsometry, and Surface Plasmon Resonance Study. *Analytical Chemistry*, 73(24), 5796–5804. <https://doi.org/10.1021/ac0106501>
- Höök, F., Rodahl, M., Brzezinski, P., & Kasemo, B. (1998). Energy Dissipation Kinetics for Protein and Antibody–Antigen Adsorption under Shear Oscillation on a Quartz Crystal Microbalance. *Langmuir*, 14(4), 729–734. <https://doi.org/10.1021/la970815u>
- Kim, J.-H., Fujita, S., & Shiratori, S. (2006). Design of a thin film for optical applications, consisting of high and low refractive index multilayers, fabricated by a layer-by-layer self-assembly method. *Colloids and Surfaces A: Physicochemical and Engineering Aspects*, 284–285, 290–294. <https://doi.org/10.1016/j.colsurfa.2005.11.081>
- Kittle, J. D., Wondraczek, H., Wang, C., Jiang, F., Roman, M., Heinze, T., & Esker, A. R. (2012). Enhanced Dewatering of Polyelectrolyte Nanocomposites by Hydrophobic Polyelectrolytes. *Langmuir*, 28(30), 11086–11094. <https://doi.org/10.1021/la3016996>
- Kittle, J., Levin, J., & Levin, N. (2021). Water Content of Polyelectrolyte Multilayer Films Measured by Quartz Crystal Microbalance and Deuterium Oxide Exchange. *Sensors*, 21(3), 3. <https://doi.org/10.3390/s21030771>
- McClelland, G. M., Erlandsson, R., & Chiang, S. (1987). Atomic Force Microscopy: General Principles and a New Implementation. In D. O. Thompson & D. E. Chimenti (Eds.), *Review of Progress in Quantitative Nondestructive Evaluation* (pp. 1307–1314). Springer US. https://doi.org/10.1007/978-1-4613-1893-4_148
- Mermut, O., Lefebvre, J., Gray, D. G., & Barrett, C. J. (2003). Structural and Mechanical Properties of Polyelectrolyte Multilayer Films Studied by AFM. *Macromolecules*, 36(23), 8819–8824. <https://doi.org/10.1021/ma034967+>
- Moreau, C., Beury, N., Delorme, N., & Cathala, B. (2012). Tuning the Architecture of Cellulose Nanocrystal–Poly(allylamine hydrochloride) Multilayered Thin Films: Influence of Dipping Parameters. *Langmuir*, 28(28), 10425–10436. <https://doi.org/10.1021/la301293r>
- Neville, G. A., Rochon, P., Rej, R. N., & Perlin, A. S. (1991). Characterization and differentiation of some complex dextran sulfate preparations of medicinal interest. *Journal of Pharmaceutical Sciences*, 80(3), 239–244. <https://doi.org/10.1002/jps.2600800310>
- Rodahl, M., Höök, F., Krozer, A., Brzezinski, P., & Kasemo, B. (1995). Quartz crystal microbalance setup for frequency and Q-factor measurements in gaseous and liquid environments. *Review of Scientific Instruments*, 66(7), 3924–3930. <https://doi.org/10.1063/1.1145396>
- Sauerbrey, G. (1959). Verwendung von Schwingquarzen zur Wägung dünner Schichten und zur Mikrowägung. *Zeitschrift für Physik*, 155(2), 206–222. <https://doi.org/10.1007/BF01337937>
- Serizawa, T., Yamaguchi, M., & Akashi, M. (2002). Enzymatic hydrolysis of a layer-by-layer assembly prepared from chitosan and dextran sulfate. *Macromolecules*, 35(23), 8656–8658. <https://doi.org/10.1021/ma012153s>
- Serizawa, T., Yamaguchi, M., Matsuyama, T., & Akashi, M. (2000). Alternating Bioactivity of Polymeric Layer-by-Layer Assemblies: Anti- vs Procoagulation of Human Blood on Chitosan and Dextran Sulfate Layers. *Biomacromolecules*, 1(3), 306–309. <https://doi.org/10.1021/bm000006g>

- Silva, J. M., Reis, R. L., & Mano, J. F. (2016). Biomimetic Extracellular Environment Based on Natural Origin Polyelectrolyte Multilayers. *Small*, 12(32), 4308–4342. <https://doi.org/10.1002/sml.201601355>
- Stenberg, E., Persson, B., Roos, H., & Urbaniczky, C. (1991). Quantitative determination of surface concentration of protein with surface plasmon resonance using radiolabeled proteins. *Journal of Colloid and Interface Science*, 143(2), 513–526. [https://doi.org/10.1016/0021-9797\(91\)90284-F](https://doi.org/10.1016/0021-9797(91)90284-F)
- Stokes, J. R., Macakova, L., Chojnicka-Paszun, A., de Kruif, C. G., & de Jongh, H. H. J. (2011). Lubrication, Adsorption, and Rheology of Aqueous Polysaccharide Solutions. *Langmuir*, 27(7), 3474–3484. <https://doi.org/10.1021/la104040d>
- Villares, A., Bizot, H., Moreau, C., Rolland-Sabaté, A., & Cathala, B. (2017). Effect of xyloglucan molar mass on its assembly onto the cellulose surface and its enzymatic susceptibility. *Carbohydrate Polymers*, 157, 1105–1112. <https://doi.org/10.1016/j.carbpol.2016.10.072>
- Yanase, Y., Hiragun, T., Ishii, K., Kawaguchi, T., Yanase, T., Kawai, M., Sakamoto, K., & Hide, M. (2014). Surface Plasmon Resonance for Cell-Based Clinical Diagnosis. *Sensors*, 14(3), 4948–4959. <https://doi.org/10.3390/s140304948>
- Yuan, Y., & Lee, T. R. (2013). Contact Angle and Wetting Properties. In G. Bracco & B. Holst (Eds.), *Surface Science Techniques* (Vol. 51, pp. 3–34). Springer Berlin Heidelberg. https://doi.org/10.1007/978-3-642-34243-1_1

Chapter 3

Layer-by-layer formation of α -glucans multilayers

Table of content

Introduction	113
1. Screening: capacity of α-glucans derivatives to form multilayers	116
<u>1.1. Multilayers based on dextrans sulfate (DexS).....</u>	<u>117</u>
1.1.1. <i>Poly(allylamine hydrochloride) and dextran sulfate multilayers (PAH/DexS 40).....</i>	118
1.1.2. <i>Diethylaminoethyl-dextran and dextran sulfate multilayers (Dex-DEAE 150/DexS 40) ..</i>	122
<u>1.2. Multilayers based on α-glucans.....</u>	<u>126</u>
1.2.1. <i>Poly(allylamine hydrochloride) and α-glucans (PAH/ α-glucans)</i>	127
1.2.2. <i>Diethylaminoethyl-dextran and α-glucans (Dex-DEAE 150/ α-glucans).....</i>	131
<u>1.3. Summarized information on multilayers films.....</u>	<u>135</u>
2. Growth mechanisms of PAH/DexS multilayers.....	137
<u>2.1. Physico-chemical characterization of PAH/DexS.....</u>	<u>138</u>
2.1.1. <i>Water content</i>	138
2.1.2. <i>Surface morphology.....</i>	139
<u>2.2. Formation mechanisms for DexS/PAH films.....</u>	<u>141</u>
2.2.1. <i>Tentative mechanism for (PAH/DexS H40) i.e. type A.....</i>	142
2.2.2. <i>Tentative mechanism for (PAH/DexS L40) i.e. type B</i>	143
Conclusion.....	145
References	146
Annexes	149

This chapter is partially adapted from the article:

Delvart, A., Moreau, C., D'orlando, A., Falourd, X., & Cathala, B. (2022). Dextran-based polyelectrolyte multilayers: Effect of charge density on film build-up and morphology. Colloids and Surfaces B: Biointerfaces, 210, 112258. <https://doi.org/10.1016/j.colsurfb.2021.112258>

Introduction

Bacterial α -glucans are a family of α -glucans naturally produced by bacteria from sucrose, regrouping dextrans, alternans, reuterans and mutans. Main chain consists of D-glucose units linked by α -(1 \rightarrow 6), α -(1 \rightarrow 4) or α -(1 \rightarrow 3) type glycosidic bonds which displays backbone with various size and ramifications, depending on the bacterium involved during production (Díaz-Montes, 2021). Within the increasing interest in the elaboration of bio-based materials, α -glucans are attractive polymers due to their wide availability and their diversified structure differing in branching patterns or molar mass. Also, the occurrence of hydroxyl groups on the surface of the main chain and branches gives them interesting functionalization abilities (Antonini et al., 1964; Heinze et al., 2006). Especially, dextrans, partially degraded-dextrans and dextran derivatives find numerous applications in various areas as for instance, in the biomedical field, food science, cosmetics formulation and environmental field (de Belder, 1996; Leathers, 2002; Naessens et al., 2005; Robyt, 1985).

Charged modified dextrans, such as dextrans sulfate, have also been used for coatings and thin films elaboration. Their charged groups promote interactions with other polyelectrolytes (PEs) and thus, their inclusion in polymers assemblies such as polyelectrolyte multilayers (PEMs) (Serizawa et al., 2002; Balabushevich et al., 2003; Pescosolido et al., 2011; Matsusaki et al., 2007). Due to their availability and biocompatibility, dextrans have already been successfully incorporated in PEMs with various positively charged PEs for biological and biomedical applications. However, apart from dextrans and dextran derivatives, other bacterial α -glucans such as alternans, reuterans and their derivatives are not currently used or studied in the field of multilayered materials.

Films of PEs can be typically formed using the layer-by-layer (LbL) technique, introduced by Decher *et al.* in the 1990 (Decher, 1997; Decher *et al.*, 1992), based on the alternative adsorption of cationic and anionic charged PEs, *via* the contribution of various driving forces (chapter 1, section 2.2.1). Among all interactions, electrostatics between oppositely charged PEs was thought to be the main driving force for multilayers formation (Decher *et al.*, 1992), and the film growth is explained by charge density of the adsorbing PEs and associated charge matching between poly-ions (Schoeler *et al.*, 2002; Voigt *et al.*, 2003). Schlenoff *et al.* have reported studies on charge balance in PEMs based on the charge overcompensation and distribution in films and proposed a modelling method to determine growth mechanism of PEMs (Schlenoff *et al.*, 1998; Schlenoff & Dubas, 2001). Furthermore, several works reveal the contribution of other driving non-electrostatic forces, such as hydrophobic forces or hydrogen bonds, especially when polysaccharides are involved (Cerclier *et al.*, 2010; Crouzier & Picart, 2009; Kotov, 1999). A linear growth of the film thickness with the number of deposited layers is commonly obtained with strong PEs leading to stable PEMs. On the other hand, PEMs constructed from weakly charged PEs, polysaccharides or polypeptides are often characterized by a non-linear growth processes, due to the fast diffusion of both PE types into PEM films (Boulmedais *et al.*, 2003; Elzbieciak *et al.*, 2009; Picart *et al.*, 2001, 2002). Moreover, LbL assemblies generally entrap significant amount of water (Schmitt *et al.*, 1993) and swelling/deswelling character of PEMs affects their properties and structures (chapter 1, section 2.3.1).

In the present study, we report the possibility to grow multilayer films containing Poly(allylamine hydrochloride) (PAH) or Diethylaminoethyl-Dextran (Dex-DEAE) as polycations and Dextran Sulfates (DexS) or oxidized α -glucans as polyanions. We investigate the films growth mode by Quartz Crystal Microbalance with Dissipation Monitoring (QCM-D) to screen the different polyelectrolytes and systems for the formation of PEMs. As we obtained various types of growth behavior for each system, we decided in a second time to focus our study on two systems: PAH/DexS multilayers, with result in opposite behavior depending on the charge density of DexS (DexS H for higher charge density *vs* DexS L for lower charge density). We investigated the physico-chemical properties, and mainly the structure, of the two PEMs in order to understand the mechanism behind the multilayer growth and to easily link the growth type with the film structure obtained. By analysis of the water content of (PAH/DexS) by QCM-D and Surface Plasmon Resonance (SPR) and the morphologies of the PEM surfaces by Atomic Force Microscopy (AFM), we were able to

propose two growth mechanisms for the LbL assembly of (PAH/DexS). The tentative mechanisms result from the understanding of the analyzed multilayer structures and allow to regroup all the α -glucans PEMs in two categories of films and structures.

1. Screening: capacity of α -glucans derivatives to form multilayers

Adsorptions of PEs solutions were monitored by QCM-D at 20°C and carried out in 25 mM NaCl followed by a rinsing step in pure water to remove all loosely bound polymers or salt excess as in classical LbL process (Figure 3.1).

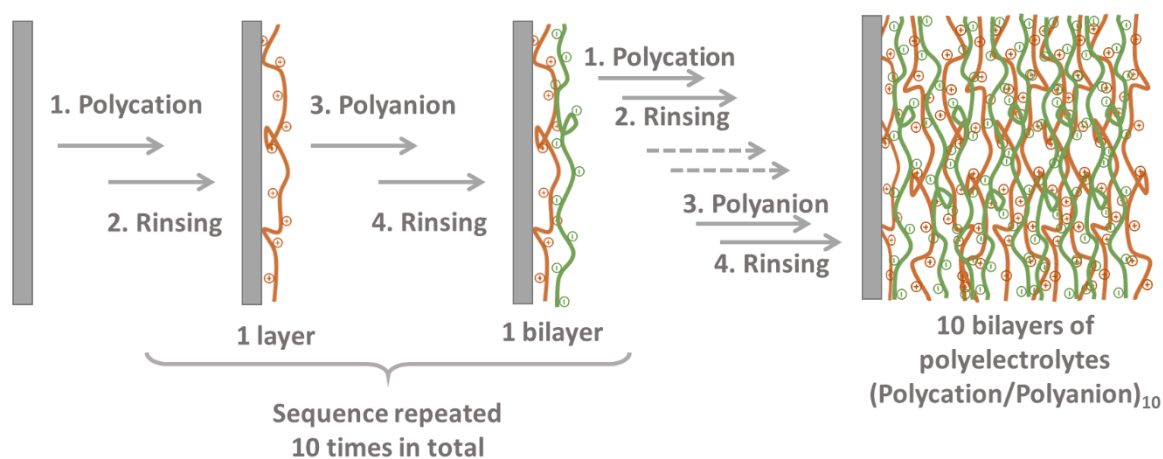


Figure 3.1. Scheme of the LbL formation of films from polycation (orange chains), and polyanion (green chains) in solid substrate (grey bar).

These conditions are in agreement with previous studies on salt concentration effect, as it is well known that ionic strength can affect thickness, surface roughness and the structure of the films (Elosua et al., 2013; Elźbieciak-Wodka et al., 2015; Lourenço et al., 2004; Moreau et al., 2012). For similar films with PAH, NaCl concentration used is between 10 mM NaCl and 1 M NaCl (Elosua et al., 2013; Elźbieciak-Wodka et al., 2015; Lourenço et al., 2004; Moreau et al., 2012). Polymer concentrations can also influence the multilayer film assembly and its adsorption kinetics; polycation concentration (0.1 g.L^{-1}) and polyanion concentration (0.5 g.L^{-1}) were chosen according to our previous studies on LbL growth using QCM-D (Dubas & Schlenoff, 1999; Moreau et al., 2012).

Using the same experimental conditions but different polyelectrolyte couples, we present in this part the typical growth types we obtained from our systems during this PhD work.

1.1. Multilayers based on dextrans sulfate (DexS)

Figure 3.2 presents the structure of the dextrans sulfate used in this study. DexS have the same molar mass ($40\,000\text{ g}\cdot\text{mol}^{-1}$) and the same D-glucose backbone linked by α -(1 \rightarrow 6) glycosidic linkages (Figure 3.2).

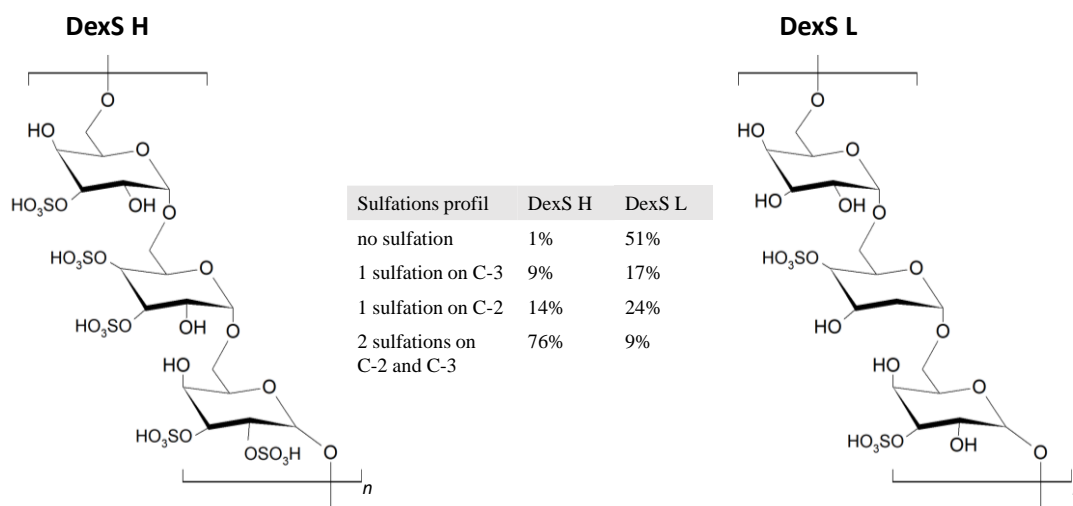


Figure 3.2. Chemical structures of dextrans sulfate with high sulfate content DexS H (on the left) and low sulfate content DexS L (on the right); sulfation patterns of both DexS are indicated.

They differ only by charge densities and accordingly sulfate substitution patterns as determined by ^1H NMR (Figure 3.A1). DexS with high sulfate content (DexS H) is mainly disubstituted since NMR spectra displays peaks for simultaneous sulfation at C-2/C-3 (76%) and -or monosubstituted either at C-2 or C-3 (14 and 9 %, respectively). On the contrary, DexS with low sulfate content (DexS L) shows peaks for monosulfation at C2 and C3 (24 and 17%) and little amount of disulfation (9%). A majority of unsulfated glucose units were also detected (51%) for DexS L. In summary, all glucose units of DexS H bear at least one charge, a majority being double charged leading to an average charge density of 1.75 charges per glucose unit, while, in the case of DexS L, only 0.6 glucose groups in average are charged. The difference of charge density between the two DexS is significant and relevant to explain their possible adsorption behaviors. We decided to explore films growth using an intermediate molar mass available among both the DexS L and DexS H: DexS H40 ($40\,000\text{ g}\cdot\text{mol}^{-1}$) and DexS L40 ($40\,000\text{ g}\cdot\text{L}^{-1}$). First, the capacity of DexS H40 and DexS L40 to grow multilayer films with different polyelectrolyte was investigated.

1.1.1. Poly(allylamine hydrochloride) and dextran sulfate multilayers (PAH/DexS 40)

On a first part, we focused on poly(allylamine hydrochloride) (PAH) as polycation (Figure 3.3) and two dextran sulfates (DexS) as polyanions. PAH contains 1 amino group per monomer unit considering the neutral pH of the polymer solution so that all the amino groups are charged leading to the presence of 1 charge per monomer.

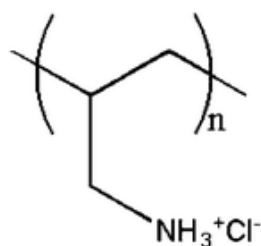


Figure 3.3. Chemical structure of poly(allylamine hydrochloride) (PAH).

Formation of PAH/DexS multilayers. The successful growth of (PAH/DexS)₁₀ PEMs on gold surface is demonstrated by QCM-D traces shown in Figure 3.3a. A decrease of frequency at each layer deposition is observed for both DexS indicating PE adsorption. In addition, the formation of stable PEMs is observed as frequency signal remains constant after the rinsing step. Different Δf values after 10 bilayers due to hydrated mass deposition were observed indicating different adsorption behavior. The mass absorbed at each step during the film process is given using the Voigt model for viscoelastic films and values are reported in Figure 3.4b.

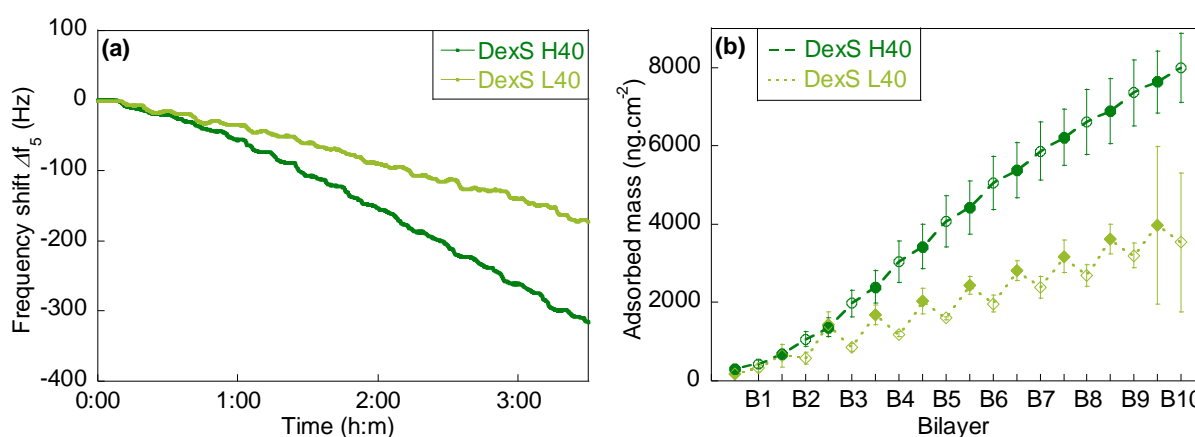


Figure 3.4. (a) Graph of $\Delta f_5/5$ vs time for (PAH/DexS)₁₀ multilayer with DexS H40 (dark green) and DexS L40 (light green) building on gold coated surface. (b) Adsorbed mass evaluated with Voigt model for (PAH/DexS)₁₀ multilayer with DexS H40 (dark green) and DexS L40 (light green). B_n corresponds to the nth (PAH/DexS) bilayer of the multilayer.

Table 3.1. Final frequency shift measured with QCM-D and mass obtained with Voigt model and Sauerbrey equation after 10 bilayers and rinsing step, for PAH/DexS 40 multilayers.

System	$\Delta f_s/5$ after 10 bilayers (Hz)	Absorbed mass after 10 bilayers (ng.cm ⁻²) (Voigt model)	Approximative adsorbed mass after 10 bilayers (ng.cm ⁻³) (Sauerbrey equation)
PAH/DexS H40	-320	8000 ± 870	~6000
PAH/DexS L40	-165	3600 ± 1770	~3000

Films based on PAH/DexS H40 result in a final frequency shift of -320 Hz for a total mass absorbed of about 8000 ± 870 ng.cm⁻² while films based on PAH/DexS L40 result in a final frequency shift of -165 Hz for a total mass absorbed of 3600 ± 1770 ng.cm⁻² for 10 bilayers as reported in Table 3.1. For both dextrans, two regimes were observed (Figure 3.4b). The first one between bilayer 1 and bilayer 3 and a second one after bilayer 3, as previously observed for others systems during multilayer assembly (Caruso et al., 1997; Pinto et al., 2010). The first one, *i.e.* before the bilayer 3, is mainly driven by the substrate surface properties while the second one is related to the formation of a surface charge excess only related to bilayer structure. Thus the adsorption behavior of the PE couple (PAH/DexS) becomes independent from the surface chemistry of the substrate (Caruso et al., 1997; de Villiers et al., 2011). In the case of PAH/DexS H40, the second regime highlights also a linear growth with an average mass increase of 858 ng.cm⁻² per bilayer. Whatever the PE deposited, PAH or DexS H40, the adsorbed mass increases. However, it may be noted that PAH deposition yields to a lower value (338 ng.cm⁻²) while DexS H40 deposition yields to a higher value (520 ng.cm⁻²). The amount being evaluated by QCM-D, associated water must also be considered, and will be discussed after. The (PAH/DexS L40)₁₀ PEMs also exhibited a linear regime after bilayer 3 but a lower mass increment of 375 ng.cm⁻² is found for bilayer deposition in average. Remarkably, the growth pattern displays non-monotonous zig-zag shaped growth (Figure 3.4b). PAH layer adsorption on DexS L40 layer presents an increase of average mass deposition of 835 ng.cm⁻² while adsorption of DexS L40 layer on PAH layer displays an average mass loss of 460 ng.cm⁻². This behavior has already been observed and was associated to an adsorption-desorption process of hydrated polymers that can either be removed from the surface due to loose attachment or expulsion of water and/or counterions from the film (Calvo et al., 2010; Ghostine et al., 2013). Moreover, even though both PEs allow to build stable films, they display different adsorption behaviors (symmetric linear growth vs asymmetric linear growth) as well as a higher amount of polymer adsorbed for (PAH/DexS H40)₁₀ films.

Viscoelastic behavior of PAH/DexS films. The frequency and dissipation shifts of both (PAH/DexS H40)₁₀ and (PAH/DexS L40)₁₀ assemblies are displayed for the third, fifth and seventh overtones on Figure 3.5a,c. Qualitatively, the comparison between the different overtones of frequencies and dissipation signals gives information on structural and viscoelasticity properties of the adsorbed film.

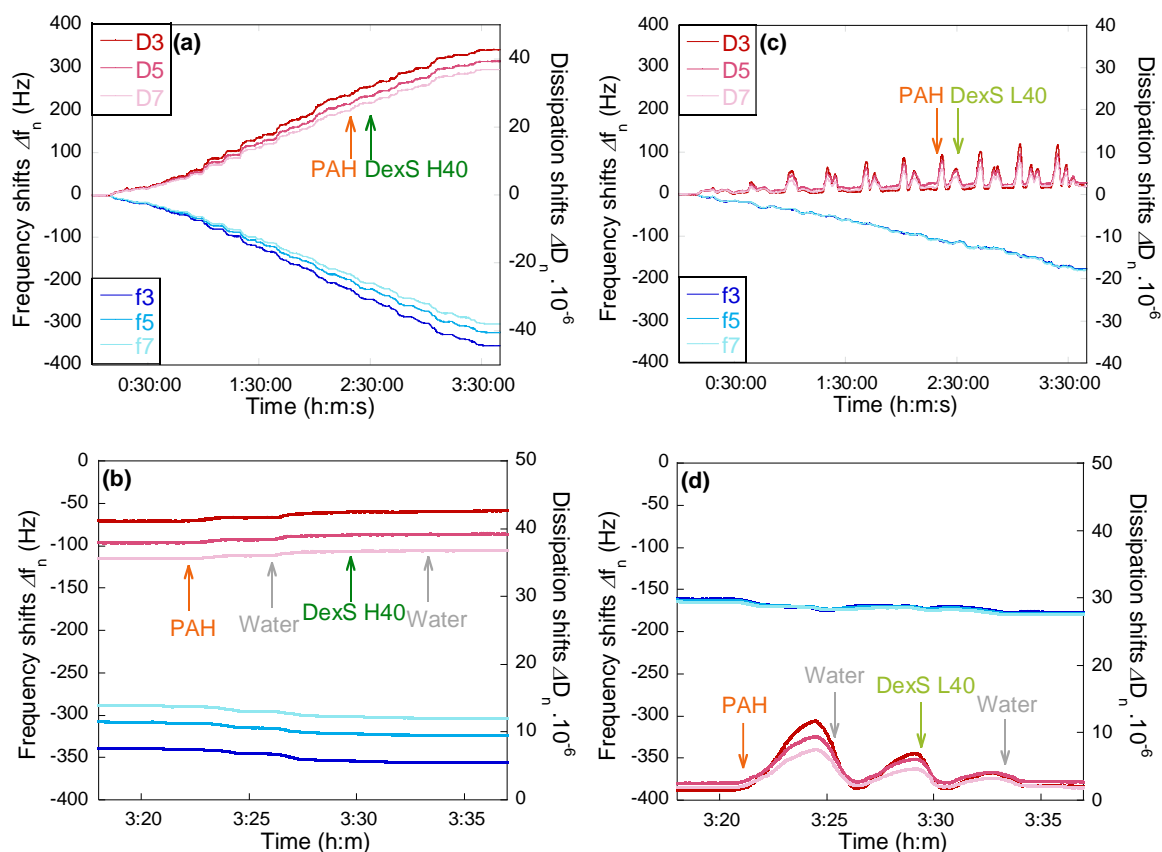


Figure 3.5. (a), (c) $\Delta f_n/n$ and ΔD_n as a function of time for (PAH/DexS 40)₁₀ multilayers on gold coated quartz crystal using QCM-D. The frequency (blue) and dissipation (red) change for the third, fifth and seventh overtones are depicted. (b), (d) Zoom on the bilayer 10 build-up with adsorption of PAH (orange), rinsing with pure water (grey), adsorption of DexS 40 (green).

As observed in Figure 3.5a, a splitting of frequencies for (PAH/DexS H40) is observed during the 10 bilayers build-up. (PAH/DexS L40) PEMs do not behave similarly since the frequencies are almost superimposable (Figure 3.4c). Expanding closer on the formation of the bilayer 10 (Figure 3.5b,d) confirms the absence of splitting between frequencies for films based on DexS L40 while a difference of 50 Hz between the 3rd and the 7th overtones is observed for DexS H40. In addition, as illustrated on Figures 3.5b and 3.5d, (PAH/DexS H40) films present an average final dissipation of 30×10^{-6} while (PAH/DexS L40) PEMs display an average final dissipation of 2×10^{-6} , respectively. This indicates different viscoelastic

properties with a more rigid film for (PAH/DexS L40) as compared to (PAH/DexS H40) films.

These properties can be qualitatively compared through the comparison between ΔD et Δf values reported on Figure 3.6a,b and the $-\Delta D/\Delta f$ ratio calculated from final frequencies and dissipation values reported on Figure 3.6c,d. The ratio corresponds to a normalization of dissipation variation per unit of mass adsorbed, corresponding to the relative softness of the films: a lower value indicates a more rigid film (inspired by ‘relative rigidity’ proposed by (Towle et al., 2020)). Here, we calculated the relative softness at given point: at the end of a polyelectrolyte adsorption step, before and after rinsing. The variations of ΔD as a function of Δf allow to access the changes in the viscoelastic regime of the film during its formation (Jaafar et al., 2019; Palasingh et al., 2021). As explained previously, the negative frequency is correlated with the amount of adsorbed mass. In the same time, the increasing dissipation value indicates a film viscoelastic property change, the bigger the dissipation is, the “softer” is the film. A higher slope of the $\Delta D/\Delta f$ plot can indicate a “softer” film and more water inside the layers.

The viscoelastic properties (Figure 3.6a) and the relative softness (Figure 3.6c) of (PAH/DexS H40) do not show important variations with $0.105 \times 10^{-6} \text{ Hz}^{-1}$ for bilayer 5 after rinsing and $0.122 \times 10^{-6} \text{ Hz}^{-1}$ for bilayer 10 after rinsing. On the contrary, it is notable by looking at the variation of ΔD_5 as function of $\Delta f_5/5$ on Figure 3.5b that viscoelastic properties of (PAH/DexS L40) vary a lot during the film construction. In particular, an increase of relative softness from less than $0.02 \times 10^{-6} \text{ Hz}^{-1}$ to $0.08 \times 10^{-6} \text{ Hz}^{-1}$ can be observed by rinsing the 10th DexS layer of (PAH/DexS L40) and the same is observed for bilayer 5 as reported on Figure 3.5d. Those results highlight once again how the system and its viscoelastic properties are highly dependent on the polyelectrolyte injected but also on the rinsing step. Final ratio $-\Delta D_5/\Delta f_5$ (after rinsing of bilayer 10) for (PAH/DexS L40) films is an order of magnitude lower ($>0.08 \times 10^{-6} \text{ Hz}^{-1}$) than (PAH/DexS H40) value ($0.122 \times 10^{-6} \text{ Hz}^{-1}$) (Figure 3.6c,d) which confirms that the PAH/DexS L40 film is more rigid than the PAH/DexS H40. From literature, value of about $0.3 \times 10^{-6} \text{ Hz}^{-1}$ have been measured for poly(acrylic acid)/poly-L-lysine pairs (Towle et al., 2020) and values varying from 0.1 to $0.5 \times 10^{-6} \text{ Hz}^{-1}$ have been found for PEMs based on cellulose nanocrystals/hemicellulose, *i.e.* non-electrostatic based systems (Jaafar et al., 2019). This clearly indicates that (PAH/DexS 40) PEMs are quite rigid compared to values obtained for systems based on natural polymers.

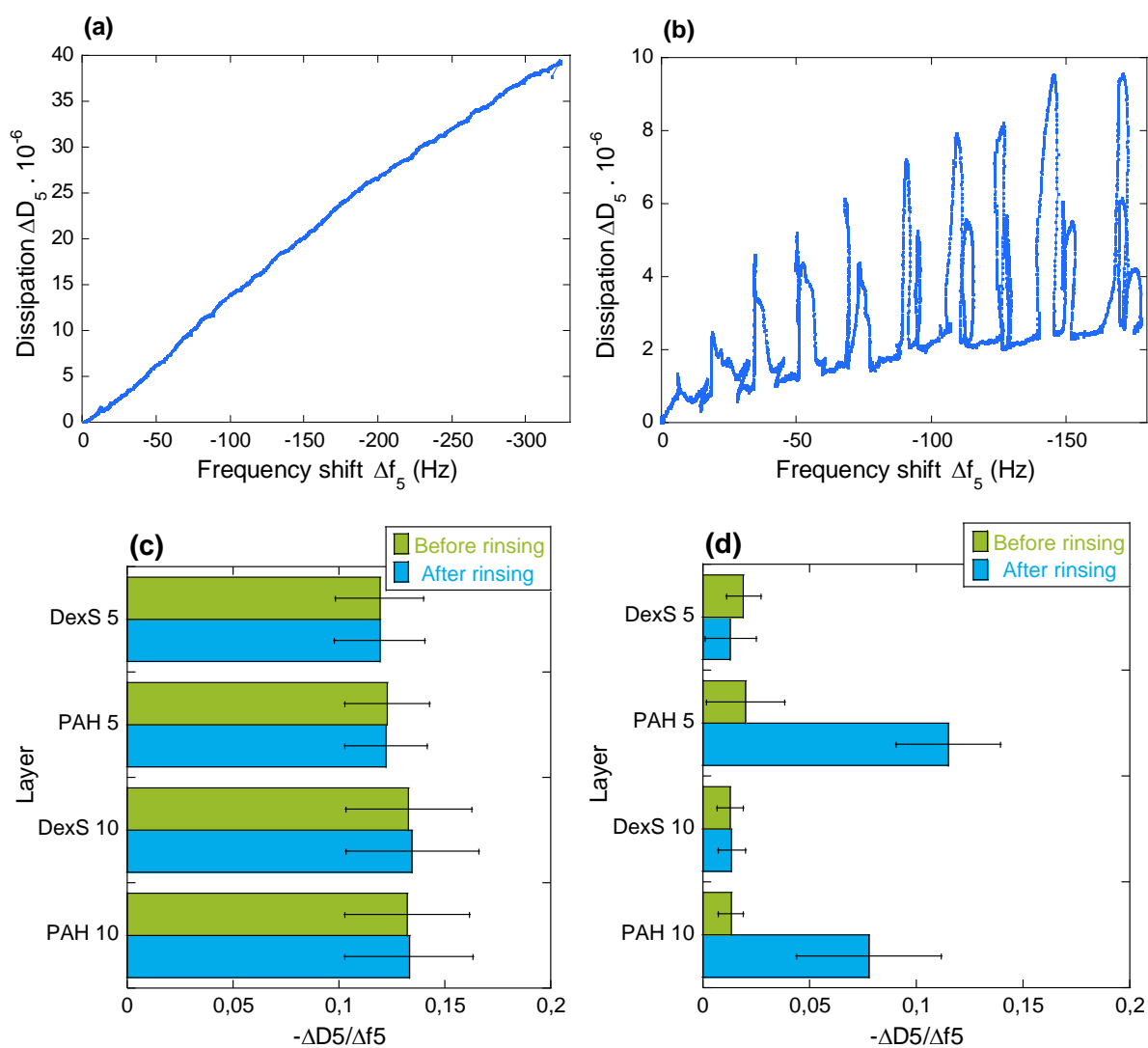


Figure 3.6. ΔD_5 as a function of $\Delta f_5/5$ of (a) the construction of (PAH/DexS H40)₁₀ films and (b) the construction of (PAH/DexS L40)₁₀. Relative softness calculated from ΔD_5 and $\Delta f_5/5$ for adsorption step of PAH layer (PAH 5) and DexS layer (DexS 5) of bilayer 5 and PAH layer (PAH 10) and DexS layer (DexS 10) of bilayer 10 for (c) (PAH/DexS H40)₁₀ and (d) (PAH/DexS L40)₁₀.

1.1.2. Diethylaminoethyl-dextran and dextran sulfate multilayers (Dex-DEAE 150/DexS 40)

We chose to extend the study of dextrans sulfate-based multilayers to another polycation: the Diethylaminoethyl-Dextran (Dex-DEAE) (Figure 3.7) in order to investigate systems entirely based on dextrans. Among the different molecular masses available, we decided to work in a first attempt with a Dex-DEAE with a molar mass similar to the one of

PAH. Thus, multilayers of Dex-DEAE and DexS were built and characterized using Dex-DEAE 150 ($140\,000 - 180\,000\text{ g}\cdot\text{mol}^{-1}$). Diethylaminoethyl-Dextran (Dex-DEAE) contains tertiary amino groups and quaternary amino groups, with 1 charged group per three monomer units. As the two tertiary groups have a pK_a of approximately 5.5 and a pK_a of approximately 9.2 and there is the presence of a quaternary amino group, Dex-DEAE remains positively charged for all pH values.

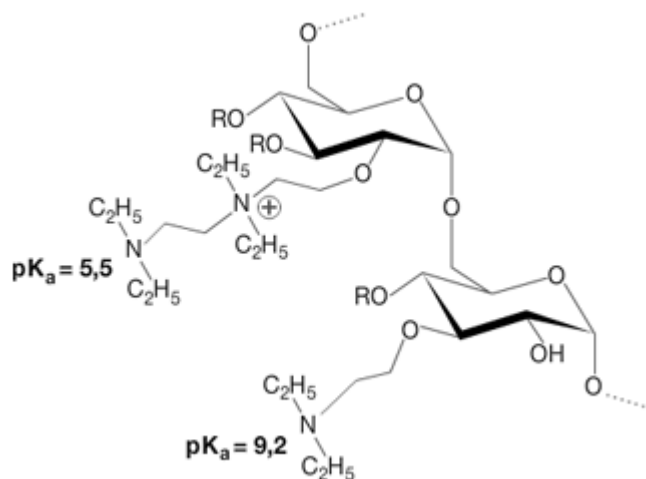


Figure 3.7. Chemical structures of diethylaminoethyl-Dextran (Dex-DEAE).

Formation of Dex-DEAE 150/DexS multilayers. Figure 3.8a shows the growth of $(\text{Dex-DEAE } 150/\text{DexS})_{10}$ PEMs on gold-coated quartz crystal, followed by QCM-D. For both DexS H40 and DexS L40, a decrease of frequency is observed for the buildup of the first bilayers. However, the decreasing frequency reaches a plateau after two hours (equivalent to 6 bilayers) with the approximate same Δf final value after 10 bilayers: -64 Hz and -68 Hz for DexS H40 and DexS L40, respectively. Thus, the growth of both films stops after some bilayers adsorption but remains stable after the rinsing step. Using the Voigt model, the mass absorbed at each step during the film process is given for viscoelastic films and values are reported in Figure 3.8b.

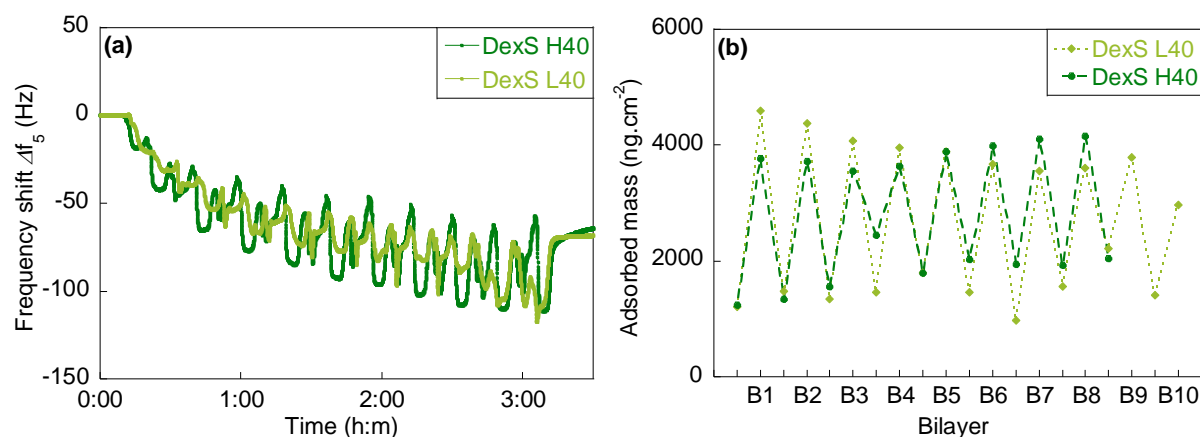


Figure 3.8. (a) Graph of $\Delta f_5/5$ vs time for (Dex-DEAE 150/DexS)₁₀ multilayer with DexS H40 (dark green) and DexS L40 (light green) building on gold coated surface. (b) Adsorbed mass evaluated with Voigt model for (Dex-DEAE 150/DexS)₁₀ multilayer with DexS H40 (dark green) and DexS L40 (light green). B_n corresponds to the nth (Dex-DEAE 150/DexS) bilayer of the multilayer. (Adsorbed masses for bilayer 9 and bilayer 10 of (Dex-DEAE 150/DexS H40)₁₀ were not integrated in the data as the Voigt model does not fit for those two points).

Unlike (PAH/DexS) films, (Dex-DEAE 150/DexS)₁₀ multilayers based on DexS H40 and DexS L40 display a loss in frequency (around -65 Hz), and thus in mass, that can be observed on the frequency shift depending on the adsorption step during the buildup. After the formation of the 3rd bilayer, the frequency of both films shows important variations. For both systems, average adsorbed masses oscillated between 1000 ng.cm⁻² after rinsing of Dex-DEAE 150 layers and 4500 ng.cm⁻² after rinsing of DexS layers. No global increase can be observed with addition of bilayers during the buildup of (Dex-DEAE 150/DexS H40) and of (Dex-DEAE 150/DexS L40). In addition to the plateau observed on frequency values, masses indicate that 1) we don't have a multilayer for systems based on Dex-DEAE 150 and DexS and 2) the system is destabilized by each injection of polyelectrolyte or water for rinsing.

Viscoelastic behavior of Dex-DEAE 150/DexS films. The frequency shifts of both (Dex-DEAE 150/DexS H40)₁₀ and (Dex-DEAE 150/DexS L40)₁₀ assemblies are displayed for the third, fifth and seventh overtones on Figure 3.9a,c. As it can be seen on Figure 3.9a,b, the adsorption behavior of (Dex-DEAE 150/DexS H40)₁₀ and (Dex-DEAE 150/DexS L40)₁₀ seem similar to the one observed for (PAH/DexS L40): growth with peaks in frequencies and dissipation. However, unlike (PAH/DexS L40) multilayers, those films based on Dex-DEAE 150 reach a plateau after a few bilayers.

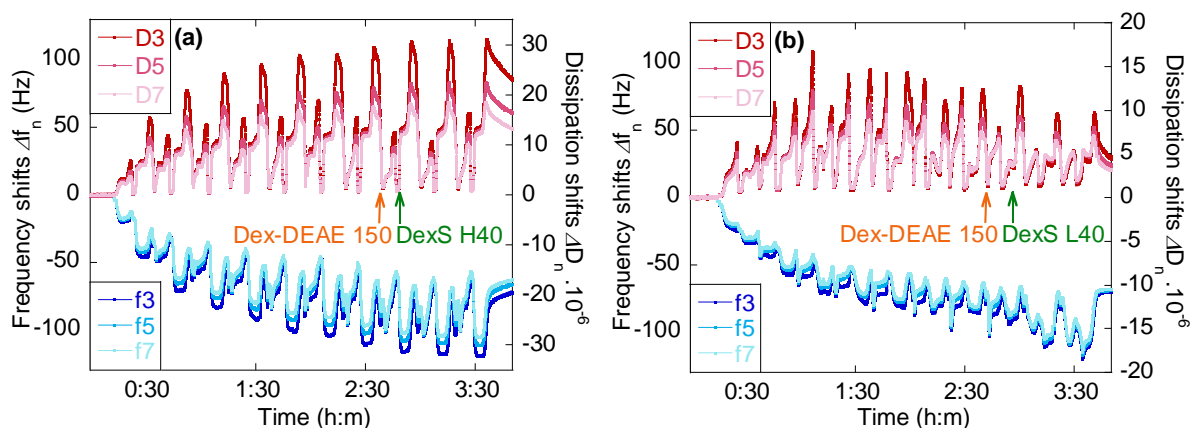


Figure 3.9. (a), (b) $\Delta f_n/n$ and ΔD_n as a function of time for (Dex-DEAE 150/DexS 40)₁₀ multilayer on gold coated quartz crystal using QCM-D. The frequency (blue) and dissipation (red) changes for the third, fifth and seventh overtones are depicted with adsorption of Dex-DEAE 150 (orange) and adsorption of DexS 40 (green).

For (Dex-DEAE 150/DexS H40), the adsorption of Dex-DEAE 150 layer for the formation of the 10th bilayer results in a decrease in frequency signal from -72 Hz to -96 Hz, followed by a peak with an increase (from -96 Hz up to -79 Hz) that ends with a new decrease until the frequency reaches -100 Hz before the rinsing step. The rinsing step of Dex-DEAE 150 results in a final frequency of -58 Hz which is a frequency shift less important than before Dex-DEAE 150 adsorption, as if material was removed from the surface with injection of Dex-DEAE 150. The adsorption of DexS H40 leads to a decrease in frequency of -52 Hz but rinsing DexS H40 leads to an increase frequency of +64 Hz, for a total frequency shift of the adsorption and rinsing of DexS of +6 Hz. The total 10th bilayer of (Dex-DEAE 150/DexS H40) ends in a positive frequency shift of +7 Hz and so there is a loss of mass onto the surface according to QCM-D results. The same is observed for (Dex-DEAE 150/DexS L40) as the adsorption of the 10th bilayer results in an increase in frequency from -74 Hz to -68 Hz for a total frequency shift of +6 Hz. The same type of variations during PAH adsorption appears for (Dex-DEAE 150/DexS L40) as well. Dissipations for both systems oscillate as well, with important peaks during injection and rinsing steps. Analysis of frequencies and dissipations confirms the instability of (Dex-DEAE 150/DexS 40) systems and the failure of the multilayer formation with those two polyelectrolytes couples.

1.2. Multilayers based on α -glucans

Among the polyanions available for this PhD work, we investigated interaction capabilities of α -glucans and α -glucans derivatives designed by TBI (Toulouse) in the project framework. These polysaccharides were synthesized, as presented previously, by the action of different enzymes on saccharose and seven α -glucans were obtained with different structures and high molar masses ($>10^8$ g.mol⁻¹). Information provided by HPSEC analysis, ¹H NMR and ¹³C NMR analysis, FT-IR analysis by TBI are summarized in Table 3.2.

Table 3.2. Structure of different bacterial α -D-glucans synthesized and provided by TBI.

Notation	Type of α -linkages	Linearity	Molar mass (g.mol ⁻¹)
Dex DSR-OK	97% of (1 → 6), 3% of (1 → 3)	Linear	$\sim 2 \times 10^9$
Dex DSR-OK-a3	55% of (1 → 6), 45% of (1 → 3)	Linear with branches in α -(1 → 3)	$> 2 \times 10^9$
Dex DSR-OK-a2	60% of (1 → 6), 40% of (1 → 2)	Linear with branches in α -(1 → 2)	$> 2 \times 10^9$
Dex DSR-S	97% of (1 → 6), 3% of (1 → 3)	Linear	$\sim 10^8$
Dex DSR-S-a3	56% of (1 → 6), 44% of (1 → 3)	Linear with branches in α -(1 → 3)	$\sim 10^8$
Dex DSR-S-a2	64% of (1 → 6), 36% of (1 → 2)	Linear with branches in α -(1 → 2)	$\sim 10^8$
Alternan	65% of (1 → 6), 35% of (1 → 3)	Alternate between α -(1 → 6) and A-(1 → 3)	$\sim 10^8$
Reuteran	41% of (1 → 6), 59% of (1 → 4)	Alternate between α -(1 → 6) and α -(1 → 4)	$\sim 10^8$

In addition to those neutral polymers, TBI used TEMPO-oxidation in the presence of laccase to functionalize α -glucans. Oxidized α -glucans were analyzed by acid hydrolysis to determine their oxidation rate and by HPAEC-PAD analysis to obtain their molar masses. The different functionalized α -glucans with their oxidation degrees are presented in Table 3.3.

Table 3.3. Notation and oxidation degrees of the different oxidized α -glucans provided by TBI.

Notation	Functionalized from	Oxidation degree (%)
Ox1-Dex	Dex DSR-OK-a2	32.9
Ox2-Dex	Dex DSR-OK-a2	30.8
Ox3-Dex	Dex DSR-OK-a2	25.8
Ox-Alt	Alternan	36
Ox1-Reu	Reuteran	44.8
Ox2-Reu	Reuteran	29.3

Among neutral α -glucans and charged α -glucans, only a few of them were soluble in water or in 25mM NaCl at 0.5 g.L⁻¹ and at 20°C. We thus only investigated polymers soluble in water for LbL formation ability. The following α -glucans were used as polyanions:

- Dex DSR-OK-a2, Ox1-Dex, Ox2-Dex, Ox3-Dex
- Alternan, Ox-Alt
- Reuteran, Ox1-Reu, Ox2-Reu

Even considering the differences in terms of characteristic groups, charge density and molar masses, the same experimental conditions were conserved in a first time.

1.2.1. Poly(allylamine hydrochloride) and α -glucans (PAH/ α -glucans)

On this part, we propose to study the formation of multilayers with PAH and the α -glucans and functionalized α -glucans presented previously. PAH is described in section 1.1.1.

Formation of PAH/ α -glucans multilayers. The growths of 10 bilayers (PAH/ α -glucan) films on gold-coated quartz monitored by QCM-D are reported on Figure 3.10a. The use of neutral α -glucans leads in both cases (neutral alternan and neutral reuteran) to a plateau in frequency shift Δf after adsorption of maximum 2 bilayers. For neutral α -glucans, a final frequency shift is reached after at most 2 bilayers with a final Δf_5 value of -67 Hz for (PAH/Alternan)₁₀ and -88 Hz for (PAH/Reuteran)₁₀. The decrease in frequency seems mainly due to the adsorption of the first PAH layer by interaction with the substrate. However, it can be observed that (PAH/Reuteran)₁₀ shows a decrease of frequency from -8 to -20 Hz by injection of reuteran and rinsing during the formation of the bilayer 1. While it can be due to non-electrostatic interactions between PAH and Reuteran, the absence of frequency decrease after the 1st bilayer may suggest that the adsorption is due to: 1) hydration of PAH layer, 2) salt adsorption by PAH layer or 3) impurities (enzymes, etc.) in reuteran solution from their preparation. Moreover, a signal derivation, *i.e.* a slow decrease of frequency shifts can be observed for both films that may be for similar reasons.

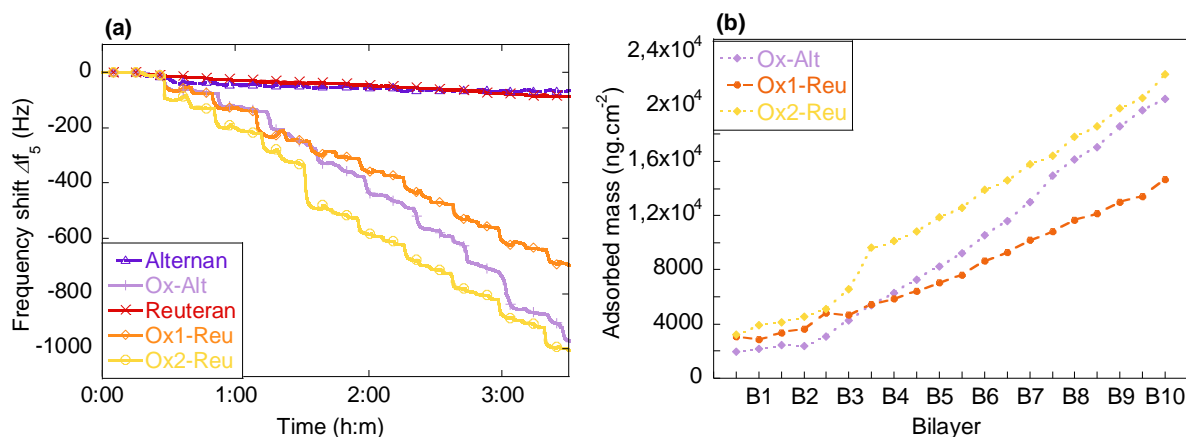


Figure 3.10. (a) Graph of $\Delta f_5/5$ vs time for (PAH/ α -glucan)₁₀ multilayer with PAH and neutral alternan (dark purple), Ox-Alt (light purple), neutral reuteran (dark orange), Ox1-Reu (orange) and Ox2-Reu (yellow) building on gold coated surface. (b) Adsorbed mass evaluated with Voigt model for 10 bilayers multilayer with PAH and oxidized α -glucan Ox-Alt (light purple), Ox1-Reu (orange) and Ox2-Reu (yellow). B_n corresponds to the nth (PAH/ α -glucan) bilayer of the multilayer.

Table 3.4. Final frequency shift measured with QCM-D and mass obtained with Voigt model after 10 bilayers and rinsing step, for PAH/oxidized α -glucans multilayers.

System	$\Delta f_5/5$ after 10 bilayers (Hz)	Adsorbed mass after 10 bilayers (ng.cm ⁻²)
PAH/Ox-Alt	-1055	20700
PAH/Ox1-Reu	-780	14700
PAH/Ox2-Reu	-1100	22400

For oxidized reuterans and oxidized alternan, a successful growth of stable (PAH/ α -glucan)₁₀ films is observed as frequency decrease occurs at each layer deposition for every oxidized α -glucans indicating of PE adsorption in Figure 3.10b, and the values obtained are much higher than the ones we obtained for DexS. Moreover, depending on the nature (alternan or reuteran) as well as on the oxidation degree, the evolution of Δf for (PAH/Ox-Alt)₁₀, (PAH/Ox1-Reu)₁₀ and (PAH/Ox2-Reu)₁₀ presents different final values (between -600 and -1000 Hz) but a similar general behavior. Frequency values and masses obtained for (PAH/Ox-Alt), (PAH/Ox1-Reu) and (PAH/Ox2-Reu) are reported in Table 3.4. For all multilayers, two linear regimes can be observed on the mass evaluation on Figure 3.10b: a first regime during the formation of bilayer 1 to bilayer 2 for Ox-Alt, bilayer 3 for Ox1-Reu and bilayer 4 for Ox2-Reu and a second one starting from bilayer 2, 3 or 4 depending on the polyanion. In each case, no notable difference can be observed between the masses resulting from the adsorption of PAH or the adsorption of oxidized α -glucan. As explained previously in 1.1.1, the presence of those two regimes is due to the substrate surface properties that affect

the LbL formation of the first bilayers. The adsorption behavior of all (PAH/oxidized α -glucans) multilayers seems to be similar to (PAH/DexS H40) formation, *i.e.* two regimes with linear mass growth. However, average masses adsorbed for (PAH/oxidized α -glucan)₁₀ are 1.5 – 2.5 times higher than the values obtained for (PAH/DexS H40). In addition to a different charge groups on their surface as well as a different charge density, oxidized α -glucans (10^8 – 10^9 g.mol⁻¹) present higher molar masses than dextrans sulfate (40 000 g.mol⁻¹). As far as we know, there is no data on LbL prepared with polyelectrolyte with molar masses from the range of oxidized α -glucans (10^8 – 10^9 g.mol⁻¹) in literature. Moreover, unlike for (PAH/DexS 40) PEMs, the augmentation of charges *i.e.* augmentation of oxidation degree between Ox1-Reu and Ox2-Reu leads to a higher mass absorbed for the higher oxidation rate (Ox2-Reu) but not to a change in adsorption behavior. Both present a linear growth of the films with 14700 ng.cm⁻² for (PAH/Ox1-Reu) and 22400 ng.cm⁻² for (PAH/Ox2-Reu) for an increase of around 15% between the oxidation rate of Ox1-Reu and the oxidation rate of Ox2-Reu.

Viscoelastic behavior of PAH/oxidized α -glucans films. To access qualitative information on structural and viscoelasticity properties of (PAH/oxidized α -glucans) films, we investigated the QCM-D frequency and dissipation shifts as well. The frequency shifts of both (PAH/Ox-Alt)₁₀ and (PAH/Ox1-Reu)₁₀ assemblies are displayed for the third, fifth and seventh overtones on Figure 3.11a,b. The frequency and dissipation shifts of (PAH/Ox2-Reu) can be found in Annexes (Annexes, Figure 3.A4). On Figure 3.11a,b, it is observed that the adsorption behavior of (PAH/Ox-Alt)₁₀ and (PAH/Ox1-Reu)₁₀ are alike in terms of adsorption behavior though their frequency shifts and their final adsorption are not in the same range. However, they present contrast for dissipation shifts.

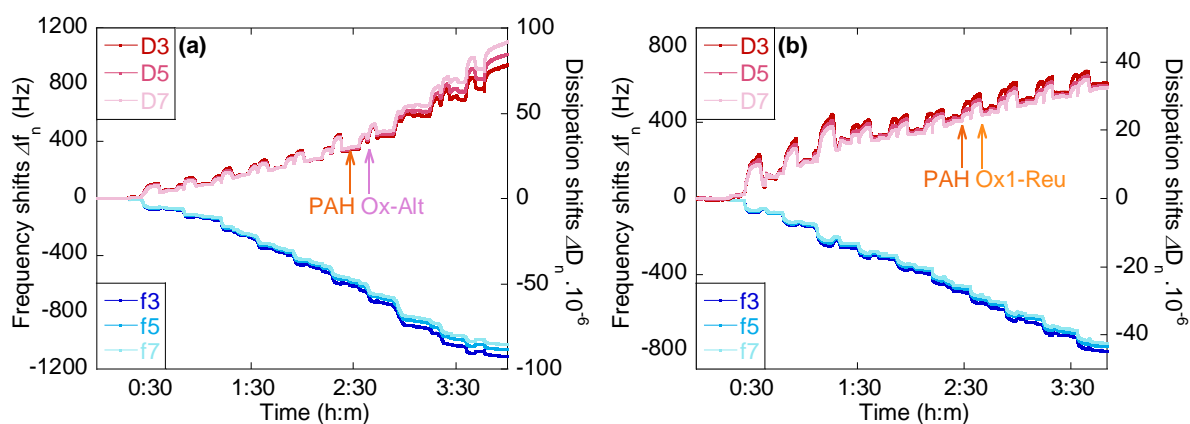


Figure 3.11. (a), (b) $\Delta f_n/n$ and ΔD_n as a function of time for (PAH/Ox-Alt)₁₀ and (PAH/Ox1-Reu)₁₀ multilayer on gold coated quartz crystal using QCM-D. The frequency (blue) and dissipation (red)

changes for the third, fifth and seventh overtones are depicted with adsorption of PAH (orange), adsorption of Ox-Alt (purple) and adsorption of Ox1-Reu (orange).

As observed in Figure 3.11a and in Figure 3.11b, Ox-Alt and Ox1-Reu both lead to growth with peak in dissipation depending on the adsorption of polycation or polyanion, as we found out for (PAH/DexS L40) before. (PAH/Ox-Alt)₁₀ films show an average final dissipation of 80×10^{-6} while (PAH/Ox1-Reu)₁₀ PEMs display an average final dissipation of 35×10^{-6} , respectively. Both films are quite viscous compared to what we observed for (PAH/DexS 40) multilayers, (PAH/Ox1-Reu)₁₀ seems more rigid than (PAH/Ox-Alt)₁₀. Moreover, starting with the build-up of bilayer 7, we observe a change in adsorption behavior for (PAH/Ox-Alt) with a notable splitting of frequencies (Figure 3.11b). A change can be seen with (PAH/Ox1-Reu) as well: the frequencies remain superimposable during all the deposition, but the peaks in dissipation seems to be lower after the formation of bilayer 3.

In addition to those results, ΔD values as a function of Δf values reported on Figure 3.12a,b indicate the changes in the viscoelastic regime of the film during its formation and qualify the viscoelastic behavior of (PAH/Ox-Alt)₁₀ and (PAH/Ox1-Reu)₁₀ multilayers.

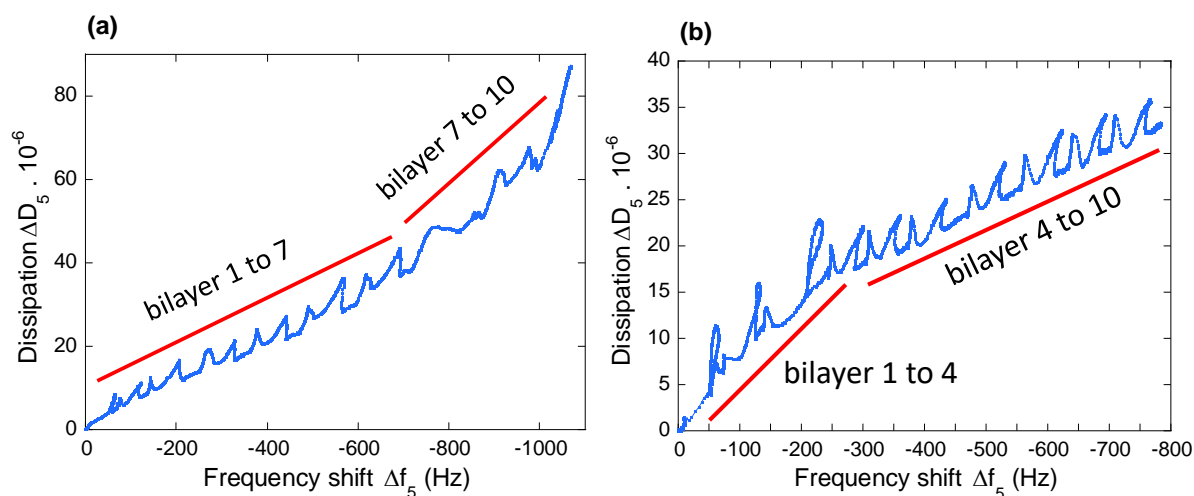


Figure 3.12. ΔD_5 as a function of $\Delta f_5/5$ of (a) the construction of (PAH/Ox-Alt)₁₀ films and (b) the construction of (PAH/Ox1-Reu)₁₀.

The viscoelasticity in the systems (Figure 3.12a,b) presents a variation for both (PAH/Ox-Alt)₁₀ and (PAH/Ox1-Reu)₁₀ films. However, in the case of (PAH/Ox-Alt)₁₀, those variations are not as remarkable as the ones observed during the formation of (PAH/DexS L40). For (PAH/Ox1-Reu), the bursts of dissipation with frequency observed is about 10×10^{-6} , similar to what we obtained for (PAH/DexS L40) films. The final relative softness or ratio -

$\Delta D_5/\Delta f_5$ (after rinsing of bilayer 10) for (PAH/Ox1-Reu) films is in the same order of magnitude ($>0.05 \times 10^{-6} \text{ Hz}^{-1}$) of (PAH/Ox1-Alt) value ($0.08 \times 10^{-6} \text{ Hz}^{-1}$). The variations in viscoelasticity of the systems as well as the final relative softness indicate that (PAH/Ox1-Reu) has a viscoelastic behavior quite similar to (PAH/DexS L40) (dissipation peaks and films more rigid) while (PAH/Ox1-Reu) is more likely to be a mix between (PAH/DexS H40) and (PAH/DexS L40) (lower dissipation peaks and films less rigid). In both case, films present a change in viscoelastic regime, with two apparent slopes $\Delta D_5/\Delta f_5$ during the film formation as illustrated on Figure 3.10. For (PAH/Ox-Alt), we note that the film becomes “softer” after bilayer 7, indicated by an increase of slope $\Delta D_5/\Delta f_5$. In the case of (PAH/Ox1-Reu), the opposite is observed as after bilayer 4, the slope $\Delta D_5/\Delta f_5$ decreases resulting in a more rigid multilayer.

1.2.2. Diethylaminoethyl-dextran and α -glucans (Dex-DEAE 150/ α -glucans)

Even though the formation of (Dex-DEAE 150/DexS 40) multilayers were not successful, we evaluated the assembly of Dex-DEAE 150 and oxidized α -glucans in the same experimental conditions. The difference between DexS and oxidized α -glucans, in terms of charged groups, charge density as well as molar masses, may have a positive influence on the LbL assembly with Dex-DEAE 150.

Formation of Dex-DEAE 150/ α -glucans multilayers. The growth of (Dex-DEAE 150/ α -glucan)₁₀ PEMs on gold surface is reported in Figure 3.13a. Neutral dextran, Dex-DSR-OK-a2, leads to a plateau in frequency shift Δf after adsorption of the first Dex-DEAE 150 layer. In the case of neutral dextran *i.e.* Dex-DSR-OK-a2, frequency $\Delta f_5/5$ goes from a value of - 8 Hz after the first layer of Dex-DEAE 150 to a final value $\Delta f_5/5$ of -20 Hz after 10 bilayers. The plateau obtained after Dex-DEAE 150 layer indicates that no LbL is formed with the system (Dex-DEAE 150/ Dex-DSR-OK-a2) after adsorption of Dex-DEAE 150 onto the substrate.

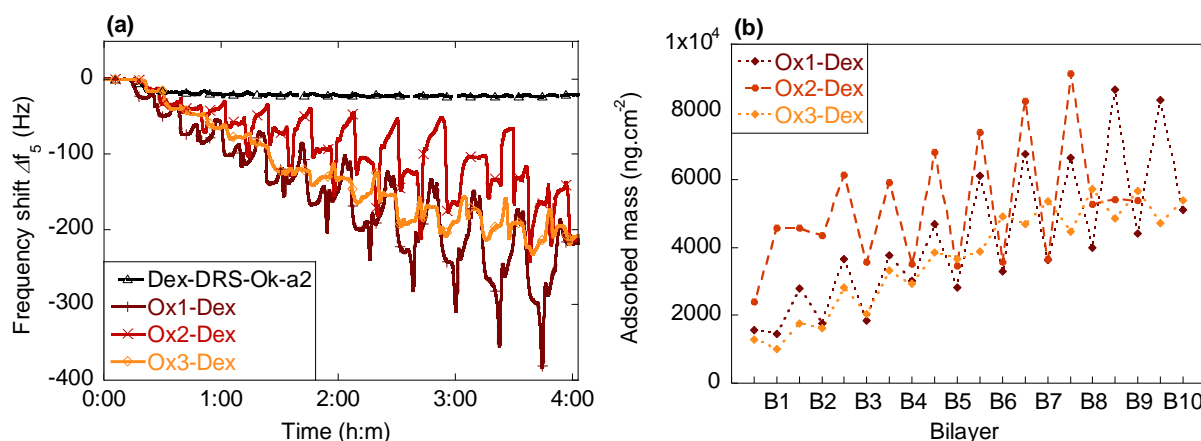


Figure 3.13. (a) Graph of $\Delta f_5/5$ vs time for (Dex-DEAE 150/ α -glucan)₁₀ multilayer with Dex-DEAE 150 and neutral Dex-DRS-OK-a2 (black), Ox1-Dex (brown), Ox2-Dex (dark orange) and Ox3-Dex (orange) built on gold coated surface. (b) Adsorbed mass evaluated with Voigt model for 10 bilayers multilayer with Dex-DEAE 150 and oxidized α -glucan Ox1-Dex (brown), Ox2-Dex (dark orange) and Ox3-Dex (orange). B_n corresponds to the nth (Dex-DEAE 150/ α -glucan) bilayer of the multilayer.

Table 3.5. Final frequency shift measured with QCM-D and mass obtained with Voigt model after 10 bilayers and rinsing step, for Dex-DEAE 150/oxidized α -glucans multilayers.

System	$\Delta f_5/5$ after 10 bilayers (Hz)	Absorbed mass after 10 bilayers (ng.cm ⁻²)
Dex-DEAE 150/Ox1-Dex	-217	5100
Dex-DEAE 150/Ox2-Dex (bilayer 9, unfit model for bilayer 10)	-214	5400
Dex-DEAE 150/Ox3-Dex	-208	5400

For oxidized dextrans, Ox-Dex, though there is an important variation of frequencies during the adsorption steps, a decrease of frequency at each layer deposition can be observed for all of them. Similar Δf values after 10 bilayers and rinsing due to hydrated mass deposition are noted. Values of the adsorbed masses for charged α -glucans are obtained using the Voigt model and are reported in Figure 3.13b for each adsorption step. Multilayers based on Dex-DEAE 150 and oxidized α -glucans result to a similar final frequency after formation of 10 bilayers as reported in Table 3.5. As illustrated in Figure 3.13b, the films seem to present a non-monotonous zig-zag shaped growth with asymmetric values between polycation and polyanions as it was observed for (PAH/DexS L40) multilayers formation (Figure 3.13b). However, the asymmetry is more remarkable for Ox1-Dex and Ox2-Dex, with a difference of mass adsorbed between Dex-DEAE 150 and oxidized dextrans up to 4000 ng.cm⁻², than for Ox3-Dex for which the mass difference is of 1000 ng.cm⁻². The phenomenon is more notable with Ox1-Dex and Ox2-Dex that are more charged (oxidation degree of 31 – 33%) than Ox3-Dex (oxidation rate of 26%).

Viscoelastic behavior of Dex-DEAE 150/oxidized α -glucans films. We studied the viscoelasticity of (Dex-DEAE 150/oxidized α -glucans) systems with a detailed examination of the frequency and dissipation shifts obtained by QCM-D. The frequency shifts of both (Dex-DEAE 150/Ox1-Dex)₁₀ and (Dex-DEAE 150/Ox3-Dex)₁₀ multilayers are presented for the third, fifth and seventh overtones on Figure 3.14a,b. The frequency and dissipation shifts of (Dex-DEAE 150/Ox2-Dex)₁₀ can be found in Annexes (Annexes, Figure 3.A5). As systems based on Dex-DEAE 150 and DexS, both frequency shifts and dissipation shifts present important peaks during the film formation. However, films from Dex-DEAE 150 and oxidized dextrans actually result in stable multilayers after 10 bilayers.

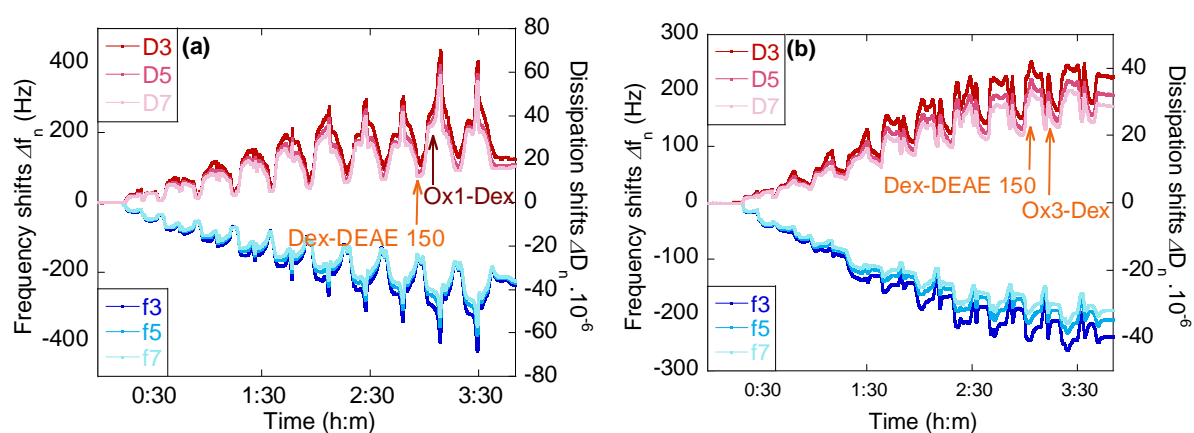


Figure 3.14. $\Delta f_n/n$ and ΔD_n as a function of time for (a) (Dex-DEAE 150/Ox1-Dex)₁₀ and (b) (Dex-DEAE 150/Ox3-Dex)₁₀ multilayer on gold coated quartz crystal using QCM-D. The frequency (blue) and dissipation (red) changes for the third, fifth and seventh overtones are depicted with adsorption of PAH (orange), adsorption of Ox1-Dex (brown) and adsorption of Ox3-Dex (orange).

For (Dex-DEAE 150/Ox1-Dex), the formation of 10 bilayers leads to final frequencies around -200 Hz associated with final dissipation shifts of $\sim 20 \times 10^{-6}$. The values of frequencies and dissipations highlight variations during the LbL process, with oscillations up to 200 Hz in the case of frequencies and up to 35×10^{-6} for dissipation (Figure 3.14a). However, there are not important splitting of frequencies and dissipations observed at the end of the film formation, indicating that the viscoelasticity of the system varies a lot during the adsorption steps but results in stable films (frequency, dissipation) after 10 bilayers. For (Dex-DEAE 150/Ox3-Dex), the multilayer obtained presents final frequencies between -200 and -250 Hz associated with final dissipation shifts between 30×10^{-6} and 40×10^{-6} (Figure 3.14b). As for Ox1-Dex, the system based on Ox3-Dex shows a lot of variation in terms of both frequencies and dissipation, but also a splitting of frequencies and dissipations by the end of the process.

Higher values of dissipations as well as the slipping of dissipations indicate that (Dex-DEAE 150/Ox3-Dex)₁₀ results in quite softer films after rinsing of 10 bilayers.

The high variations in the slope $\Delta D_5/\Delta f_5$ during the multilayers of both (Dex-DEAE 150/Ox1-Dex) and (Dex-DEAE 150/Ox3-Dex) makes the analysis and comparison of relative softness between the two films difficult. ΔD values as a function of Δf values reported on Figure 3.15a,b present the changes in the viscoelasticity of the film for (Dex-DEAE 150/Ox1-Dex)₁₀ and (Dex-DEAE 150/Ox3-Dex)₁₀ assemblies.

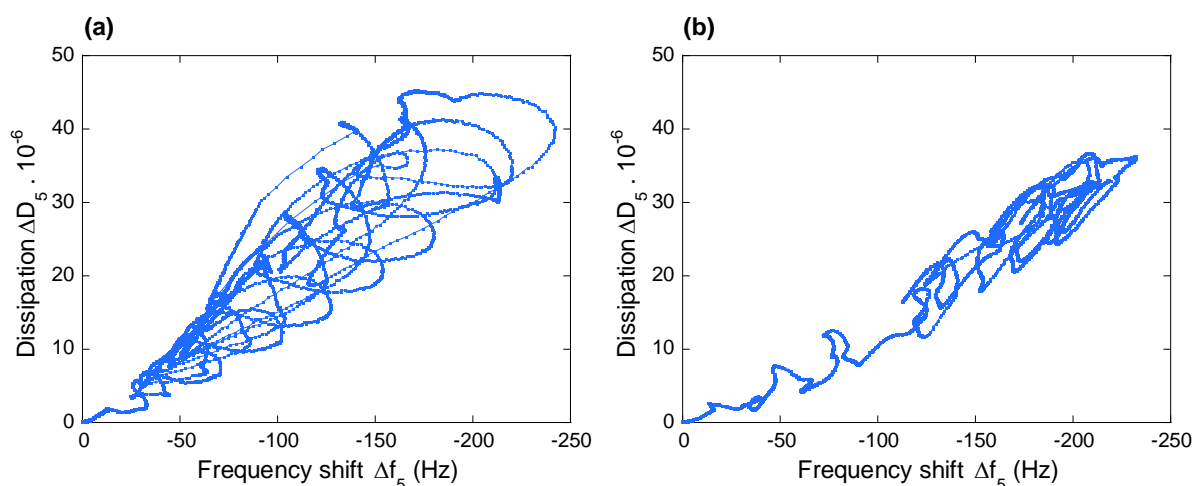


Figure 3.15. ΔD_5 as a function of $\Delta f_5/5$ of (a) the construction of (Dex-DEAE 150/Ox1-Dex)₁₀ films and (b) the construction of (Dex-DEAE 150/Ox3-Dex)₁₀.

In the case of (Dex-DEAE 150/Ox1-Dex)₁₀ multilayers, the variations appear like loops and make it impossible to identify the different adsorption steps after bilayer 1. For (Dex-DEAE 150/Ox3-Dex)₁₀ multilayers, the lack of differentiation between adsorption steps appears later, after bilayer 4. By calculating the final relative softness or ratio $-\Delta D_5/\Delta f_5$ at a certain time (after the rinsing of bilayer 10), we can see that the value for (Dex-DEAE 150/Ox1-Dex) films ($0.156 \times 10^{-6} \text{ Hz}^{-1}$) is close to (Dex-DEAE 150/Ox3-Dex) value ($0.154 \times 10^{-6} \text{ Hz}^{-1}$) which demonstrates that both films have an equivalent relative softness at the end of their formation. Among all other systems studied for the LbL formation, films from (Dex-DEAE 150/oxidized dextrans) are in fact the less rigid multilayers with (PAH/DexS H40) films and (PAH/ oxidized dextrans).

1.3. Summarized information on multilayers films

In this part, we decided to give an overview of all the information obtained on the construction of films based on dextran derivatives, dextrans sulfate and oxidized α -glucans. In Table 3.6, we reported the final values of frequency $\Delta f_5/5$, dissipation ΔD_5 , information on the mass adsorption (symmetric, asymmetric/zig-zag, no formation), the different slopes $\Delta D_5/\Delta f_5$ observed.

Table 3.6. Summarized information on multilayers studied in section 1, after 10 bilayers formation.

Systems	$\Delta f_5/5$ (Hz)	ΔD_5 ($\cdot 10^{-6}$)	Mass adsorbed ($\text{ng}\cdot\text{cm}^{-2}$)	Characteristics of the adsorption	Multilayer formation	Slopes $\Delta D_5/\Delta f_5$ ($10^{-6}\cdot\text{Hz}^{-1}$)
PAH/DexS H40	-320	30	8000	Linear, symmetric	Yes	0.122
PAH/DexS L40	-165	30	3600	Linear, zig-zag	Yes	Variable with final value at 0.08
DEAE-Dex 150/DexS H40	-63	17	~4500	No increase, zig-zag	No	-
DEAE-Dex 150/DexS L40	-66	4	~4500	No increase, zig-zag	No	-
PAH/Ox-Alt	-1055	80	20700	Linear, symmetric	Yes	0.05 (bilayer 1 to 7) 0.08 (from bilayer 7)
PAH/Ox1-Reu	-780	32	14700	Linear, symmetric	Yes	0.07 (bilayer 1 to 4) 0.04 (from bilayer 4)
Dex-DEAE 150/Ox1-Dex	-217	21	5100	Linear, zig-zag	Yes	0.156
Dex-DEAE 150/Ox3-Dex	-208	32	5400	Linear, zig-zag	Yes	0.154

As one can see, we obtained PEMs with a wide range of absorbed mass and various viscoelastic behavior after 10 bilayers. In general, systems based on the same type of polyelectrolytes lead to the same type of construction. For instance, (Dex-DEAE 150/DexS) systems do not allow to form films with neither DexS H40 or DexS L40. Both (PAH/Ox-Alt) and (PAH/Ox1-Reu) result in multilayers presenting linear symmetric mass growth with two different viscoelastic regimes (two slopes $\Delta D_5/\Delta f_5$) for a final film which can be considered as rigid. (Dex-DEAE 150/Ox1-Dex) and (Dex-DEAE 150/Ox3-Dex) systems both result in quite ‘soft’ films with zig-zag mass growth. Only systems based on PAH and DexS lead to multilayers with a different type of mass growth and different viscoelastic behavior during the construction and after the construction of 10 bilayers. We obtained soft films with a linear symmetric growth of the mass deposited in the case for DexS H40 and quite rigid films with a linear zig-zag mass growth in the case of DexS L40.

Moreover, we also observed some differences between systems based on PAH/DexS and systems based on DEAE-Dex 150/DexS, as the first one allows to obtain multilayer when the second does not, no matter the charge density of DexS (1 charge/1 monomer for DexS L40 and 1.67 charge/1 monomer for DexS H40). The difference between the two results is the charge density of the polycation, as PAH has 1 charge/1 monomer when DEAE-Dex 150 has 0.33 charge/1 monomer.

The (DEAE-Dex 150 and oxidized α -glucans) system also results in multilayers when the system (DEAE-Dex 150 and DexS) does not. Oxidized α -glucans present 1 charge/1 monomer for Ox1-Dex and 0.8 charge/1 monomer for Ox3-Dex which is similar to the charge density of DexS L40. However, the molar mass of oxidized α -glucans is clearly higher than the one of DexS: $10^8 - 10^9$ g.mol⁻¹ for oxidized α -glucans and 40 000 g.mol⁻¹ for DexS. We have thus an impact of the higher molecular weight on mass growth and viscoelastic behavior in addition to the charge equilibrium effect.

The parameters impacting the film growth and their structures will be studied in details in Chapter 4.

2. Growth mechanisms of PAH/DexS multilayers

After the successful growth of films based on the polyelectrolyte couples chosen, we decided to focus on the understanding of (PAH/DexS H40) and (PAH/DexS L40) films building mechanisms. In fact, those two PEMs based on the same polyelectrolytes, with only the exception of the charge density of DexS, results in opposite growth behaviors. (PAH/DexS H40) multilayer results in an adsorbed mass growth with a linear increase of adsorbed amount of PEs at each adsorption step and a single slope $-\Delta D_5/\Delta f_5$ of $0.122 \times 10^{-6} \text{ Hz}^{-1}$ during the entire formation. In parallel, (PAH/DexS L40) multilayer results in an asymmetric growth of the mass adsorbed between deposition of polycation and polyanion, as well as important variations of the dissipation and the ratio $-\Delta D_5/\Delta f_5$ during the whole build-up. Moreover, despite the variations observed, the film obtained was more rigid than the (PAH/DexS H40) film with a final relative softness $-\Delta D_5/\Delta f_5$ of $0.08 \times 10^{-6} \text{ Hz}^{-1}$ for the formation of 10-bilayer film. As they are the systems which present the most remarkable differences in terms of adsorption and viscoelastic behavior, we decided to propose growth mechanisms based on the understanding of their formation.

In order to do that, we investigate their physico-chemical characteristics: water content and surface morphology. Those characteristics combined with information collected of the mass adsorbed and the viscoelasticity behavior of the multilayers, we are able to propose a comprehensive description of the growth mechanism of multilayer based on PAH and DexS H40 or DexS L40. The global approach used to characterize multilayers and understand the growth mechanisms is described in Figure 3.16.

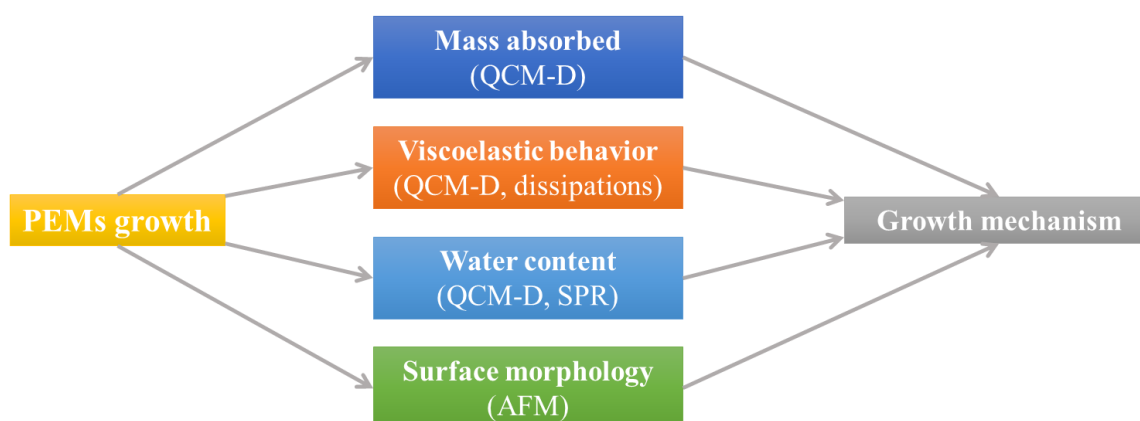


Figure 3.16. Schematic representation of the experimental approach to characterize multilayers: from growth of QCM-D to tentative mechanisms.

We combined QCM-D and Surface Plasmon Resonance (SPR) techniques to determine the water content of PEMs. Those two techniques allow quantitative, real-time, *in situ*, non-invasive and highly sensitive detection and determination of the adsorbed molecules on various type of surfaces, including biopolymers and polysaccharides (Höök et al., 2001; Mosley et al., 2021). QCM-D is an oscillating piezoelectric sensor that probes the variations in total mass and viscoelastic properties of the adsorbed species coupled with solvent *i.e.* the “wet” film formed on a surface. The qualitative viscoelastic information is obtained by analysis of the dissipation of the energy *i.e.* the signal damping when the direct current is stopped. SPR allows the determination of the “dry” mass of the adsorbed film from change of refractivity of the surface caused by the adsorption of molecules. A combination of those methods supplies significant information of the LbL adsorption mechanism, structural changes and the extent of hydration of the adsorbed layer. Moreover, a surface analysis of the films by Atomic Force Microscopy (AFM) was carried out to access the morphology of the films and relate the impact of growth type/mechanism on the surface properties.

2.1. Physico-chemical characterization of PAH/DexS

2.1.1. Water content

Besides information provided by QCM-D on hydrated adsorbed mass on substrate, SPR allows to calculate a “dry” polymer mass, *i.e.* the mass of polymer contained in the films without the contribution of the water bound. From equation (4) and equation (5), SPR adsorbed masses are determined to be 130 ng.cm^{-2} for (PAH/DexS H)₂ PEMs and 120 ng.cm^{-2} for (PAH/DexS L40)₂ PEMs (Annexes, Figure 3.A2). Meanwhile, hydrated masses from QCM-D are 1100 ng.cm^{-2} for (PAH/DexS H40)₂ PEMs and 570 ng.cm^{-2} (PAH/DexS H40)₂ PEMs, which suggest that (PAH/DexS L40)₂ films contain more water than (PAH/DexS L)₂. Based on QCM-D and SPR data, water content $\text{H}_2\text{O}_{\text{SPR/QCM}}(\%)$ was found to be about 72% in the case of DexS H and 50% in the case of DexS L (Figure 3.17a). Water content has also been evaluated from $\text{H}_2\text{O}/\text{D}_2\text{O}$ exchange experiment as monitored by QCM-D, *i.e.* $\text{H}_2\text{O}_{\text{exchange}}(\%)$ (J. Kittle et al., 2021). Figure 3.17b shows the change in frequency ($\Delta f_n/n$) versus time for the (PAH/DexS)₂ PEMs switched from H_2O to D_2O and back to H_2O . The calculated water content of films was lower for (PAH/DexS L40) films (44.5 %) than for the (PAH/DexS H40) films (66.8%).

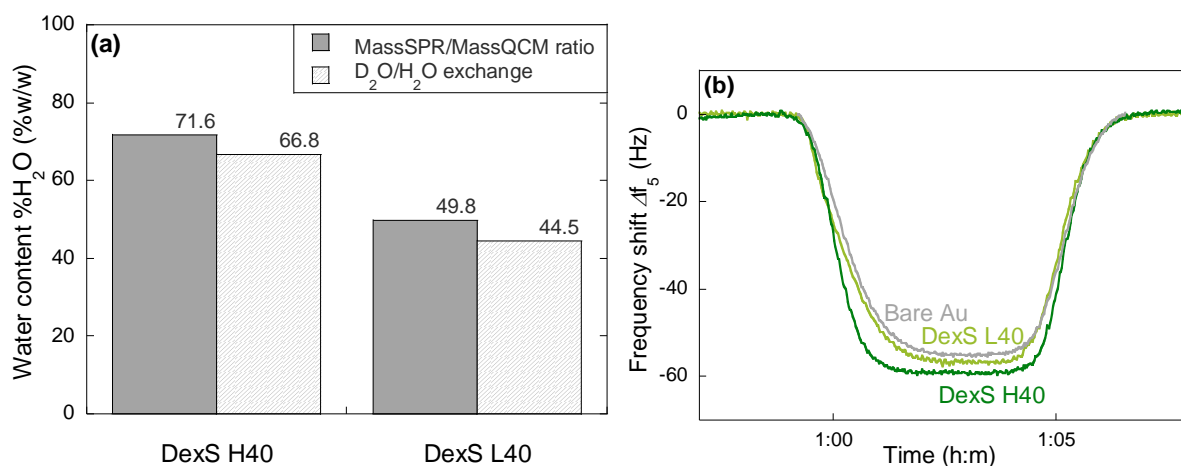


Figure 3.17. (a) Water content (%w/w) of the films calculated from the ratio of adsorbed mass obtained by SPR and adsorbed mass obtained by QCM-D on the 2nd bilayer and the value calculated from D₂O-H₂O exchange on the 2nd bilayer. (b) $\Delta f_5/5$ vs time for D₂O-H₂O exchange on the 2nd bilayer of (PAH/DexS H40) multilayer (dark green), of (PAH/DexS L40) multilayer (light green) and on bare gold (bare Au, grey).

Both analyses give consistent values of water content around 66 – 72% of water for (PAH/DexS H40)₂ PEMs and 44 – 50% of water for (PAH/DexS L40)₂ PEMs (Figure 3.17b). As discussed in the previous section, PEMs built from DexS H40 are more hydrated than PEMs built from DexS L40 which is consistent with a rather softer film structure.

2.1.2. Surface morphology

AFM was performed to analyze the surface morphology and roughness of the (PAH/DexS 40) adsorbed layers on the silicon wafer after adsorption, in a dry state, and images are reported on Figure 3.18. After drying of 5 (PAH/DexS H40/L40) and 10 (PAH/DexS H40/L40) adsorbed bilayers, different patterns are observed on both films as illustrated on Figure 3.18. (PAH/DexS H40) PEMs exhibit a surface displaying fibrillar network pattern while (PAH/DexS L40) PEMs present a more granular surface with “puddle-like” aggregates. Similar aggregates in the dry state were previously observed for various porous PEMs based on synthetic and natural polymers (Barroso et al., 2019; Elzbieciak et al., 2009; Ghavidel Mehr et al., 2015; Picart et al., 2001), proteins and complex of biopolymers and proteins (Davantès et al., 2019; Liu et al., 2018) and microporous surfaces (Fu et al., 2002; Hollman & Bhattacharyya, 2004). For both dextrans sulfate, increasing the number of bilayers seems to lead to a better surface coverage, as AFM images for PAH10 and DexS10

show a lower contrast than images for PAH5 and DexS5. Moreover, in the case of (PAH/DexS L40), the surface morphology seems to change between the PAH adsorption step and the DexS adsorption step. Images on PAH10 show better surface coverage than images on DexS10, *i.e.* the adsorption of DexS10 on PAH10 seems to reduce covered surface.

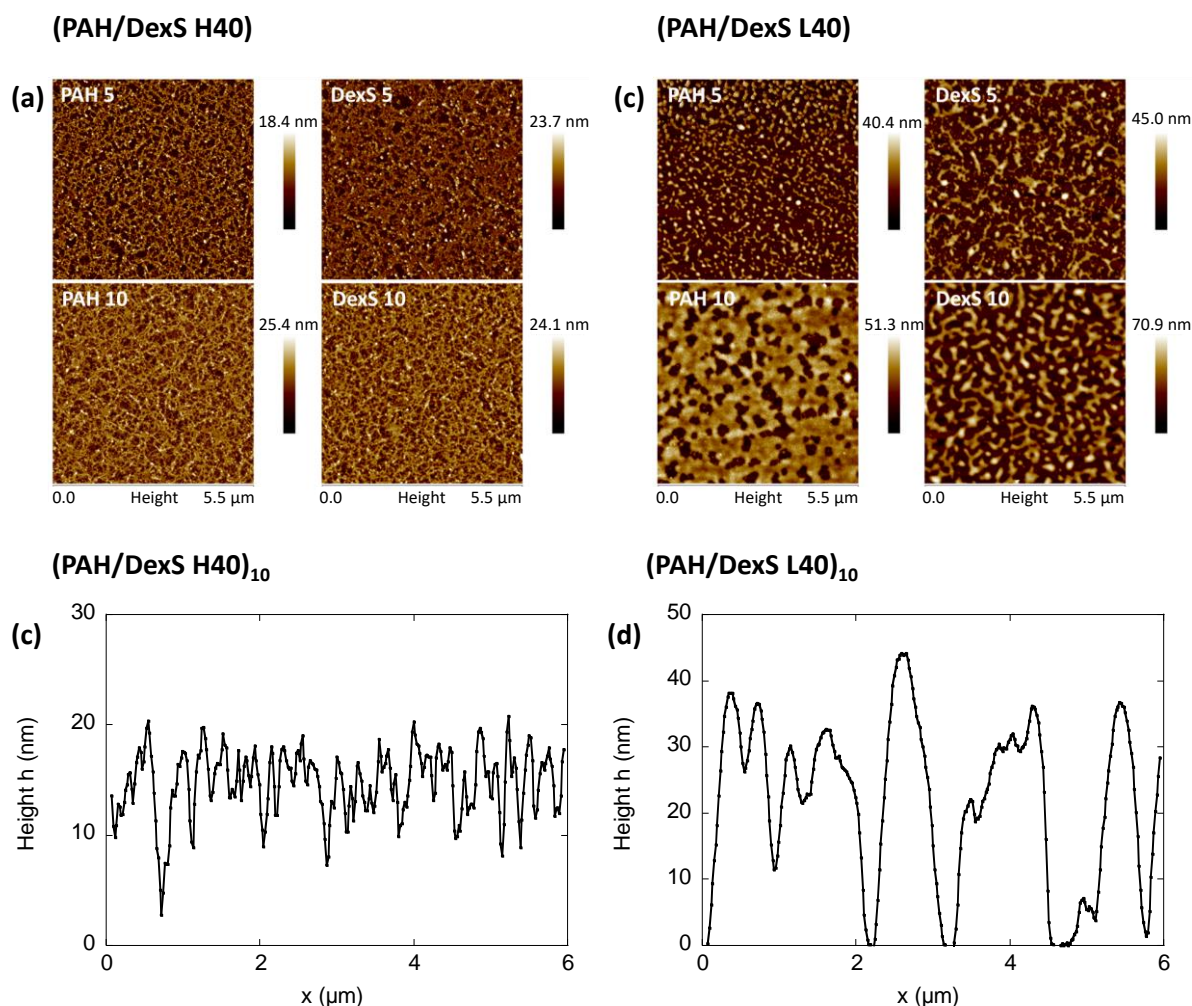


Figure 3.18. AFM topography images from (a) (PAH/DexS H40) multilayer and (b) (PAH/DexS L40) multilayer of (at the top) the PAH 5 (bilayer 4.5 *i.e.* outermost layer of PAH before bilayer 5), the DexS 5 (bilayer 5), and of (at the bottom) PAH 10 (bilayer 9.5 *i.e.* outermost layer of PAH before bilayer 10) and DexS 10 (bilayer 10). Height profiles of (c) (PAH/DexS H40)₁₀ and (d) (PAH/DexS L40)₁₀ using AFM topography images on scratched surface (Annexes, Figure 3.A3).

Additionally, thicknesses of the layers were determined by AFM topography images of scratched dry layers and height profiles are presented in Annexes (Annexes, Figure 3.A3). Using the scratch method on the 10th bilayer, *i.e.* DexS10 layers, height ranges and roughness of surfaces are obtained. (PAH/DexS H40)₁₀ composites present a height of $15.01 \text{ nm} \pm 4.78 \text{ nm}$ and a RMS roughness of $4.06 \text{ nm} \pm 0.79 \text{ nm}$. (PAH/DexS L40) PEMs building leads to a

thicker and a rougher surface; “puddle-like” aggregates of (PAH/DexS L40)₁₀ present an average height of 19.87 nm \pm 1.51 nm and an average RMS roughness of 24.49 nm \pm 12.05 nm indicating a heterogeneous structure due to holes between aggregates. The holes can be clearly identified on height profile of (PAH/DexS L40) given on Figure 3.18d, unlike (PAH/DexS H40) structures given on Figure 3.18c. The film built based on DexS L40 presents a higher thickness after drying and a different surface morphology compared to the film built with DexS H40.

2.2. Formation mechanisms for DexS/PAH films

By combining QCM-D analysis and the physico-chemical characterization done on multilayers, it is possible to understand the mechanism behind the formation of those films. In the case of DexS H, the (PAH/DexS H) system allowed the film to grow linearly with an increase of adsorbed amount of PEs at each adsorption step. QCM-D data, dissipation values and $-\Delta D_5/\Delta f_5$ ratio highlighted the fact that (PAH/DexS H40) PEMs presented a viscoelastic behavior in agreement with higher water content (~69%) than (PAH/DexS L40)₁₀ systems that led to less soft films as evidenced by the lower $-\Delta D_5/\Delta f_5$ ratio and water amount as compared to (PAH/DexS H40) PEMs (~47%). Interestingly, (PAH/DexS L40) PEMs present an asymmetric growth between polycation and polyanion adsorption with high hydrated mass adsorbed from PAH while a mass loss is observed for DexS L40 adsorption. In addition, DexS H40 or DexS L40 surface morphology of films obtained after drying investigated by AFM also presents dissimilarities. (PAH/DexS H40) thin films display fibril-like surface while (PAH/DexS L40) PEMs lead to rougher films forming “puddle-like” aggregates. Moreover, while (PAH/DexS H40) PEMs present similar surface morphology with PAH or DexS ending, (PAH/DexS L40) PEMs surfaces differ between PEMs ending with PAH and PEMs ending with DexS L40. The morphology observed in AFM confirms the influence of charge density of DexS H40 and DexS L40 on film architecture, but also the impact of DexS L40 adsorption on the internal restructuration of (PAH/DexS L40) PEMs. The specific surface pattern recalls the surface morphology previously observed for others systems and attributed to the formation of polyelectrolyte-complexes (Feng et al., 2005), that may indicate the complexation of PAH and DexS L40 onto the surface. This complexation can be due to complete or partial charge neutralization in the films and thus lead to water removal and an increase of hydrophobic content of the film as it was previously observed by Kittle *et al.* (J. D.

Kittle et al., 2012). More than the charge density itself, the charge neutralization is a result of the charge density of both polyelectrolytes and the difference between each. A charge neutralization occurs when charges (in addition to other structural parameters) of one polyelectrolyte can be fully compensated by the charges of the second polyelectrolyte. With this phenomenon, polyelectrolytes complexes are often obtained. However, in this case, a charge inversion on the surface and construction of the PEMs are limited.

From all information collected in this study, we proposed two tentative mechanisms of film building explaining the differences observed in the two systems (PAH/DexS H40) and (PAH/DexS L40) on Figure 3.19 and Figure 3.20. The two growth mechanisms will be defined as Type A and Type B, and they will be used to categorize most of the multilayers built in this thesis.

2.2.1. Tentative mechanism for (PAH/DexS H40) i.e. type A

In the case of (PAH/DexS H40) films, illustrated on Figure 3.19, the amount of negative charges from DexS H40 are likely high enough to overcompensate the charges coming from the previous PAH layer that might provide high surface charge density after DexS H40 adsorption (Figure 3.19) (Glinel et al., 2002).

(PAH/DexS H40)



Figure 3.19. Proposed mechanism for the build-up of (PAH/DexS H40) PEMs starting from bilayer 4 on PEMs previously ending with DexS.

In *Step 1*, the adsorption of PAH on adsorbed DexS H40 layer leads to an increase in mass and in dissipation as hydrated PAH is adsorbed. During *Step 2*, water rinsing does not seem to induce any mass loss which indicates that previous layers were charged enough to be strongly linked to the surface underneath. Thus, the (PAH/DexS H40) system leads to the formation of stable and charged layers. Then, the adsorption of DexS H40 on the previous PAH layer (*Step 3*) followed by the rinsing step (*Step 4*) leads to surface charge inversion and

no significant DexS H40 and counterion excess removing. During these four steps, the amount of water in the layer is stable and PE forms stable and highly charged layers.

2.2.2. Tentative mechanism for (PAH/DexS L40) i.e. type B

For (PAH/DexS L40) systems (Figure 3.20), the adsorption mechanism is more complex. At the *Step 1*, the adsorption of PAH induces an increase of film hydration and a decrease of the film rigidity followed by an internal film restructuration.

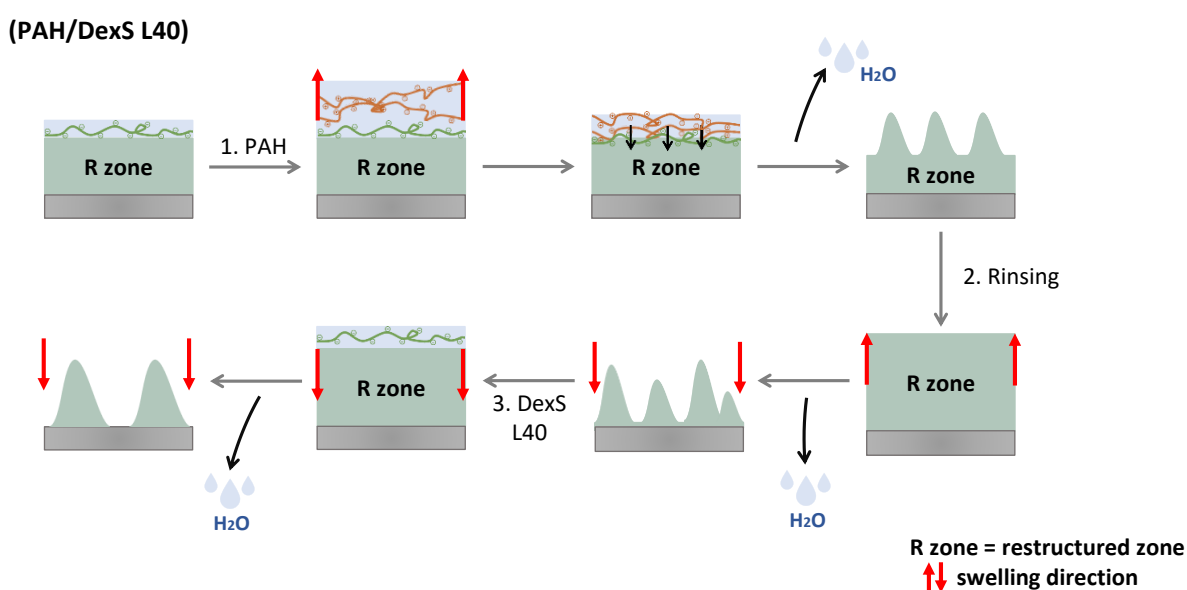


Figure 3.20. Proposed mechanism for the build-up of (PAH/DexS L40) PEMs starting from bilayer 4 on PEMs previously ending with DexS.

As DexS L40 presents a number of charges per monomer comparable to the number of charges presents on PAH monomer, a partial neutralization of sub-layers with PE adsorption occurs, which contributes to the diffusion of the adsorbed PAH into the (PAH/DexS L40) PEMs. During the rinsing in *Step 2*, the film swells again which may promote further internal diffusion and restructuration of PEMs. Charge neutralization itself generates a water removal as shown by Kittle *et al.* (2012) (J. D. Kittle et al., 2012). During *Step 3*, as soon as DexS L40 diffusion starts after adsorption, charge compensation between PAH and DexS L40 occurs inside the films which likely promotes charge neutralization then complexation between PAH and DexS L40. Formation of PE-complexes decreases the electrostatic repulsion between PEs and the affinity with bonding-water of highly hydrated PAH/DexS L40 decreases which results in the water expulsion from the film. This film dehydration, also named deswelling or

dewatering, favors short range interactions within the final system (Höök et al., 2001; J. Kittle et al., 2021) and induces PAH/DexS L40 aggregation onto the surface leading to the “puddle-like” pattern (*Step 3*) (Feng et al., 2005).

For (PAH/DexS H40) systems, the high amount of charges on the surface due to charge overcompensation leads to the construction of (PAH/DexS H) PEMs with typical symmetric linear growth and homogeneous thin films defined as Type A. In contrast, (PAH/DexS L) PEMs present an asymmetric growth between polycation and polyanion adsorption, which suggests a restructuration and a loss of water during LbL process defined as Type B.

Conclusion

In this chapter, we investigated the growth of multilayers based on poly(allylamine hydrochloride) (PAH) or Diethylaminoethyl-dextran (Dex-DEAE 150) with dextrans sulfate (DexS 40) or oxidized α -glucans (Ox-Alt, Ox1-Reu, Ox2-Reu, Ox1-Dex, Ox2-Dex and Ox3-Dex). Dextrans sulfate (PAH/DexS) PEMs films with linear growth were successfully constructed and we demonstrated that the difference of charge density between DexS H40 and DexS L40 resulted in a distinct adsorption capacity and influenced the type of adsorption as well as the film surface morphology. For (PAH/DexS H40) systems, the high amount of charges on the surface due to charges overcompensation led to the construction of (PAH/DexS H40) PEMs with typical symmetric linear growth and homogenous thin films. In contrast, (PAH/DexS L40) PEMs presented an asymmetric growth between polycation and polyanion adsorption, which suggests a restructuration and a loss of water during LbL process. The effect of restructuration on film surface morphology also influences the film morphology as the formation of PEMs with different pattern is obtained. (PAH/DexS L40) multilayer surfaces display “puddle-like” aggregates with pores similar to ones obtained with PE-complex. Moreover, while the system (Dex-DEAE 150/DexS) did not result in stable multilayers, the LbL formation with oxidized α -glucans was successful. (PAH/Ox-Alt) and (PAH/Ox1-Reu) PEMs present a linear growth and variations in their viscoelastic properties during the process indicating a small possible restructuration as well. A difference of final viscoelasticity of the films is also notable as (PAH/Ox1-Reu)₁₀ are more rigid than (PAH/Ox-Alt)₁₀. In parallel, (Dex-DEAE 150/Ox1-Dex) and (Dex-DEAE 150/Ox3-Dex) PEMs result in a linear asymmetric growth and important variations in their viscoelastic regime during the formation highlighting a restructuration or several restructurations with adsorption steps. Finally, results on (PAH/DexS) systems allow us to propose two formation behaviors and mechanisms defined as growth type A for linear symmetric growth, softer films and growth type B for linear asymmetric growth, more rigid and “puddle-like” films.

References

- Antonini, E., Bellelli, L., Bruzzesi, M. R., Caputo, A., Chiancone, E., & Rossi-Fanelli, A. (1964). Studies on dextran and dextran derivatives. I. Properties of native dextran in different solvents. *Biopolymers*, 2(1), 27–34. <https://doi.org/10.1002/bip.1964.360020105>
- Balabushevich, N., Tiourina, O., Volodkin, D., Larionova, N., & Sukhorukov, G. (2003). Loading the multilayer dextran sulfate/protamine microsized capsules with peroxidase. *Biomacromolecules*, 4(5), 1191–1197. <https://doi.org/10.1021/bm0340321>
- Barroso, N., Guaresti, O., Pérez-Álvarez, L., Ruiz-Rubio, L., Gabilondo, N., & Vilas-Vilela, J. L. (2019). Self-healable hyaluronic acid/chitosan polyelectrolyte complex hydrogels and multilayers. *European Polymer Journal*, 120, 109268. <https://doi.org/10.1016/j.eurpolymj.2019.109268>
- Boulmedais, F., Ball, V., Schwinte, P., Frisch, B., Schaaf, P., & Voegel, J.-C. (2003). Buildup of Exponentially Growing Multilayer Polypeptide Films with Internal Secondary Structure. *Langmuir*, 19(2), 440–445. <https://doi.org/10.1021/la0264522>
- Calvo, E. J., Flexer, V., Tagliazucchi, M., & Scodeller, P. (2010). Effects of the nature and charge of the topmost layer in layer by layer self assembled amperometric enzyme electrodes. *Physical Chemistry Chemical Physics*, 12(34), 10033–10039. <https://doi.org/10.1039/C0CP00449A>
- Caruso, F., Niihara, K., Furlong, D. N., & Okahata, Y. (1997). 1. Ultrathin Multilayer Polyelectrolyte Films on Gold: Construction and Thickness Determination. *Langmuir*, 13(13), 3422–3426. <https://doi.org/10.1021/la960821a>
- Cerclier, C., Cousin, F., Bizot, H., Moreau, C., & Cathala, B. (2010). Elaboration of Spin-Coated Cellulose-Xyloglucan Multilayered Thin Films. *Langmuir*, 26(22), 17248–17255. <https://doi.org/10.1021/la102614b>
- Crouzier, T., & Picart, C. (2009). Ion Pairing and Hydration in Polyelectrolyte Multilayer Films Containing Polysaccharides. *Biomacromolecules*, 10(2), 433–442. <https://doi.org/10.1021/bm8012378>
- Davantès, A., Nigen, M., Sanchez, C., d'Orlando, A., & Renard, D. (2019). Adsorption of Hyperbranched Arabinogalactan-Proteins from Plant Exudate at the Solid–Liquid Interface. *Colloids and Interfaces*, 3(2), 2. <https://doi.org/10.3390/colloids3020049>
- de Belder, D. (1996). *Polysaccharides in Medicinal Applications*. Marcel Dekker, New York, 505–524.
- de Villiers, M. M., Otto, D. P., Strydom, S. J., & Lvov, Y. M. (2011). Introduction to nanocoatings produced by layer-by-layer (LbL) self-assembly. *Advanced Drug Delivery Reviews*, 63(9), 701–715. <https://doi.org/10.1016/j.addr.2011.05.011>
- Decher, G. (1997). Fuzzy Nanoassemblies: Toward Layered Polymeric Multicomposites. *Science*, 277(5330), 1232–1237. <https://doi.org/10.1126/science.277.5330.1232>
- Decher, G., Hong, J. D., & Schmitt, J. (1992). Buildup of ultrathin multilayer films by a self-assembly process: III. Consecutively alternating adsorption of anionic and cationic polyelectrolytes on charged surfaces. *Thin Solid Films*, 210–211, 831–835. [https://doi.org/10.1016/0040-6090\(92\)90417-A](https://doi.org/10.1016/0040-6090(92)90417-A)
- Díaz-Montes, E. (2021). Dextran: Sources, Structures, and Properties. *Polysaccharides*, 2(3), 554–565. <https://doi.org/10.3390/polysaccharides2030033>
- Dubas, S. T., & Schlenoff, J. B. (1999). Factors Controlling the Growth of Polyelectrolyte Multilayers. *Macromolecules*, 32(24), 8153–8160. <https://doi.org/10.1021/ma981927a>
- Elosua, C., Lopez-Torres, D., Hernaez, M., Matias, I. R., & Arregui, F. J. (2013). Comparative study of layer-by-layer deposition techniques for poly(sodium phosphate) and poly(allylamine hydrochloride). *Nanoscale Research Letters*, 8(1), 539. <https://doi.org/10.1186/1556-276X-8-539>
- Elzbiaciak, M., Kolasińska, M., Zapotoczny, S., Krastev, R., Nowakowska, M., & Warszyński, P. (2009). Nonlinear growth of multilayer films formed from weak polyelectrolytes. *Colloids and Surfaces A: Physicochemical and Engineering Aspects*, 343(1–3), 89–95. <https://doi.org/10.1016/j.colsurfa.2009.01.034>
- Elzbiaciak-Wodka, M., Kolasińska-Sojka, M., Nowak, P., & Warszyński, P. (2015). Comparison of permeability of poly(allylamine hydrochloride) and poly(diallyldimethylammonium chloride)/poly(4-styrenesulfonate) multilayer films: Linear vs. exponential growth. *Journal of Electroanalytical Chemistry*, 738, 195–202. <https://doi.org/10.1016/j.jelechem.2014.11.035>
- Feng, Q., Zeng, G., Yang, P., Wang, C., & Cai, J. (2005). Self-assembly and characterization of polyelectrolyte complex films of hyaluronic acid/chitosan. *Colloids and Surfaces A: Physicochemical and Engineering Aspects*, 257–258, 85–88. <https://doi.org/10.1016/j.colsurfa.2004.10.099>

- Fu, Y., Bai, S., Cui, S., Qiu, D., Wang, Z., & Zhang, X. (2002). Hydrogen-Bonding-Directed Layer-by-Layer Multilayer Assembly: Reformation Yielding Microporous Films. *Macromolecules*, 35(25), 9451–9458. <https://doi.org/10.1021/ma0207881>
- Ghavidel Mehr, N., Hoemann, C. D., & Favis, B. D. (2015). Chitosan surface modification of fully interconnected 3D porous poly(ϵ -caprolactone) by the LbL approach. *Polymer*, 64, 112–121. <https://doi.org/10.1016/j.polymer.2015.03.025>
- Ghostine, R. A., Markarian, M. Z., & Schlenoff, J. B. (2013). Asymmetric Growth in Polyelectrolyte Multilayers. *Journal of the American Chemical Society*, 135(20), 7636–7646. <https://doi.org/10.1021/ja401318m>
- Glinel, K., Moussa, A., Jonas, A. M., & Laschewsky, A. (2002). Influence of Polyelectrolyte Charge Density on the Formation of Multilayers of Strong Polyelectrolytes at Low Ionic Strength. *Langmuir*, 18(4), 1408–1412. <https://doi.org/10.1021/la0113670>
- Heinze, T., Liebert, T., Heublein, B., & Hornig, S. (2006). Functional Polymers Based on Dextran. In D. Klemm (Ed.), *Polysaccharides II* (Vol. 205, pp. 199–291). Springer Berlin Heidelberg. https://doi.org/10.1007/12_100
- Hollman, A., & Bhattacharyya, D. (2004). Pore assembled multilayers of charged polypeptides in microporous membranes for ion separation. *Langmuir*, 20(13), 5418–5424. <https://doi.org/10.1021/la049688+>
- Höök, F., Kasemo, B., Nylander, T., Fant, C., Sott, K., & Elwing, H. (2001). Variations in Coupled Water, Viscoelastic Properties, and Film Thickness of a Mefp-1 Protein Film during Adsorption and Cross-Linking: A Quartz Crystal Microbalance with Dissipation Monitoring, Ellipsometry, and Surface Plasmon Resonance Study. *Analytical Chemistry*, 73(24), 5796–5804. <https://doi.org/10.1021/ac0106501>
- Jaafar, Z., Mazeau, K., Boissière, A., Le Gall, S., Villares, A., Vigouroux, J., Beury, N., Moreau, C., Lahaye, M., & Cathala, B. (2019). Meaning of xylan acetylation on xylan-cellulose interactions: A quartz crystal microbalance with dissipation (QCM-D) and molecular dynamic study. *Carbohydrate Polymers*, 226, 115315. <https://doi.org/10.1016/j.carbpol.2019.115315>
- Kittle, J. D., Wondraczek, H., Wang, C., Jiang, F., Roman, M., Heinze, T., & Esker, A. R. (2012). Enhanced Dewatering of Polyelectrolyte Nanocomposites by Hydrophobic Polyelectrolytes. *Langmuir*, 28(30), 11086–11094. <https://doi.org/10.1021/la3016996>
- Kittle, J., Levin, J., & Levin, N. (2021). Water Content of Polyelectrolyte Multilayer Films Measured by Quartz Crystal Microbalance and Deuterium Oxide Exchange. *Sensors*, 21(3), 3. <https://doi.org/10.3390/s21030771>
- Kotov, N. A. (1999). Layer-by-layer self-assembly: The contribution of hydrophobic interactions. *Nanostructured Materials*, 12(5), 789–796. [https://doi.org/10.1016/S0965-9773\(99\)00237-8](https://doi.org/10.1016/S0965-9773(99)00237-8)
- Leathers, T. D. (2002). Dextran. *Biopolymers*, 5, 299–321.
- Liu, W., Wijeratne, S., Yang, L., & Bruening, M. (2018). Porous star-star polyelectrolyte multilayers for protein binding. *Polymer*, 138, 267–274. <https://doi.org/10.1016/j.polymer.2018.01.055>
- Lourenço, J. M. C., Ribeiro, P. A., Botelho do Rego, A. M., Braz Fernandes, F. M., Moutinho, A. M. C., & Raposo, M. (2004). Counterions in Poly(allylamine hydrochloride) and Poly(styrene sulfonate) Layer-by-Layer Films. *Langmuir*, 20(19), 8103–8109. <https://doi.org/10.1021/la049872v>
- Matsusaki, M., Sakaguchi, H., Serizawa, T., & Akashi, M. (2007). Controlled release of vascular endothelial growth factor from alginate hydrogels nano-coated with polyelectrolyte multilayer films. *Journal of Biomaterials Science-Polymer Edition*, 18(6), 775–783. <https://doi.org/10.1163/156856207781034160>
- Moreau, C., Beury, N., Delorme, N., & Cathala, B. (2012). Tuning the Architecture of Cellulose Nanocrystal–Poly(allylamine hydrochloride) Multilayered Thin Films: Influence of Dipping Parameters. *Langmuir*, 28(28), 10425–10436. <https://doi.org/10.1021/la301293r>
- Mosley, R. J., Talarico, M. V., & Byrne, M. E. (2021). Recent applications of QCM-D for the design, synthesis, and characterization of bioactive materials. *Journal of Bioactive and Compatible Polymers*, 36(4), 261–275. <https://doi.org/10.1177/08839115211014216>
- Naessens, M., Cerdobbel, A., Soetaert, W., & Vandamme, E. J. (2005). *Leuconostoc* dextranase and dextran: production, properties and applications. *Journal of Chemical Technology & Biotechnology*, 80(8), 845–860. <https://doi.org/10.1002/jctb.1322>
- Palasingh, C., Ström, A., Amer, H., & Nypelö, T. (2021). Oxidized xylan additive for nanocellulose films – A swelling modifier. *International Journal of Biological Macromolecules*, 180, 753–759. <https://doi.org/10.1016/j.ijbiomac.2021.03.062>
- Pescosolido, L., Schuurman, W., Malda, J., Matricardi, P., Alhaique, F., Coviello, T., van Weeren, P. R., Dhert, W. J. A., Hennink, W. E., & Vermonden, T. (2011). Hyaluronic Acid and Dextran-Based Semi-IPN Hydrogels as Biomaterials for Bioprinting. *Biomacromolecules*, 12(5), 1831–1838. <https://doi.org/10.1021/bm200178w>

- Picart, C., Lavalle, Ph., Hubert, P., Cuisinier, F. J. G., Decher, G., Schaaf, P., & Voegel, J.-C. (2001). Buildup Mechanism for Poly(L-lysine)/Hyaluronic Acid Films onto a Solid Surface. *Langmuir*, 17(23), 7414–7424. <https://doi.org/10.1021/la010848g>
- Picart, C., Mutterer, J., Richert, L., Luo, Y., Prestwich, G. D., Schaaf, P., Voegel, J.-C., & Lavalle, P. (2002). Molecular basis for the explanation of the exponential growth of polyelectrolyte multilayers. *Proceedings of the National Academy of Sciences*, 99(20), 12531–12535. <https://doi.org/10.1073/pnas.202486099>
- Pinto, E. M., Barsan, M. M., & Brett, C. M. A. (2010). Mechanism of Formation and Construction of Self-Assembled Myoglobin/Hyaluronic Acid Multilayer Films: An Electrochemical QCM, Impedance, and AFM Study. *The Journal of Physical Chemistry B*, 114(46), 15354–15361. <https://doi.org/10.1021/jp107107b>
- Robyt, J. F. (1985). Dextran. *Encyclopaedia of Polymer Science*. Wiley-Vch, 4, 753–767.
- Schlenoff, J. B., & Dubas, S. T. (2001). Mechanism of Polyelectrolyte Multilayer Growth: Charge Overcompensation and Distribution. *Macromolecules*, 34(3), 592–598. <https://doi.org/10.1021/ma0003093>
- Schlenoff, J. B., Ly, H., & Li, M. (1998). Charge and Mass Balance in Polyelectrolyte Multilayers. *Journal of the American Chemical Society*, 120(30), 7626–7634. <https://doi.org/10.1021/ja980350+>
- Schmitt, J., Gruenewald, T., Decher, G., Pershan, P. S., Kjaer, K., & Loesche, M. (1993). Internal structure of layer-by-layer adsorbed polyelectrolyte films: a neutron and x-ray reflectivity study. *Macromolecules*, 26(25), 7058–7063. <https://doi.org/10.1021/ma00077a052>
- Schoeler, B., Kumaraswamy, G., & Caruso, F. (2002). Investigation of the Influence of Polyelectrolyte Charge Density on the Growth of Multilayer Thin Films Prepared by the Layer-by-Layer Technique. *Macromolecules*, 35(3), 889–897. <https://doi.org/10.1021/ma011349p>
- Serizawa, T., Yamaguchi, M., & Akashi, M. (2002). Enzymatic hydrolysis of a layer-by-layer assembly prepared from chitosan and dextran sulfate. *Macromolecules*, 35(23), 8656–8658. <https://doi.org/10.1021/ma012153s>
- Towle, E. G., Ding, I., & Peterson, A. M. (2020). Impact of molecular weight on polyelectrolyte multilayer assembly and surface properties. *Journal of Colloid and Interface Science*, 570, 135–142. <https://doi.org/10.1016/j.jcis.2020.02.114>
- Voigt, U., Jaeger, W., Findenegg, G. H., & Klitzing, R. v. (2003). Charge Effects on the Formation of Multilayers Containing Strong Polyelectrolytes. *The Journal of Physical Chemistry B*, 107(22), 5273–5280. <https://doi.org/10.1021/jp0256488>

Annexes

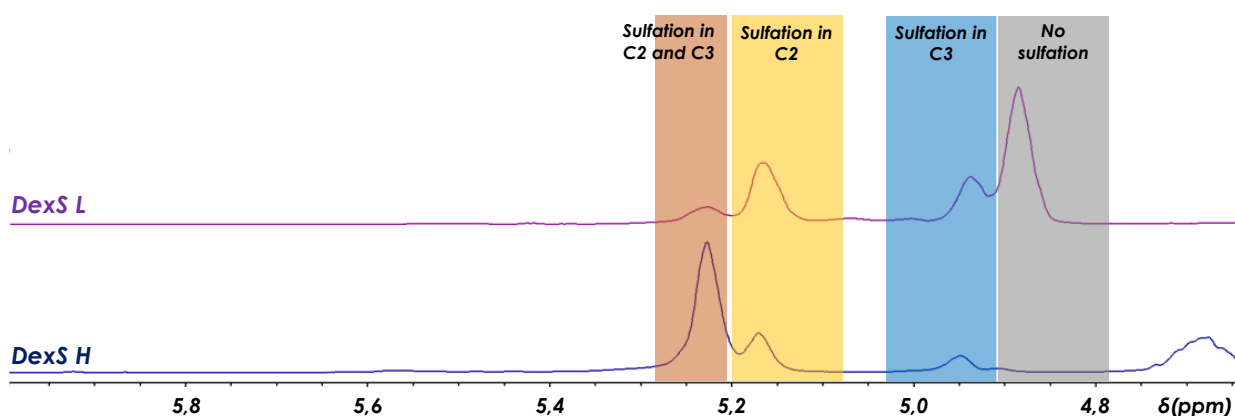


Figure 3.A1. ^1H NMR spectrum for DexS H and DexS L showing sulfation from peaks on C2 and C3 at 5.2-5.3 ppm, on C2 (5.1-5.2 ppm) and on C3 (4.9-5.0 ppm) and no sulfation from peaks at 4.8-4.9 ppm.

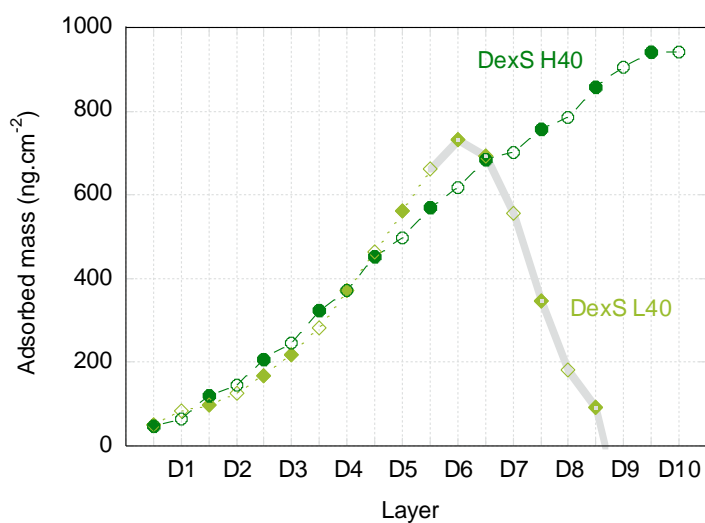


Figure 3.A2. Adsorbed mass obtained by SPR analysis on gold-coated sensors, where D_n represents the number of bilayers deposited. (PAH/DexS H40) is represented in dark green, (PAH/DexS L40) is represented in light green. In grey is indicated, the values where (PAH/DexS L40) seems to detach itself from the substrate and the total adsorbed mass detected drop during the measurement.

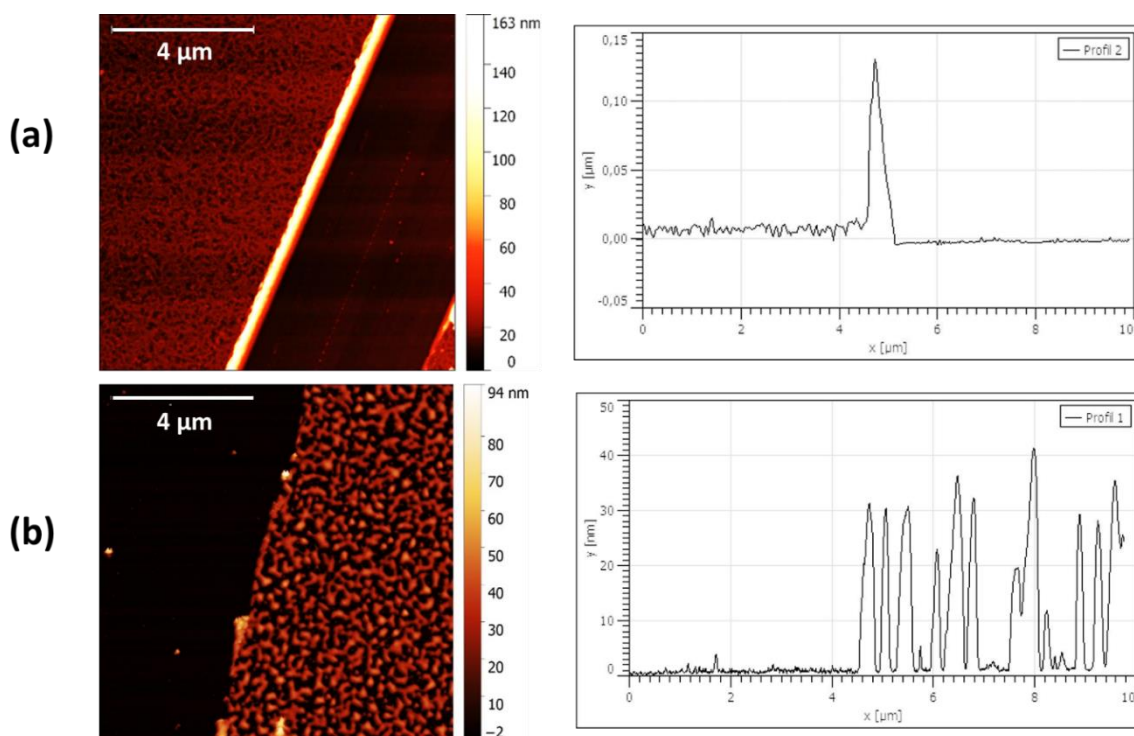


Figure 3.A3. AFM topography images ($10\mu\text{m} \times 10\mu\text{m}$) and the corresponding height profiles of the 10th layer of DexS after scratching method applied on (a) $(\text{PAH}/\text{DexS H40})_{10}$ and (b) $(\text{PAH}/\text{DexS L40})_{10}$ PEMs. AFM scratching method applied on PEMs $(\text{PAH}/\text{DexS H40})$ and $(\text{PAH}/\text{DexS L40})$. Height profiles of $(\text{PAH}/\text{DexS H40})$ PEMs section on the top and of $(\text{PAH}/\text{DexS L40})$ PEMs section on the bottom. Height profiles of the 10th layer of DexS for (a) $(\text{PAH}/\text{DexS H40})$ and (b) $(\text{PAH}/\text{DexS L40})$.

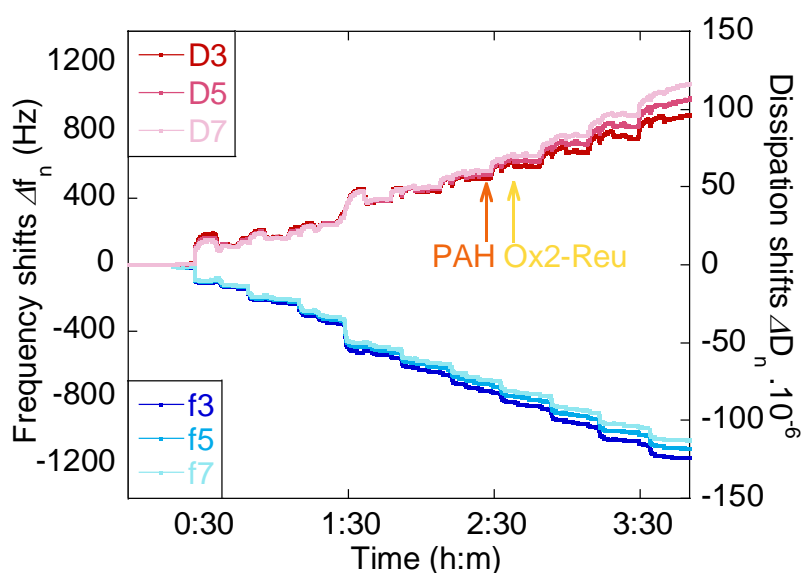


Figure 3.A4. $\Delta f_n/n$ and ΔD_n as function of time for $(\text{PAH}/\text{Ox2-Reu})_{10}$ multilayer on gold coated quartz crystal using QCM-D. The frequency (blue) and dissipation (red) changes for the third, fifth and seventh overtone are depicted with adsorption of PAH (orange) and adsorption of Ox2-Reu (yellow).

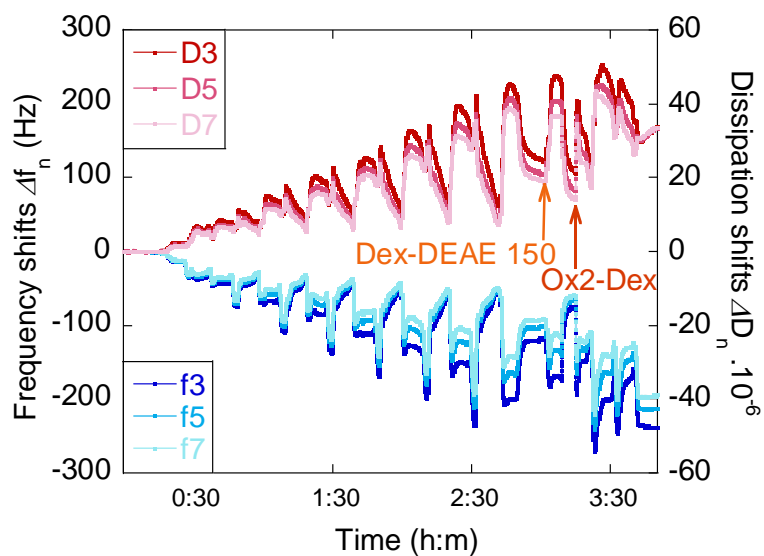


Figure 3.A5. $\Delta f_n/n$ and ΔD_n as function of time for (Dex-DEAE 150/Ox2-Dex)₁₀ multilayer on gold coated quartz crystal using QCM-D. The frequency (blue) and dissipation (red) changes for the third, fifth and seventh overtone are depicted with adsorption of Dex-DEAE 150 (orange) and adsorption of Ox2-Dex (dark orange).

Chapter 4

Structure and surface properties modulation

Table of content

Introduction	157
1. Influence of the charge density on the structure of multilayered films.....	159
<u>1.1. Impact of the charge density on film growth and viscoelastic behavior</u>	<u>159</u>
<i>1.1.1. Dextrans sulfate -based multilayers</i>	<i>160</i>
<i>1.1.2. Oxidized dextrans-based multilayers</i>	<i>162</i>
<u>1.2. Impact of charge density on film characteristics and properties</u>	<u>163</u>
<i>1.2.1. Morphology and structural colors.....</i>	<i>164</i>
<i>1.2.2. Wetting properties</i>	<i>166</i>
2. Influence of the ionic strength on the structure of multilayered films	168
<u>2.1. Impact of the ionic strength on film growth and viscoelastic behavior.....</u>	<u>168</u>
<i>2.1.1. Dextrans with high charge density</i>	<i>168</i>
<i>2.1.2. Dextrans with low charge density</i>	<i>170</i>
<u>2.2. Impact of the ionic strength on film characteristics and properties.....</u>	<u>171</u>
<i>2.2.1. Morphology and structural colors.....</i>	<i>172</i>
<i>2.2.2. Wetting properties</i>	<i>175</i>
3. Impact of the molar masses of PE on the structure of multilayered films.....	177
<u>3.1. Impact of molar mass of polyelectrolytes on film growth and viscoelastic behavior</u>	<u>177</u>
<u>3.2. Impact of molar masses on film characteristics and properties.....</u>	<u>179</u>
<i>3.2.1. Surface morphology and structural colors</i>	<i>179</i>
<i>3.2.2. Wetting properties</i>	<i>181</i>
Conclusion.....	183
References	185
Annexes	Erreur ! Signet non défini.

Introduction

With the LbL technique, we have the ability to monitor the characteristics of the films (Chapter 1, section 2.3.1): thickness, roughness, structural colors, wettability, swelling behavior, *etc.* (Petrila et al., 2021). As presented in Chapter 1, section 2.3.2., the physico-chemical properties of multilayers can be tailored by adjusting the experimental conditions. This includes the control of critical parameters such as polymer functionality, polymer concentration, pH, ionic strength or number of layers (Dubas & Schlenoff, 1999; Guzmán et al., 2020). Fine modulation of the characteristics of LbL assemblies allows the development of materials with innovative properties such as hydrophobicity, stimuli-responsiveness or flexibility (Richardson et al., 2016; Wågberg & Erlandsson, 2021). In particular, new nano-objects such as films, capsules and hydrogels with natural polyelectrolytes are of great interest to the scientific community and industry (La Fuente Arias et al., 2021; Lombardo & Villares, 2020; Nie et al., 2019).

The study in the previous chapter (chapter 3) on systems using (PAH/DexS H40) and (PAH/DexS L40) allows us to identify two different types of film growth as a function of charge density. The differences between the two growth mechanisms explained in chapter 3 (section 2) lead to films with distinct characteristics. In the case of these two dextran derivatives, a lower charge density leads to a stiffer film with a more porous 10 bilayer surface morphology while a higher charge density leads to a more hydrated film with a high coverage surface morphology. Furthermore, the use of other polyelectrolyte systems also leads to one of these two types of growth mechanisms. As described in Chapter 1 (Section 2.3.), there are multiple experimental conditions that can affect multilayer growth and its properties, suggesting that we could tune the growth type of each polyelectrolyte system by adjusting these parameters. In this way, we could control the film constitution and internal structure, which are essential for tuning their physico-chemical properties.

In Chapter 4, we decided to investigate the possibility of modulating the growth type and characteristics of α -glucan-based films by adjusting the experimental conditions. In this objective, we also seek to understand the correlation between the formation of the films, their internal structure, their properties, and the assembly conditions. We investigate the impact of the following parameters on the formation of functionalized α -glucan-based films as follows:

1. Charge density of polyelectrolytes (section 1)
2. Ionic strength of polyelectrolyte solutions (section 2)

3. Molar mass of polyelectrolytes (section 3)

First, we studied the impact of each parameter on the key “features” for LbL assemblies: the growth mode of the systems and their viscoelastic behavior. For this purpose, the construction of a 5-layer film was studied using a quartz crystal microbalance with dissipation control (QCM-D). Then, we proposed to obtain a higher scale of film fabrication using spin-assisted deposition and 40 bilayer films to have materials with usable features. An analysis of the influence of parameters on the surface characteristics (morphology, thickness, roughness) is presented as well as the resulting properties (structural color, surface wettability). The surface morphologies and roughness of the multilayers were studied by atomic force microscopy (AFM). The structural colors resulting from the structure and their thickness were observed by camera images and analyzed to calculate the theoretical thickness of the multilayers. Finally, we measured the contact angle of water on the surface to determine the wettability of our multilayers.

1. Influence of the charge density on the structure of multilayered films

Based on the differences observed with (PAH/DexS 40) systems, we decided to expand my study on charge density to all polyelectrolyte couples used for the film buildup. We successfully managed to build films on multiple α -glucans (Dex-DEAE, DexS, Ox-Alt, Ox-Reu and Ox-Dex) in the previous chapter. Thus, polyelectrolytes from the same nature with an important variation of charge density were chosen to deepen the overview on the impact of charge density on α -glucans based system. From all systems, we should be able to have a wide range of structures and properties controlled by the charge density of polyelectrolytes introduced in the multilayers.

We used the same experimental parameters that those used in Chap 3. In this section, only polyelectrolyte types and their charge density are changing in the solutions used. Salt concentration were fixed at 25 mM NaCl, and polymer concentrations fixed at 0.1 g.L⁻¹ and 0.5 g.L⁻¹ for polyanions and for polycations, respectively. Adsorptions of PEs solutions were done at 20°C regardless of the build-up method used, each adsorption step was followed by a rinsing step in MilliQ water to eliminate unbound materials.

1.1. Impact of the charge density on film growth and viscoelastic behavior

The first step was to study the influence of charge density on the film construction *i.e.* the film growth. In this part, we decided to work with 5 bilayers instead of 10 bilayers as we saw in the previous chapter (chapter 3) that the film growth reaches a regime where the growth no longer depends on the substrate characteristics after bilayer 3.

All systems of polyelectrolytes studied in this section and information on their charge density are given in Table 4.1.

Table 4.1. Systems based on different polyelectrolyte couples, charge type and charge density of polycation (PC) and polyanion (PA) used for each system.

System	Charge type PC	Charge density PC	Charge type PA	Charge density PA
(PAH/DexS H40)	NH ₂ ⁺ groups	1 charge / 1 monomer	SO ₃ ⁻ groups	1.75 charge / 1 monomer
(PAH/DexS L40)	NH ₂ ⁺ groups	1 charge / 1 monomer	SO ₃ ⁻ groups	0.6 charge / 1 monomer
(PAH/DexS H5)	NH ₂ ⁺ groups	1 charge / 1 monomer	SO ₃ ⁻ groups	1.75 charge / 1 monomer

(PAH/DexS L5)	NH ₂ ⁺ groups	1 charge / 1 monomer	SO ³⁻ groups	0.6 charge / 1 monomer
(Dex-DEAE 150/Ox1-Dex)	NH ⁺ and N ⁺ groups	0.33 charge / 1 monomers	COO ⁻ groups	1 charge / 1 monomer
(Dex-DEAE 150/Ox3-Dex)	NH ⁺ and N ⁺ groups	0.33 charge / 1 monomers	COO ⁻ groups	0.8 charge / 1 monomer

The use of a large choice of molar masses for the polyanions (5 000 g.mol⁻¹ and 40 000 g.mol⁻¹ for DexS and 10⁸ g.mol⁻¹ for Ox-Dex) as well as different charge types for both polyanion and polycation (charges in Table 4.1) will allow us to highlight the impact of the charge density for different polyelectrolyte structures. We fixed the pH of all polyelectrolyte solutions at pH 6.5. Hence, COOH groups of oxidized α -glucans are all in the COO⁻ form during film formation.

1.1.1. Dextran sulfate -based multilayers

Using (PAH/DexS) systems, we studied the growth of 5 bilayers of (PAH/DexS H40), (PAH/DexS L40), (PAH/DexS H5) and (PAH/DexS L5) on gold-coated quartz with QCM-D. For PAH and DexS systems, the frequency shifts, $\Delta f_5/5$, reported on Figure 4.1a, give a comparison between all systems for adsorbed quantity of material. The ΔD values as a function of Δf values reported on Figure 4.1b allows a qualitative evaluation of the rigidity/softness of the films built.

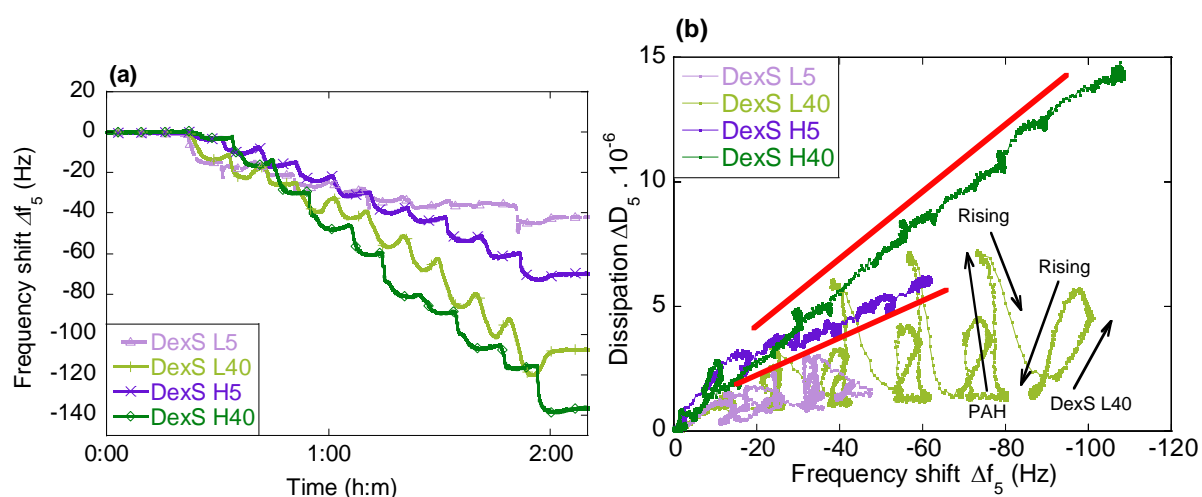


Figure 4.1. (a) Graph of $\Delta f_5/5$ vs time for 5 bilayers of (PAH/DexS L5) films (light purple), (PAH/DexS H5) films (dark purple), (PAH/DexS L40) films (light green) and (PAH/DexS H40) films (dark green) built on gold coated surface. (b) ΔD_5 as a function of $\Delta f_5/5$ of the construction of (PAH/DexS L5)₅ films (light purple), (PAH/DexS H5)₅ films (dark purple), (PAH/DexS L40)₅ films (light green) and (PAH/DexS H40)₅ films (dark green). Relative softness *i.e.* slopes in red.

The summarized information is provided in Table C4.

As presented in Chapter 3, we can see that both systems lead to a general decrease of frequencies with adsorption of polyelectrolytes and film build-up. The (PAH/DexS H40) film presents a lower final frequency shift than the (PAH/DexS L40) system with -136 Hz and -107 Hz, respectively. The analysis of frequency and dissipation on the 5th harmonic frequency highlights the difference between the film growth as $\Delta D_5/\Delta f_5$ slopes (indicative of the relative softness), on Figure 4.2b, during the construction are not similar. The entire PAH/DexS H40 film formation appears to be linear, as we observed in Chapter 3 (section 2.1.1). The slope $-D_5/\Delta f_5$, *i.e.* the relative softness, is around $0.13 \times 10^{-6} \text{ Hz}^{-1}$ (Figure 4.1b). Meanwhile, the formation of PAH/DexS L40 leads to a change in value of relative softness at both the polyelectrolyte adsorption or the rinsing step as it was presented in Chapter 3 (section 2.1.1).

If we look now at the construction of (PAH/DexS H5) and (PAH/DexS L5) films ($5000 \text{ g}\cdot\text{mol}^{-1}$) on Figure 4.2a, it can be observed that the frequency variations have the same behavior, as the two systems lead to a decrease of frequency at each bilayer adsorption. Moreover, DexS H5 results in a film with a lower frequency value, -70 Hz, than films based on DexS L5 with a final frequency of -42 Hz. In addition to frequencies, the analysis of dissipations reported on Figure 4.2b highlights a similar behavior in terms of viscoelasticity of the layers as well. As it can be observed on purple curves on Figure 4.2b, DexS H5 (dark purple) results in a general slope from the second bilayer ($-\Delta D_5/\Delta f_5$ about $0.07 \times 10^{-6} \text{ Hz}^{-1}$), *i.e.* from the frequency Δf_5 around -30 Hz. As we observed with (PAH/DexS H40), the first bilayers (1 – 2) show a different adsorption regime as compared to the following due to the influence of substrate properties. In the opposite, DexS L5 film results in several variations of its viscoelastic properties and relative rigidity during its construction recalling the behavior of PAH/DexS L40 films.

DexS with a high charge density (1.75 charge/monomer) results in a higher value of final frequency shift $-\Delta f_5$ that a DexS with a low charge density (0.6 charge/monomer), for both molar masses of DexS. Those observations on DexS H5/L5 confirm what we observed for DexS H40/L40: dextrans with low sulfate content, we have a hydration/dehydration process as well as a change in structure of the multilayers due to their diffusion inside the film (Kittle et al., 2012). This leads to the mechanism presented in Chapter 3 for PAH/DexS 40 (section 3.2). In fact, the charge density of both DexS L may not be high enough to obtain a

total charge inversion onto the surface, that is necessary for the formation of classic LbL assembly (Glinel et al., 2002).

1.1.2. Oxidized dextrans-based multilayers

Figure 4.3a reports the frequency shift Δf_5 during the construction of (Dex-DEAE 150/Ox1-Dex) and (Dex-DEAE 150/Ox3-Dex) multilayers, with Ox1-Dex as the polyanion with the higher charge density (1 charge/monomer) and Ox3-Dex as the polyanion with the lower charge density (0.8 charge/monomer). The ΔD values as a function of Δf values are reported on Figure 4.3b.

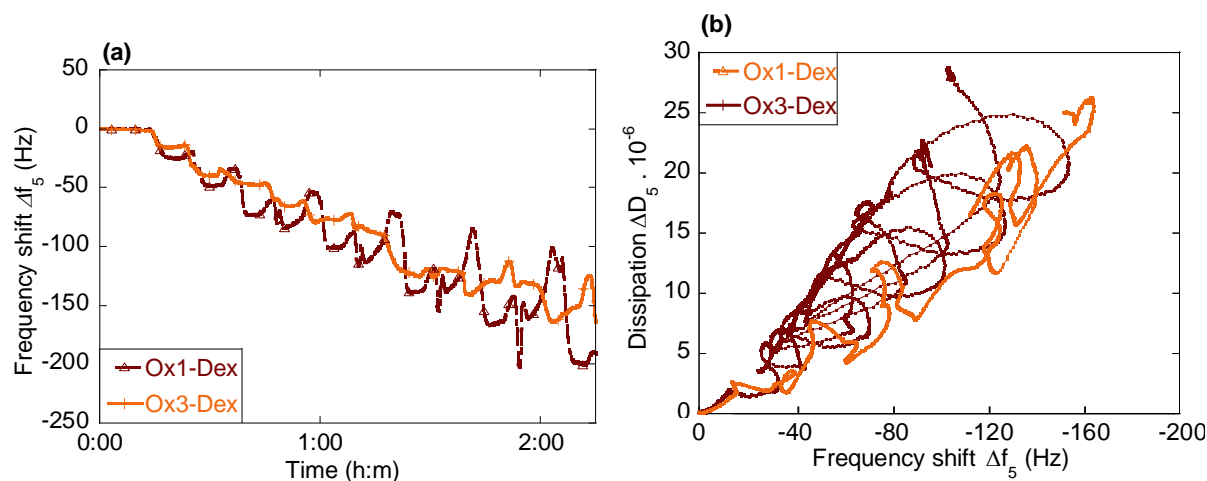


Figure 4.2. (a) Graph of $\Delta f_5/5$ vs time for 5 bilayers of (Dex-DEAE 150/Ox1-Dex) films (brown), and (Dex-DEAE 150/Ox3-Dex) films (orange) built on gold coated surface. (b) ΔD_5 as a function of $\Delta f_5/5$ of the construction of (Dex-DEAE 150/Ox1-Dex)₅ films (brown) and (Dex-DEAE)₅ films (orange).

The summarized information is provided in Table C4.

In these systems based on two functionalized dextrans, we also observe that the higher charge density results in the higher frequency shift. On Figure 4.3a, we can see that Dex-DEAE 150/Ox1-Dex (1 charge/monomer) leads to -198 Hz while Dex-DEAE 150/Ox3-Dex (0.8 charge/monomer) leads to -164 Hz after adsorption of 5 bilayers. Moreover, the use of Ox1-Dex with high charge density leads to lower variation amplitude in dissipation (Figure 4.3b, orange) than during the formation with Ox3-Dex which has a lower charge density (Figure 4.3b, brown).

It can be due to the lower difference between charge densities of Ox1-Dex (1 charge / 1 monomer) and Ox3-Dex (0.8 charge / 1 monomer) and charge densities of DexS H (1.75 charge / 1 monomer) and DexS L (0.6 charge / 1 monomer). While DexS H5 and DexS H40 layer are able to overcompensate the sub-layer of PAH to form films (mechanism from Chapter 3, section 3.1), DexS L40 and DexS L5 are charged enough to allow film formation, but by the formation of PE-complexes instead of organized layers (mechanism from Chapter 3, section 3.2). In comparison, Dex-DEAE 150/Ox3-Ox may lead to film formation by PE-complexation as well, while Dex-DEAE 150/Ox1-Dex may be a mix between the two types of formations.

If charge density is an important parameter to control the growth of multilayers, other parameters such as molar masses and ionic strength must be considered as well and will be studied in section 3.

1.2. Impact of charge density on film characteristics and properties

In addition to the control of film growth, the modulation of the properties of films could be useful for the elaboration of materials applied to various fields. Among the different properties of multilayers presented in Chapter 1 (section 2.3), we decided to focus this study on the surface properties of films including:

- Structural colors
- Surface morphology
- Wettability

The characteristics of films presented in Table 4.2 were studied in this part.

Table 4.2. Systems based on different polyelectrolyte couples, charge density of polycation (PC) and polyanion (PA) and number of bilayers used for each system.

System	Charge density PC	Charge density PA	Number of bilayers
(PAH/DexS H40) ₄₀	1 charge / 1 monomer	1.75 charge / 1 monomer	40 bilayers
(PAH/DexS L40) ₄₀	1 charge / 1 monomer	0.6 charge / 1 monomer	40 bilayers

As the impact of charge density was found to be the same for each system studied in the previous section (section 1.1), we decided to focus on the influence on (PAH/DexS)₄₀ films as a representative for all films. (PAH/DexS)₄₀ films were formed by varying the charge

density from polyelectrolytes containing 25mM NaCl: the polycation (PAH) has 1 charge per monomer while DexS H40 and DexS L40 have 1.75 charge per monomer and 0.6 charge per monomer, respectively. In order to analyze film properties, we worked with 40 bilayers films obtained by spin-assisted dipping method since the resulting thickness of the films makes it easier to observe (visually or with a camera) any potential changes.

1.2.1. Morphology and structural colors

The structural colors of these films were studied by eyes and camera pictures while the morphology of these multilayers was examined using the AFM. 2D and 3D images of 40 bilayers of (PAH/DexS H40) and (PAH/DexS L40) and the photos of the surface are shown on Figure 4.3. We note that the structural colors of (PAH/DexS H40) and (PAH/DexS L40) films were stable in air and at room temperature (%RH between 30 – 60).

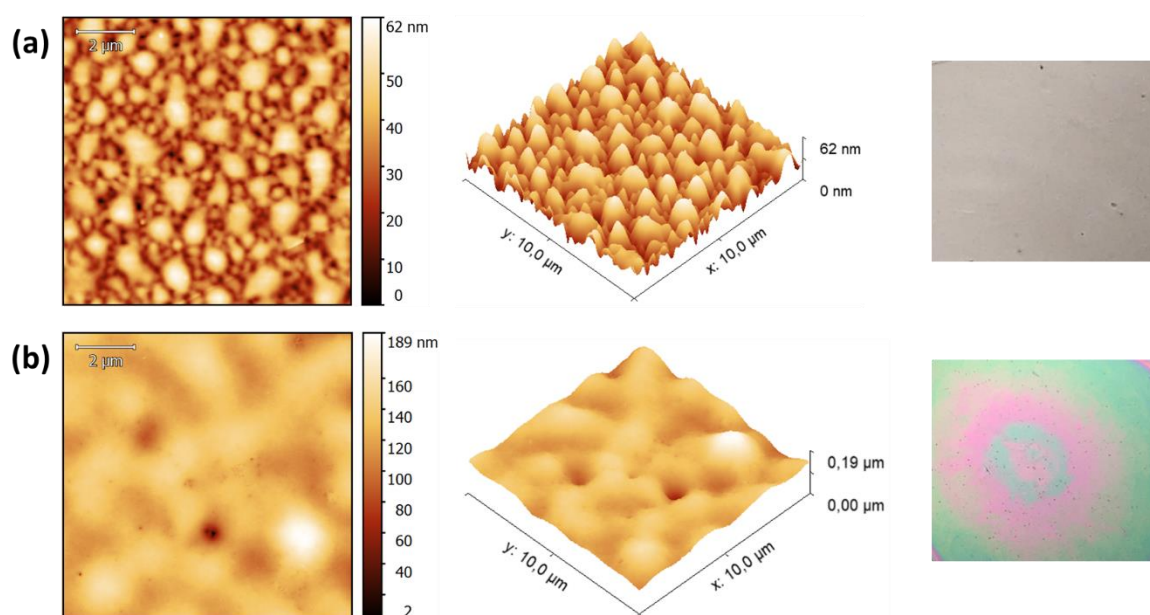


Figure 4.3. AFM 2D and 3D images (10×10 μm) and photos of the surface for 40 bilayers of (a) (PAH/DexS H40) and (b) (PAH/DexS L40) built by spin-assisted dipping method onto silicon wafer at 25mM NaCl.

On AFM images from Figure 4.3, it can be seen that 40 bilayers of (PAH/DexS H40) lead to surface morphology with peaks unlike surfaces from (PAH/DexS L40) with a quite flat morphology. The surface roughness RMS (root mean square) measured is $3.273 \text{ nm} \pm 0.588 \text{ nm}$ for 40 bilayers of (PAH/DexS H40) and $1.197 \text{ nm} \pm 0.366 \text{ nm}$ for 40 bilayers of (PAH/DexS L40). Moreover, at 40 bilayers, the (PAH/DexS L40) film presents a colorful

surface with two concentric circles with important heterogeneity (magenta and blue-green, Figure 4.3a) when DexS has a low charge density and a surface with a very light brown (Figure 4.3b) when DexS has a higher charge density. The concentric circles observed on DexS L40 -based multilayers indicate a non-regular spread of polyelectrolytes by spin-assisted deposition, and especially, of DexS L40 as we do not observe the problem with PAH/DexS H40.

We could not measure the thickness on AFM with the scratching method, as it was impossible to obtain a clear scratch on films this thick. So, we determined a theoretical thickness using the equation 9 and equation 10 (chapter 2, section 2.4.2) on constructive and destructive light interferences in thin films. As presented in Chapter 2 (section 2.4.2), we are considering white light perpendicularly incident on the film and a refractive index of 1.48 for the whole multilayers. Thus, the blue-green zones (~520 nm) should have a thickness of ~178 nm ($m=1$) using constructive light interferences equation (equation 9). Magenta is a mix of blue and red, so we consider that we have destructive interferences for green wavelength (~550 nm) for magenta zones. Using equation 10, magenta zones have a theoretical thickness of ~93 nm ($m=1$). For (PAH/DexS H40), the light brown observed on the surface is a set of wavelengths with a low saturation, principally red and green light. Hence, for brownish films, we consider that we have destructive interferences for blue wavelength (~400 nm). Using equation 11, we obtain a theoretical thickness of ~70 nm ($m=0$).

AFM images and height profiles of (PAH/DexS 40) at 10 bilayers presented in Chapter 3 (section 2.1.2) show average thickness of $15.01 \text{ nm} \pm 4.78 \text{ nm}$ for (PAH/DexS H40)₁₀ and of $19.87 \text{ nm} \pm 1.51 \text{ nm}$ for (PAH/DexS L40)₁₀. As the absorbed mass of the film increases linearly with the number of bilayers, 40 bilayers of (PAH/DexS H40) and of (PAH/DexS L40) should result in approximately 60 nm and 80 nm respectively, which is close to the theoretical values calculated with equation 9 and equation 10. Only the theoretical thickness of the magenta zones of (PAH/DexS L40) are largely above the value calculated. In addition to a different thickness, we may have a localized change in the internal structure of the film that can result in a different refractive index n . Since the n chosen is a refractive index valid for rigid dry films entirely made of the polymer, the equation may not be accurate for all films or all zones (Nolte et al., 2004; Wang et al., 2018).

The surface morphologies of 40-bilayers films are quite different from the 10 bilayers, as seen in Chapter 3 (section 2.1.3). At 10 bilayers, these films result to a “fibrillar-like”

morphology with high coverage for (PAH/DexS H40) and a “puddle-like” morphology with low coverage for (PAH/DexS L40). However, by increasing the number of bilayers up to 40 bilayers, we obtain a higher surface coverage with DexS L40 than with DexS H40. This may be the result of the nucleation of clusters with number of bilayers: the “puddles” observed for DexS L40 tend to decrease in size while the clusters increase in size until they are no more puddles onto the surface. In the case of DexS H40, the morphology obtained for 40 bilayers may also be the consequence of the growth of “fibrils” observed at 10 bilayers. The distinctions observed between the films at 10 bilayers and 40 bilayers are not surprising, as the number of layers/bilayers is one of the key factor to control the surface morphology and properties (Buron et al., 2009; Gholami et al., 2020).

1.2.2. Wetting properties

To characterize wetting properties of multilayer, we measure the contact angle on both surfaces. The measurements were done after 80 seconds, and the contact angle of both multilayers was stable onto the surface. Contact angle obtained after 80 seconds are reported on Figure 4.4.

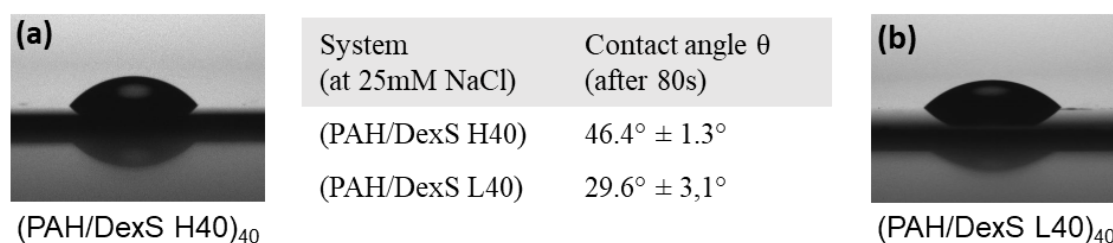


Figure 4.4. Contact angle images and corresponding values obtained for 40 bilayers of (a) (PAH/DexS H40) and (b) (PAH/DexS L40) built by spin-assisted dipping method onto silicon wafer at 25mM NaCl.

As it is reported in Figure 4.4, the contact angle of (PAH/DexS L40) ($29.6^\circ \pm 3.1^\circ$) is generally lower than the contact angle obtained for (PAH/DexS H40) ($46.4^\circ \pm 1.3^\circ$). The contact angle of both films remains in the range of hydrophilic surfaces ($0^\circ < \theta < 90^\circ$) with $\sim 46.4^\circ$ for DexS H40 and $\sim 29.6^\circ$ for DexS L40, which is not surprising as both polyelectrolytes used are hydrophilic polysaccharides (Almodóvar et al., 2011). The roughness achieved by varying the charge density is not high enough to result in hydrophobic surfaces ($90^\circ < \theta < 150^\circ$) or superhydrophobic surfaces ($\theta > 150^\circ$). The lower contact angle of

DexS L40 compared to DexS H40 can be explained by the different morphologies and the decrease in roughness observed from AFM images. An increase in roughness of the surface results in an increase of interfacial tension at the water/film interface and thus, droplets with a lower contact area onto the surface (Bracke et al., 1988; Kwok & Neumann, 1999; Marmur, 2006). (PAH/DexS L40)₄₀ has a RMS of 1.197 nm ± 0.366 nm that leads to a smaller interfacial tension at the interface than (PAH/DexS H40)₄₀ which has a RMS of 3.273 nm ± 0.588 nm.

To summarize, we observed that α -glucans with higher charge densities tend to lead to film growth of type A and to thicker “hydrated” films. On the contrary, with a lower charge density, α -glucans are more likely to result in film growth of type B. This evolution of the film growth type and internal structure was noted, regardless the charge density of the counter-polyion used. However, it is likely that the value of charge density, necessary to switch between film growth from one type to another, is dependent of the characteristics of the second polyelectrolyte. The charge density affects the surface morphology as well, as a lower charge density results in a thicker and more heterogeneous “dry” film than the use of α -glucans with a higher charge density. Though, at 40 bilayers, films based on dextrans sulfate with lower charge density appear to be smoother and to have a lower roughness in general. The smoother morphology and lower roughness also result in a variation of surface hydrophilicity: α -glucans with lower charge density leads to lower water contact angle.

2. Influence of the ionic strength on the structure of multilayered films

Among the factors controlling the growth of films, the ionic strength is one of the key factors that impact the formation and structure of multilayers as explained in Chapter 1 (section 2.3) (Dubas & Schlenoff, 2001; Steitz et al., 2001; v. Klitzing, 2006). Information on all systems of polyelectrolytes studied in this section and on the salt concentrations (NaCl) used are given in Table 4.3.

Table 4.3. Systems based on different polyelectrolyte couples, charge density and ionic strength (as NaCl concentration) of polycation (PC) and polyanion (PA) used for each system.

System	Charge density PC	NaCl concentration PC	Charge density PA	NaCl concentration PA
(PAH/DexS H40)	1 charge / monomer	0mM NaCl	1.75 charge / monomer	0mM NaCl
		5mM NaCl		5mM NaCl
		25mM NaCl		25mM NaCl
(PAH/DexS L40)	1 charge / monomer	0mM NaCl	0.6 charge / monomer	0mM NaCl
		5mM NaCl		5mM NaCl
		25mM NaCl		25mM NaCl

As previously explained, the experimental conditions were chosen according to literature and to conditions fixed in previous parts of the thesis's work. In this part, (PAH/DexS H40) and (PAH/DexS L40) systems were used in the same conditions as in chapter 3, i.e. 0.1 g.L⁻¹ for all polycations and 0.5 g.L⁻¹ for all polyanions, but the salt concentration is varied here : 0 mM NaCl, 5 mM NaCl and 25 mM NaCl.

2.1. Impact of the ionic strength on film growth and viscoelastic behavior

2.1.1. Dextrans with high charge density

First, we study the impact of ionic strength on high sulfate content DexS, i.e. DexS with the higher charge density. Figure 4.5a reports the evolution of $\Delta f_5/5$ signal of the film growth for the couple (PAH/DexS H40) at different ionic strengths, given by the salt concentration in polymer solutions (0mM, 5mM and 25mM NaCl). On Figure 4.5b are reported the ΔD values as a function of Δf values from which the $-\Delta D_5/\Delta f_5$ slope, i.e. the relative softness, is a qualitative evaluation of the viscoelastic behavior of the film.

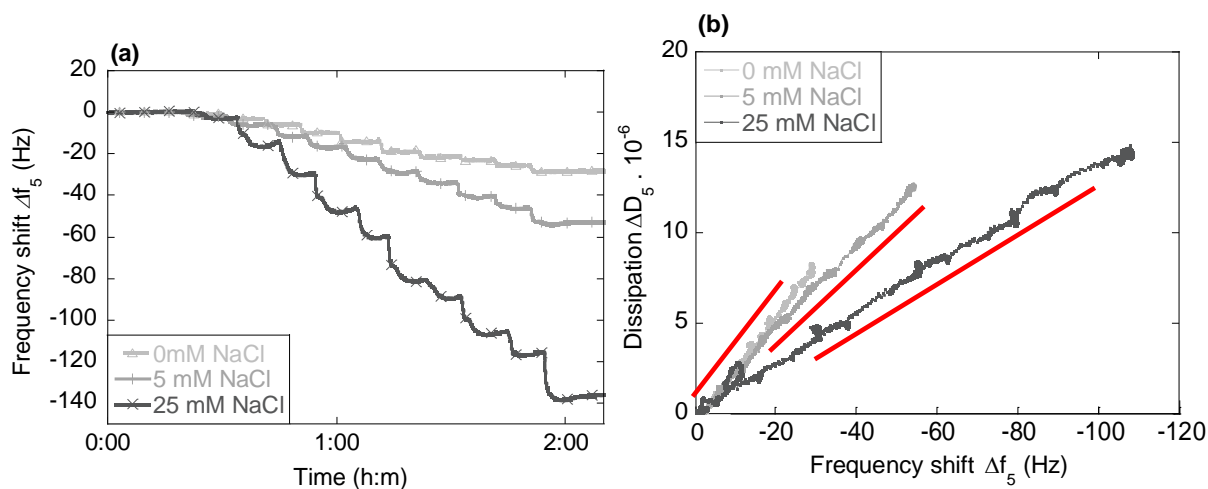


Figure 4.5. (a) Graph of $\Delta f_5/5$ vs time for 5 bilayers of (PAH/DexS H40) films for 0 mM NaCl (light grey), for 5 mM NaCl (grey) and for 25mM NaCl (dark grey) built on gold coated surface. (b) ΔD_5 as a function of Δf_5 of the construction of (PAH/DexS H40)₅ films for 0 mM NaCl (light grey), for 5 mM NaCl (grey) and for 25mM NaCl (dark grey). Relative softness *i.e.* slopes in red.

The summarized information is provided in Table C4.

It can be seen from Figure 4.5a that an increase of ionic strength, *i.e.* an increase of NaCl concentration, leads to an overall decrease in the frequency shift $\Delta f_5/5$. 5 bilayers of (PAH/DexS H40) at 0mM NaCl leads to a final frequency shift $\Delta f_5/5$ of -28 Hz, 5 bilayers of (PAH/DexS H40) at 5mM NaCl leads to a final frequency shift $\Delta f_5/5$ of -53 Hz and 5 bilayers of (PAH/DexS H40) at 25mM NaCl leads to a final frequency shift $\Delta f_5/5$ of -136 Hz. Thus, the increase of ionic strength for DexS with high charge density leads to an increase of mass absorbed. The addition of NaCl also have an impact on the film softness as we can observe from Figure 4.5b. The $-\Delta D_5/\Delta f_5$ slopes or relative softnesses obtained for (PAH/DexS H40) are $0.27 \times 10^{-6} \text{ Hz}^{-1}$, $0.21 \times 10^{-6} \text{ Hz}^{-1}$ and $0.13 \times 10^{-6} \text{ Hz}^{-1}$ at 0mM NaCl, 5mM NaCl and 25mM NaCl for the entire film formation. The relative softness $-\Delta D_5/\Delta f_5$ decreases with the decrease of NaCl concentration. However, at all NaCl concentrations, the dissipation increases linearly as a function of the frequency for DexS H40 based multilayer, meaning that the salt and the ionic strength do not affect the type of film growth despite impacting the hydrated mass adsorbed.

This behavior is often observed in literature, as ionic strength of polyelectrolyte solutions influences the conformation of polyelectrolytes in solution (Chapter 1, section 2.3) (Dubas & Schlenoff, 2001; v. Klitzing, 2006). In the absence of salt, polyelectrolytes adopt an extended conformation in solution due to the repulsion between the charges along the polymer

chain. The increase of ionic strength, *i.e.* addition of counterions, leads to the screening of these electrostatic interactions and a random coil conformation of polyelectrolytes (Feldötö et al., 2010). This conformation results in most cases in an increase of mass adsorption like we observed in PAH/DexS H40 case. The introduction of counterions inside the film structure results in thicker films, thus softer films (Schoeler et al., 2002). With screening of charges, the polymer is in “coil” conformation and more hydrated polymer packets can be adsorbed. Moreover, with addition of salt, a part of the surface charge is compensated by Na^+ and Cl^- ions present in polymer solution that remain inside the film structure. Due to the hydration shell of each ion, a more important quantity of water is trapped in the films at 25mM NaCl than in films at 0 mM NaCl and at 5mM NaCl at the end (Farhat et al., 1999). However, at equal thickness, films at 25mM NaCl are more rigid and less hydrated.

2.1.2. Dextrans with low charge density

Then, low sulfate content DexS, *i.e.* DexS with the lower charge density was also studied. The result obtained by QCM-D for the couple (PAH/DexS L40) at different ionic strengths, given by the salt concentration in polymer solutions (0, 5 and 25mM NaCl), are reported on Figure 4.6a and on Figure 4.6b.

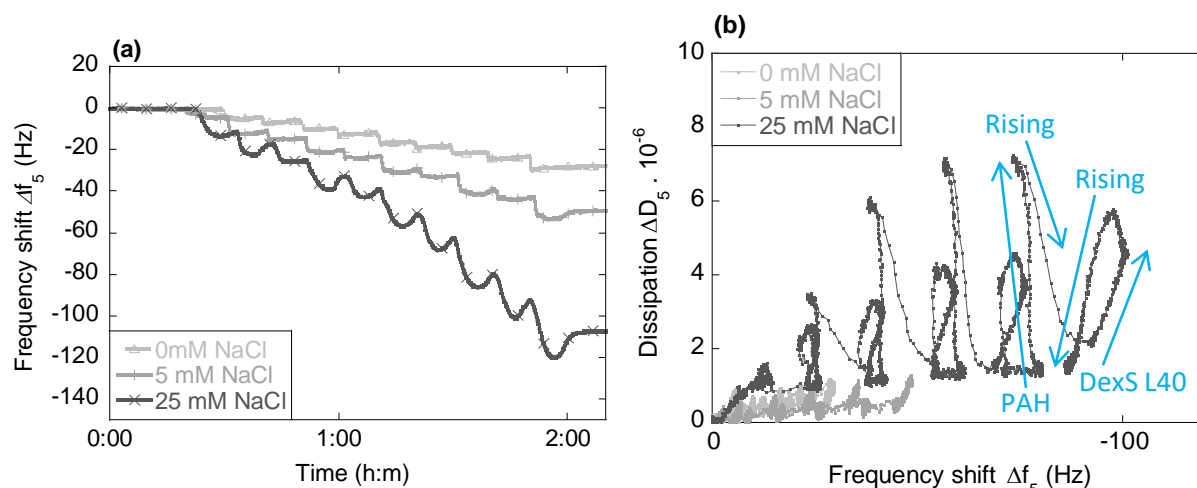


Figure 4.6. (a) Graph of $\Delta f_s/5$ vs time for 5 bilayers of (PAH/DexS L40) films for 0 mM NaCl (light grey), for 5 mM NaCl (grey) and for 25mM NaCl (dark grey) built on gold coated surface. (b) ΔD_s as a function of $\Delta f_s/5$ of the construction of (PAH/DexS L40)₅ films for 0 mM NaCl (light grey), for 5 mM NaCl (grey) and for 25mM NaCl (dark grey).

As for DexS H40, we observe on Figure 4.6a that increasing the NaCl concentration in polymers solution leads to a decrease of the final frequency shift $\Delta f_s/5$ of films formed with

PAH and DexS L40. The use of 25mM NaCl results in a final frequency shift of -107 Hz after 5 bilayers of (PAH/DexS L40) which is the film with the most important mass absorbed. 5mM NaCl leads to -49 Hz and 0mM NaCl leads to -27 Hz for (PAH/DexS L40)₅. A modification of behavior between (PAH/DexS L40) at 25mM NaCl and (PAH/DexS L40) at 5mM NaCl and 0mM NaCl is noted on Figure 4.6b. The variations of the course of the dissipation for films at 25mM are very important compared to the one observed for 5mM NaCl and 0mM NaCl. The variation of dissipation appears as a loop going from 7×10^{-6} to 1.2×10^{-6} during the formation of the last bilayer (bilayer 5) in the case of 25mM NaCl while value of ΔD_5 around $0.5 \times 10^{-6} - 1 \times 10^{-6}$ for lower NaCl concentration. Thus, we have more polyelectrolytes adsorbed, with higher hydration and lower rigidity, due to the addition of salt in the polymer solution for DexS with lower charge density.

As for the PAH/DexS H40, the addition of salt results in a polymer conformation change in solution (“stretch” to “coiled”) and more adsorbed mass onto the surface. Moreover, as DexS L40 has less charges (0.6 charge / monomer) than DexS H40 (1.75 charge / 1 monomer), less counterions are necessary to screen their charges. Thus, the effect of the charge screening by introduction of counterions is more important on the DexS L40. However, our results indicate the opposite. We have a ratio of 4.86 between final frequency shift $\Delta f_5/5$ of (PAH/DexS H40) at 25mM and (PAH/DexS H40) at 0mM and we have a ratio of 3.96 between final frequency shift $\Delta f_5/5$ of (PAH/DexS L40) at 25mM and (PAH/DexS L40) at 0mM. What can be seen is that the introduction of counterions have a higher impact on the adsorption and/or swelling of DexS L40 films than on the adsorption and/or swelling of DexS H40 films. We suppose that the phenomenon is due to the counterions and their hydration shell trapped within the film. At 25mM NaCl, the strong presence of counterions within the structure leads to a more hydrated film, and their removal during the restructuring step of the mechanism is then more visible. At low salt concentration, this restructuring step is less visible than with 25mM NaCl, because water and salt ejection is less important during PE-complexes formation.

2.2. Impact of the ionic strength on film characteristics and properties

As for section 2.1, we screen the characteristics and properties of the films. In this part, the structure and surface properties of DexS 40 bilayers deposited on silicon wafer are

analyzed as a function of the ionic strength (0 mM NaCl, 5 mM NaCl and 25 mM NaCl). Concentrations of polymer solutions used were at 0.1 g.L⁻¹ for all polycations and 0.5 g.L⁻¹ for all polyanions.

2.2.1. Morphology and structural colors

AFM was used for the analysis of the surface morphology and its RMS, and we used camera to report the structural colors. The 2D and 3D AFM images and the photos of the structural colors of PAH/DexS H40 systems at 0mM NaCl, 5mM NaCl and 25mM NaCl at for 40 bilayers are reported on Figure 4.7.

On Figure 4.7a, we can observe that PAH/DexS H40 systems lead to colorless or very light brown films, with what appear to be homogeneous surfaces, at all ionic strengths: almost colorless at 0mM NaCl and 5mM NaCl to light brown for 25mM NaCl. On 2D and 3D images, we observe a visual increase of material quantity onto the surface with the addition of salt (based on surface coverage observed on AFM). At 0mM NaCl (Figure 4.7a), there are no obvious visual characteristics compared to the other two. At 5mM NaCl, peaks of around 0.2 – 0.5 μm are visible (Figure 4.7b) and at 25mM NaCl, peaks of around 0.5 – 1 μm are visible (Figure 4.7c). The surface roughness RMS (root mean square) of (PAH/DexS H40) is 1.890 nm \pm 0.268 nm for 0mM NaCl, 7.313 nm \pm 0.686 nm for 5mM NaCl and 3.273 nm \pm 0.588 nm for 25mM NaCl. While RMS (AFM) increases between 0mM NaCl and 5mM NaCl, it decreases for 25mM NaCl. On AFM images, the small clusters observed on (PAH/DexS H40)₄₀ films at 5mM NaCl seem to expand in size with further addition of salt in polyelectrolyte solution, that leads to a decrease of RMS at 25mM NaCl. The analysis of structural colors using the equation 11 (chapter 2, section 2.4.2) suggests that light brown (destructive interferences for 400 nm) films like (PAH/DexS H40) at 25mM have a theoretical thickness around 70 nm (m=0). So, the almost colorless surface at 0 and 5mM NaCl concentrations (Figure 4.7a,b) should have a theoretical thickness below 70 nm (m=0).

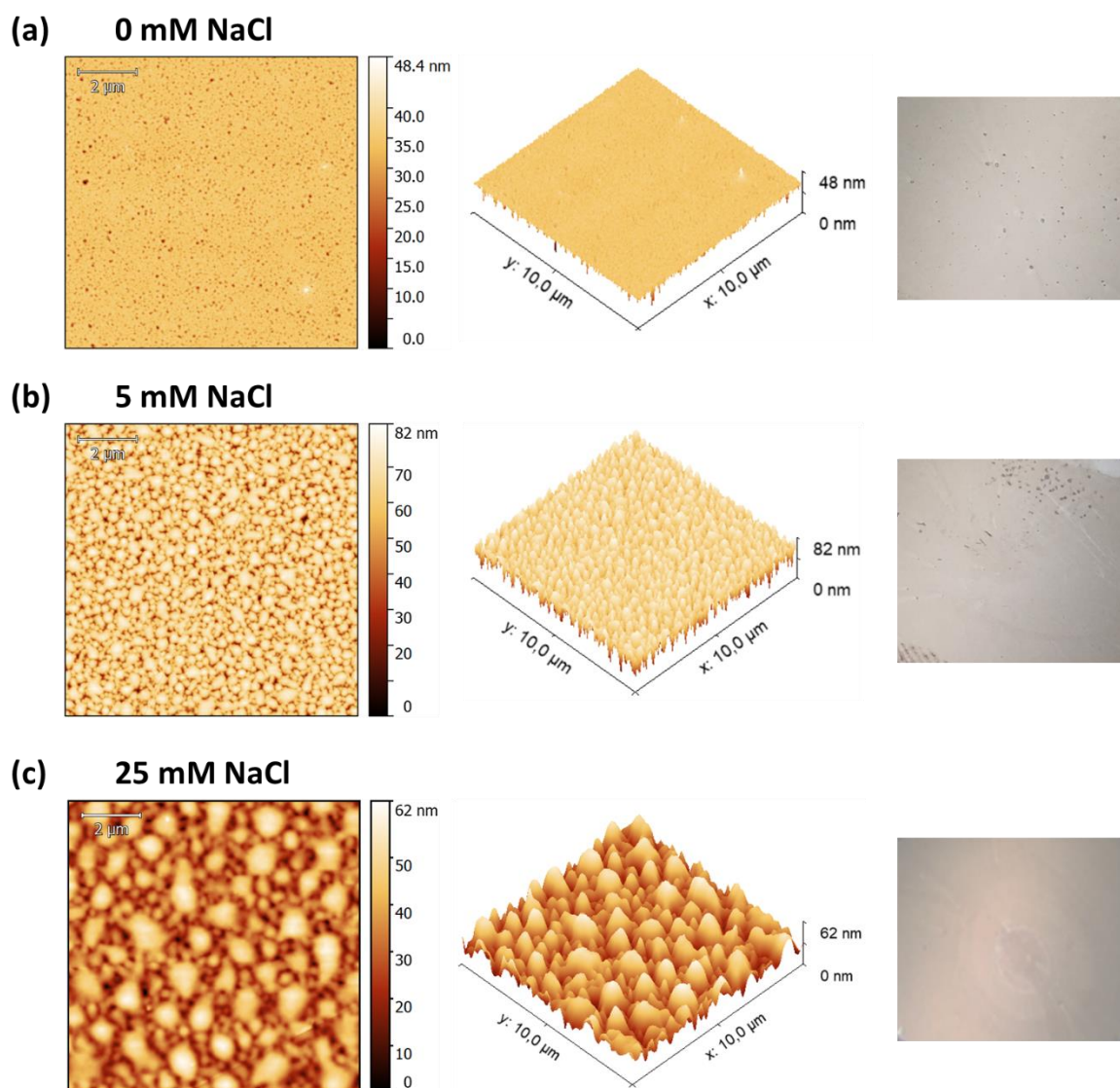


Figure 4.7. AFM 2D and 3D images ($10 \times 10 \mu\text{m}$) and photos of the surface for 40 bilayers of (PAH/DexS H40) films at (a) 0mM NaCl, (b) 5mM NaCl and (c) 25mM NaCl, built by spin-assisted dipping method onto silicon wafer.

Then, we study the impact of NaCl concentration on the surface of DexS L40 films. AFM 2D and 3D images and photos of the (PAH/DexS L40) multilayers at 40 bilayers are reported on Figure 4.8. AFM images acquisition allows to say that the morphologies are uniform independently on the localization on the surface, even for visually heterogeneous films.

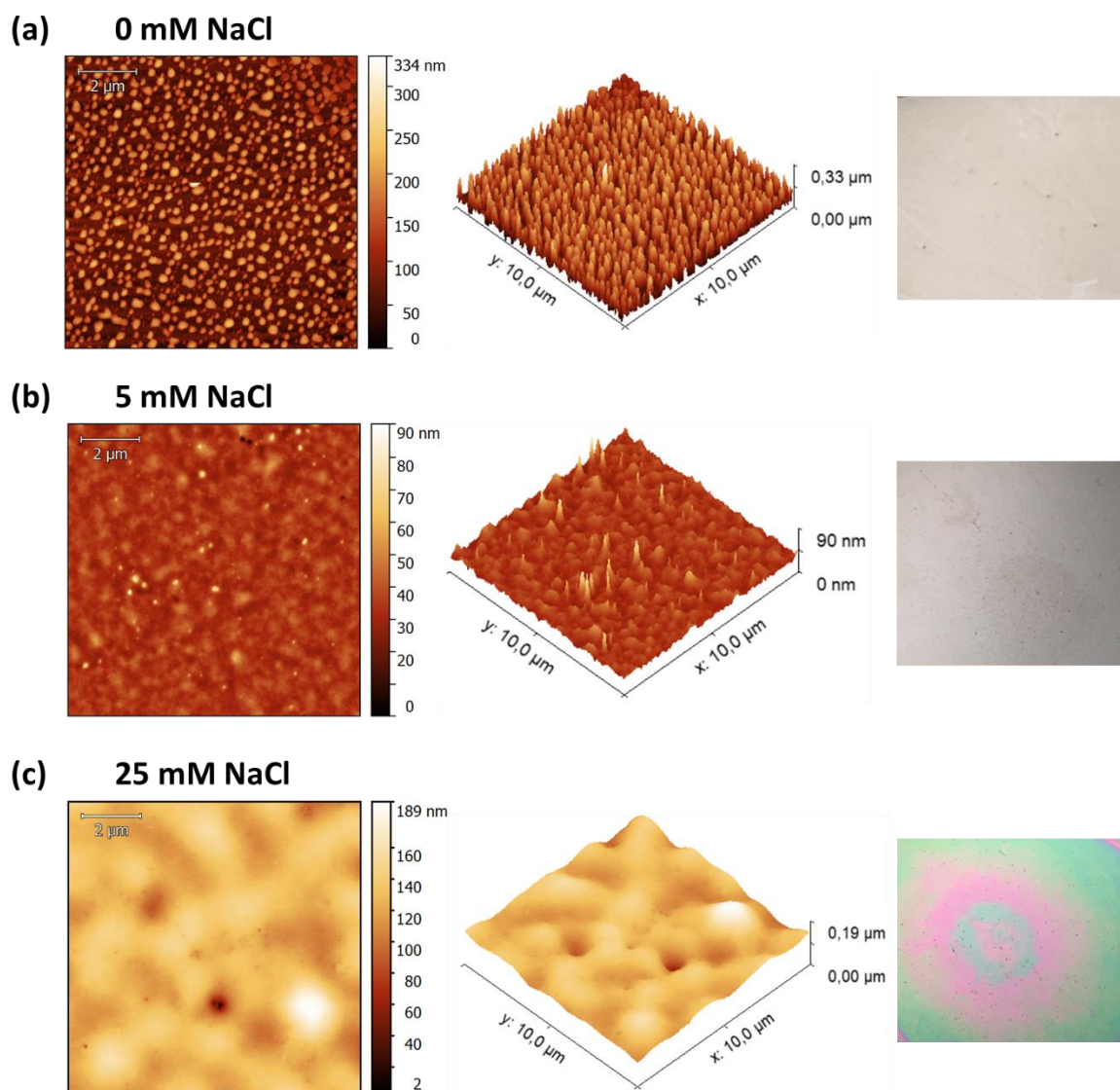


Figure 4.8. AFM 2D and 3D images ($10 \times 10 \mu\text{m}$) and photos of the surface for 40 bilayers of (PAH/DexS L40) films at (a) 0mM NaCl, (b) 5mM NaCl and (c) 25mM NaCl, built by spin-assisted dipping method onto silicon wafer.

The photos reported on Figure 4.8 show that at low NaCl concentration (0mM NaCl, 5mM NaCl), we obtained colorless surfaces while at high NaCl concentration (25mM NaCl), the film is magenta – green. The addition of salt also results in the modification of the surface morphology from beads at 0mM NaCl to smooth film at 25mM NaCl. The size of beads observed onto the surface of (PAH/DexS L40)₄₀ films without salt addition is $328 \text{ nm} \pm 90 \text{ nm}$ with a RMS of $35.871 \text{ nm} \pm 4.626 \text{ nm}$. At 5mM NaCl, we still have localized beads unevenly distributed on the surface, but their number seems to be less important. In general, we have a film with a wavy surface and a lower RMS, which is of $3.293 \text{ nm} \pm 1.418 \text{ nm}$. By increasing to 25mM NaCl, the surface obtained is smoother with a RMS of $1.197 \text{ nm} \pm 0.366$

nm and no apparent beads. The comparison between (PAH/DexS L40)₁₀ and (PAH/DexS L40)₄₀ AFM images (Chapter 3) seems to indicate that the peaks also act like clusters for nucleation with the increase of the number of bilayers. Moreover, the theoretical thickness determined with structural colors are around 70 nm (m=0) for (PAH/DexS L40) at 0 and 5mM NaCl while the magenta – green film indicates theoretical thicknesses of ~93 nm (m=1) for the magenta zones and ~178 nm (m=1) for the green zones. The nucleation seems faster and the cluster size increases faster with the addition of salt, which agrees with a faster growth of the film observed by QCM-D (Figure 4.6a) at 25mM NaCl.

2.2.2. Wetting properties

The wetting properties of multilayers were studied by the analysis of the contact angle. We measure the contact angle on each surface during 80 seconds after the contact between water drop and surfaces (Figure 4.9).

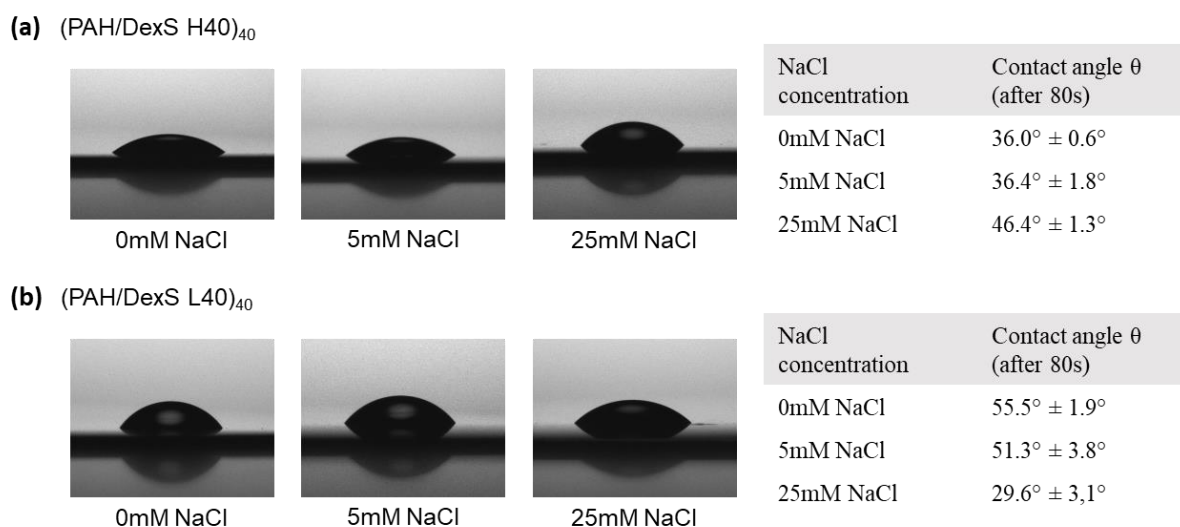


Figure 4.9. Contact angle images and contact angle values obtained for 40 bilayers of (a) (PAH/DexS H40) and (b) (PAH/DexS L40) at 0mM NaCl, 5mM NaCl and 25mM NaCl built by spin-assisted dipping method onto silicon wafer.

On Figure 4.9a, it appears that the contact angle increases with the salt concentration, with a sharp increase between 5mM and 25 mM NaCl. A contact angle of $\sim 36.0^\circ$ is obtained for (PAH/DexS H40)₄₀ at 0mM NaCl and at 5mM NaCl, while the measurement on (PAH/DexS H40)₄₀ films at 25mM NaCl results in a contact angle of $46.4^\circ \pm 1.3^\circ$. Contrary to what was observed in section 1.2.2, the variations of contact angle of those films are not

correlated with an increase of RMS (AFM images), as the high RMS was found out to be at 5mM NaCl. Here, the contact angle seems to increase with the size of peaks observed onto the surface with AFM images. The peaks around 0.2 – 0.5 μm at 5mM NaCl (Figure 4.8b) and around 0.5 – 1 μm at 25mM NaCl (Figure 4.8c) may lead to a decrease of RMS from 5mM NaCl to 25mM NaCl, but an increase of contact angle. On the contrary, the increase of ionic strength on PAH/DexS L40 leads to a decrease of the contact angle value as it is shown on Figure 4.9b. (PAH/DexS L40)₄₀ at 0mM NaCl and at 5mM NaCl, it results in a contact angle of $\sim 55^\circ$ and $\sim 51^\circ$, respectively. Increasing NaCl concentration at 25mM NaCl allows the decrease of the contact angle down to $29.6^\circ \pm 3.1^\circ$. The values of the contact angle have the same variation as the RMS found by AFM. However, the angles at 0mM NaCl and at 5mM NaCl are quite similar compared to the difference of RMS: $35.871 \text{ nm} \pm 4.626 \text{ nm}$ at 0mM NaCl and $3.293 \text{ nm} \pm 1.418 \text{ nm}$ at 5mM NaCl. Thus, in both cases, the increase/decrease of the contact angle and so the hydrophilicity of the surface is more likely linked to the type of morphology than to the RMS/surface roughness.

To resume, the impact of ionic strength on the formation of α -glucans -based multilayers is highly dependent on the charge density of the polyelectrolyte. For polyanions with a higher charge density, an increase of ionic strength leads to an increase of thickness and of relative softness but results in softer “hydrated” film at the end. Increasing ionic strength for low charge density will also result in thicker “dry” films and a surface morphology with large patterns (peaks). This change of morphology type induces a decrease of the surface hydrophilicity. In the case of α -glucans with a lower charge density, we have a thicker “hydrated” film as the ionic strength increases, with more important variations of dissipation during the construction. The “dry” film appears to be thicker as well. The main difference is the increase in surface heterogeneity at higher salt concentration and the modification of the morphology: the film becomes flatter with the increase of the ionic strength. This observation is correlated with an increase of the wettability of the surface.

3. Impact of the molar masses of polyelectrolytes on the structure of multilayered films

The study of the effect of polyanion's molar mass was carried out with PAH and DexS with high sulfate content at three different molar masses: DexS H5 (5 000 g.mol⁻¹), DexS H40 (40 000 g.mol⁻¹) and DexS H500 (500 000 g.mol⁻¹).

All systems of polyelectrolytes studied in this section and information on their molecular weight are given in Table 4.4.

Table 4.4. Systems based on different polyelectrolyte couples. Molar masses of all polycations (PC) and polyanions (PA) used for each system.

System	Molecular weight PC	Molecular weight PA
(PAH/DexS H5)	150 000 g.mol ⁻¹	5 000 g.mol ⁻¹
(PAH/DexS H40)	150 000 g.mol ⁻¹	40 000 g.mol ⁻¹
(PAH/DexS H500)	150 000 g.mol ⁻¹	500 000 g.mol ⁻¹

Other experimental conditions used to build the LbL assembly were chosen according to literature, method development and information collected during this thesis. The polymer solutions in this part were prepared in 25mM NaCl at 0.1 g.L⁻¹ for the polycation and 0.5 g.L⁻¹ for the polyanion. For QCM-D measurements, the films were assembled up to 5 bilayers on gold-coated quartz crystals while we worked with 40 bilayers on silicon wafer for the analysis of the structure and surface properties.

3.1. Impact of molar mass of polyelectrolytes on film growth and viscoelastic behavior

To study the impact of molecular weight of polyelectrolytes on the growth of films and their properties, we first followed the build-up of 5 bilayer films by QCM-D based on DexS with three different molar masses at 25mM NaCl. Figure 4.10a shows the results of the film growth from PAH and DexS with high charge density at different molecular weight (5 000 g.mol⁻¹, 40 000 g.mol⁻¹ and 500 000 g.mol⁻¹). Figure 4.10b reports the ΔD values as a function of Δf values that give a qualitative information on the viscoelastic properties of the film, and in particular, the relative rigidity defined as $-\Delta D_5/\Delta f_5$.

The summarized information is provided in Table C4.

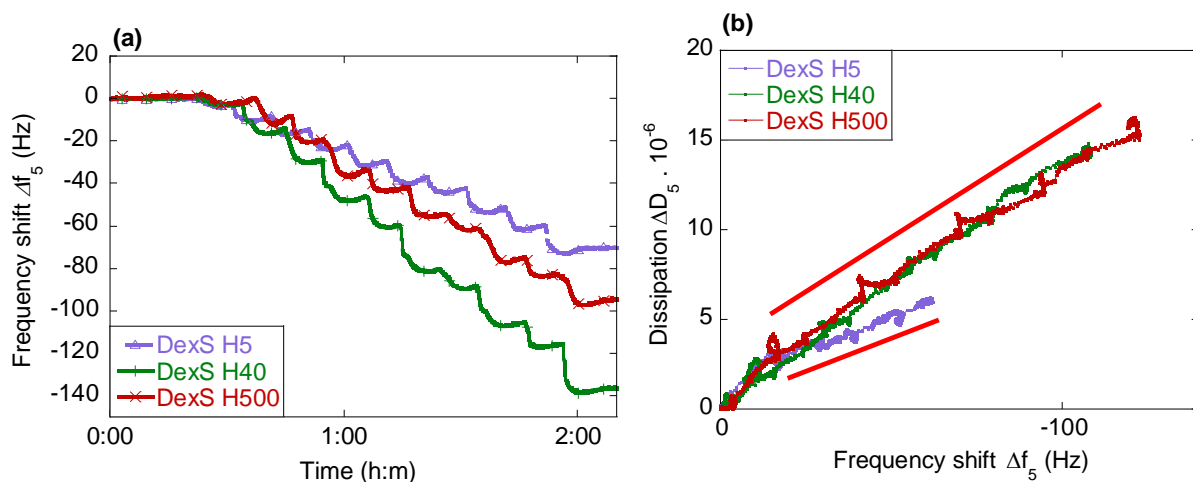


Figure 4.10. (a) Graph of $\Delta f_5/5$ vs time for 5 bilayers of (PAH/DexS H5) films (dark purple), (PAH/DexS H40) films (dark green) and (PAH/DexS H500) films (red) built on gold coated surface. (b) ΔD_5 as a function of $\Delta f_5/5$ of the construction of (PAH/DexS H5)₅ films (dark purple), (PAH/DexS H40)₅ films (dark green) and (PAH/DexS H500)₅ films (red). Relative rigidity *i.e.* slopes in red.

The frequency shifts $\Delta f_5/5$ evolution on Figure 4.10a show an increase between final frequency of (PAH/DexS H5) at -70 Hz and (PAH/DexS H40) at -136 Hz after the build-up of 5 bilayers. However, a decrease of final frequency can be seen between (PAH/DexS H40) and (PAH/DexS H500) with respectively -136 Hz and -95 Hz. By observing variations of ΔD_5 as a function of $\Delta f_5/5$ on Figure 4.10b, we can see that the dissipation of films based on PAH/DexS H40 and DexS H500 increases linearly and has approximately the same slope/relative softness with respectively 0.13×10^{-6} and 0.12×10^{-6} . Moreover, if the dissipation also presents a linear increase during the film formation of (PAH/DexS H5)₅, the slope/relative softness of the film is lower with a value of 0.07×10^{-6} . Only the use of DexS H5 results in a more rigid film in addition to a thinner film.

Most of the time, an increase of molecular weights allows thicker films to be obtained, *i.e.* more adsorbed mass during the layer formation (Cramer et al., 2017; Zan et al., 2012). But this is not always true (Lyu & Peterson, 2017; Towle et al., 2020). Our results show that we have a maximum in mass adsorbed at 5 bilayers for DexS 40 and not for DexS H500. The decrease in adsorbed mass observed between the film from DexS H40 and the film from DexS H500 can also be explained by the thermodynamic stripping phenomenon, *i.e.* pull-off of the previous adsorbed layer instead of adsorption by a polyelectrolyte, that can occur during the LbL assembly of polyelectrolytes (Alkekhia & Shukla, 2019; Sui et al., 2003). There is a

possibility that at 500 000 g.mol⁻¹, the important difference between the molecular weight of the DexS (500 000 g.mol⁻¹) and PAH (150 000 g.mol⁻¹) enhances the phenomenon (Sui et al., 2003; Towle et al., 2020). The high molar mass of DexS H500 can also affect the charge distribution into the multilayer and lead to the same phenomenon.

3.2. Impact of molar masses on film characteristics and properties

In addition to the impact of molecular weight on the multilayer growth and its viscoelastic properties during formation at 5 bilayers, we analyzed the structure and surfaces properties at 40 bilayers.

To screen the surface properties, we built 40 bilayers on silicon wafer using the spin-assisted deposition method. Concentrations of polymer solutions used were at 0.1 g.L⁻¹ for all polycations and 0.5 g.L⁻¹ for all polyanions. The salt concentration was fixed at 25mM NaCl for all systems.

3.2.1. Surface morphology and structural colors

We analyzed the surface morphology by AFM images of the dry (PAH/DexS H5), (PAH/DexS H40) and (PAH/DexS H500) films at 25mM NaCl. The structural colors were pictured by camera. On Figure 4.11, both the 2D AFM images and the photos of the surface of the (PAH/DexS H) multilayers are reported.

Figure 4.11 reports three different morphologies depending on the molar mass of DexS, and different structural colors. The (PAH/DexS H5)₄₀ film, *i.e.* the film based on the dextran with the lower molecular weight, results in a film with craters (Figure 4.11a) and colorless surface. (PAH/DexS H40)₄₀ multilayer results in clusters/large peaks we observed (Figure 4.11b) with a very light brown color. DexS H500 leads to a flatter film with a high surface coverage (Figure 4.11c) and a surface where the color observed is clearly visible: a magenta-orange color. The morphology of (PAH/DexS H5)₄₀ is quite particular compared to what we observe for AFM images of films in previous parts. The film showed craters/globules with an external diameter of 0.8 – 1.5 μm and an internal diameter of 0.2 - 1 μm, which results in a RMS of 1.587 nm ± 0.256 nm for the multilayer. Those craters look like the peaks

observed on (PAH/DexS H40), with a larger diameter and a collapse in the center of them. In comparison, the RMS of 40 bilayers of (PAH/DexS H40) is $3.273 \text{ nm} \pm 0.588 \text{ nm}$ and the one of (PAH/DexS H500) is $2.184 \text{ nm} \pm 0.446 \text{ nm}$.

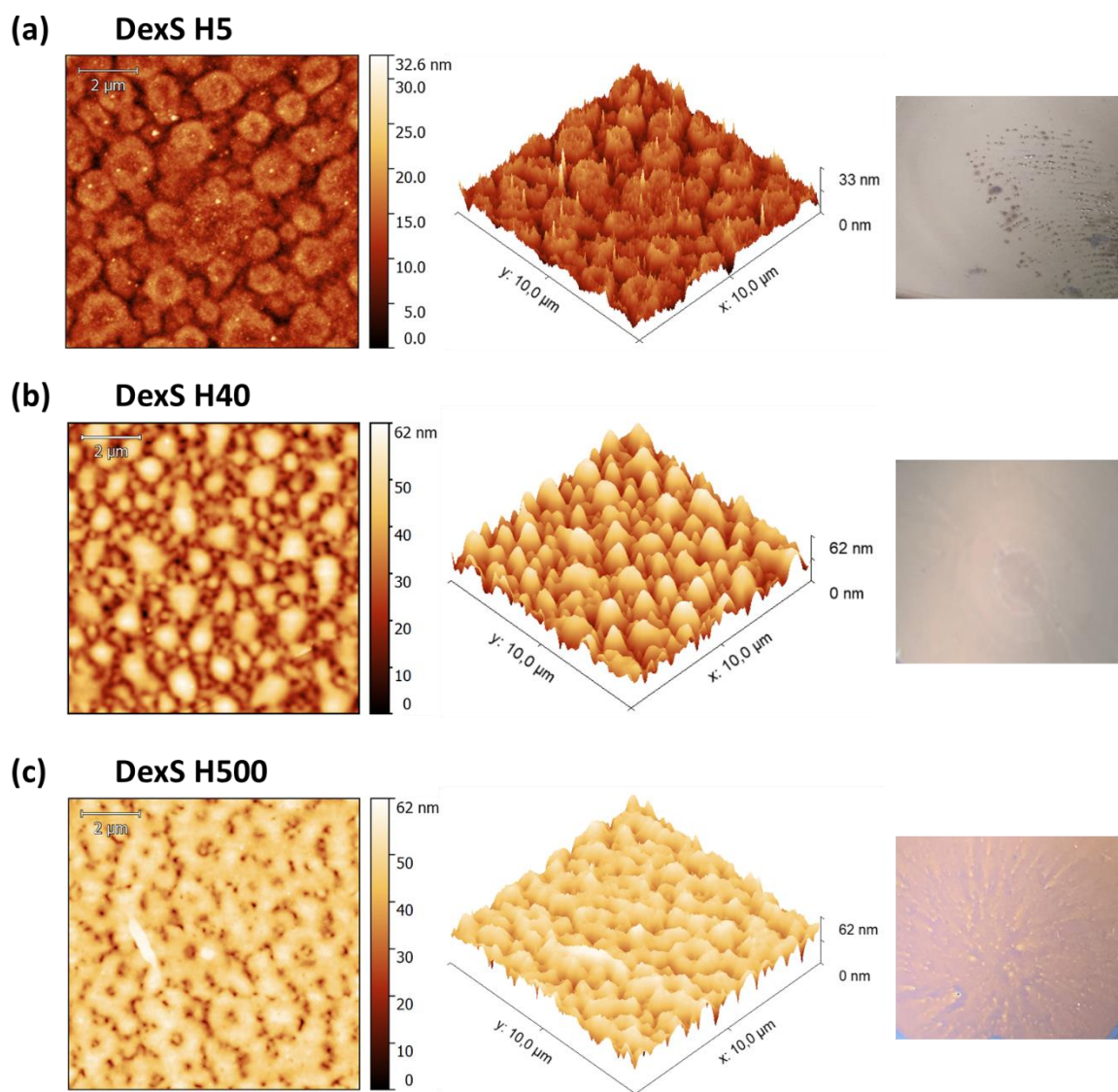


Figure 4.11. AFM 2D and 3D images ($10 \times 10 \mu\text{m}$) for 40 bilayers of (PAH/DexS H) films for DexS H with a molecular weight of (a) $5\,000 \text{ g}\cdot\text{mol}^{-1}$, (b) $40\,000 \text{ g}\cdot\text{mol}^{-1}$ and (c) $500\,000 \text{ g}\cdot\text{mol}^{-1}$, built by spin-assisted dipping method onto silicon wafer at 25 mM NaCl .

As presented in the previous section, the $(\text{PAH/DexS H5})_{40}$ film with a colorless surface have a theoretical thickness below 70 nm according to equation 9 and equation 10. For the $(\text{PAH/DexS H40})_{40}$ multilayer, its theoretical thickness is around 70 nm according to its light brown color. In the case of the $(\text{PAH/DexS H500})_{40}$ film, the surface obtained consists in a mix of magenta and orange. Thus, we chose to calculate the theoretical thickness using equation 10 on destructive interferences and the complementary colors of those two colors:

cyan (~500 nm). The theoretical thickness of (PAH/DexS H500)₄₀ film was estimated at ~85 nm (m=1). Hence, a minimal molecular mass is necessary to obtain structural colors in the same experimental conditions. We can note that we obtain a thicker and more colorful dry film using DexS H500 despite the higher amount of hydrated mass absorbed with DexS H40 on QCM-D (section 3.1). The relative rigidity of the two films is also similar, indicating a comparable hydration in hydrated state at 10 bilayers. The opposite results in dry state may be due to the number of bilayers (40 bilayers) or to the experimental set-up, the drying step in particular, that affects the structure and final colors of the film.

3.2.2. Wetting properties

An evaluation of the surface hydrophobicity and the wettability of films were carried out by measuring water contact angles. The measurement of the contact angle was done 80 seconds after the drop deposition, as each angle was stable after this time. On Figure 4.12., are reported the contact angle values for (PAH/DexS H5)₄₀, (PAH/DexS H40)₄₀ and (PAH/DexS H500)₄₀ multilayers.

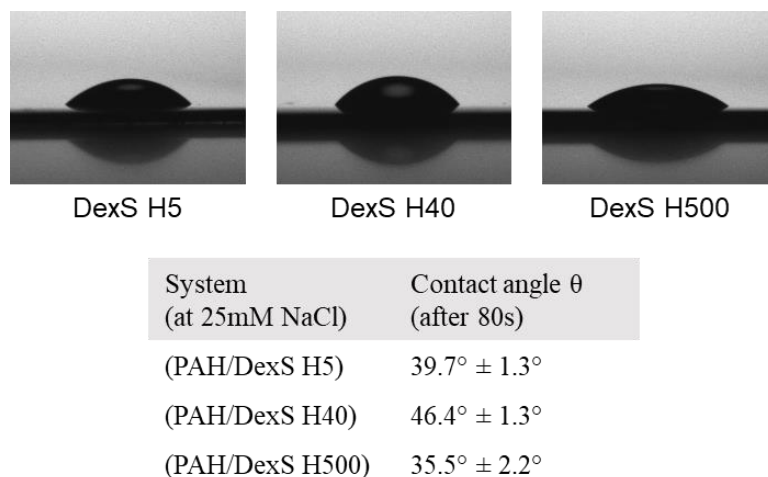


Figure 4.12. Contact angle images and contact angle values obtained for 40 bilayers of (PAH/DexS H5), (PAH/DexS H40) and (PAH/DexS H500) built by spin-assisted dipping method onto silicon wafer at 25mM NaCl.

We can see in Figure 4.12 that firstly, there is an increase of the water contact angle with the increase of molar mass between 5 000 and 40 000 g.mol⁻¹, from a value of $39.7^\circ \pm 1.3^\circ$ for the contact angle of (PAH/DexS H5)₄₀ film and of $46.4^\circ \pm 1.3^\circ$ for (PAH/DexS L40)₄₀. Then, the transition from a molar mass of 40 000 to 500 000 g.mol⁻¹ results in a

decrease of the contact angle with an angle of $35.5^\circ \pm 2.2^\circ$ for (PAH/DexS H500)₄₀ multilayers. The variations of contact angle with the molecular weight of polyelectrolyte are correlated with the variations observed of RMS obtained by AFM analysis. A higher roughness results in a higher water contact angle, and so in a lower hydrophilicity, which is similar to what we observed with morphology and wettability of (PAH/DexS H40) and (PAH/DexS L40). Here, the decrease in surface hydrophilicity is clearly linked to the increase of roughness. Moreover, it is likely that the choice of a certain molecular weight or a range of molecular weights is necessary to reach the highest surface roughness.

The use of a polyelectrolyte with a high molar mass leads in general to thicker hydrated films than films based on polymers with lower molar mass above a certain value of molecular weight. Polyions with higher molecular weights may also lead to softer film (higher relative softness) above a certain value of molecular weight. In terms of morphology, an increase of molar mass seems to result in a better surface coverage and at a higher molar mass, a flatter film is obtained. The variations of the roughness measured are similar to the variations of the contact angle. Going from the lower to the intermediate molecular weight, an increase of RMS results in a lower hydrophilicity. Going to the intermediate to the high molar mass a decrease of RMS and a higher wettability can be observed.

Conclusion

The charge density influences the film growth and its viscoelastic characteristics by affecting the charge overcompensation between a layer and its sub-layer. If the charge density of one of the polyelectrolytes is too low, the charge inversion does not occur onto the surface and there is no film formation. If the charge density is high enough, there is a charge overcompensation then a charge inversion that allows the film construction. However, there is a range of density where a partial complexation between polyelectrolytes leads to a partial neutralization of the surface. In this case, film formation is possible but not in the classic linear way. The mechanism includes an internal restructuring of the films after each adsorption and rinsing steps. The adjustment of charge density of one of the two polyelectrolytes used to build multilayers is then a way to control the growth type of the film and so their internal structure. Moreover, due to their different growth mechanisms, they also have varying structural and surface properties. For 40 bilayers, a lower charge density is the route to obtain thicker films with unmissable structural colors.

The effect of the ionic strength on the growth of multilayers is important, for both polyelectrolyte with low charge density and polyelectrolyte with high charge density. If a change in ionic strength does not seem to affect the type of film growth identified for the polyelectrolyte pair, it does have an impact of film thickness as well as on their relative rigidity. At both charge densities, the introduction of counterions in the polymer solution causes the polyelectrolyte to assume a “coiled” conformation and a thicker multilayer is formed as expected. This conformation of the polyions used also appears to affect the internal structure of the film, especially by increasing the rigidity of the multilayer. However, ionic strength does not have the same impact on the morphology of the film and on their interaction according to the charge density of the polyelectrolyte. At a lower charge density, the increase of salt concentration is a way to obtain smoother films with a better wettability. On the contrary, increasing ionic strength for polyelectrolyte with a higher charge density results in changes in morphology and a lower wettability.

The increase of the molar mass of functionalized α -glucans allows to obtain thicker hydrated films, but only above a certain value of molar mass. The effect differs depending on the thickness of “hydrated” film or “dry” film, so the thicker dry film is based on the polyelectrolyte with the higher molecular weight. Concerning the surface morphology, the film appears to be smoother with the dextran with higher molar mass, but roughness is the

highest for the intermediate molar mass, so is the contact angle. In fact, the intermediate molecular weight of dextrans sulfate results in films with the highest roughness and the lowest hydrophilicity. The difference in “hydrated” and “dry” state is surprising and can be due to multiple factors. A “stripping” phenomenon *i.e.* a partial removal of the last layer instead of adsorption can happen during the construction. The spin-assisted deposition method used as well as the number of bilayers can also affect the film formation.

References

- Alkekha, D., & Shukla, A. (2019). Influence of poly- L -lysine molecular weight on antibacterial efficacy in polymer multilayer films. *Journal of Biomedical Materials Research Part A*, 107(6), 1324–1339. <https://doi.org/10.1002/jbm.a.36645>
- Almodóvar, J., Place, L. W., Gogolski, J., Erickson, K., & Kipper, M. J. (2011). Layer-by-Layer Assembly of Polysaccharide-Based Polyelectrolyte Multilayers: A Spectroscopic Study of Hydrophilicity, Composition, and Ion Pairing. *Biomacromolecules*, 12(7), 2755–2765. <https://doi.org/10.1021/bm200519y>
- Bracke, M., Bisschop, F., & Joos, P. (1988). Contact angle hysteresis due to surface roughness. In V. Degiorgio (Ed.), *Trends in Colloid and Interface Science II* (Vol. 76, pp. 251–259). Steinkopff. <https://doi.org/10.1007/BFb0114202>
- Buron, C. C., Filiâtre, C., Membrey, F., Bainier, C., Buisson, L., Charraut, D., & Foissy, A. (2009). Surface morphology and thickness of a multilayer film composed of strong and weak polyelectrolytes: Effect of the number of adsorbed layers, concentration and type of salts. *Thin Solid Films*, 517(8), 2611–2617. <https://doi.org/10.1016/j.tsf.2008.10.036>
- Cramer, A. D., Dong, W.-F., Benbow, N. L., Webber, J. L., Krasowska, M., Beattie, D. A., & Ferri, J. K. (2017). The influence of polyanion molecular weight on polyelectrolyte multilayers at surfaces: elasticity and susceptibility to saloplasticity of strongly dissociated synthetic polymers at fluid–fluid interfaces. *Physical Chemistry Chemical Physics*, 19(35), 23781–23789. <https://doi.org/10.1039/C7CP02614E>
- Devi, M. G., Dutta, S., Al Hinai, A. T., & Feroz, S. (2014). Surface Morphology Study of Chitosan-Dextran Sulphate Multilayer Thin Films. *Journal of Chitin and Chitosan Science*, 2(4), 245–258. <https://doi.org/10.1166/jcc.2014.1069>
- Dubas, S. T., & Schlenoff, J. B. (1999). Factors Controlling the Growth of Polyelectrolyte Multilayers. *Macromolecules*, 32(24), 8153–8160. <https://doi.org/10.1021/ma981927a>
- Dubas, S. T., & Schlenoff, J. B. (2001). Swelling and Smoothing of Polyelectrolyte Multilayers by Salt. *Langmuir*, 17(25), 7725–7727. <https://doi.org/10.1021/la0112099>
- Farhat, T., Yassin, G., Dubas, S. T., & Schlenoff, J. B. (1999). Water and Ion Pairing in Polyelectrolyte Multilayers. *Langmuir*, 15(20), 6621–6623. <https://doi.org/10.1021/la990631a>
- Feldötö, Z., Varga, I., & Blomberg, E. (2010). Influence of Salt and Rinsing Protocol on the Structure of PAH/PSS Polyelectrolyte Multilayers. *Langmuir*, 26(22), 17048–17057. <https://doi.org/10.1021/la102351f>
- Gholami, F., Pakzad, L., & Behzadfar, E. (2020). Morphological, interfacial and rheological properties in multilayer polymers: A review. *Polymer*, 208, 122950. <https://doi.org/10.1016/j.polymer.2020.122950>
- Glinel, K., Moussa, A., Jonas, A. M., & Laschewsky, A. (2002). Influence of Polyelectrolyte Charge Density on the Formation of Multilayers of Strong Polyelectrolytes at Low Ionic Strength. *Langmuir*, 18(4), 1408–1412. <https://doi.org/10.1021/la0113670>
- Guzmán, E., Rubio, R. G., & Ortega, F. (2020). A closer physico-chemical look to the Layer-by-Layer electrostatic self-assembly of polyelectrolyte multilayers. *Advances in Colloid and Interface Science*, 282, 102197. <https://doi.org/10.1016/j.cis.2020.102197>
- Haselberg, R., Flesch, F. M., Boerke, A., & Somsen, G. W. (2013). Thickness and morphology of polyelectrolyte coatings on silica surfaces before and after protein exposure studied by atomic force microscopy. *Analytica Chimica Acta*, 779, 90–95. <https://doi.org/10.1016/j.aca.2013.03.066>
- Kittle, J. D., Wondraczek, H., Wang, C., Jiang, F., Roman, M., Heinze, T., & Esker, A. R. (2012). Enhanced Dewatering of Polyelectrolyte Nanocomposites by Hydrophobic Polyelectrolytes. *Langmuir*, 28(30), 11086–11094. <https://doi.org/10.1021/la3016996>
- Kwok, D. Y., & Neumann, A. W. (1999). Contact angle measurement and contact angle interpretation. *Advances in Colloid and Interface Science*, 81(3), 167–249. [https://doi.org/10.1016/S0001-8686\(98\)00087-6](https://doi.org/10.1016/S0001-8686(98)00087-6)
- La Fuente Arias, C. I., Kubo, M. T. K., Tadini, C. C., & Augusto, P. E. D. (2021). Bio-based multilayer films: A review of the principal methods of production and challenges. *Critical Reviews in Food Science and Nutrition*, 1–17. <https://doi.org/10.1080/10408398.2021.1973955>
- Lombardo, S., & Villares, A. (2020). Engineered Multilayer Microcapsules Based on Polysaccharides Nanomaterials. *Molecules*, 25(19), 4420. <https://doi.org/10.3390/molecules25194420>
- Lyu, X., & Peterson, A. M. (2017). The Princess and the Pea Effect: Influence of the first layer on polyelectrolyte multilayer assembly and properties. *Journal of Colloid and Interface Science*, 502, 165–171. <https://doi.org/10.1016/j.jcis.2017.04.091>
- Marmur, A. (2006). Soft contact: measurement and interpretation of contact angles. *Soft Matter*, 2(1), 12–17. <https://doi.org/10.1039/B514811C>
- Nie, J., Pei, B., Wang, Z., & Hu, Q. (2019). Construction of ordered structure in polysaccharide hydrogel: A review. *Carbohydrate Polymers*, 205, 225–235. <https://doi.org/10.1016/j.carbpol.2018.10.033>
- Nolte, A. J., Rubner, M. F., & Cohen, R. E. (2004). Creating Effective Refractive Index Gradients within Polyelectrolyte Multilayer Films: Molecularly Assembled Rugate Filters. *Langmuir*, 20(8), 3304–3310. <https://doi.org/10.1021/la0363229>
- Petrila, L.-M., Bucatariu, F., Mihai, M., & Teodosiu, C. (2021). Polyelectrolyte Multilayers: An Overview on Fabrication, Properties, and Biomedical and Environmental Applications. *Materials*, 14(15), 4152. <https://doi.org/10.3390/ma14154152>

- Richardson, J. J., Cui, J., Björnmalm, M., Braunger, J. A., Ejima, H., & Caruso, F. (2016). Innovation in Layer-by-Layer Assembly. *Chemical Reviews*, 116(23), 14828–14867. <https://doi.org/10.1021/acs.chemrev.6b00627>
- Schoeler, B., Kumaraswamy, G., & Caruso, F. (2002). Investigation of the Influence of Polyelectrolyte Charge Density on the Growth of Multilayer Thin Films Prepared by the Layer-by-Layer Technique. *Macromolecules*, 35(3), 889–897. <https://doi.org/10.1021/ma011349p>
- Steitz, R., Jaeger, W., & Klitzing, R. v. (2001). Influence of Charge Density and Ionic Strength on the Multilayer Formation of Strong Polyelectrolytes. *Langmuir*, 17(15), 4471–4474. <https://doi.org/10.1021/la010168d>
- Sui, Z., Salloum, D., & Schlenoff, J. B. (2003). Effect of Molecular Weight on the Construction of Polyelectrolyte Multilayers: Stripping versus Sticking. *Langmuir*, 19(6), 2491–2495. <https://doi.org/10.1021/la026531d>
- Towle, E. G., Ding, I., & Peterson, A. M. (2020). Impact of molecular weight on polyelectrolyte multilayer assembly and surface properties. *Journal of Colloid and Interface Science*, 570, 135–142. <https://doi.org/10.1016/j.jcis.2020.02.114>
- v. Klitzing, R. (2006). Internal structure of polyelectrolyte multilayer assemblies. *Physical Chemistry Chemical Physics*, 8(43), 5012. <https://doi.org/10.1039/b607760a>
- Wågberg, L., & Erlandsson, J. (2021). The Use of Layer-by-Layer Self-Assembly and Nanocellulose to Prepare Advanced Functional Materials. *Advanced Materials*, 33(28), 2001474. <https://doi.org/10.1002/adma.202001474>
- Wang, D., He, Y., Zhang, J., Li, W., Fu, X., Tian, M., Zhou, Y., & Yao, Z. (2018). Layer-by-layer assembled transparent polymeric adhesive films with adjustable refractive indices. *International Journal of Adhesion and Adhesives*, 85, 202–207. <https://doi.org/10.1016/j.ijadhadh.2018.06.010>
- Zan, X., Hoagland, D. A., Wang, T., Peng, B., & Su, Z. (2012). Polyelectrolyte uptake by PEMs: Impacts of molecular weight and counterion. *Polymer*, 53(22), 5109–5115. <https://doi.org/10.1016/j.polymer.2012.09.011>

Chapter 5

α -glucans multilayers for detection of enzymatic activity

Table of content

Introduction	193
1. Concept: colorimetric assay for enzyme-detection.....	196
2. Elaboration of colorimetric assays based on α-glucans multilayers.....	197
<u>2.1. Choice of functionalized α-glucans multilayers: colors</u>	<u>197</u>
<i>2.1.1. Type of functionalized α-glucans multilayers.....</i>	<i>197</i>
<i>2.1.2. Number of bilayers</i>	<i>199</i>
<u>2.2. Hybrid growth type and structures for film formation</u>	<u>199</u>
3. Colorimetric sensors for the detection of trypsin	202
<u>3.1. Integration of poly-L-lysine (PLL) in colorimetric assay</u>	<u>202</u>
<i>3.1.1. Formation of poly-L-lysine/dextran sulfate multilayers (PLL/DexS).....</i>	<i>202</i>
<i>3.1.2. Integration of poly-L-lysine (PLL) multilayer in α-glucans multilayers</i>	<i>203</i>
<u>3.2. Enzymatic degradation of multi-layered sensors.....</u>	<u>204</u>
Conclusion.....	207
References	209
Annexes	211

Introduction

Depending on the transduction process, biosensors can be divided in different categories such as electrochemical, optical, piezoelectric, thermal and optical sensors (Karunakaran, Rajkumar, et al., 2015; Naresh & Lee, 2021; Singh et al., 2021). Another classification can be made according to the type of receiver: microbial biosensors, genosensors, immunosensors and enzymatic biosensors. First developed by Qlark in 1956 as electrochemical sensors, enzymatic biosensors are of great interest for the scientific community due to their wide possibility of applications, in biomedical, food and environmental monitoring (Karunakaran, Madasamy, et al., 2015; Qlark Jr, 1956). Enzymatic biosensors are analytical assays based on chemical reaction between enzymes (bioreceptor) and the substrate (analyte) which results in an electric or optical signal (Newman & Setford, 2006; Sassolas et al., 2012; Zhao et al., 2017).

Therefore, organized multilayer films of enzymes or consisting of enzyme-sensitive polyelectrolytes have been used to functionalize surfaces for improving biosensors (Barsan & Brett, 2016; Brynda et al., 1998; Sabu et al., 2019). The layer-by-layer technique is an inevitable and relatively easy method for incorporating both analyte and bioreceptors into a system for the development of enzymatic sensors. In particular, assemblies prepared by LbL method allow the integration of natural polyelectrolytes sensitive to enzyme activity. The principle of these sensors is the enzymatic degradation of polyelectrolytes, but depending on the intended application, the construction strategy may vary (C. Cerclier et al., 2011; Itoh et al., 2006).

As shown in Chapters 3 and 4, functionalized α -glucans -based multilayers present various structures and structural colors as a function of the modification of experimental conditions. This makes them ideal systems for the development of colorimetric biosensors. In the early 2010s, our research team elaborated an innovative enzymatic sensor based on colored semi-reflective thin films using polysaccharides (C. Cerclier et al., 2011). Cerclier *et al.* used multilayers of cellulose and xyloglucans to detect an enzymatic activity as illustrated on Figure 5.1. (C. Cerclier et al., 2011; C. V. Cerclier et al., 2013; Guyomard-Lack et al., 2012). The colorful thin films prepared (70 – 130 nm) aimed to detect enzyme activity by the total or partial enzymatic degradation of the multilayer as illustrated on Figure 5.1a. The multilayer devices elaborated by Cerclier C. during her thesis allowed the detection of an enzymatic activity of cellulase down to $0,024 \text{ nkat.mL}^{-1}$, 15 minutes after the contact between

the film and the enzymes (C. Cerclier, 2011). This fast and easy-to-use colorimetric device was patented later on, as “Colorimetric device for detecting, in an aqueous solution of interest, hydrolytic enzymatic activity with regard to at least one polymer of interest” by Cathala B. and Cerclier C. (Cathala & Cerclier, 2012).

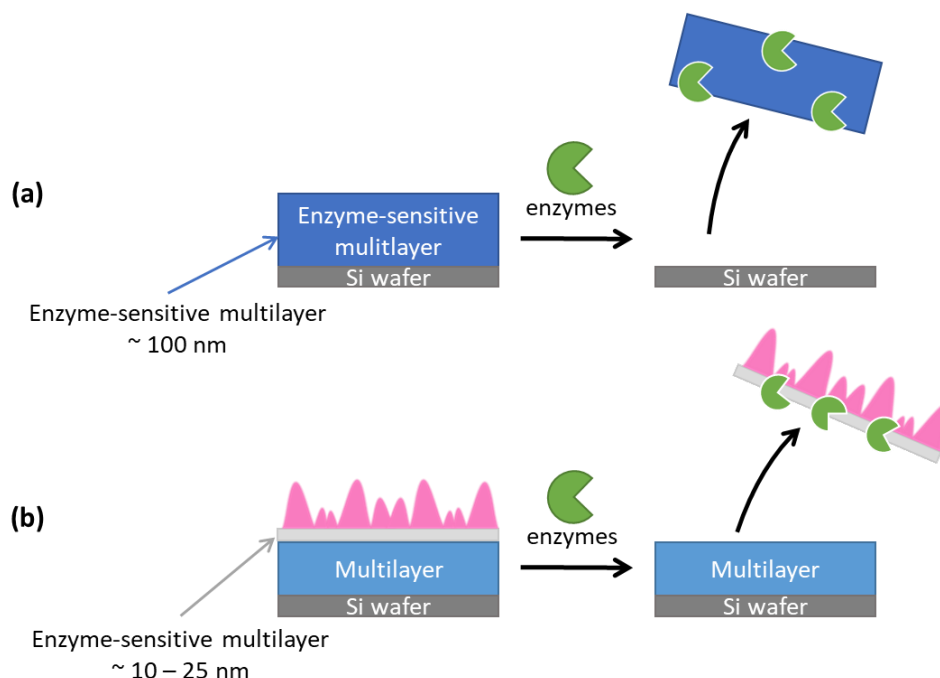


Figure 5.1. Schematic presentation of (a) the concept proposed by Cerclier *et al.* for colorimetric biosensors for detection of enzymatic activity, (b) of the concept proposed in this thesis for more sensitive colorimetric biosensors for detection of enzymatic activity.

In the present thesis, we decide to change the construction strategy by creating a three-multilayer ‘sandwich’ with enzyme-sensitive multilayer as an intermediate as schematized on Figure 5.1b. The idea is to incorporate the enzyme-sensitive multilayer between colorful functionalized α -glucans multilayers to have a thinner film (10 – 25 nm) compared to systems from Cerclier C., and so, a higher sensitivity to enzymes. Moreover, by separating the colored part and the enzyme-sensitive part, the colorimetric device could be extended to the detection of any enzymatic activity by the sole choice of the intermediate multilayer. The chosen strategy is explained in details at the beginning of this chapter. The problems related to the multilayers according to their position in the ‘sandwich’ are presented in order to guide the choice of the polyelectrolyte systems to be used for the development of the system. In particular, the functionalized α -glucans multilayers must have a colored surface and be able to grow into a film with an alternation of 3 multilayers. Their permeability to the enzyme is also an important point for the accessibility of the enzyme to the concerned layers.

Using films formed with spin-assisted deposition, we proceeded to an analysis of the structural colors as a function of the type of polyelectrolyte systems but also of the number of bilayers deposited. We chose to study the potential of (PAH/DexS H40)₄₀ and (PAH/DexS L40)₄₀ films for the device's development because of the marked difference in their structural colors. Using Quartz Crystal Microbalance with Dissipation Monitoring (QCM-D), we demonstrate the capacity of multilayered systems to form layers with distinct characteristics within an alternating multilayer. Next, we investigate the incorporation of PLL-based multilayer between two functionalized α -glucans films (PAH/DexS) to develop an assay for the trypsin detection. The construction of (PLL/DexS) was reported using QCM-D, and its successful integration into the three-multilayer device using spin-assisted deposition is also reported. Then, the visual and colorimetric detection of film degradation is investigated as a function of the concentration of enzymes used and the number of bilayers in the integrated enzyme-sensitive multilayer.

1. Concept: colorimetric assay for enzyme-detection

As illustrated on Figure 5.2, the concept is to integrate a thin enzyme-sensitive polyelectrolyte between two films with different composition and thus leading to different colors. The sensor is then constituted of three different films onto a substrate: a multilayer with color 1 at the bottom, an enzyme-sensitive film in the middle, a multilayer with color 2 on the top. The final color of the sensor is dependent of the total thickness of the three films and the refractive index, and can be predicted by equation 9 and 10 (chapter 1, section 4.2.1).

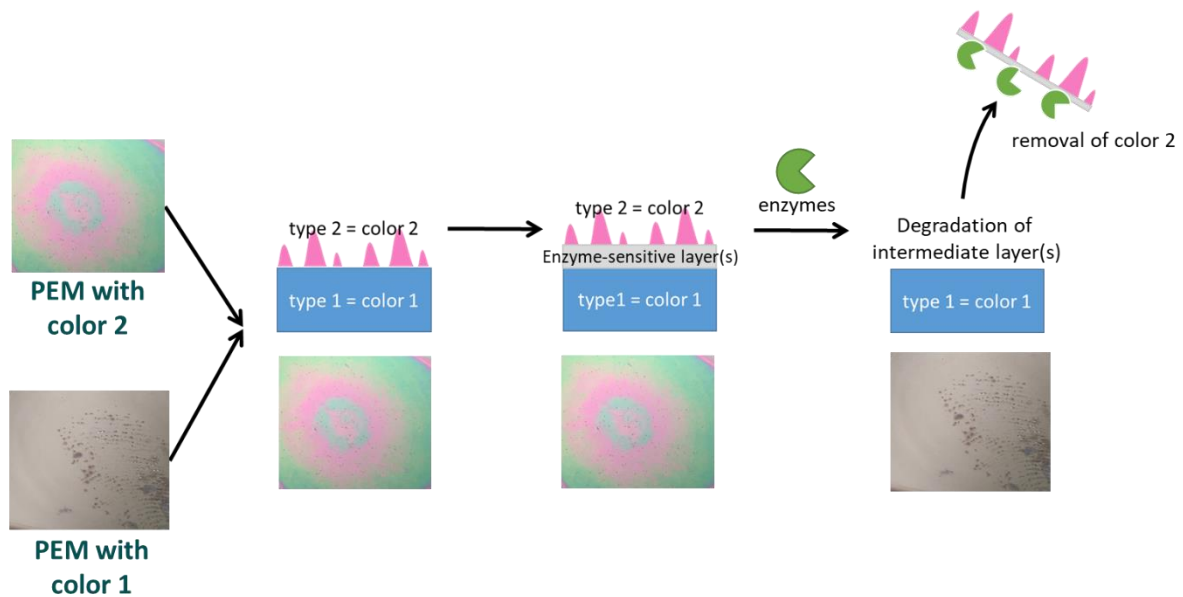


Figure 5.2. Scheme of the concept proposed for the elaboration of colorimetric biosensors for the detection of enzymes, based on multilayers of functionalized α -glucans.

In presence of the specific enzymes, the intermediate film is degraded by their action onto the enzyme-sensitive polyelectrolyte chosen, leading to the removal of the two top-parts of the sensors. By removing the multilayer with color 2 at the top (and the middle multilayer), we predict a change in the color of sensor: obtaining color 1 from multilayer at the bottom. Thus, the contact of the multilayer device with a medium containing the enzyme should lead to a visual change in its surface colors. In order to develop such devices, some issues have to be considered:

- The multilayer at the bottom and the one at the top must display different colors.
- All multilayers should be able to grow within an alternating system of multilayers.
- All multilayers should allow enzymes' diffusion.

2. Elaboration of colorimetric assays based on α -glucans multilayers

In order to build the colorimetric assays, two multilayers are necessary to ‘sandwich’ the enzyme-sensitive multilayer as explained in section 1.1.: 1) multilayer with color 1, 2) multilayer with color 2, which must be sufficiently porous to allow enzymes to have access to the enzyme-sensitive multilayer. The conception relies on: the choice of α -glucans multilayers (colors, structures), and the capacity of each multilayers to grow on each other and to keep their structure despite the mixing with other multilayers.

2.1. Choice of functionalized α -glucans multilayers: colors

The choice of the two functionalized α -glucans systems used for the elaboration of the device is based on two criteria: structural colors and structures. It is necessary that there is a marked difference between the colors of the multilayer at the bottom and the multilayer at the top. Thus, we studied the different structural colors we can obtain with functionalized α -glucans -based systems by building multilayers with spin-assisted deposition.

2.1.1. Type of functionalized α -glucans multilayers

First, we present the formation of 40 bilayers from different systems on silicon wafer using the spin-assisted deposition and the same experimental conditions: in 25mM NaCl, polycation at 0.1 g.mol^{-1} and polyanion at 0.5 g.mol^{-1} . The structural colors of these films are reported in Figure 5.3a for (PAH/DexS) systems and in Figure 5.3b for (PAH/oxidized α -glucans) and (DEAE-Dex 150/oxidized α -glucans) systems.

As we saw in Chapter 4, (PAH/DexS H40) and (PAH/DexS L40) result in films with different colors, which are dependent on the film thickness and on its refraction index. 40 bilayers of (PAH/DexS H40) lead to a very light brown color while 40 bilayers of (PAH/DexS L40) present a surface with magenta and green as main structural colors, as shown in Figure 5.3a. (PAH/DexS L40)₄₀ displays heterogeneous thickness on the entire surface resulting in different colors. However, despite the heterogeneity of visible colors, the (PAH/DexS L40) 40-bilayer assembly results in very marked colors that can be suitable as the multilayer with color 2. Moreover, the important difference between the structural colors (PAH/DexS H40)

and (PAH/DexS L40) corresponds to the needs identified for the elaboration of the colorimetric device.

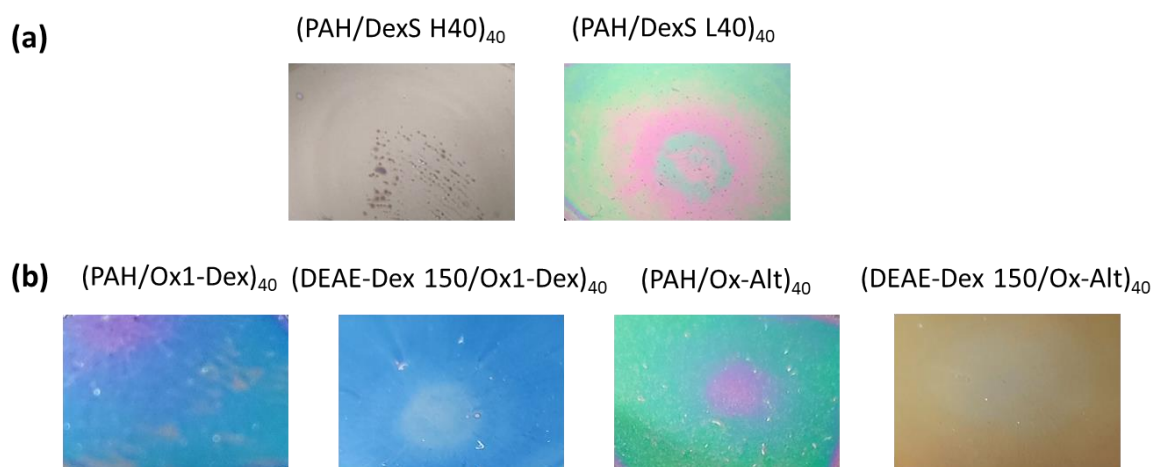


Figure 5.3. Photos and colors of (a) (PAH/DexS) 40-bilayer films and (b) (PAH/oxidized α -glucans) and (DEAE-Dex 150/oxidized α -glucans) 40-bilayer films. Multilayers were built on silicon wafers at 25mM NaCl using spin-assisted coating method.

Due to their greater mass adsorption, as discussed in Chapter 3, i.e., and greater resulting thickness, the formation of 40 bilayer films based on oxidized α -glucans leads to colored surfaces for each system (Figure 5.3b). In Figure 5.3b, we notice that DEAE-Dex 150-based films lead to more homogeneous structural colors than PAH-based films. For example, the (PAH/Ox1-Dex)₄₀ film shows both magenta and blue with a significant heterogeneous surface area while the (DEAE-Dex 150/Ox1-Dex)₄₀ film gives a homogeneous blue surface. The same is true for Ox-Alt based films such as the (PAH/Ox-Alt)₄₀ film which is both magenta and green and the (DEAE-Dex 150/Ox-Alt)₄₀ film which is a homogeneous orange/gold surface. While the observed structural colors are suitable for the development of colorimetric devices, the surface heterogeneity of the (PAH/oxidized α -glucans) films may affect the equal spread of the enzyme-sensitive multilayer on their surface during deposition. Thus, the (PAH/ α -oxidized glucan)₄₀ films are more likely to correspond to multilayer 2 (at the top) in the device structure while the (DEAE-Dex 150/ α -oxidized glucan)₄₀ films are more likely to be suitable as multilayer 1 (at the bottom).

2.1.2. Number of bilayers

In addition to the type of multilayers, we studied the structural colors for different number of bilayers in order to optimize the colors of the device. We reported on Figure 5.4 the photos of (PAH/DexS L40) multilayers with different number of bilayers.

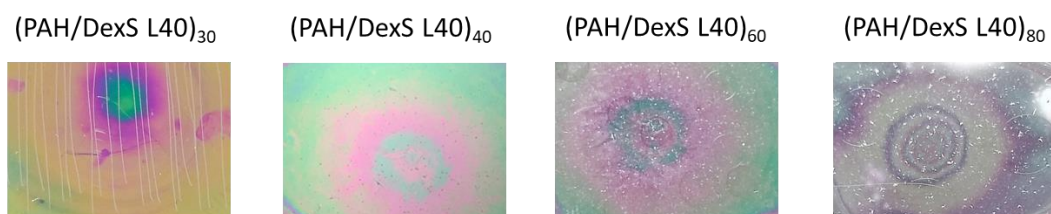


Figure 5.4. Photos of (PAH/DexS L40) films for 30 bilayers, 40 bilayers, 60 bilayers and 80 bilayers. Multilayers were built on silica wafers at 25mM NaCl using spin-assisted coating method.

In Figure 5.3, we can see that we have very marked colors for the (PAH/DexS L40) multilayers of 30 and 40 bilayers: yellow and magenta for 30 bilayers and green and magenta for 40 bilayers. However, for 60 and 80 bilayers, the structural colors of the films are less marked with visible aggregates on the surfaces. As expected, the number of bilayers has an importance on the final surface colors, but also on the surface morphology. Beyond 40 bilayers, the systems (PAH/DexS L40) do not lead to suitable surfaces for the construction of the colorimetric device because the color contrast between the two films is not strong enough. We chose to build the colorimetric device from 40 bilayers and 30 bilayers with 40 bilayers for the top and bottom multilayers. However, to optimize the construction in time and quantity of raw material, we could choose 30 bilayers.

2.2. Hybrid growth type and structures for film formation

As presented in Chapters 3 and 4, functionalized α -glucans multilayer films exhibit different growth patterns and surface morphology due to their growth mechanisms. The structures of these multilayers are important to 1) allow growth on the enzyme-sensitive polyelectrolyte multilayer on top of the first layer and, 2) allow enzyme accessibility to the enzyme-sensitive polyelectrolyte multilayer. Thus, we chose to use the PAH/DexS H40 system and the PAH/DexS L40 system for the multilayer sensor development. Indeed, in Chapter 3, we found that the PAH/DexS H40 system gives rise to a classical LbL growth with a charge inversion at the surface that allows the adsorption of the next layer. Since the top

layer is charged, adsorption of a polyelectrolyte of opposite charge should be possible in order to construct another multilayer. Furthermore, a (PAH/DexS H40) multilayer of 10 bilayers gave a "fibrillar" surface morphology with high coverage as well as a homogeneous surface, *i.e.* homogeneous structural colors regardless of the number of bilayers, which should facilitate the adsorption of the next layer. In the case of PAH/DexS L40, the analysis conducted in Chapter 3 showed that the system leads to partial charge neutralization and formation of PE complexes, which can block the growth of the next layer on its surface. However, we have highlighted that a (PAH/DexS L40) multilayer of 10 layers leads to "puddle" type surfaces with a lower coverage, *i.e.* a more "porous" structure than the (PAH/DexS H40) multilayer. This type of surface is more likely to be permeable to enzymes and can be used as the top layer of sensors to trap the enzyme-sensitive polyelectrolyte multilayer. In addition to its higher porosity, PAH/DexS L40 also generates highly colored surfaces, despite their heterogeneity, which can be clearly identified by the naked eye if removed.

The challenge is to be able to alternate two or three types of multilayers with a distinct structure and avoid diffusion between the types of multilayers. Thus, we studied the formation of 5 bilayers of (PAH/DexS L40) on top of 5 bilayers of (PAH/DexS H40) on QCM-D to see if we are able to keep the original growth type of (PAH/DexS L40) despite the presence of the other multilayer underneath. The frequency and dissipation shifts of 5 bilayers of (PAH/DexS H40) followed by the deposition of 5 bilayers of (PAH/DexS L40), *i.e.* (PAH/DexS H40)₅/(PAH/DexS L40)₅ assemblies, are displayed for the third, fifth, and seventh harmonics in Figure 5.5a.

For the assembly of 5 bilayers of (PAH/DexS L40) on top of 5 bilayers of (PAH/DexS H40) reported in Figure 5.5a,b, two different viscoelastic regimes can be observed. The first regime corresponds to the adsorption of (PAH/DexS H40) between 20min and 2h while the second regime corresponds to the adsorption of (PAH/DexS L40) from 2h onwards (Figure 5.5a). For the first 5 bilayers of (PAH/DexS H40)₅/(PAH/DexS L40)₅ *i.e.* (PAH/DexS H40)₅, we find the same mass adsorption and viscoelasticity behavior that we observed for (PAH/DexS H40) (Chapter 3). Then, the adsorption of the next 5 bilayers, *i.e.* (PAH/DexS L40)₅, leads to a change in the dissipation signal variations plotted in Figure 5.5a and the $\Delta D_5/\Delta f_5$ slope in Figure 5.5b. The dissipation variations/peaks observed for the (PAH/DexS L40) system (Chapter 3) can be observed here from bilayer 6 despite the presence of a (PAH/DexS H40) multilayer (bilayers 1 to 5). Furthermore, the transition from the single

slope $\Delta D_5/\Delta f_5$ viscoelastic behavior of (PAH/DexS H40) to the different slopes/loops linked to the construction of (PAH/DexS L40) can be clearly identified. The same result was observed when we performed multilayer adsorption of 15 bilayers with (PAH/DexS H40)₅/(PAH/DexS L40)₅/(PAH/DexS H40)₅ on QCM-D as well (Annexes, Figure 5.A1).

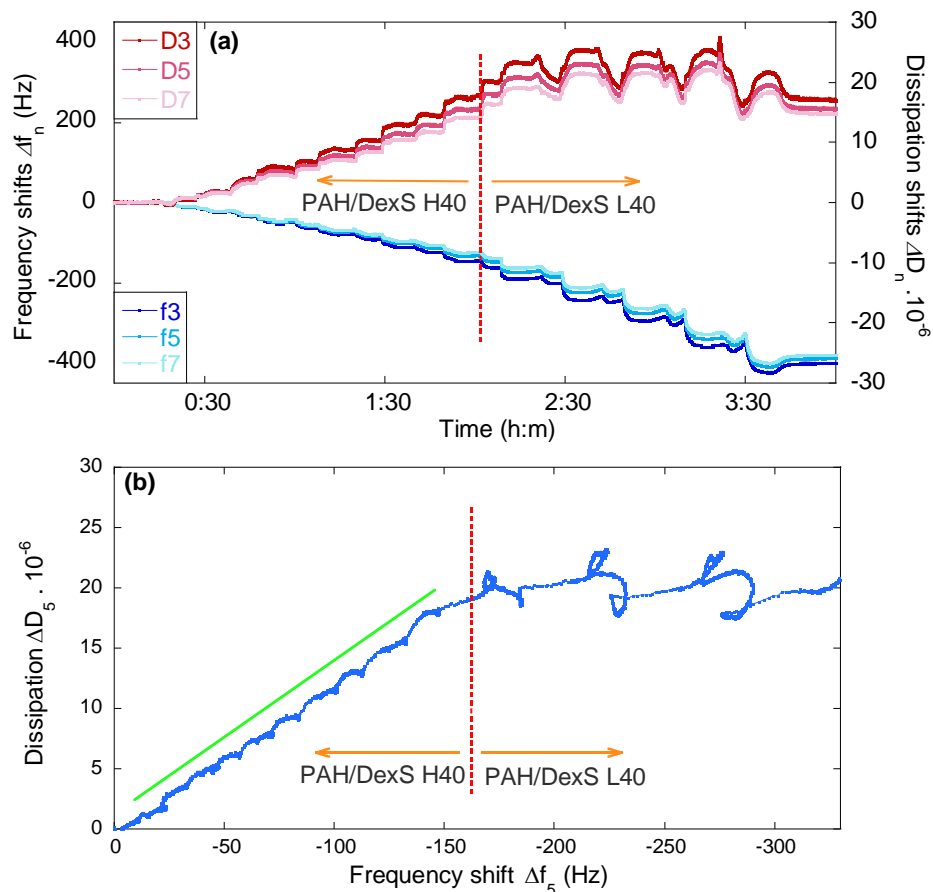


Figure 5.5. (a) $\Delta f_n/n$ and ΔD_n as a function of time for deposition of (PAH/DexS H40)₅/(PAH/DexS L40)₅ on gold coated surface using QCM-D. (b) ΔD_5 as a function of $\Delta f_5/5$ with the switch of regime between (PAH/DexS H40)₅ and (PAH/DexS L40)₅ in orange.

The systems result in successful multilayers with clearly separated growth types: each multilayer (PAH/DexS) retains its distinct structures. Therefore, the (PAH/DexS H40) and (PAH/DexS L40) 40 bilayer systems are suitable for the development of colorimetric devices, as the former is not colored at 40 bilayers while the DexS L40 based films have really marked colors. Moreover, growing both multilayers on top of each other allows to maintain their structures, so their integration in a multilayer system with an enzyme-sensitive polyelectrolyte multilayer should be possible and not hinder their characteristics.

3. Colorimetric sensors for the detection of trypsin

The next step in the development of our colorimetric assay is to integrate an enzyme-sensitive multilayer between the two α -glucans films to evaluate the feasibility of such a 3-multilayer device. We decided to use ϵ -poly-L-lysine (PLL), a positively charged natural polymer commonly used in LbL assemblies, for the formation of the enzyme-sensitive layers. PLL is a homo-polyamino acid characterized by the peptide bond between the carboxyl and ϵ -amino groups of L-lysine (Yoshida & Nagasawa, 2003), as illustrated on Figure 5.6.

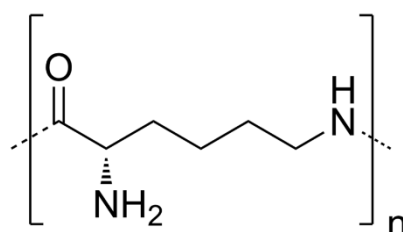


Figure 5.6. Structure of ϵ -poly-L-lysine (PLL).

PLL presents an antimicrobial activity that is particularly interesting for the formation of materials for the biomedical and tissue engineering domains (Hyldgaard et al., 2014; Shi et al., 2016; Shima et al., 1984). In particular, PLL has been successfully used in the formulation of multilayers coating in such areas as the promotion of cellular adhesion, microencapsulation or antibacterial coating (Hamano, 2011; Tuersuntuoheti et al., 2019). PLL has also been used in multilayers for its sensitivity to specific enzymes. In fact, the release of macromolecules by enzyme-trigger degradation of PLL has been proven with trypsin, α -chymotrypsin and pronase (Itoh et al., 2006; Marchenko et al., 2012). Moreover, both the stability at high temperature and the antimicrobial activity of PLL can be useful for the long conservation of a colorimetric device (Hiraki, 2000).

3.1. Integration of poly-L-lysine (PLL) in colorimetric assay

3.1.1. Formation of poly-L-lysine/dextran sulfate multilayers (PLL/DexS)

Itoh *et al.* reported in 2008 the formation of capsules based on (CHI/DexS/PLL) multilayers, highlighting the possibility to form assemblies based on DexS and PLL (Itoh et al., 2008a). Hence, we decided to study of formation of multilayers based on PLL with functionalized α -glucans, and especially with DexS, on QCM-D. The formation of 10 bilayers

of (PLL/DexS H40) and of 10 bilayers of (PLL/DexS L40) on QCM-D should allow to check if we can build stable films based on those polyelectrolytes in order to integrate them into the colorimetric device. The frequency and dissipation shifts of 10 bilayers of (PLL/DexS H40)₁₀ and of (PLL/DexS L40)₁₀ assemblies are displayed for the third, fifth and seventh overtones on Figure 5.7a,b.

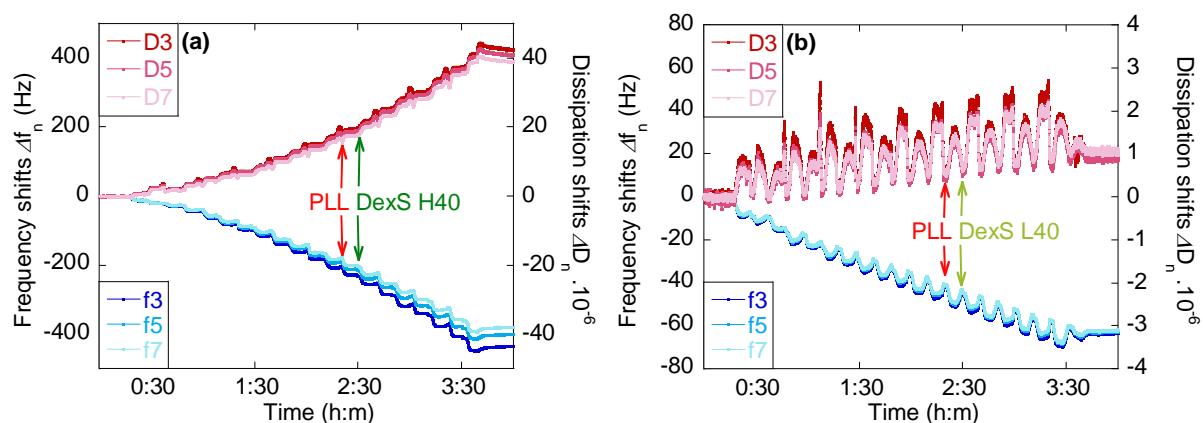


Figure 5.7. $\Delta f_n/n$ and ΔD_n as a function of time for (a) (PLL/DexS H40)₁₀ multilayer and (b) (PLL/DexS L40)₁₀ multilayer on gold coated quartz crystal using QCM-D. The frequency (blue) and dissipation (red) changes for the third, fifth and seventh overtones are depicted.

As shown by Figure 5.7a,b, both systems based on PLL and DexS result in stable multilayer films, with respectively a final frequency shift Δf_5 of -410 Hz and of -63 Hz for (PLL/DexS H40)₁₀ and (PLL/DexS L40)₁₀. In addition to a frequency shift higher for (PLL/DexS H40), the two multilayers display different viscoelastic behavior. (PLL/DexS H40) presents a relatively linear increase of the dissipation in the course of the adsorption process (Figure 5.7a), which is similar to what we observed for (PAH/DexS H40). In parallel, (PLL/DexS L40) shows a sudden change in dissipation values with peaks up from 3×10^{-6} to 1×10^{-6} (Figure 5.7b). This behavior is similar to the one noted for (PAH/DexS L40).

3.1.2. Integration of poly-L-lysine (PLL) multilayer in α -glucans multilayers

As we were able to obtain stable films on QCM-D, the (PLL/DexS) multilayers were integrated within the colorful functionalized α -glucans -based multilayers. Films were built on silica wafers using spin-assisted deposition using the same experimental conditions as mentioned in section 1.2.1. First, we found out that we are not able to build (PLL/DexS) films directly onto silica wafer as we observed (naked eyes, AFM) no deposition onto the surface.

Then, we decided to build $(\text{PAH/DexS H40})_{40}/(\text{PLL/DexS H40})_1/(\text{PAH/DexS L40})_{40}$ films based on the results obtained previously. We reported, on Figure 5.8, the film surface observed during the construction.

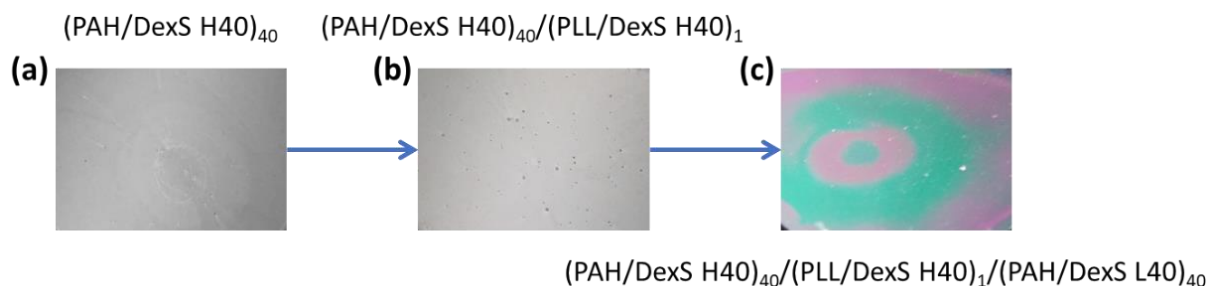


Figure 5.8. Photos and colors of (a) $(\text{PAH/DexS H40})_{40}$ film, of (b) $(\text{PAH/DexS H40})_{40}/(\text{PLL/DexS H40})_1$ film and of (c) $(\text{PAH/DexS H40})_{40}/(\text{PLL/DexS H40})_1/(\text{PAH/DexS L40})_{40}$ film.

As presented on Figure 5.8, the integration of PLL -based multilayer within the colorimetric assay is successful and does not impact the final color of the device. Based on the colors obtained for the three multilayers structure, (PLL/DexS H40) system at 1 bilayer results in a film that allows the formation of (PAH/DexS L40) onto it. Moreover, the colorless character of the 1-bilayer (PLL/DexS H40) does not change the final color of the film, allowing the obtention of a marked color by the construction of (PAH/DexS L40) . A variation between 1 to 10 of the number of (PLL/DexS H40) bilayers leads to the same result. For instance, the formation of both $(\text{PAH/DexS H40})_{40}/(\text{PLL/DexS H40})_5/(\text{PAH/DexS L40})_{40}$ and $(\text{PAH/DexS H40})_{40}/(\text{PLL/DexS H40})_{10}/(\text{PAH/DexS L40})_{40}$ show heterogeneous surface with both magenta and green.

3.2. Enzymatic degradation of multi-layered sensors

One of the enzymes specific for the degradation of poly-L-lysine (PLL) is trypsin, an endopeptidase (Levin et al., 1956; Waley & Watson, 1953). Multiple studies reported the hydrolysis of PLL by action of trypsin, including the degradation of LbL assemblies (Itoh et al., 2008a). Thus, we proposed to evaluate the colorimetric assay developed with PLL for the detection of trypsin activity. In order to do that, we propose to dip the device $(\text{PAH/DexS H40})_{40}/(\text{PLL/DexS H40})_n/(\text{PAH/DexS L40})_{40}$ (for $n= 1, 5$ or 10) in trypsin solution at different concentration (1 mg.mL^{-1} , 0.1 mg.mL^{-1} and 0.01 mg.mL^{-1}) in 0.1 M phosphate buffer (pH 6) for 30 minutes, at 38°C .

We used the $(\text{PAH/DexS H40})_{40}/(\text{PLL/DexS H40})_{10}/(\text{PAH/DexS L40})_{40}$ system to determine the lowest trypsin concentration between 1 mg.mL^{-1} ($\sim 1.6 \times 10^5 \text{ nkat.mL}^{-1}$), 0.1 mg.mL^{-1} ($\sim 1.6 \times 10^4 \text{ nkat.mL}^{-1}$) and 0.01 mg.mL^{-1} ($\sim 1.6 \times 10^3 \text{ nkat.mL}^{-1}$) for which we have a colorimetric change on the surface i.e. a degradation of the PLL-based multilayer. We chose to use 10-bilayer (PLL/DexS H40) intermediate multilayers for this step as we supposed that it was the most sensitive systems to enzymes between the three systems. At 10 bilayers, (PLL/DexS H40) films are around 20 nm. We reported the photos of surface of $(\text{PAH/DexS H40})_{40}/(\text{PLL/DexS H40})_{10}/(\text{PAH/DexS L40})_{40}$ before and after dipping for 30 min in presence of 1 mg.mL^{-1} , 0.1 mg.mL^{-1} and 0.01 mg.mL^{-1} trypsin.

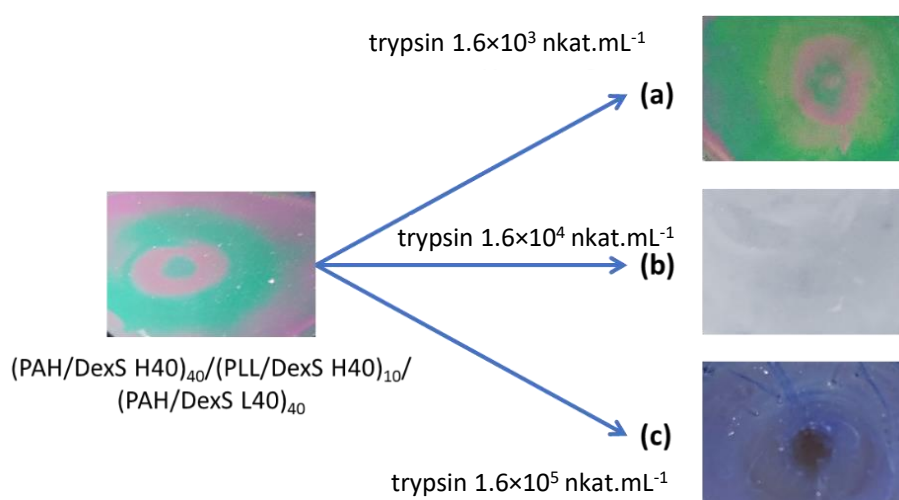


Figure 5.9. Photos of $(\text{PAH/DexS H40})_{40}/(\text{PLL/DexS H40})_{10}/(\text{PAH/DexS L40})_{40}$ before and after dipping in presence of (a) 1 mg.mL^{-1} , (b) 0.1 mg.mL^{-1} and (c) 0.01 mg.mL^{-1} trypsin.

On Figure 5.9a, a light color change can be observed by the action of enzyme of the multilayer at 1 mg.mL^{-1} trypsin *i.e.* $\sim 1.6 \times 10^5 \text{ nkat.mL}^{-1}$. After dipping for 30 min in the trypsin solution, the surface appears to be less bright, but a radical change cannot be observed. For dipping in 0.1 mg.mL^{-1} ($\sim 1.6 \times 10^4 \text{ nkat.mL}^{-1}$) or 0.01 mg.mL^{-1} ($\sim 1.6 \times 10^3 \text{ nkat.mL}^{-1}$) trypsin solution, $(\text{PAH/DexS H40})_{40}/(\text{PLL/DexS H40})_{10}/(\text{PAH/DexS L40})_{40}$ results in a cloudy surface, proof of the action of enzymes on the PLL intermediate multilayer. However, we do not obtain the color of $(\text{PAH/DexS H40})_{40}/(\text{PLL/DexS H40})_{10}$ multilayers, but a very light cloudy blue at 0.1 mg.mL^{-1} trypsin solution and a cloudy blue at 0.01 mg.mL^{-1} trypsin solution. Above $1.6 \times 10^3 \text{ nkat.mL}^{-1}$, we are not able to observe a change of structural colors.

At very high trypsin concentration ($\sim 1.6 \times 10^5 \text{ nkat.mL}^{-1}$), we may have formation of an enzyme layer on the top that decrease or block the enzyme diffusion rate. This “crowding” of enzymes on the surface can be a resulting effect of the electrostatic interactions between the

charges of the top multilayer and enzymes (Ma & Nussinov, 2013). At lower trypsin concentrations, 1.6×10^4 nkat.mL⁻¹ and $\sim 1.6 \times 10^3$ nkat.mL⁻¹, we have a diffusion of enzymes within the structure leading to changes in structural colors. However, it is clear that we do not obtain a total removal of the two top films. Those observations can be explained by a partial hydrolysis of PLL by trypsin, leading to the partial degradability of the PLL -based multilayers. The degradation of PLL may not be sufficient to eliminate all interactions with the film underneath and lead to the removal. Another hypothesis is that following the degradation of the PLL, we have pieces of polyelectrolyte (polymer, dimer or monomer) that re-adsorb on the surface.

The preparation of (PAH/DexS H40)₄₀/(PLL/DexS H40)₁₀/(PAH/DexS H40)₄₀ was also not successful as the 90-bilayer blue surface observed after formation remains blue after dipping in trypsin media (Annexes, Figure 4.A2). It may be due to the ‘more closed’ surface of (PAH/DexS H40) we observed in AFM (Chapter 3) that does not permit the trypsin to access the PLL layers. Moreover, we tried to reduce the number of (PLL/DexS H40) bilayers to 5 bilayers and to 1 bilayer, but we did not observe any color modification on the surface after 30 min or 1h of dipping in trypsin solution.

Compared to systems developed by our research team with multilayers, the system present in this thesis has a lower sensitivity to enzymes. As it stands, the three-multilayer colorimetric sensors developed during this thesis detects a minimum activity of 1.6×10^3 nkat.mL⁻¹ for an incorporated 20 nm PLL thin film.

Conclusion

In this chapter, we proposed a colorimetric device for enzyme detection, using the functionalized α -glucans multilayers studied in chapter 3 and chapter 4. The concept of our colorimetric assay is based on the structural colors that can be obtained by assembling charged α -glucans. We proposed to "sandwich" an enzyme-sensitive intermediate multilayer using two films of two different colors. In the presence of a specific enzyme, a chemical reaction between the enzyme-sensitive polyelectrolyte and the enzyme is expected to occur, leading to the complete or partial degradation of this intermediate multilayer. As a consequence of this degradation, the interactions between the intermediate layers and the other multilayers should be minimized, which should lead to the removal of the intermediate and the top substrate multilayer. Using colored films, we planned to identify the enzymatic action by a colorimetric change on the surface that can be observed by the naked eye. The construction of such a device requires specific characteristics for each of the three multilayers used.

1) The lower multilayer of color 1 must allow the formation of an enzyme-sensitive multilayer on it and the upper multilayer of color 2 must have strong structural colors and a structure that allows accessibility of the intermediate layers by enzymes. We have investigated the colors that we can achieve with our different polyelectrolyte systems. (PAH/DexS L40) and (PAH/ α -glucans oxidized) are more likely to match the top multilayer, due to their heterogeneity and marked colors. (PAH/DexS H40) and (DEAE-Dex 150/ α -oxidized glucans) are more likely to match the lower multilayer, as they have a more homogeneous surface even if (PAH/DexS H40) is not colored. Furthermore, the structural colors of these multilayers can be tuned by the number of bilayers. However, in the case of (PAH/DexS L40), increasing the number of bilayers beyond 40 bilayers results in less marked colors and aggregates on the surface. As the structure is important for the test development, we also studied the stability of the film structure by combining the growth of two multilayers. Using PAH/DexS H40 and PAH/DexS L40, we demonstrated that mixing two films with a different type of growth results in a successful multilayer and each multilayer (PAH/DexS) maintains its distinct structures.

2) The enzyme-sensitive intermediate must grow as a multilayer on top of the lower functionalized α -glucans multilayers and must not obstruct the features of the other multilayers to allow enzymatic degradation. Poly-L-lysine and a specific enzyme, trypsin, were used as a model for the intermediate multilayer and its degradation. We demonstrated

that the enzyme-sensitive poly-L-lysine can form 10-layer multilayers with DexS H40 and DexS L40, and exhibit a growth pattern similar to (PAH/DexS H40) and (PAH/DexS L40) respectively. Then, we integrated the PLL-based multilayer with functionalized α -glucans multilayers to construct the colorimetric assay. Integrating such an intermediate multilayer with 1 bilayer, 5 bilayers and 10 bilayers successfully forms a (PAH/DexS H40)₄₀/(PLL/DexS H40)_n/(PAH/DexS L40)₄₀ system, without affecting the final surface colors. To test the effectiveness of the three-layer device, the system was immersed in a trypsin solution, which is expected to result in a change in surface color. (PAH/DexS H40)₄₀/(PLL/DexS H40)_n/(PAH/DexS L40)₄₀ exhibited a color change at low trypsin concentration. However, decreasing the number of PLL-based bilayers to 1 or 5 does not allow degradation and/or removal of the intermediate and upper layers, as no color change was observed. The sensibility of the device based on a 20 nm-thick PLL multilayer was around $1.6 \times 10^3 \text{ nkat.mL}^{-1}$ which needs improvement.

References

- Barsan, M. M., & Brett, C. M. A. (2016). Recent advances in layer-by-layer strategies for biosensors incorporating metal nanoparticles. *TrAC Trends in Analytical Chemistry*, 79, 286–296. <https://doi.org/10.1016/j.trac.2015.11.019>
- Brynda, E., Houska, M., Skvor, J., & Ramsden, J. (1998). Immobilisation of multilayer bioreceptor assemblies on solid substrates. *Biosensors & Bioelectronics*, 13(2), 165–172. [https://doi.org/10.1016/S0956-5663\(97\)00107-3](https://doi.org/10.1016/S0956-5663(97)00107-3)
- Cathala, B., & Cerclier, C. (2012). Colorimetric device for detecting, in an aqueous solution of interest, hydrolytic enzymatic activity with regard to at least one polymer of interest (Patent No. FR2962545).
- Cerclier, C. (2011). Films multicouches à base de polymères végétaux : Elaboration et application à la détection d'activités enzymatiques. Université de Nantes.
- Cerclier, C., Guyomard-Lack, A., Moreau, C., Cousin, F., Beury, N., Bonnin, E., Jean, B., & Cathala, B. (2011). Coloured Semi-reflective Thin Films for Biomass-hydrolyzing Enzyme Detection. *Advanced Materials*, n/a-n/a. <https://doi.org/10.1002/adma.201101971>
- Cerclier, C. V., Guyomard-Lack, A., Cousin, F., Jean, B., Bonnin, E., Cathala, B., & Moreau, C. (2013). Xyloglucan–Cellulose Nanocrystal Multilayered Films: Effect of Film Architecture on Enzymatic Hydrolysis. *Biomacromolecules*, 14(10), 3599–3609. <https://doi.org/10.1021/bm400967e>
- Guyomard-Lack, A., Cerclier, C., Beury, N., Jean, B., Cousin, F., Moreau, C., & Cathala, B. (2012). Nano-structured cellulose nanocrystals-xyloglucan multilayered films for the detection of cellulase activity. *The European Physical Journal Special Topics*, 213(1), 291–294. <https://doi.org/10.1140/epjst/e2012-01676-1>
- Hamano, Y. (2011). Occurrence, Biosynthesis, Biodegradation, and Industrial and Medical Applications of a Naturally Occurring ϵ -Poly-L-lysine. *Bioscience, Biotechnology, and Biochemistry*, 75(7), 1226–1233. <https://doi.org/10.1271/bbb.110201>
- Hiraki, J. (2000). ϵ -Polylysine; its development and utilization. *Fine Chem.*, 29, 18–25.
- Hyldgaard, M., Mygind, T., Vad, B. S., Stenvang, M., Otzen, D. E., & Meyer, R. L. (2014). The Antimicrobial Mechanism of Action of Epsilon-Poly-L-Lysine. *Applied and Environmental Microbiology*, 80(24), 7758–7770. <https://doi.org/10.1128/AEM.02204-14>
- Itoh, Y., Matsusaki, M., Kida, T., & Akashi, M. (2006). Enzyme-responsive release of encapsulated proteins from biodegradable hollow capsules. *Biomacromolecules*, 7(10), 2715–2718. <https://doi.org/10.1021/bm060289y>
- Karunakaran, C., Madasamy, T., & Sethy, N. K. (2015). Enzymatic Biosensors. In *Biosensors and Bioelectronics* (pp. 133–204). Elsevier. <https://doi.org/10.1016/B978-0-12-803100-1.00003-7>
- Karunakaran, C., Rajkumar, R., & Bhargava, K. (2015). Introduction to biosensors. In *Biosensors and bioelectronics* (pp. 1–68). Elsevier.
- Levin, Y., Berger, A., & Katchalski, E. (1956). Hydrolysis and transpeptidation of lysine peptides by trypsin. *Biochemical Journal*, 63(2), 308–316. <https://doi.org/10.1042/bj0630308>
- Ma, B., & Nussinov, R. (2013). Structured Crowding and Its Effects on Enzyme Catalysis. In J. Klinman & S. Hammes-Schiffer (Eds.), *Dynamics in Enzyme Catalysis* (Vol. 337, pp. 123–137). Springer Berlin Heidelberg. https://doi.org/10.1007/128_2012_316
- Manouchehri, S., Zarrintaj, P., Saeb, M. R., & Ramsey, J. D. (2021). Advanced Delivery Systems Based on Lysine or Lysine Polymers. *Molecular Pharmaceutics*, 18(10), 3652–3670. <https://doi.org/10.1021/acs.molpharmaceut.1c00474>
- Marchenko, I., Yashchenok, A., Borodina, T., Bukreeva, T., Konrad, M., Möhwald, H., & Skirtach, A. (2012). Controlled enzyme-catalyzed degradation of polymeric capsules templated on CaCO₃: Influence of the number of LbL layers, conditions of degradation, and disassembly of multicompartments. *Journal of Controlled Release*, 162(3), 599–605. <https://doi.org/10.1016/j.jconrel.2012.08.006>
- Newman, J. D., & Setford, S. J. (2006). Enzymatic Biosensors. *Molecular Biotechnology*, 32(3), 249–268. <https://doi.org/10.1385/MB:32:3:249>
- Qlark Jr, L. (1956). Monitor and control of blood and tissue oxygen tensions. *Asaio Journal*, 2(1), 41–48.
- Sabu, C., Henna, T. K., Raphey, V. R., Nivitha, K. P., & Pramod, K. (2019). Advanced biosensors for glucose and insulin. *Biosensors and Bioelectronics*, 141, 111201. <https://doi.org/10.1016/j.bios.2019.03.034>
- Sassolas, A., Blum, L. J., & Leca-Bouvier, B. D. (2012). Immobilization strategies to develop enzymatic biosensors. *Biotechnology Advances*, 30(3), 489–511. <https://doi.org/10.1016/j.biotechadv.2011.09.003>
- Shi, C., Zhao, X., Liu, Z., Meng, R., Chen, X., & Guo, N. (2016). Antimicrobial, antioxidant, and antitumor activity of epsilon-poly-L-lysine and citral, alone or in combination. *Food & Nutrition Research*, 60(1), 31891. <https://doi.org/10.3402/fnr.v60.31891>
- Shima, S., Matsuoka, H., Iwamoto, T., & Sakai, H. (1984). Antimicrobial action of .EPSILON.-poly-L-lysine. *The Journal of Antibiotics*, 37(11), 1449–1455. <https://doi.org/10.7164/antibiotics.37.1449>

- Singh, A., Sharma, A., Ahmed, A., Sundramoorthy, A. K., Furukawa, H., Arya, S., & Khosla, A. (2021). Recent Advances in Electrochemical Biosensors: Applications, Challenges, and Future Scope. *Biosensors*, 11(9), 336. <https://doi.org/10.3390/bios11090336>
- Tuersuntuoheti, T., Wang, Z., Wang, Z., Liang, S., Li, X., & Zhang, M. (2019). Review of the application of ϵ -poly-L-lysine in improving food quality and preservation. *Journal of Food Processing and Preservation*, 43(10). <https://doi.org/10.1111/jfpp.14153>
- Waley, S. G., & Watson, J. (1953). The action of trypsin on polylysine. *Biochemical Journal*, 55(2), 328–337. <https://doi.org/10.1042/bj0550328>
- Yoshida, T., & Nagasawa, T. (2003). ϵ -Poly-l-lysine: microbial production, biodegradation and application potential. *Applied Microbiology and Biotechnology*, 62(1), 21–26. <https://doi.org/10.1007/s00253-003-1312-9>
- Zhao, W.-W., Xu, J.-J., & Chen, H.-Y. (2017). Photoelectrochemical enzymatic biosensors. *Biosensors and Bioelectronics*, 92, 294–304. <https://doi.org/10.1016/j.bios.2016.11.009>

Annexes

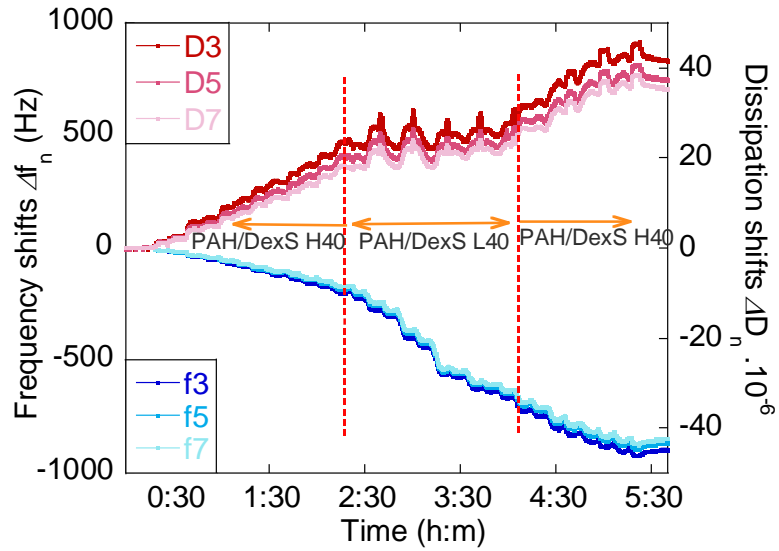


Figure 5.A1. Δf_n and ΔD_n as a function of time for deposition of $(\text{PAH/DexS H40})_5/(\text{PAH/DexS L40})_5/(\text{PAH/DexS H40})_5$ on gold coated surface using QCM-D.

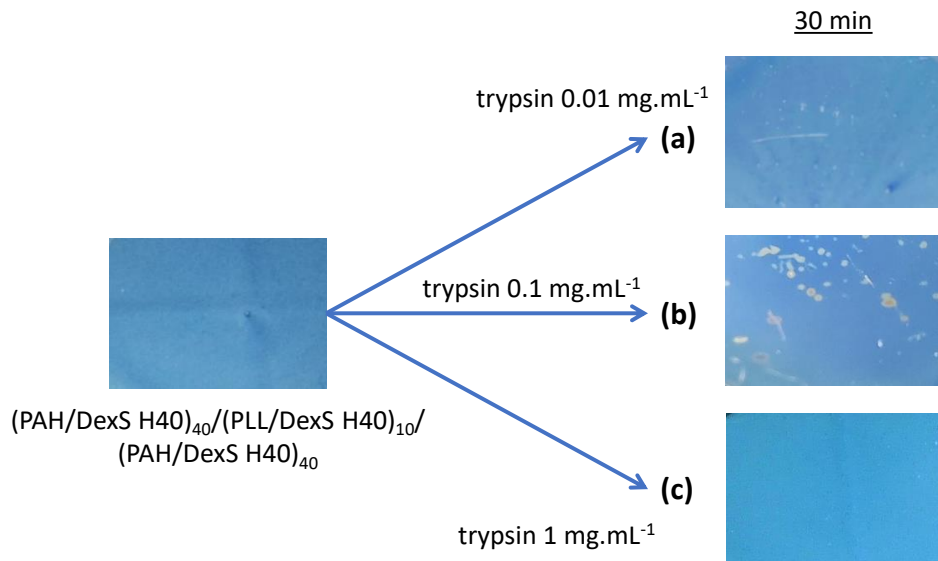


Figure 5.A2. Photos of $(\text{PAH/DexS H40})_{40}/(\text{PLL/DexS H40})_{10}/(\text{PAH/DexS H40})_{40}$ before and after dipping in presence of (a) 0.01 mg.mL^{-1} , (b) 0.1 mg.mL^{-1} and (c) 1 mg.mL^{-1} trypsin.

Conclusion and outlooks

The formation of layer-by-layer assemblies is the focus of this work, during which we are interested in the construction of multilayer films from functionalized α -glucans. The objectives are multiple: to understand the formation of the films, to control the growth of the films and their characteristics and to develop new enzymatic sensors. The films and their characteristics are studied at two scales:

1. 10 bilayers by dipping methods for analysis for layer formation (mass adsorption, viscoelastic behavior) and understanding of growth mechanisms
2. 40 bilayers by spin-assisted deposition method for the analysis of film characteristics and properties

In the first part of this thesis, several couples of functionalized glucans are studied as potential nanostructured films. This includes original oxidized glucans of very high molecular weight, because to our knowledge the only functionalized α -glucans used in multilayers are DexS and DEAD-Dex with molar masses lower than $500\,000\text{ g}\cdot\text{mol}^{-1}$. We show that it is possible to construct films with the PAH/DexS, PAH/oxidized α -glucans and DEAD-Dex/oxidized α -glucans systems. With each system, we find that differences in growth and viscoelastic behavior appear. In particular, we highlight that a difference in the loading of this DexS (DexS H40 vs Dex L40) leads for this couple to multilayer films with quite distinct characteristics. The first one allows us to obtain films with a classical linear growth and a unique viscoelastic regime. The second one allows to obtain films with a zig-zag growth and a viscoelastic regime that changes dramatically at each step of the film construction. The analysis of the physicochemical characteristics of these two films shows that the two types of growth gave films with different hydration rates as well as totally different surface morphologies. Thanks to this information, we are able to propose two construction mechanisms based on the understanding of the impact of their charges. In the case of DexS H40, the sufficient amount of charges creates a charge overcompensation and charge reversal at the surface allowing the adsorption of the counter polyelectrolyte. This mechanism results in less rigid or softer films with a “fibrillar-like” surface and high coverage. In the case of Dex L40, the lower amount of charges leads to the formation of PE complexes related to internal film restructuration and water and counter-ions ejection with polyelectrolyte adsorption and rinsing. This second mechanism leads to rigid films with a very particular “puddle-like” morphology.

In the second part, we choose to further understand several experimental parameters on the construction of the films with the idea of being able to control their growth and

characteristics. We study the impact of charge density, ionic strength and molar mass of functionalized α -glucans on the formation of the films. The studied characteristics are surface morphology, thickness and roughness and the studied properties are structural colors and surface wettability. First, we show that the charge density of polyelectrolytes influenced the type of film growth and its viscoelastic characteristics. Thus, the restructuring generated by a charge density too low to be overcompensated leads to the formation of a thicker film with more pronounced structural colors. We also notice that at 40 bilayers the surface roughness of the films is lower for a low charge density, contrary to what was observed at 10 bilayers. This lower roughness also leads to a decrease of the contact angle, *i.e.* a better wettability. Secondly, we show that the ionic strength has an impact on the viscoelasticity of the wet film but also on its final thickness and thus its color. Increasing the ionic strength allows us to modulate the conformation of the polyelectrolytes in solution: charge screening by adding counter ions allows us to obtain polymers in a “coiled” conformation that increases its adsorption potential, as well as its softness. We also investigate that the impact of the salt concentration on the morphology, its roughness and thus its wettability is different depending on the charge density. Finally, we demonstrate that there is an optimal molar mass value for film growth in thickness that depends on the system. In general, the results obtained with the different molar masses are surprising. The thickness/mass trends are reversed in the “wet” or “dry” state, with no change in viscoelasticity observed with the different molar masses. Similarly, we find that we obtain the best wettability for the intermediate molar mass despite the highest roughness for this system. We speculate that a difference in molar mass between the polyanion and the polycation may lead to a “stripping” phenomenon but also that the method of layer formation may have some impact.

In the last chapter, we propose the realization of a first enzymatic colorimetric sensor based on functionalized α -glucans multilayers. By an innovative construction, we wish to improve the sensitivity of existing sensors in the literature by reducing the amount of polyelectrolytes to be degraded by the enzymes. For this purpose, we realize a sandwich with three multilayers: 1) a very colorful multilayer - on the top, 2) an enzyme-sensitive multilayer - in the center and 3) a multilayer with a very different color from the first one - on the bottom. The choice of multilayers used for the design is made by observing the structural colors as a function of the polyelectrolyte systems and the number of bilayers. We demonstrate that by growing two films with each other, we are able to obtain a stable hybrid film while maintaining the characteristics of each multilayer. This observation allows the

incorporation of an enzyme-sensitive multilayer without fearing the total modification of the multilayer structure. Thus, it is possible to integrate a PLL/DexS H40 multilayer in the middle of a very light brown (PAH/DexS H40)₄₀ multilayer and a pink-green “porous” (PAH/DexS L40)₄₀ multilayer. The previously observed porous multilayer structure (PAH/DexS L40) seems to allow some permeability to enzymes, and allows enzymes to access the enzyme-sensitive middle multilayer. Similarly, incorporating 1–10 bilayers of PLL/DexS H40 corresponding to 10 nm - 25 nm does not affect the color of the fabricated sensor. When the 3-multilayer film is put in contact with trypsin, we find that we have a color change for concentrations between 0.1 mg.mL⁻¹ (~1.6×10⁴ nkat.mL⁻¹) and 0.01 mg.mL⁻¹ (~1.6×10³ nkat.mL⁻¹) of trypsin for 10 PLL-based multilayers. Below and above these concentrations, we do not observe any color change, for thinner PLL either. With our current enzymatic sensor, we obtain a sensitivity of 1.6×10³ nkat.mL⁻¹ for a thin PLL film of about 20 nm.

In the continuity of this thesis work, it would be interesting to improve the sensitivity of the enzymatic sensor developed. This would involve the choice of polyelectrolytes, in particular by trying to form sensors with oxidized α -glucans. This would allow to test other film porosities and permeabilities to enzymes but also to reduce the number of layers necessary to obtain a marked color. By reducing the number of layers of the enzyme permeable part, it would be possible to improve the accessibility between the layer to be degraded and the enzymes, and thus the sensitivity. A second perspective concerns the diversity of applications of functionalized α -glucans-based multilayers. It would be interesting to exploit the different structures observed at other levels, especially on the morphology which appears closed and 'non-porous' for the development of barrier coatings (gas barrier for example). Moreover, in the idea of the Grafting project, we wish to diversify the type of functions on α -glucans by enzymatic routes. In particular, we are talking about introducing phosphate groups that could be useful for the development of flame-retardant coatings.

Résumé en français

Introduction

Les α -glucanes bactériens présentent un grand intérêt pour la communauté scientifique en raison de leur production par l'action de bactéries et de leur possibilité de fonctionnalisation par voie chimique (Baptista & Freitas, 2021; Naessens et al., 2005). Plus récemment, les progrès notables réalisés par l'équipe TBI (Toulouse, France), sur la production d' α -glucanes par voie enzymatique, ont ouvert le champ des modifications enzymatiques possibles de ces polysaccharides par voie non chimique (Grimaud et al., 2018). Elles offrent alors une opportunité pour une utilisation plus massive des α -glucanes dans l'industrie. En particulier, leur utilisation dans la construction de matériaux permettrait de remplacer une partie des polymères synthétiques chargés pour former les matériaux. Le principal challenge consiste à comprendre et à contrôler les interactions des/avec les α -glucanes fonctionnalisés pour développer des matériaux aux propriétés comparables à celles des matériaux à base de polymères synthétiques. Une technique versatile et pratique pour construire de tels matériaux est l'assemblage couche par couche (layer-by-layer, LbL) de polyélectrolytes, basé sur l'adsorption alternée de polycations et de polyanions sur un substrat, comme décrit sur la Figure R.1. (Decher, 1997; Decher & Hong, 1991).

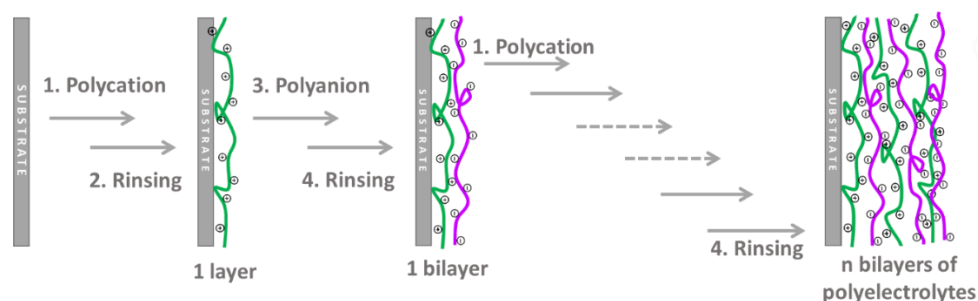


Figure R.1. Représentation schématique des différentes étapes de la fabrication de multicouches de polyélectrolytes (PEM) par la méthode couche par couche (layer-by-layer).

Dans ce contexte, le projet ANR (Agence Nationale de la Recherche) « Grafting » vise à améliorer et diversifier la production d' α -glucanes chargés en développant des voies de fonctionnalisation plus 'vertes' comme la fonctionnalisation par voie enzymatique. En parallèle du développement de la fonctionnalisation biologique, le projet aspire également à évaluer la possibilité d'élaborer de nouveaux matériaux à partir de ces nouveaux polyélectrolytes biosourcés tout en explorant leurs propriétés d'interaction notamment dans l'assemblage LbL.

Ma partie du projet a été réalisée dans l'équipe Nano de l'INRAE BIA (Biopolymères, Interactions et Assemblages) à Nantes (France). Ainsi, mon projet de thèse s'est concentré sur trois objectifs majeurs pour l'élaboration de matériaux innovants basés sur de nouvelles multicouches d' α -glucanes bactériens : 1) Évaluation des capacités d'adsorption des α -glucanes bactériens, 2) Contrôle de la fabrication couche par couche (LbL) de multicouches à base d' α -glucanes bactériens, 3) Examen des propriétés des films multicouches pour la sélection d'applications spécifiques.

Mon manuscrit de thèse s'organise en trois volets. 1) L'évaluation de la capacité des α -glucanes bactériens fonctionnalisés à former des films multicouches. 2) La modulation des croissances de films et des propriétés de surfaces. 3) Le développement de dispositifs pour la détection d'activité enzymatique.

1. Construction de multicouches à partir de α -glucanes fonctionnalisés

1.1. Sélection des α -glucanes fonctionnalisés pour la formation de films

Nous avons obtenu des PEMs avec une large gamme de masse absorbée et un comportement viscoélastique varié après 10 bicouches. En général, les systèmes basés sur les deux mêmes types de polyélectrolytes conduisent au même type de construction. Par exemple, les systèmes (DEAE-Dex 150/DexS) ne permettent pas de former des films avec ni DexS H40 ni DexS L40 alors que les systèmes PAH/DexS fonctionnent (Figure R.2).

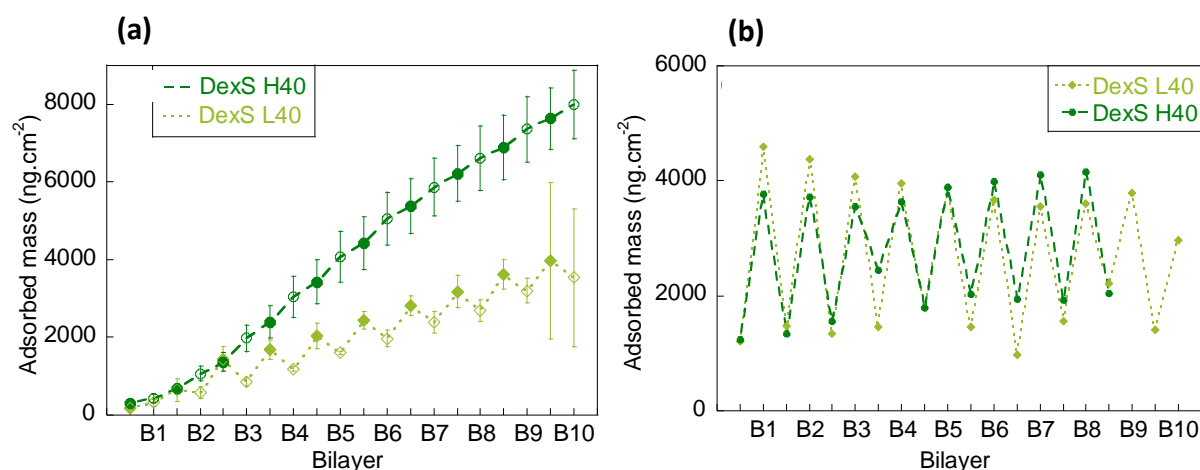


Figure R.2. Masse adsorbée évaluée avec le modèle de Voigt pour un multicouche de (a) (PAH/DexS)₁₀ and (b) (Dex-DEAE 150/DexS)₁₀ avec DexS H40 (vert foncé) et DexS L40 (vert clair). Bn correspond à la nième bicouche du multicouche.

Les systèmes (PAH/Ox-Alt) et (PAH/Ox1-Reu) conduisent tous deux à des multicouches présentant une croissance de masse symétrique linéaire avec deux régimes viscoélastiques différents pour un film final qui peut être considéré comme rigide. Les systèmes (Dex-DEAE 150/Ox1-Dex) et (Dex-DEAE 150/Ox3-Dex) conduisent tous deux à des films assez "mous" avec une croissance de masse en zigzag. Seuls les systèmes à base de PAH et DexS conduisent à des multicouches avec un type de croissance de masse différent et un comportement viscoélastique différent pendant la construction et après la construction de 10 bicouches. Nous avons obtenu des films mous avec une croissance symétrique linéaire de la masse déposée dans le cas du DexS H40 et des films assez rigides avec une croissance de la masse en zig-zag dans le cas du DexS L40 (Figure R.2).

1.2. Exemple de mécanismes de croissance

Après le balayage de la croissance des films basés sur les α -glucanes fonctionnalisés, nous avons décidé de nous concentrer sur la compréhension des mécanismes de construction des films (PAH/DexS H40) et (PAH/DexS L40). En effet, ces deux PEMs basés sur les mêmes polyélectrolytes, à la seule exception de la densité de charge du DexS, présentent la différence la plus remarquable en termes d'adsorption et de comportement viscoélastique. Nous avons décidé basés sur la compréhension de leur formation. Les caractéristiques physico-chimiques (teneur en eau, morphologie de surface), combinées aux informations recueillies sur la masse adsorbée et le comportement viscoélastique des multicouches par QCM-D, permettent de proposer une description complète du mécanisme de croissance des multicouches à base de PAH/DexS.

Dans le cas des films (PAH/DexS H40), illustrés sur la figure R.3, la quantité de charges négatives provenant du DexS H40 est probablement suffisamment élevée pour compenser largement les charges provenant de la couche de PAH précédente qui pourrait fournir une densité de charge de surface élevée après l'adsorption du DexS H40 (Glinel et al., 2002).

Pour les systèmes (PAH/DexS L40) (Figure R.3), le mécanisme d'adsorption est plus complexe. Comme le DexS L40 présente un nombre de charges par monomère comparable au nombre de charges présentes sur le monomère PAH, une neutralisation partielle des sous-couches avec adsorption de PE s'est produite, ce qui contribue à la diffusion du PAH adsorbé dans les PEMs (PAH/DexS L40). Le gonflement du film pendant l'étape de rinçage peut

favoriser une diffusion supplémentaire interne et la restructuration des PEMs. La neutralisation des charges génère elle-même une élimination de l'eau (Kittle et al., 2012). Une compensation de charge entre PAH et DexS L40 se produit au sein des films, favorisant une nouvelle fois la neutralisation des charges puis la complexation entre PAH et DexS L40. La formation de complexes de PE diminue la répulsion électrostatique entre les PE et l'affinité avec l'eau de la PAH et du DexS L40, ce qui provoque une expulsion de l'eau contenue dans le film.

(PAH/DexS H)



(PAH/DexS L)

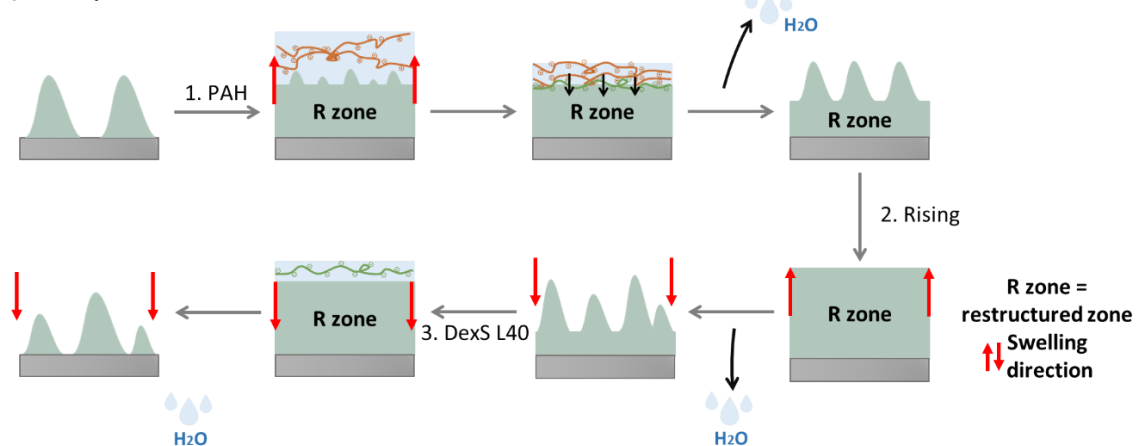


Figure R.3. Mécanismes proposés pour la construction de (a) multicouche (PAH/DexS H40) et de (b) multicouche (PAH/DexS L40).

2. Contrôle de la structure et des caractéristiques des films

Comme nous travaillons principalement avec des polyélectrolytes forts (en dehors des α -glucanes oxydés préparés par l'équipe TBI), nous étudions l'impact des paramètres suivants sur la constitution de films à base d' α -glucanes fonctionnalisés : 1) densité de charge des polyélectrolytes, 2) force ionique des solutions de polyélectrolytes, 3) masse molaire des polyélectrolytes. Nous étudions l'impact de chaque paramètre sur le type de croissance des multicouches et sur leurs comportements viscoélastiques au cours de leur formation. Ensuite,

une analyse de l'influence de ces paramètres sur les propriétés structurales et de surface est présentée : couleur structurale, morphologie et mouillabilité.

2.1. Impact de la densité de charge

Nous avons observé que les α -glucanes avec une densité de charge plus élevée ont tendance à conduire à une croissance du film de type A et à un film "hydraté" plus épais. Cette évolution du type de croissance du film et de la structure interne a été constatée, quelle que soit la densité de charge du contre-polyion utilisé. Cependant, il est probable que la valeur de la densité de charge, nécessaire pour passer d'une croissance de film de type A à une croissance de type B, dépende des caractéristiques du second polyélectrolyte.

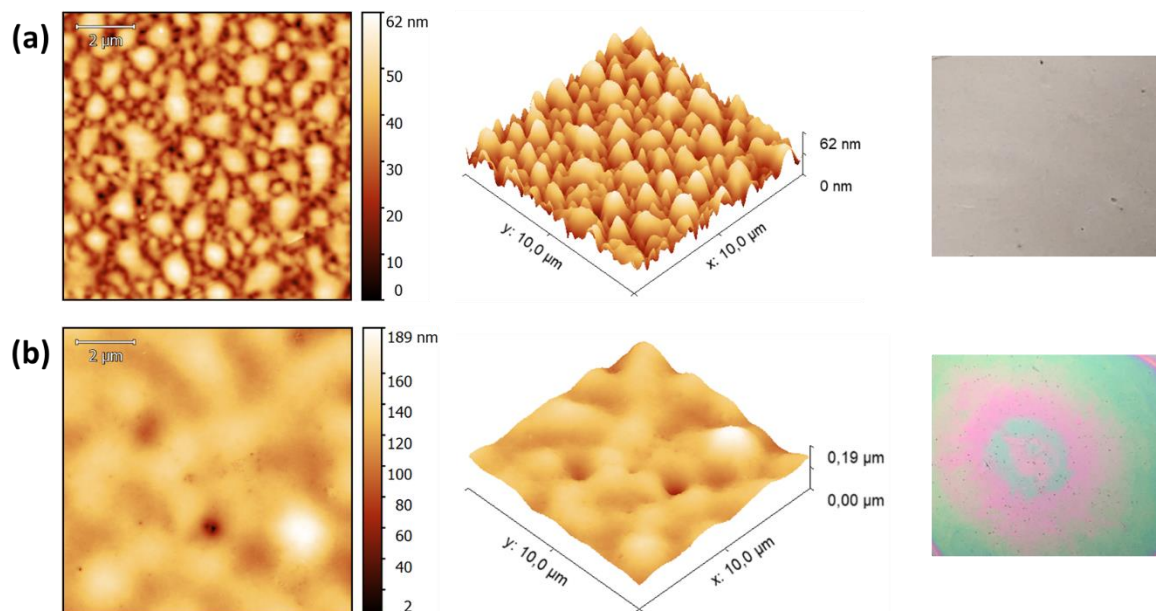


Figure R.4. Images AFM 2D et 3D (10×10 μm) ainsi que les photos des surfaces pour 40 bicouches de (a) (PAH/DexS H40) et (b) (PAH/DexS L40) construites par la méthode de trempage assistée par rotation sur silicium à 25mM NaCl.

La densité de charge affecte également la morphologie de la surface, car une densité de charge plus faible donne un film "sec" plus épais et plus hétérogène que l'utilisation d'un α -glucane avec une densité de charge plus élevée (Figure R.4). À 40 bicouches, les films à base de sulfate de dextrane avec une densité de charge inférieure semblent être plus plats. La morphologie plus plate et la rugosité plus faible se traduisent également par une variation de l'hydrophilie de surface : les α -glucanes avec une densité de charge plus faible conduisent à un angle de contact avec l'eau plus faible.

2.2. Impact de la force ionique

L'impact de la force ionique sur la formation de multicouches à base d' α -glucanes dépend fortement de la densité de charge du polyélectrolyte. Pour les polyanions ayant une densité de charge plus élevée, une augmentation de la force ionique conduit à un film "hydraté" plus épais et plus mou (rigidité relative plus faible). L'augmentation de la force ionique pour une densité de charge élevée entraîne également des films "secs" plus épais et une morphologie de surface avec de grands motifs (pics). Ce changement de type de morphologie induit une diminution de l'hydrophilie de surface. Dans le cas des α -glucanes ayant une densité de charge plus faible, nous avons un film "hydraté" plus épais lorsque la force ionique augmente, avec des variations de dissipation plus importantes lors de la construction. Le film "sec" semble également plus épais. La principale différence est l'augmentation de l'hétérogénéité de surface à plus forte concentration en sel et la modification de la morphologie : le film devient plus plat avec l'augmentation de la force ionique. Cette observation est corrélée à une augmentation de la mouillabilité de la surface.

2.3. Impact de la masse molaire des polyélectrolytes

L'utilisation d'un polyélectrolyte de masse molaire élevée conduit généralement à des films "hydratés" plus épais que les films à base de polymères de masse molaire inférieure au-dessus d'une certaine valeur de poids moléculaire. Les polymères de masse moléculaire plus élevée peuvent également conduire à un film plus mou au-dessus d'une certaine valeur de masse moléculaire. En termes de morphologie, comme illustrés sur la figure R.5, une augmentation de la masse molaire semble entraîner une meilleure couverture de surface et à la masse molaire la plus élevée, un film plus plat est obtenu. Les variations de la rugosité mesurée sont similaires aux variations de l'angle de contact. En passant de la masse moléculaire inférieure à la masse moléculaire intermédiaire, une augmentation du RMS entraîne une hydrophilie plus faible. En passant de la masse molaire intermédiaire à la masse molaire élevée, on observe une diminution du RMS et une plus grande mouillabilité.

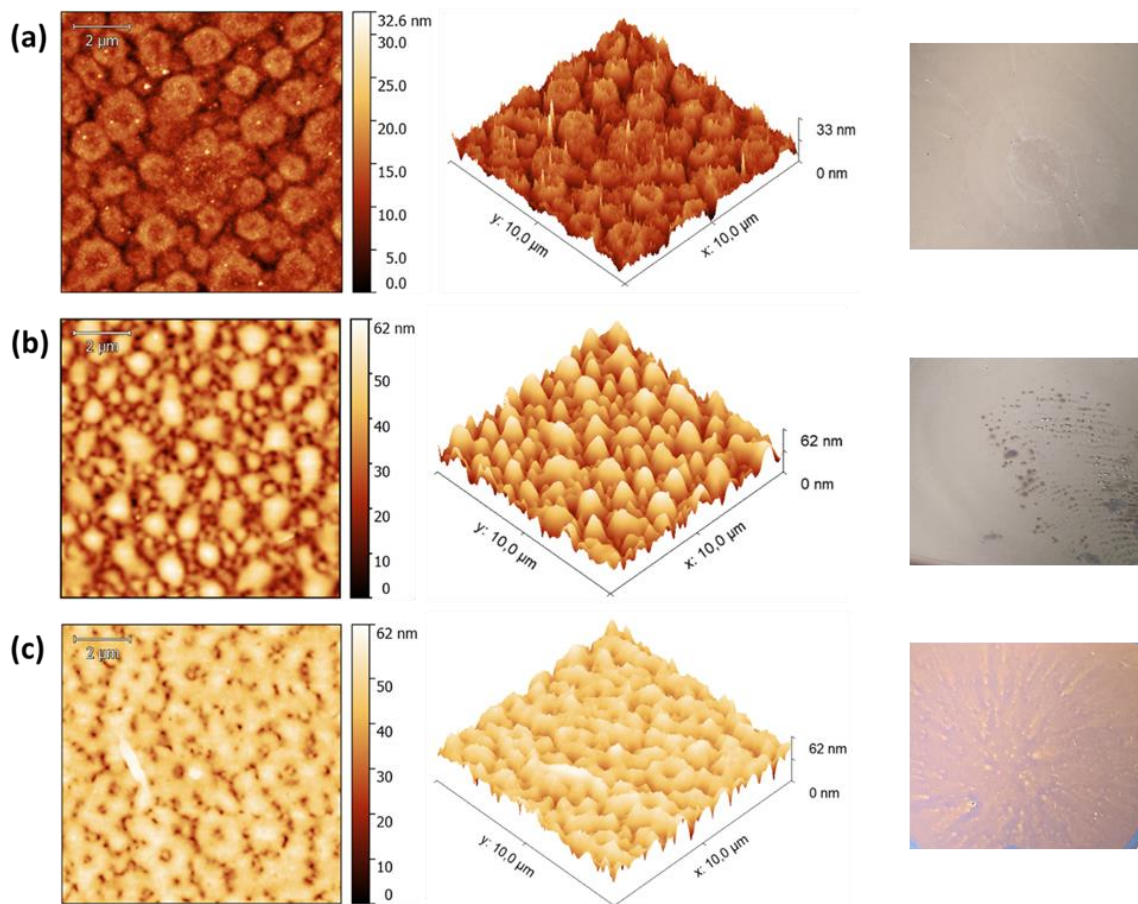


Figure R.5. Images AFM 2D et 3D ($10 \times 10 \mu\text{m}$) ainsi que les photos des surfaces pour 40 bicouches de (PAH/DexS H) pour le DexS H avec un poids moléculaire de (a) $5\,000 \text{ g.mol}^{-1}$, (b) $40\,000 \text{ g.mol}^{-1}$ and (c) $500\,000 \text{ g.mol}^{-1}$ construites par la méthode de trempage assistée par rotation sur silicium à 25mM NaCl .

3. Multicouches d' α -glucanes pour dispositifs de détection d'enzymes

Nous proposons la réalisation d'un dispositif de détection d'enzymes original : Le concept est d'intégrer en sandwich un polyélectrolyte sensible aux enzymes entre deux films de couleurs structurales différentes. Le capteur est alors constitué de trois films différents sur un substrat : une multicouche de couleur 1, un film sensible aux enzymes, une multicouche de couleur comme présenté sur la Figure R.6. La construction d'un tel dispositif nécessite des caractéristiques spécifiques pour chacune des trois multicouches utilisées.

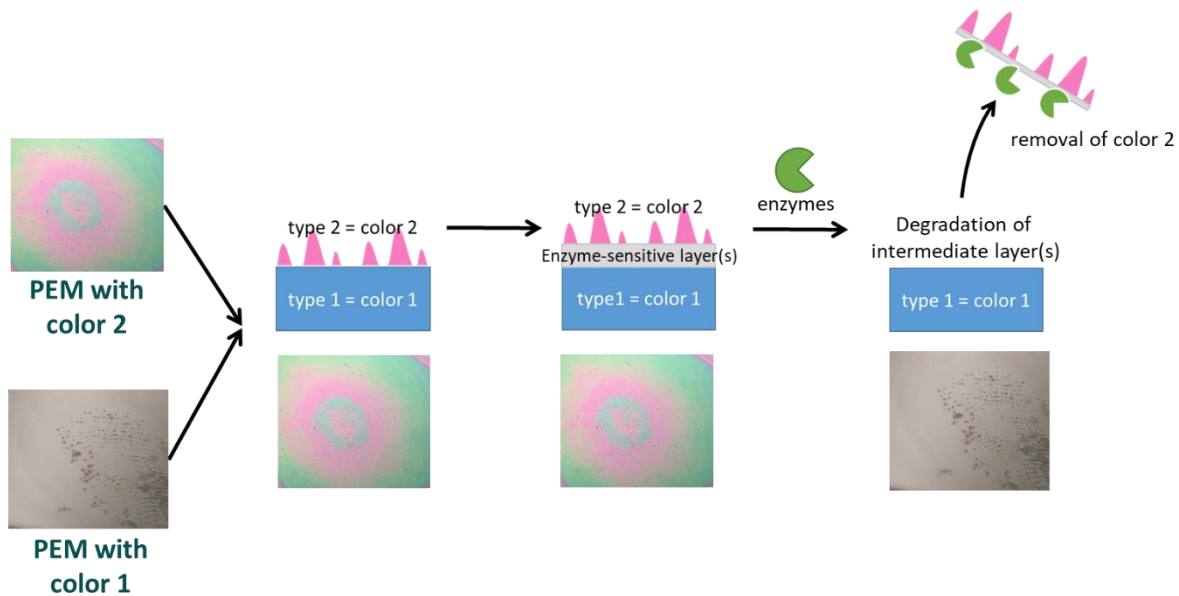


Figure R.6. Présentation schématique du concept proposé pour l'élaboration de biocapteurs colorimétriques pour la détection d'enzymes, basés sur des multicouches d' α -glucanes fonctionnalisés.

2.1. Choix des multicouches d' α -glucanes fonctionnalisés : couleurs et structures

Le choix des deux systèmes d' α -glucanes fonctionnalisés utilisés pour l'élaboration du dispositif est basé sur deux critères : les couleurs et les structures. Si le multicouche de couleur 1 ne doit pas présenter une couleur marquée, la couleur du multicouche 2 doit être suffisamment colorée pour identifier un changement s'il est supprimé. Ainsi, nous avons étudié les différentes couleurs structurales que nous pouvons obtenir avec des systèmes à base d' α -glucanes fonctionnalisés en construisant des multicouches avec un dépôt assisté par spin.

Nous avons étudié les couleurs que nous pouvons obtenir avec nos différents systèmes de polyélectrolytes. (PAH/DexS L40) (Figure R.7) et (PAH/ α -glucanes oxydés) sont plus susceptibles de correspondre à la multicouche supérieure, en raison de leur hétérogénéité et de leurs couleurs marquées. (PAH/DexS H40) et (DEAE-Dex 150/ α -glucanes oxydés) sont plus susceptibles de correspondre à la multicouche inférieure, car ils présentent une surface plus homogène même si (PAH/DexS H40) n'est pas coloré. De plus, les couleurs structurales de ces multicouches peuvent être accordées par le nombre de bicouches. Cependant, dans le cas de (PAH/DexS L40), l'augmentation du nombre de bicouches au-delà de 40 bicouches entraîne des couleurs moins marquées et des agrégats sur la surface.

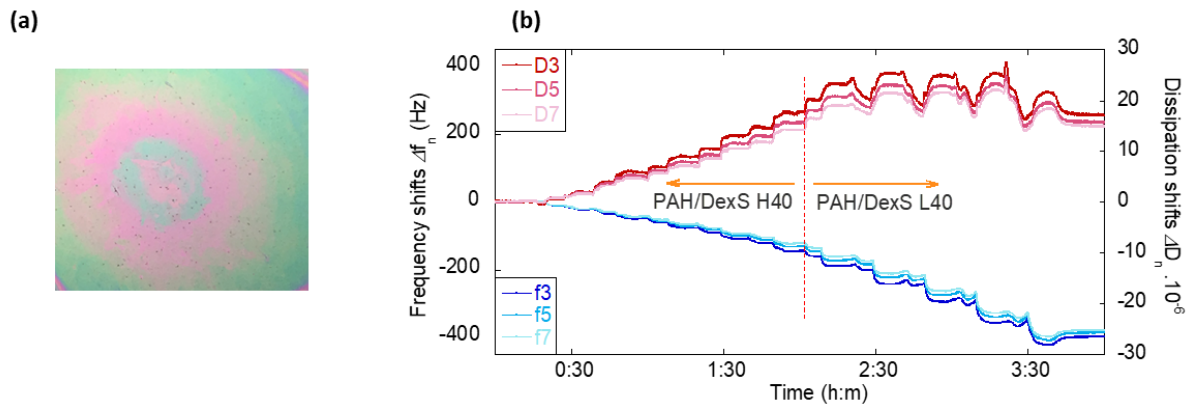


Figure R.7. (a) Photo et couleurs d'un film de 40 bicouches (PAH/DexS L40). (b) $\Delta f_n/n$ et ΔD_n en fonction du temps pour le dépôt de (PAH/DexS H40)₅/(PAH/DexS L40)₅ sur une surface d'or en utilisant QCM-D.

Comme la structure est importante pour l'élaboration du test, nous avons également étudié le maintien de la structure du film en combinant la croissance de deux multicouches comme nous pouvons le voir sur la Figure R.7b. En utilisant PAH/DexS H40 et PAH/DexS L40, nous avons démontré que le mélange de deux films avec un type de croissance différent résulte en une multicouche réussie et que chaque multicouche (PAH/DexS) maintient ses structures distinctes.

3.2. Capteurs colorimétriques pour la détection de la trypsine

La poly-L-lysine et une enzyme spécifique, la trypsine, ont été utilisées comme modèle pour la multicouche intermédiaire et sa dégradation. Nous avons démontré que la poly-L-lysine sensible à l'enzyme peut former des multicouches de 10 couches avec DexS H40 et DexS L40, et présenter un type de croissance similaire à (PAH/DexS H40) et (PAH/DexS L40) respectivement. Ensuite, nous avons intégré la multicouche à base de PLL avec des multicouches d' α -glucanes fonctionnalisées pour construire le test colorimétrique comme montrés sur la Figure R.8. L'intégration d'une telle multicouche intermédiaire à 1 bicouche, 5 bicouches et 10 bicouches permet de former avec succès un système (PAH/DexS H40)₄₀/(PLL/DexS H40)_n/(PAH/DexS L40)₄₀, sans affecter les couleurs finales de la surface.

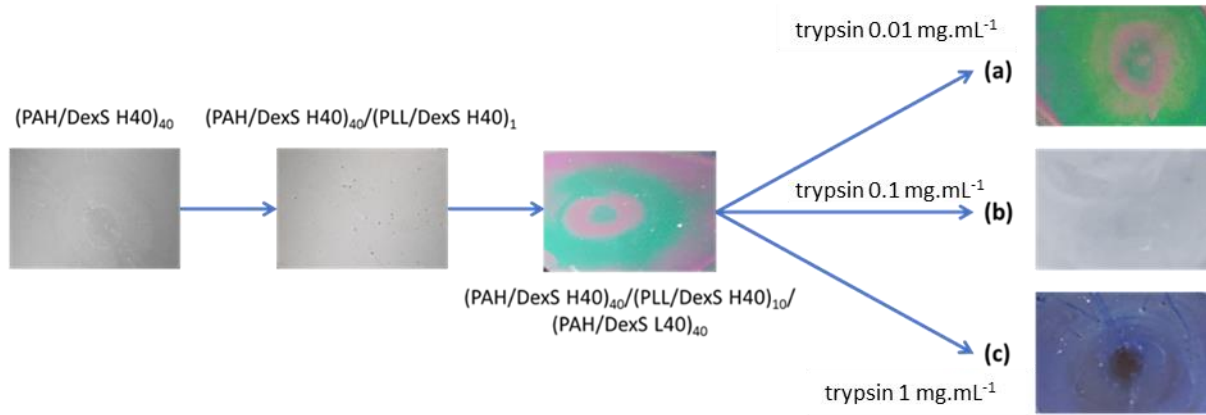


Figure R.8. Photos de l'élaboration du film $(\text{PAH/DexS H40})_{40}/(\text{PLL/DexS H40})_1/(\text{PAH/DexS L40})_{40}$ et de sa dégradation par trempage en présence de (a) 0.01 mg.mL⁻¹, (b) 0.1 mg.mL⁻¹ et (c) 1 mg.mL⁻¹ de trypsine.

Pour tester l'efficacité du dispositif à trois multicouches, le système a été immergé dans une solution de trypsine qui devrait entraîner une modification de la couleur de la surface. $(\text{PAH/DexS H40})_{40}/(\text{PLL/DexS H40})_n/(\text{PAH/DexS L40})_{40}$ présentait un changement de couleur à faible concentration de trypsine dû à une dégradation partielle du film intermédiaire de PLL. Cependant, la diminution du nombre de bicouches à base de PLL à 1 ou 4 ne permet pas la dégradation/élimination des couches intermédiaires et supérieures, puisqu'aucun changement de couleur n'a été observé.

Titre : Propriétés d'adsorption d' α -glucanes fonctionnalisés pour l'élaboration de matériaux biosourcés innovants.....

Mots clés : α -glucanes ; adsorption ; film multicouche ; couche-par-couche ; biocapteur

Résumé : Les α -glucanes sont de potentiels candidats pour l'élaboration de matériaux innovants. Au-delà de leur disponibilité dans la nature, ils présentent un intérêt de par leurs diverses structures et compositions chimiques. Le projet "GRaFTING" vise à développer des voies vertes de fonctionnalisation des α -glucanes puis à valoriser les α -glucanes fonctionnalisés par la fabrication de matériaux. La thèse est réalisée en réponse au second point : les α -glucanes permettent la construction de matériaux par la technique layer-by-layer (LbL), basée sur le dépôt alterné de polycations et de polyanions. Ce travail est constitué de trois parties. 1) Formation de multicouches avec des α -glucanes chargés. 2) Contrôle de la croissance des films et de leurs structures. 3) Elaboration de matériaux innovants.

L'adsorption des α -glucanes fonctionnalisés est évaluée par la formation de multicouches avec la Microbalance à Cristal de Quartz avec contrôle de la Dissipation (QCM-D). Les dextrans sulfate (DexS) forment des multicouches avec le poly(hydrochlorure d'allylamine) (PAH) mais pas avec le diéthylaminoéthyl-dextrane (Dex-DEAE) et les α -glucanes oxydés forment des films avec les deux polycations. Différents comportements d'adsorption et de viscoélasticité sont identifiés permettant de proposer deux mécanismes de croissance. Nous avons ensuite étudié l'impact de la densité de charge, de la force ionique et de la masse moléculaire des polyélectrolytes sur les films et leurs propriétés (morphologie, couleurs, mouillabilité). Les caractéristiques des films ont permis de créer des dispositifs colorimétriques pour la détection d'enzymes.

Title : Adsorption properties of functionalized α -glucans for the elaboration of innovative biobased materials.....

Keywords : α -glucans ; adsorption ; multilayer film ; layer-by-layer ; biosensor

Abstract : Among biopolymers, α -glucans exhibit potential as candidates for the elaboration of innovative materials. Beyond from their availability in nature, α -glucans demonstrate great interests regarding their diverse structures and chemical compositions. The project "GRaFTING" aims to develop green routes concerning α -glucans functionalization then to valorize functionalized α -glucans for assembling materials. The thesis was carried out in response to the second point: α -glucans were used to build materials by layer-by-layer (LbL) technique, based on the alternative deposition of polycations and polyanions. This work was constituted of three main parts. 1) Formation of multilayer films with functionalized α -glucans. 2) Control of the growth of LbL assemblies and their structures. 3) Elaboration of materials based on the specific properties of the films.

The adsorption capacity of functionalized α -glucans was evaluated by formation of multilayer films using Quartz Crystal Microbalance with Dissipation monitoring (QCM-D). Dextran sulfates (DexS) form multilayers with poly(allylamine hydrochloride) (PAH) but not with diethylaminoethyl-Dextran (Dex-DEAE) while oxidized α -glucans result in multilayers with both polycations. Different adsorption and viscoelastic behaviors were identified allowing to propose two mechanisms for (PAH/DexS) growth. Then, our work studied the impact of charge density, ionic strength and molecular weight of polyelectrolytes on the films and their properties (morphology, structural colors, wettability). Finally, we took advantage of their characteristics to develop bio-based colorimetric devices for enzyme-detection